Genome-scale DNA Methylation Changes in Endothelial Cells by Disturbed Flow and its Role in Atherosclerosis

A Dissertation
Presented to
The Academic Faculty

by

Jessilyn Dunn

In Partial Fulfillment
of the Requirements for the Degree
Doctor of Philosophy in Biomedical Engineering in the
Wallace H. Coulter Department of Biomedical Engineering

Georgia Institute of Technology
Emory University
May 2015

Genome-scale DNA Methylation Changes in Endothelial Cells by Disturbed Flow and its Role in Atherosclerosis

Approved by:

Dr. Hanjoong Jo, Chair
Department of Biomedical Engineering
School of Medicine, Division of Cardiology
Georgia Institute of Technology and Emory University

Dr. Xiaodong Cheng
Department of Biochemistry
Emory University

Dr. Yuhong Fan
School of Biology
Georgia Institute of Technology

Dr. I. King Jordan
School of Biology
Georgia Institute of Technology

Dr. Melissa Kemp
Department of Biomedical Engineering
Georgia Institute of Technology

Dr. Larry V. McIntire
Department of Biomedical Engineering
Georgia Institute of Technology

Date Approved: March 19, 2015

This work is dedicated to my family. Thank you for your unwavering love, support, and encouragement.

ACKNOWLEDGEMENTS

Thank you to my grandma, grandpa, mom, and dad for instilling in me the values to do my best work, for listening to me on the good days and the bad, and for always giving me good advice to live by. Thank you to my sister Erin for always believing in me. Thank you Zach for consistently reminding me of what is most important.

I am incredibly appreciative of my thesis committee members for constantly pushing me to improve and for making my work better than I could imagine. The care with which my committee has analyzed my findings, asked relevant and detailed questions, and shared their insight and advice was beyond words.

A special thank you to Dr. Jo for your guidance throughout this journey, and for helping me to discover my interests and enabling me to develop my skills, both in the wet lab and in computational biology. Thank you to Dr. Cheng and Dr. Fan for sharing your incredible breadth of knowledge on DNA methylation and epigenetics. Thank you Dr. Jordan for enabling me to discover and pursue my interests in bioinformatics, for arming me with the tools and knowledge for success, and for believing in my ability to become a "bona fide bioinformaticist." Thank you Dr. Kemp for your vast knowledge of systems biology and your perpetual interest and excitement about this work. Thank you Dr. McIntire for providing your expertise on cardiovascular disease mechanisms and the potential clinical applications of this work.

The combined expertise of my thesis committee allowed me to design the most relevant experiments, iterate through data analyses, and draw proper conclusions to construct this thesis project, and I am forever grateful for their time and dedication.

Thank you to my former lab mates and collaborators Haiwei Qiu, Soyeon Kim, Inhwan Jang, Chanwoo Kim, and Sandeep Kumar for their advice in lab and life, and to the Jo Lab graduate students and postdocs who have made the time I spent in lab lighter and more enjoyable. Thank you to Dong won and Sunkum Kang for your continued support and help with keeping organized in the lab. Thank you to the Biomedical Engineering Department for providing such wonderful resources, and especially to Shannon Sullivan and Sally Gerrish for your help and guidance along the way.

A big thank you to my collaborator Dr. Daudi Jjingo who taught my biologically-oriented mind to think like a computer scientist. This project and my future research directions would not be the same without your influence. Thank you also to my undergraduate research assistants Ryan Hoffman and Daniel Kim, who have gone on to create their own research successes in graduate and medical school, respectively.

Thank you to my friends, both new and old, from Florida, in Atlanta, and across the globe, for making life fun, keeping my morale up during graduate school, and jumping on board with my wild ideas, arts and crafts projects, and costume parties.

In all, this thesis was a team effort. Without those around me who have shaped my methods of thinking and long-term goals, none of this would have been possible, and I will be forever grateful.

TABLE OF CONTENTS

LIST OF TABLES

LIST OF FIGURES

Page

LIST OF SYMBOLS AND ABBREVIATIONS

A	Adenine
C	Cytosine
CG (or CpG)	Cytosine guanine dinucleotide
CVD	Cardiovascular Disease
DF (or d-flow)	Disturbed flow
DMR	Differentially methylated region
DNMT	DNA (cytosine-5-)-methyltransferase
gDNA	Genomic deoxyribonucleic acid
EC	Endothelial cell
G	Guanine
GC	Greater curvature
HAEC	Human aortic endothelial cell
HOX	Homeobox
HUVEC	Human umbilical vein endothelial cell
Klf	Kruppel-like factor
LCA	Left common carotid artery
LC	Lesser curvature
LDL	Low density lipoprotein
LS	Unidirectional, steady, laminar shear
miRNA	Micro ribonucleic acid
mRNA	Messenger ribonucleic acid
OS	Oscillatory shear or bidirectional, steady, laminar shear

oxLDL	Oxidized low density lipoprotein
PCL	Partial carotid ligation
PECAM1	Platelet endothelial cell adhesion molecule
PL	Post-ligation
RCA	Right common carotid artery
RRBS	Reduced representation bisulfite sequencing
T	Thymine
TNFα	Tumor necrosis factor alpha
U	Uracil
UTR	Untranslated region
VE-Cadherin	Vascular endothelial cadherin

SUMMARY

Cardiovascular disease (CVD) is the number one cause of death in the US. Atherosclerosis, an inflammatory disease characterized by plaque accumulation on the arterial walls, is the major cause of CVD[1,2]. Atherosclerotic plaque rupture (thrombosis and embolism) blocks blood flow and oxygen delivery to tissues thereby causing a heart attack or stroke[3]. While there are several known risk factors and behaviors that increase the likelihood of developing atherosclerosis, the underlying cause of the disease remains unknown[4].

Atherosclerosis typically occurs in curves or branches in the vasculature where disturbed blood flow alters gene expression and induces endothelial cell (EC) dysfunction. Blood flow generates shear stress on vascular ECs. Unidirectional, laminar shear stress (LS, or s-flow) is crucial for normal vascular function, whereas low, disturbed flow (d-flow), and oscillatory shear stress (OS) causes vascular dysfunction and disease [5-9]. ECs have dramatically altered gene expression patterns when exposed to d-flow versus s-flow [10-15].

Epigenetics controls aberrant gene expression in many diseases, but the mechanism of flow-induced epigenetic gene regulation in ECs via DNA methylation has not been well studied until very recently. The goal of this project was to determine how the DNA methylome responds to flow, causes altered gene expression, and regulates atherosclerosis development. The majority of our findings were published in the Journal of Clinical Investigation in May 2014 our research article titled Flow-dependent epigenetic DNA methylation regulates endothelial gene expression and atherosclerosis[16]. We found that d-flow increases DNA Methyltransferase 1 (DNMT1) expression in ECs, and we hypothesized that this causes a shift in the EC methylome and transcriptome

towards a pro-inflammatory, pro-atherosclerotic gene expression program, and further that this leads to atherosclerosis development.

To test this hypothesis, we employed both in vitro and in vivo experimental approaches combined with genome-wide studies of the transcriptome and DNA methylome and computational systems biology analyses according to the following three specific aims: 1) to elucidate the role of DNA Methyltransferase 1 in EC function, 2) to uncover the DNA methylation-dependent EC gene expression response to flow, and 3) to discover and examine master regulators of EC function that are controlled by DNA methylation.

Our in vivo technique, mouse partial carotid ligation, induces d-flow in the left carotid artery (LCA) while the s-flow right carotid artery (RCA) serves as an internal control. Data from our lab's previous *in vivo* mouse carotid artery mRNA microarrays implicated DNMT1 as a potentially functionally important mechanosensitive gene in EC biology that is upregulated by d-flow[17]. In Aim 1, we found that DNMT1 is upregulated by d-flow at the transcript and protein level *in vivo* and *in vitro*. DNMT1 inhibition using the chemical inhibitor 5-Aza-2'deoxycytdine (5Aza) or DNMT1 siRNA was done *in vitro* prior to shear in HUVECs, and 5Aza was used in mouse models of atherosclerosis to determine the functional outcome of blocking DNMT1 overexpression in d-flow. We show that DNMT1 inhibition by 5Aza inhibits inflammation and global methylation in ECs *in vitro* and plaque development in both acute and chronic murine models of d-flow-induced atherosclerosis *in vivo.* Preliminary studies exploring the mechanism of upstream DNMT1 regulation point to the mir29 family as potential mechanosensitive regulators of

this pathway. This work establishes the importance of DNMT1 in EC biology and atherosclerosis.

In the second aim we sought to determine the functional importance of DNMT1 overexpression by d-flow and also the mechanism of action of DNMT inhibition by 5Aza in d-flow-exposed endothelium. Since DNMT1 is known to methylate genomic DNA and DNA methylation is a regulator of gene expression, we designed two parallel "omics" studies to examine the effects of both d-flow and DNMT inhibition on the EC DNA methylome and transcriptome *in vivo*. We carried out reduced representation bisulfite sequencing (RRBS) using EC-enriched genomic DNA (gDNA) obtained from the RCA and LCA of partially ligated mice at two different time points of two days and one week post-ligation. To further determine whether the flow-dependent DNA methylation changes were regulated in a DNMT-dependent manner, mice treated with 5Aza were compared to a saline vehicle control. Moreover, to determine which mechanosensitive genes have transcriptional dysregulation, potentially by DNA hypermethylation, we carried out a concomitant gene transcript microarray study using EC-enriched RNA obtained from the LCA and RCA of partially-ligated mice treated with either saline (RCA vs. LCA) or 5Aza (Aza-RCA vs. Aza-LCA). From these studies we found that DNMT inhibition by 5Aza rescues global gene expression in the d-flow-exposed LCA to a healthy state. While genome-wide DNA methylation and specific functional genomic elements did not have dramatically changed methylation under these conditions, we followed a specific hypothesis and discovered a subset of genes that have d-flow-induced promoter hypermethylation correlating with gene suppression, both of which were 5Aza-reversible. Based on systems biology and further bioinformatics analysis, we found that

gene promoters containing cyclic AMP Response Elements (CRE) are preferentially demethylated at their CG sites as compared to other promoter CG sites in the RCA. Additionally, these promoter CRE CG sites are specifically hypermethylated by d-flow. We further discovered that, on the genome scale, CRE CG hypermethylation corresponds to decreased gene expression. These studies, described in detail in Aim 2, used "omics" datasets to uncover a key regulatory network regulated by DNA methylation that had never before been studied in the context of atherosclerosis.

To discover genes that are important in EC biology and regulated by DNA methylation, we performed detailed examination of the methylome and transcriptome data described in Aim 2. To determine the mechanisms by which 5Aza inhibited atherosclerosis in vivo and EC inflammation in vitro (as described in Aim 1), we tested the specific hypothesis that d-flow induces hypermethylation of anti-atherogenic EC genes at their promoter thereby silencing their expression, and that 5Aza treatment prevents this hypermethylation, leading to prevention of atherosclerosis. We found 11 genes that were strongly hypermethylated and had suppressed expression in d-flow, and these were reversed by treatment with 5Aza. These included *HoxA5, Tmem184b, Adamtsl5, Klf3, Cmkrl1, Pkp4, Acvrl1, Dok4, Spry2, Zfp46,* and *F2rl1*. We also found that genes containing promoter cyclic AMP response elements (CRE) are enriched in this subset of promoter hypermethylated, d-flow suppressed genes. In addition to HoxA5, we found that the entire family of Hox genes, including the co-localized mir10 family, had strong flow-dependent methylation changes in the same manner as described for the 11 genes. We further examined the role of several novel genes, including HoxA5 and Klf3, in EC biology using knockdown combined with EC inflammation assays. The findings

described in Aim 3 uncover the importance of DNMT-dependent mechanosensitive gene regulation by promoter methylation in EC function and highlight novel EC genes as that may provide useful targets for future atherosclerosis therapies.

The work presented here has resulted in new knowledge about the epigenetic EC shear response, details the previously unstudied EC methylome, and implicates specific loci within the genome for additional studies on their role in EC biology and atherosclerosis. This work provides a foundation for future studies to develop more targeted therapeutic strategies for CVD.

CHAPTER 1 INTRODUCTION

Clinical Significance of Atherosclerosis

Atherosclerosis is the major cause of cardiovascular disease, including coronary artery disease, coronary microvascular disease, carotid artery disease, peripheral arterial disease, and chronic kidney disease[1]. Coronary artery disease is the number one cause of death in the US[1,2]. In addition to acute symptoms caused by atherosclerosis, a number of associated chronic pathologies also burden the healthcare system, including angina (chest pain), heart failure (reduced blood flow from the heart due to a weakening of the muscle), and arrhythmias (loss of rhythm of the heartbeat). While there are several known risk factors and behaviors that increase the likelihood of developing atherosclerosis, the underlying cause of the disease remains unknown [4].

Atherosclerosis, Hemodynamics, and Endothelial Gene Expression

Atherosclerosis is an inflammatory disease characterized by plaque accumulation on the arterial walls[18]. Endothelial cells (ECs) lining the inner wall of the blood vessels become a dysfunctional, permeable barrier to low density lipoprotein and immune cell infiltration and lose proper nitric oxide regulation to control vessel dilation.[19] Atherosclerotic plaque rupture (thrombosis and embolism) blocks blood flow and oxygen delivery to tissues thereby causing a heart attack or stroke.[3]

Blood flow generates shear stress on the vascular walls. Unidirectional, laminar shear stress (LS) is crucial for normal vascular function, whereas low, disturbed flow (d-flow), and oscillatory shear stress (OS) causes vascular dysfunction and disease.[5-9] ECs have dramatically altered gene expression patterns when exposed to disturbed versus unidirectional flow.[10-15] Atherosclerosis preferentially develops in areas of d-flow, where

the dysfunctional EC phenotype initiates and perpetuates plaque accumulation.[20] D-flow-induced genes are mainly involved in apoptosis, inflammation, angiogenesis, and smooth muscle cell proliferation.

High throughput genome-wide microarray studies have generated clear evidence of the endothelial cells' keen ability to sense and convert mechanical stimuli into biochemical signaling responses.[6,8,21-23] Endothelial cells have mechanoreceptors that sense regions of d-flow and initiate a complex cascade of inflammatory events that results in global gene expression changes, endothelial dysfunction, and plaque buildup on the vessel wall.[24] Numerous key regulatory pathways as well as novel mechanosensitive genes and functional gene clusters have been illuminated from these high throughput studies.[25,26] The data continues to support the working hypothesis that laminar, unidirectional flow upregulates "atheroprotective" genes and downregulates "pro-atherogenic" genes while disturbed, reversing, or stagnant flow results in the opposite phenomenon of enhancing pro-atherogenic genes and suppressing atheroprotective genes. However, the mechanism by which disturbed flow causes changes in EC gene expression is unknown.

The discovery of master regulators that control a large network of genes is of high interest to vascular biologists because such biomolecules would serve as excellent therapeutic targets for disease treatment and prevention. Potentially important master regulators include epigenetic modifiers and transcription factors that participate in pre-transcriptional regulation, microRNAs involved in pre-translational regulation of protein expression, and post-translational modifiers. Epigenetic modifications such as DNA methylation, histone modifications, and chromatin remodeling complexes, alter the

genomic DNA structure and accessibility.[27] Transcription factors are recruited to specific regions of a gene promoter to form a transcriptional complex that assists RNA polymerase to bind and transcribe the gene to messenger RNA (mRNA). MicroRNAs have a complementary sequence to specific mRNAs and can block their translation or cause their degradation. Once mRNA has been successfully translated into protein, post-translational modifications control their activity and stability. Putative key microRNAs (miR21, miR712, miR10a) and epigenetic chromosome structural organizers (HDACs, DNA-binding proteins) are currently the subject of extensive research to determine their role in large-scale gene network regulation.

Epigenetics and DNA Methylation

Epigenetics refers to the modification of genetic information in a sequence-independent manner. Genomic DNA in an open, relaxed conformation is referred to as euchromatin and is associated with acetylated histones and unmethylated DNA. Genes in euchromatin are usually transcriptionally active. On the other hand, heterochromatin is condensed and is associated with repressive marks such as trimethylated-histone 3 lysine 9 (H3K9), trimethylated-histone 3 lysine 27 (H3K27), and DNA methylation. Heterochromatin generally contains repeat elements and transcriptionally silent genes, and its compaction predominantly occurs during development and differentiation.[28-32] Shear stress has been found to mediate chromatin remodeling and histone modifications and this is thought to play a role in shear-induced gene expression changes.[33,34]

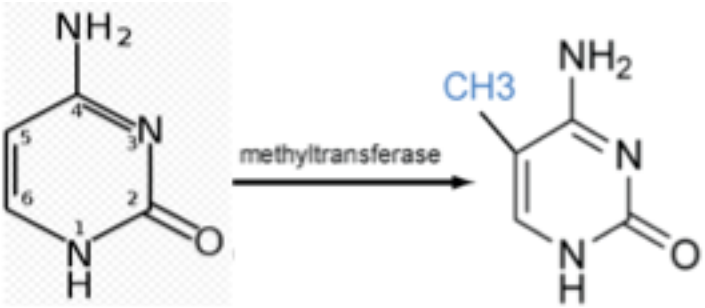

Figure 1.1: DNA methylation is placed by DNA methyltransferases at the fifth carbon of the cytosine ring.

DNA methylation is the most stable epigenetic modification and involves the addition of a methyl group to the 5' carbon of a cytosine base pair, which is then known as 5-methylcytosine (5mC) (Figure 1.1). This modification occurs most frequently in the context of a CpG (or CG) dinucleotide.[35,36] CpG islands are dense regions of CG sites with a higher than expected CG content (generally defined as > 50% with an observed vs. expected ratio of >0.6, over a distance of at least 200 base pairs) and are normally unmethylated.[37] Approximately 40% of human genes are associated with CpG islands.[38-41] Repetitive elements such as Alu, Line1, and B1 elements, and imprinted loci, are generally highly methylated.[39] CG sites are otherwise sparse throughout the genome due to a high rate of C to T mutation caused by spontaneous deamination of methylated cytosine, and only functionally important CG sites are thought to be evolutionarily protected from this mutation.[42-45]

DNA Methylation in disease

DNA methylation is a regulatory mechanism of gene expression known to play a key role in cancer development, particularly in the silencing of tumor suppressor genes via aberrant hypermethylation, but its role in many other diseases remains poorly understood. Atherosclerosis is characterized by endothelial dysfunction, including

hyperproliferation, migration, and inflammation, which are phenotypes also shared by cancer cells.

Recently, DNA methylation has been implicated as a novel risk factor for atherosclerosis in smooth muscle cells (SMCs).[46-50] Three genes are known to be methylated at the promoter in atherosclerotic SMCs: estrogen receptors ER-α, ER-β, and fibroblast growth factor 2 (FGF2).[51,52,53] Loss of estrogen receptor expression in SMCs causes a switch from the quiescent to the proliferative state. Hypermethylation of the ER-α promoter as well as high plasma homocysteine levels were found in atherosclerosis patients.[51,54] Age-related promoter hypermethylation of genes such as c-fos, c-myc, DBCCR1, E-cadherin, HIC1, IGF2, MYOD1, N33, PAX6, P15, and versican have been reported.[55] 5-methylcytosine (5mC) has been shown to be elevated in the intima of ApoE$^{-/-}$ mice fed western diet, and high 5mC levels are linked LDLR and p53 mutation in vascular cells.[45,50] 15-lipoxygenase, a gene implicated in oxidative modification of LDL, is regulated by DNA methylation.[56]

Aberrant DNA methylation is a well-known phenomenon in many cancers, and hypomethylating drugs that inhibit DNA methyltransferases have proven to be promising treatment options. 5Aza-2'-deoxycytidine (5Aza) is a well-studied DNMT1 preferential inhibitor.[57-62] 5Aza is a nucleoside analog that works by trapping DNMT1 in a covalent complex with DNA, resulting in DNMT1 degradation. 5Aza is commercially known as Decitabine and is used as a chemotherapeutic agent for cancers, more specifically, acute myeloid leukemia and myelodysplastic syndromes. Decitabine is thought to work by causing demethylation of oncogenes.[58-62] However, it is somewhat cytotoxic to bone marrow cells and this limits its therapeutic capacity. Current research explores the use of

antisense RNA therapy and specific chemical inhibitors to target DNMT1 more effectively.

CHAPTER 2 SPECIFIC AIMS

Significance and Impact

Prior to the conception of this project there were no studies on the regulation of epigenetics in endothelial cells (ECs) by mechanical forces generated by blood flow, and further no studies on the role of DNA methyltransferases (DNMTs) in ECs. Early reports of shear stress effects on epigenetics described novel pathways by which shear stress mediates chromatin remodeling and histone modifications in cultured endothelial cells [63,64]. However, until very recently, detailed endothelial cell epigenetic responses to shear stress were unknown. During the culmination of this thesis project, several research groups in vascular mechanobiology independently converged on the seminal finding that DNA methyltransferases are shear responsive proteins that regulate flow-mediated endothelial gene expression programs via DNA methylation [16,65,66]. These studies point to the opportune timing of our studies, and highlight the pertinence and novelty of this work to the field of vascular mechanobiology and disease.

This study was the first to examine the global effects of blocking DNA methylation pathways using DNMT inhibition in ECs. 5Aza-2'deoxycytidine (5Aza) and short interfering RNA (siRNA) treatments allowed us to directly observe the functional consequence of DNMT1 inhibition on global EC DNA methylation patterns and EC biology. Results from our *in vitro* studies predicated the question of whether there would be a functional effect of DNMT1 inhibition on disease outcome. We used two *in vivo* models of acute d-flow-induced and chronic diet-induced atherosclerosis as a robust system to analyze DNMT inhibition effects on disease development. The question of

whether DNMT1 inhibition affects EC inflammation *in vitro* and atherosclerotic plaque development *in vivo* has never been addressed before this point.

Many of the discoveries that are detailed in this dissertation were also published in the *Journal of Clinical Investigation*, and our work garnered international recognition through presentations at international conferences and coverage by various media outlets including the *American Heart Association Science News* [16]. This work provides a foundation for future studies to develop more targeted therapeutic strategies for CVD.

Rationale

Data from our lab's previous high throughput gene expression studies of endothelial cells in the *in vivo* mouse carotid artery using mRNA microarrays implicated DNA methyltransferase 1 as a potentially functionally important mechanosensitive gene [17]. DNA Methyltransferase 1 (DNMT1) was highlighted in the pool of ~600 shear-sensitive endothelial cell (EC) genes discovered by microarray in the mouse partial carotid ligation model due to its flow-sensitivity (~2.4 fold expression increase in the 48 hour disturbed flow LCA as compared with the control RCA) and its functional importance in development and disease. The other catalytically active DNA methyltransferases, DNMT3a, DNMT3b, and DNMT3L, were not found to be strongly flow-responsive in this model.

Preliminary results established significant DNMT1 upregulation in ECs under oscillatory shear (OS) *in vitro* and in disturbed flow (d-flow) *in vivo*. Therefore it was hypothesized that DNMT1 may have an important role in the EC shear response, which is the gateway to d-flow-induced atherosclerosis development. The effect of DNMT1 inhibition by 5Aza was tested on OS-induced EC inflammation, which is a major

hallmark of atherosclerosis, and on *in vivo* plaque development in atheroprone mice. Based on results demonstrating that DNMT1 inhibition reduces inflammatory signaling in ECs *in vitro* and plaque development *in vivo*, combined with the fact that the functional role of DNMT1 is to methylate DNA, the most probable and relevant downstream effect of DNMT1 upregulation is an alteration of DNA methylation. Resolving the EC methylome and transcriptome under disturbed versus unidirectional flow conditions enabled us to discover methylation and gene expression changes due to d-flow exposure. To implicate DNMT1 specifically in d-flow-induced methylation changes, the effect of DNMT1 inhibition on ECs under flow was also tested. We expected that DNMT1 inhibition would prevent the d-flow-induced methylation changes if DNMT1 is indeed the key player in establishing those methylation changes. Based on our discovery that DNMT1 is increased in d-flow, we hypothesized that d-flow leads to site-specific methylation changes that cause loss of anti-atherosclerotic gene expression by DNA methylation at the promoter. We further expected that DNMT1 inhibition by 5Aza would rescue these genes and prevent the pro-atherosclerotic phenotype.

Using a systems biology approach, the functional consequences of d-flow-induced DNA methylation and gene expression changes were explored to implicate novel genes that were previously unstudied in the context of the endothelial flow response and atherosclerosis. Discovery and validation of gene-specific methylation changes that cause gene expression changes produced a set of genes for further analysis. A subset of these genes were discovered by gene ontology analysis as transcription factors, and they were studied based their potential functional role as key network regulators. The effect of blocking d-flow-induced methylation changes in these genes on EC inflammation, which

is a hallmark of atherosclerosis, was explored. The work presented here has resulted in new knowledge about the epigenetic EC shear response, details the previously unstudied endothelial cell methylome, and implicates specific loci within the genome for additional studies on their role in EC biology and atherosclerosis.

Innovation

The finding that atherosclerosis is induced by disturbed blood flow (d-flow) is relatively recent, and is supported by the fact that global gene expression changes occur in ECs exposed to d-flow that cause a dysfunctional, pro-inflammatory EC phenotype. However, the mechanism by which these global gene expression changes take place is unknown, and the possibility of epigenetic gene regulation remained unexplored prior to this study.

Major advancements in methylomics were established with the advent of new technologies to resolve genome-level methylation at the nucleotide scale. The Human Epigenome Project and the NIH Roadmap Epigenomics Mapping Consortium are part of a major undertaking across multiple research facilities to create high-resolution DNA methylation and other epigenomic maps in various cell types.[67] While progress has been made, there is a clear lack of methylome data for ECs. One dataset using the Illumina 450k methylation array in static cultured HUVECs is publicly available, but there are no *in vivo* EC datasets, and furthermore none under varying flow and treatment conditions. The study described herein was the first to tackle this missing puzzle piece, with six new methylome datasets (ECs exposed to d-flow for either 2 or 7 days *in vivo*, and also with DNMT1 inhibition by 5Aza) that are critical for both cardiovascular and epigenomic research advancements.

A major challenge in the "omics" field is data mining to produce intelligible results from vast arrays of uninterpretable raw data. Data analysis can often act as a bottleneck in the pipeline from benchtop experiments to elucidation of therapeutic candidates. The data analysis performed for this project produced specific candidate genes as targets of d-flow-induced methylation. The systematic *a posteriori* search for global trends combined with the *a priori* pattern filtering creates a robust methodology to analyze methylomics on the genome and single gene, and even single nucleotide, scale.

Project Objective

While we know that laminar, unidirectional flow upregulates "atheroprotective" genes and downregulates "pro-atherogenic" genes while disturbed, reversing, or stagnant flow results in the opposite phenomenon, the mechanism by which flow controls EC gene expression is unknown. The goal of this project was to determine how the DNA methylome responds to flow, causes altered gene expression, and regulates atherosclerosis development.

Overall Hypothesis

Disturbed flow increases DNA Methyltransferase 1 (DNMT1) expression in endothelial cells. This in turn causes a shift in the EC methylome and transcriptome towards a pro-inflammatory, pro-atherosclerotic gene expression program which leads to atherosclerosis development. More specifically, we hypothesize that DNMT1 overexpression induces site-specific DNA hypermethylation in the promoter of key gene network regulators, which suppresses their expression and changes the endothelial transcriptome to a pro-atherosclerotic state.

Specific Aim 1: Elucidate the role of DNA Methyltransferase 1 in endothelial cell function

Data from our lab's previous *in vivo* mouse carotid artery mRNA microarrays implicated DNMT1 as a potentially functionally important mechanosensitive gene in EC biology. The mRNA array showed that DNMT1 expression was ~2.4-fold higher in the LCA exposed to d-flow for 48h following the partial ligation than in the contralateral RCA exposed to s-flow [17]. In Chapter 3, we show that DNMT1 is upregulated by d-flow at the transcript and protein level *in vivo* and *in vitro*. DNMT1 inhibition using the chemical inhibitor 5-Aza-2'deoxycytdine (5Aza) or DNMT1 siRNA was done *in vitro* prior to shear in HUVECs, and 5Aza was used in mouse models of atherosclerosis to determine the functional outcome of blocking DNMT1 overexpression in d-flow. We show that DNMT1 inhibition by 5Aza inhibits inflammation and global methylation in ECs *in vitro* and plaque development in both acute and chronic murine models of disturbed flow-induced atherosclerosis *in vivo*. Preliminary studies exploring the mechanism of upstream DNMT1 regulation point to the mir29 family as potential mechanosensitive regulators of this pathway. This work establishes the importance of DNMT1 in EC biology and atherosclerosis.

Specific Aim 2: Examine the DNA methylation-dependent endothelial gene expression response to flow

Specific aim 2 was designed to determine the mechanistic importance of DNMT1 overexpression by d-flow and also the mechanism of action of DNMT inhibition by 5Aza in disturbed-flow-exposed endothelium. Since DNMT1 is known to methylate genomic DNA and DNA methylation is a regulator of gene expression, we designed two parallel

"omics" studies to examine the effects of both disturbed flow and DNMT inhibition on the endothelial cell DNA methylome and transcriptome *in vivo*. We carried out the reduced representation bisulfite sequencing (RRBS) study using endothelial-enriched genomic DNA (gDNA) obtained from the RCA and LCA of partially ligated mice at two different time points of two days and one week post-ligation. To further determine whether the flow-dependent DNA methylation changes were regulated in a DNMT-dependent manner, mice treated with 5Aza were compared to a saline vehicle control. Moreover, to determine which mechanosensitive genes have transcriptional dysregulation, potentially by DNA hypermethylation, we carried out a concomitant gene transcript microarray study using endothelial-enriched RNA obtained from the LCA and RCA of partially-ligated mice treated with either saline (RCA vs. LCA) or 5Aza (Aza-RCA vs. Aza-LCA). From these studies we found that DNMT inhibition by 5Aza rescues global gene expression in the d-flow-exposed LCA to a healthy state. While genome-wide DNA methylation and specific functional genomic elements did not have dramatically changed methylation under these conditions, we followed a specific hypothesis and discovered a subset of genes that have d-flow-induced promoter hypermethylation correlating with gene suppression, both of which were 5Aza-reversible. Based on systems biology and further bioinformatics analysis, we found that gene promoters containing cyclic AMP Response Elements (CRE) are preferentially demethylated at their CG sites as compared to other promoter CG sites in the RCA. Additionally, these promoter CRE CG sites are specifically hypermethylated by d-flow. We further discovered that, on the genome scale, CRE CG hypermethylation corresponds to decreased gene expression. These studies, described in detail in Chapter 4, used

"omics" datasets to uncover a key regulatory network regulated by DNA methylation that can provide a basis for future studies on novel therapeutic targets for atherosclerosis.

Specific Aim 3: Discover and examine master regulators of endothelial function that are controlled by DNA methylation

To discover genes that are important in endothelial biology and regulated by DNA methylation, we performed detailed examination of the methylome and transcriptome data described in Chapter 4. To determine the mechanisms by which 5Aza inhibited atherosclerosis in vivo and endothelial cell inflammation in vitro (as described in Chapter 3), we tested the specific hypothesis that d-flow induces hypermethylation of anti-atherogenic endothelial genes at their promoter thereby silencing their expression, and that 5Aza treatment prevents this hypermethylation, leading to prevention of atherosclerosis. We found 11 genes that were strongly hypermethylated and had suppressed expression in d-flow, and these were reversed by treatment with 5Aza. These included *HoxA5, Tmem184b, Adamtsl5, Klf3, Cmkrl1, Pkp4, Acvrl1, Dok4, Spry2, Zfp46,* and *F2rl1*. We also found that genes containing promoter cyclic AMP response elements (CRE) are enriched in this subset of promoter hypermethylated, d-flow suppressed genes. In addition to HoxA5, we found that the entire family of Hox genes, including the co-localized mir10 family, had strong flow-dependent methylation changes in the same manner as described for the 11 genes. We further examined the role of several novel genes, including HoxA5 and Klf3, in endothelial biology using knockdown combined with endothelial inflammation assays. The findings described in Chapter 5 uncover the importance of DNMT-dependent mechanosensitive gene regulation by promoter

methylation in endothelial cell function and highlight novel endothelial genes as potential therapeutic targets for atherosclerosis.

Study Approval

All animal procedures were approved by the Institutional Animal Care and Use Committee at Emory University.

CHAPTER 3 THE ROLE OF DNA METHYLTRANSFERASE 1 IN ENDOTHELIAL CELL FUNCTION

Summary

Data from our lab's previous *in vivo* mouse carotid artery mRNA microarrays implicated the DNA methyltransferases as potentially functionally important mechanosensitive genes. The mRNA array showed that DNMT1 expression was ~2.4-fold higher in the LCA exposed to d-flow for 48h following the partial ligation than in the contralateral RCA exposed to s-flow[17]. D-flow-induced DNMT1 upregulation was validated at the transcript and protein level *in vivo* and *in vitro*. DNMT1 inhibition using the chemical inhibitor 5-Aza-2'deoxycytdine or DNMT1 siRNA was done *in vitro* prior to shear in HUVECs, and 5Aza was used in chronic and acute models of atherosclerosis to determine the functional outcome of blocking DNMT1 overexpression in d-flow. A major portion of Chapter 3 was published as follows: Dunn, J., Qiu, H., Kim, S., Jjingo, D., Hoffman, R., Kim, C. W., Jang, I., Son, D. J., Kim, D., Pan, C., Fan, Y., Jordan, I. K. Jo, H. Flow-dependent epigenetic DNA methylation regulates endothelial gene expression and atherosclerosis. *J Clin Invest* 124, 3187-3199[16]. Here, we demonstrated that disturbed, oscillatory shear stress induces DNMT1 overexpression at the transcript and protein level *in vivo* and *in vitro* and that DNMT1 inhibition by 5Aza inhibits inflammation and global methylation in ECs *in vitro*, and plaque development in both acute and chronic murine models of disturbed flow-induced atherosclerosis *in vivo*. Preliminary studies exploring the mechanism of upstream DNMT1 regulation point to the mir29 family as a potential mechanosensitive regulator of this pathway. This work establishes the importance of DNMT1 in EC biology and atherosclerosis.

Introduction

The Role of Fluid Mechanics in Endothelial Cell Gene Expression, the Endothelial Response to Blood Flow, and Atherosclerosis Development

Endothelial cells that line the blood vessel intima contain mechanoreceptors that sense regions of disturbed flow and initiate a complex cascade of inflammatory events that results in endothelial dysfunction and plaque buildup on the vessel wall.[24] Global gene expression in endothelial cells is altered, and newly expressed genes are involved in apoptosis, inflammation, angiogenesis, and smooth muscle cell proliferation.

Mechanosensitive Endothelial Cell Genes

Traditionally, gene expression studies conducted in vascular tissue were limited to single gene analyses of mechanical responsiveness and functional role in regulating cell shape and behavior with regard to vascular homeostasis and disease development.[68,69] Model systems engineered to study the effect of fluid shear stress on endothelial cells included shear-exerting bioreactors (e.g. cone and plate viscometer, parallel plate perfusion flow chamber)[22,70,71] for *in vitro* studies and porcine, murine, and canine models for *in vivo* studies. While bioreactor systems offered the advantage of precise control over flow conditions by bioreactor construction specifications, fluid composition, and environmental conditions, and allowed freedom to study human cells, they lacked several important factors that exist in the *in vivo* setting such as mechanical cell-substrate interactions, crosstalk with local and circulating cells and molecules, and variable rheologic properties.

In the early 1990s the idea of single gene analysis was advanced by the discovery of shear stress response elements (SSREs), or common cis-acting elements of gene promoters that are regulated by a single shear-controlled transcription factor. SSREs enable co-regulation of a host of genes under specific environmental conditions that activate their common transcription factor. Resnick et al. discovered the first SSRE common to the key signaling molecules platelet-derived growth factor beta (PDGF-B), tissue plasminogen activator, intercellular adhesion molecule 1 (ICAM1), and transforming growth factor beta 1 (TGFB1) that are all induced by laminar shear conditions.[72] SSREs have also been identified in other key genes such as Vascular Endothelial Growth Factor (VEGFR) and endothelial nitric oxide synthase (eNOS) and there are likely many SSREs that remain to be discovered.[14,73]

Genome-Wide Analysis and Discovery of Mechanosensitive Signaling Pathways

Because *in vitro* environments cannot fully recapitulate the effects of shear stress on the vascular endothelium *in vivo*, microarray studies evolved to *in vivo* settings to reveal the pathophysiological relevance of gene expression profiles in vascular endothelium exposed to specific flow conditions. Though there has been progress in the characterization of endogenous flow profiles *in vivo*,[9] the necessity for more detailed studies of gene function *in vivo* begot the development of the mouse partial carotid ligation model by our lab.[74] In this model, disturbed flow is induced in the left common carotid artery by ligation while the right common carotid artery remains untouched as an internal control. Our lab also developed a novel endothelial mRNA and microRNA collection technique that enabled the use of microarray technology to study global gene expression changes in mouse endothelium exposed to disturbed flow in an *in vivo* setting.

The dataset generated findings of 523 mechanosensitive genes changed within two days of disturbed flow exposure, including numerous genes previously undescribed in the context of the cardiovascular system.[17]

High throughput genome-wide microarray studies have demonstrated that endothelial cells respond to different shear stresses by altering their transcriptional networks.[6,8,21-23] Through these experiments, numerous key shear sensitive regulatory pathways as well as novel mechanosensitive genes and functional gene clusters have been illuminated and studied in great detail based on their role in endothelial cell homeostasis and disease development.[21,25,26] Specific intracellular signaling pathways that become prevalent under low/oscillatory, atheroprone shear stress are juxtaposed with pathways that dominate under high, atheroprotective, laminar shear areas, cyclic stretch, and appropriate hydrostatic pressure (Figure 3.1).[11] A host of mechanosensitive, atheroprotective genes that are highly expressed in laminar, unidirectional flow conditions have been uncovered. This includes eNOS, the gene responsible for nitric oxide production and maintenance of vascular tone, and several other genes involved in cell survival that have anti-thrombotic, anti-inflammatory, and anti-oxidant properties such as the Kruppel-like factor family (namely Klf2 and Klf4), and Superoxide Dismutases (Mn-SOD, EC-SOD).[75] Additional mechanosensitive genes involved in immune response activation (MCP-1,[23,76] VCAM-1, ICAM-1[77], NKFB[12])[78], reactive oxygen species production (NADPH Oxidases), and extracellular matrix reorganization causing vascular remodeling (TIMP-3, MMP-1) are found to be pro-atherogenic genes whose expression is suppressed under unidirectional laminar flow conditions and overexpressed under deleterious disturbed flow conditions. Many mechanosensitive cell

cycle regulators involved in endothelial cell homeostasis, including p53, GADD45, p21[5], ERK, play a key role in growth and proliferation suppression or activation.

One area of special interest lies in the discovery of master regulators that control a large network of genes (Figure 3.2). These biomolecules would serve as excellent therapeutic targets for disease studies. Potentially important master regulators include epigenetic modifiers and transcription factors that participate in pre-transcriptional regulation, microRNAs involved in pre-translational regulation of protein expression, and post-translational modifiers such as kinases. Epigenetic modifications such as DNA methylation, histone modifications, and chromatin remodeling, alter the genomic DNA structure and accessibility. Transcription factors are proteins recruited to specific regions of a gene promoter to form a transcriptional complex that assists RNA polymerase to bind and transcribe the gene to messenger RNA (mRNA). MicroRNAs have a complementary sequence to specific mRNAs and can block their translation or cause their degradation. Once the mRNA has been successfully translated into protein, post-translational modifications control their activity and stability. For example, kinases can activate or deactivate a protein by phosphorylation, and the post-translational modifier ubiquitin may ubiquitinylate a protein to target it for destruction by the proteasome. Putative key microRNAs (miR21, miR712, miR10a[79]) and epigenetic chromosome structural organizers (HDACs, DNA-binding proteins) are currently the subject of extensive research to determine their role in large-scale gene network regulation.

Mechanoreceptors Transduce Mechanical Forces into Biochemical Signaling in Endothelial Cells

Mechanoreceptors recognize blood flow patterns and transduce signals within

endothelial cells, which respond to unhealthy, disturbed flow by initiating plaque buildup in the vessel walls (known as atherosclerosis, a major component of cardiovascular disease). Several endothelial cell mechanoreceptors have been identified, including ion channels, cytoskeleton, tyrosine kinase receptors, caveolae, G proteins, and cell-matrix and cell-cell junction molecules such as integrins, platelet endothelial cell adhesion molecule- 1 (PECAM-1) and adherens junctions.[80,81] However, the mechanisms by which these mechanoreceptors recognize disturbed flow and transduce a signal that results in altered global gene expression in endothelial cells is largely unknown. Possible mechanisms involved in altered transcriptional activity include changes in transcription factor activity and epigenetic changes.

A subset of the mechanosensitive genes mentioned previously have been found to be vital for the endothelial cell's ability to sense mechanical stimuli. When their expression or normal activity is interrupted, cells lose phenotypic or gene expression changes associated with a specific mechanical stimulus, for example the transformation from a polygonal shape to align with the direction of flow under laminar shear stress conditions [82]. The intact mechanosensory complex at endothelial cell junctions consisting of PECAM-1, VECadherin, and VEGFR2, is crucial for the endothelial cell to be able to activate anti-atherosclerotic gene programs in response to laminar flow[81]. Several other important mechanotransduction pathways begin at the cell membrane, including integrins (FAK), cell membrane proteins [RTKs (PDGFRa[72], EGFR), GPCRs], ion channels (Ca^{2+}), and intercellular junctions, and travel biochemically through the cytosol or mechanically via the cytoskeleton to ultimately affect gene expression in the nucleus.[8,83]

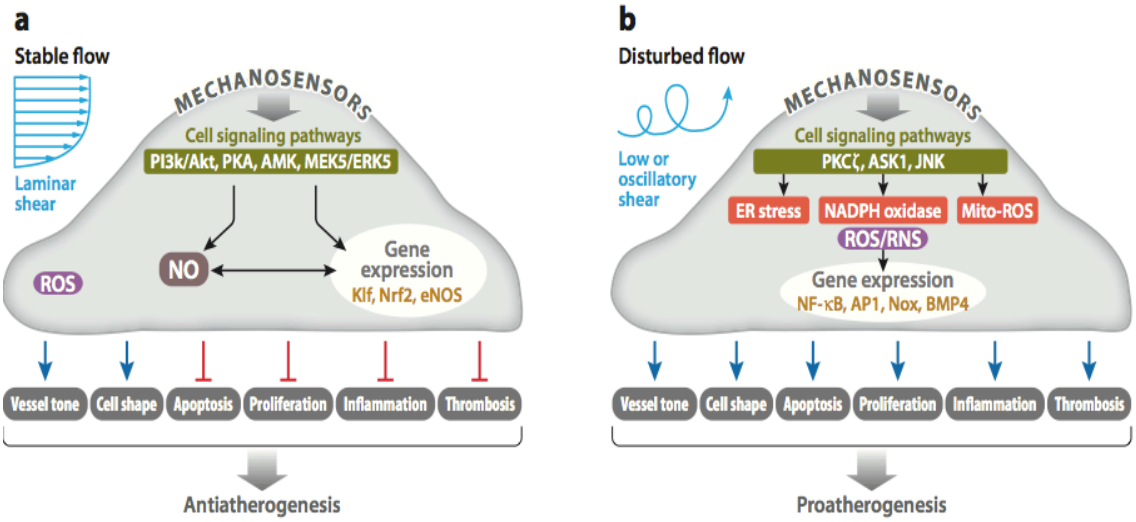

Figure 3.1: Mechanotransduction signaling pathways in endothelial cells in response to either (A) laminar or (B) oscillatory shear stress stimuli. Laminar shear stress stabilizes a healthy, anti-inflammatory state in endothelial cells that results in cytoskeletal remodeling and endothelial cell alignment in the direction of flow, as well as increased nitric oxide production and suppression of inflammatory cell adhesion molecules. Conversely, disturbed flow or oscillatory shear stress induces an inflammatory and thrombotic state characterized by high expression of cell adhesion molecules and production of inflammatory cytokines, high oxidative stress, lack of cell alignment with flow, and a leaky endothelial cell barrier that allows infiltration of smooth muscle cells and immunomodulatory cell types[84,85] .

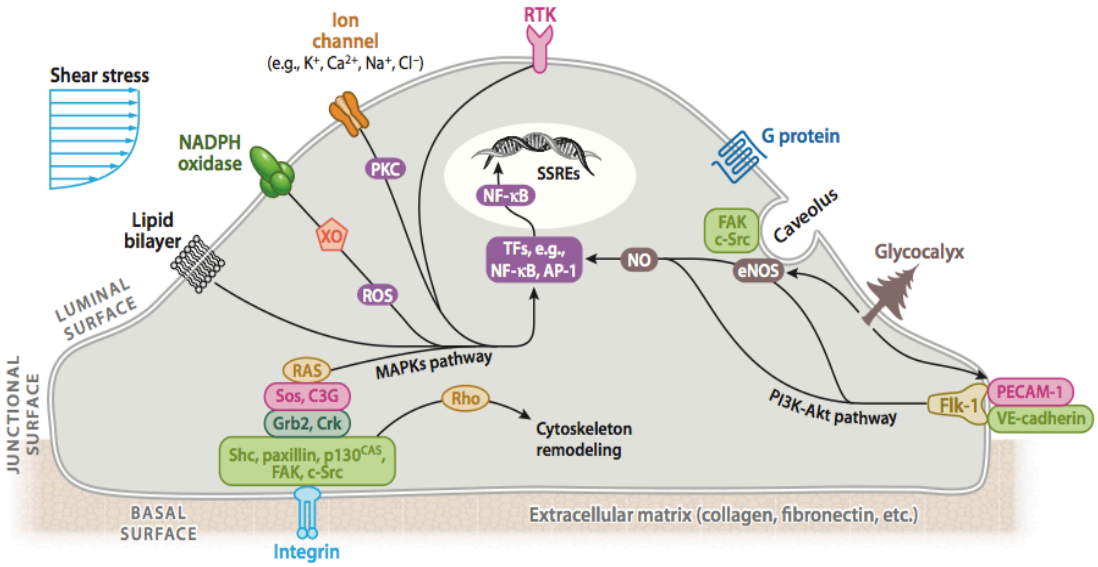

Figure 3.2: Mechanosensory pathways utilize surface mechanoreceptors to induced biochemical cell signaling events. Mechanoreceptors include ion channels (K+, Ca2+, Na+, Cl-), receptor tyrosine kinases, G-protein coupled receptors, etc., cell-

cell and cell-matrix adhesion complexes (PECAM1/VE-Cadherin/VEGFR2 complex, Focal Adhesion Kinases, etc.), the glycocalyx, and cytoskeletal elements that transduce signals and result in downstream signal amplification via master regulators such as kinase cascades and transcription factor networks. These signaling events alter the endothelial cell phenotype and behavior in response to extracellular biomechanical stimuli [7,84].

DNA Methyltransferases

DNA methyltransferases (DNMTs) catalyze the addition of the methyl group to cytosine. DNMT1 is thought to preferentially methylate hemimethylated DNA, meaning that the complementary strand of a CG dinucleotide often carries the same methylation markings. Although DNMT1 is classically referred to as a maintenance methylase, it also has *de novo* methylation capabilities.[86,87] Both DNMT1 overexpression and DNMT1 deficiency are embryonic lethal, and DNMT1 deletion causes genome-wide hypomethylation while DNMT1 overexpression causes genome-wide hypermethylation.[88-91] DNMT3a and DNMT3b are classically referred to as *de novo* methyltransferases that preferentially add methyl groups to fully unmethylated DNA. DNMT3a and DNMT3b establish global DNA methylation patterns during embryogenesis and gametogenesis.[92]

microRNAs

MicroRNAs (miRs) are potent regulators of gene expression that act post-transcriptionally to repress a gene by blocking mRNA translation or causing its degradation, and there are several miRs that are known to target DNMTs in cancer. Additionally, flow is known to regulate several miRs[93-101].

DNMT1 is verified as a direct target gene for miR-148a and miR-152, and the miR29 family.[102-104] The miR29 family is known to regulate the methylation status of

specific genes via regulation of DNMT1, DNMT3a, and DNMT3b, and it is known to be dysregulated in several cancers.[105,106] The transcription factor Myc, which is overexpressed in several cancers, suppresses mir29c.[107] Chen et al. showed that oxidized low-density lipoprotein upregulates mir29b expression, which downregulates DNMT3b and decreases MMP2/9 DNA methylation levels, leading to increased primary human aortic smooth muscle cell migration.[108] This was implicated as a novel mechanism for cardiovascular disease. Additional studies support the epigenetic regulation of MMP2 and MMP9 in carcinogenesis[109,110]. Viral infection induces miR29b, which decreases DNMT activity[111]. This very interestingly induces COX2 expression via demethylation of its promoter CRE, which also supports our interest in the mechanisms of DNMT-regulated global gene expression by promoter CRE methylation that is explored in Chapter 4.[111] Further, shear stress is known to upregulate COX2 expression via increased promoter CRE binding by AP1 and C/EBPβ in osteocytes[112]. Taken together, these findings suggest that the mir29 family contains potential DNMT1 regulators that may be useful in controlling downstream flow-controlled DNA methylation pathways in endothelial cells.

Methods

Techniques to Analyze Shear Stress Effects on Endothelial Cells

Partial Carotid Ligation in ApoE or C57Bl6 mice

8-week-old C57BL/6 or ApoE$^{-/-}$ mice (Jackson Laboratories) were used for all animal studies according to the approved Institutional Animal Care and Use Committee protocol by Emory University. Mice were partially ligated under isofluorane anesthesia and the resultant disturbed flow conditions in the LCA were determined by ultrasound

measurements as described previously [113]. Briefly, 3 out of 4 caudal branches of the LCA (left external carotid, internal carotid, and occipital artery) were ligated with 6-0 silk suture, while the superior thyroid artery was left intact (Figure 3.3). Mice were sacrificed by CO_2 inhalation and were subsequently perfused with saline containing heparin for 5 minutes Total carotid intimal RNA or genomic DNA was isolated by flushing the RCA and LCA with Qiazol or Buffer AL, respectively, by our method that we have demonstrated to be endothelial-enriched without any significant contamination of smooth muscle cells and leukocytes [17,101,113].

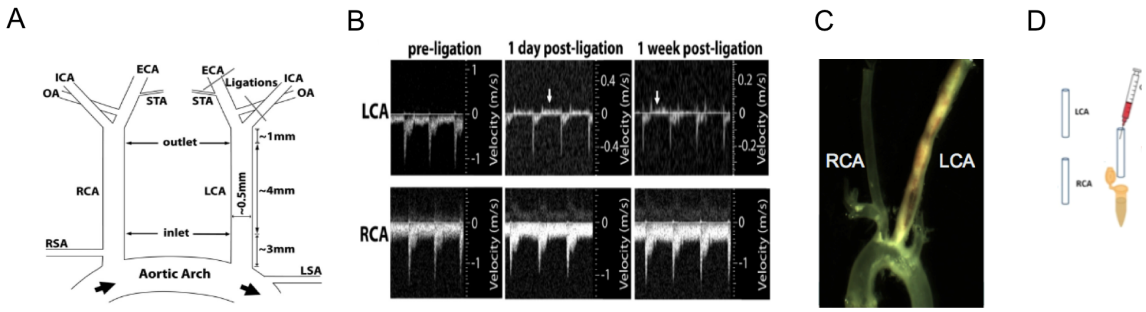

Figure 3.3: A scheme of the partial carotid ligation mouse surgery model. A) Location of sutures at the external carotid, internal carotid, and occipital arteries for partial ligation. B) Low and reversing flow in the LCA one day and one week post-ligation by ultrasound. C) Plaque accumulation in the LCA 4 weeks post-ligation on a high fat diet. D) Carotid flushing for intimal RNA or gDNA[114].

In vitro systems: cell culture and shear stress systems

Human Umbilical Vein Endothelial Cells (HUVEC, Lonza cc-2519) were maintained in M199 (Fisher MT10060CV) base culture medium containing 20% Fetal Bovine Serum (SH30071), 10% penicillin/streptomycin/fungizone (Gibco 15240-062), 10% glutaMax (Mediatech, 25-005-cl), 10% endothelial cell growth serum, and 0.4% heparin (McKesson Medical 404867). In vitro shear stress was applied to passage 6 HUVECs in 10cm culture plates for 24 hours using a cone and plate viscometer that exerts 15 dynes/cm^2 of unidirectional flow (laminar shear stress, or LS conditions) and ±

5 dynes/cm^2 of bidirectional flow (oscillatory shear stress, or OS) (Figure 3.4). The cell culture plates were secured in place at the bottom by a vacuum pump and the incubator was maintained at 5% CO_2 and 37°C. Total RNA or genomic DNA was collected by scraping cells in Qiazol (Qiagen) or Buffer AL (Qiagen DNeasy Blood & Tissue Kit), respectively.

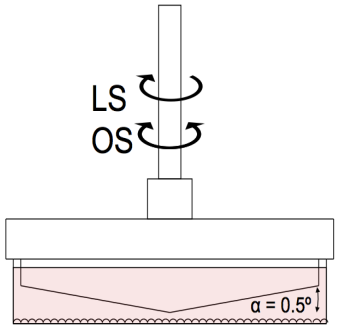

Figure 3.4: *In vitro* Cone-Plate Shear System (10 (LS) or ±5 (OS) dynes/ cm^2 exerted on EC monolayer)

RNA Extraction from Cultured Endothelial cells or Mouse Carotid Artery for Gene Expression Analysis

Microarray

Using the mouse partial carotid ligation model and the Illumina Bead Chip DNA microarray containing 45,281 gene probes, our lab previously identified ~600 "mechanosensitive" genes whose expression changes in ECs exposed to disturbed flow in the left carotid artery (LCA) as compared to unidirectional flow in the right carotid artery (RCA) for 12 and 48 hours (C57Bl6 mice; n=3 for each timepoint, each n contains 3 pooled carotid samples).[17] We have additional subsequent array data using the Affymetrix Mouse HT-MG-430 array platform for 12, 24, 48 hours and 2 weeks post-ligation (C57Bl6 mice; n=5 for each timepoint, each n is one individual carotid sample).

qPCR

Total carotid intimal RNA isolated by flushing the RCA and LCA with 150 ul Qiazol was purified by the Qiagen miREasy Kit and reverse-transcribed into cDNA using SuperScript III and random primers (Invitrogen). Total RNA was collected from HUVEC cultures in 700 ul of Qiazol and purified by the same method as above. QPCR for specific genes was performed using Brilliant II SYBR Green qPCR Master Mix (Stratagene) with custom designed primers (Table 3.1) on the ABI StepOne Plus Real-Time PCR System. Results were normalized to the 18S housekeeping gene and the fold change between siRNA-treated and negative control samples were determined using the $\Delta\Delta C_t$ method [115].

Table 3.1: Primers used for qPCR or bisulfite sequencing (BS-Seq).

	Forward	Reverse
dnmt1 (mouse)	AAGGGGGCCCTGACCGCTTC	CCGAAATGCCTGGGCTGCCG
DNMT1 (human)	TGCCAGCTGAGCGTGGTGGT	GCATGCGGGCAGCCACCAAT
dnmt3a (mouse)	GAGGGAACTGAGACCCCAC	CTGGAAGGTGAGTCTTGGCA
dnmt3b (mouse)	CGCACAACCAATGACTCTGCTG	GGTGACTTCAGAAGCCATCCGT
HoxA5 (mouse)	CGCAAGCTGCACATTAGTCACG	GAGAGGCAAAGGGCATGAGCTA
HOXA5 (human)	GCGCAAGCTGCACATAAG	CGGTTGAAGTGGAACTCCTT
Klf3 (mouse)	CCTCTCATGGTTTCCTTGTCGG	CCTCTGTGGTTCAATTCCAGGC
KLF3 (human)	CTCATGGTCTCCTTATCGGAGG	TGTCCTCTGTGGTTCGATCCCA
HoxA5 BS-Seq (mouse)	GAATTGAGGTTATAGTTTATTATGGTAAAA	AATTATTATAAATAATTCTAAATCACCACC

Immunohistochemistry and Oil-Red-O Staining on Mouse Carotid Arteries and Aortic Arch

Frozen blocks containing the heart, aortic arch, and carotid arteries were prepared in TissueTek and stored at -80°C. Immunohistochemistry was performed on selected sections from specific intervals of the frozen blocks using the following antibodies: 5-methylcytidine (Eurogentec, BY-MECY), DNMT1 (Santa Cruz sc-20701), DNMT3b

(Abcam ab2851), DNMT3a (Abcam ab23565), and CD45 (eBioscience 13-0454). Selected sections from specific intervals from the blocks were stained with Oil-Red-O by fixing the frozen tissues with 10% formalin for two minutes, rinsing twice with distilled water for five minutes, orbital shaking in 100% propanediol for ten minutes and incubation in 0.2% Oil Red-O solution for five minutes at 85°C. For hematoxylin staining, the previous method was followed by two rinses with distilled water, a hematoxylin dip for 30 seconds, two rinses with distilled water, one rinse with Scott's water, two rinses with distilled water, and then mounting. Plaque size was quantified using ImageJ software.

5-Aza-2-Deoxycytidine and siRNA treatment of HUVECs *in vitro*

Optimal 5-Aza-2'-deoxycytidine (5Aza; Sigma A3656) treatment conditions were determined by a dose-curve using 0, 0.5, 1, 5, and 20 μM 5Aza for 5 days, and by duration curve of 5uM 5Aza for 0, 0.5, 1, 2, 3, 5, and 7 days. DNMT enzymatic activity and DNMT1 protein expression assays indicated the optimal dose of 5 μM. For shear studies, 5 μM 5Aza was treated for 5 days prior to in vitro shear, and the LS or OS conditions were applied for 24 additional hours.

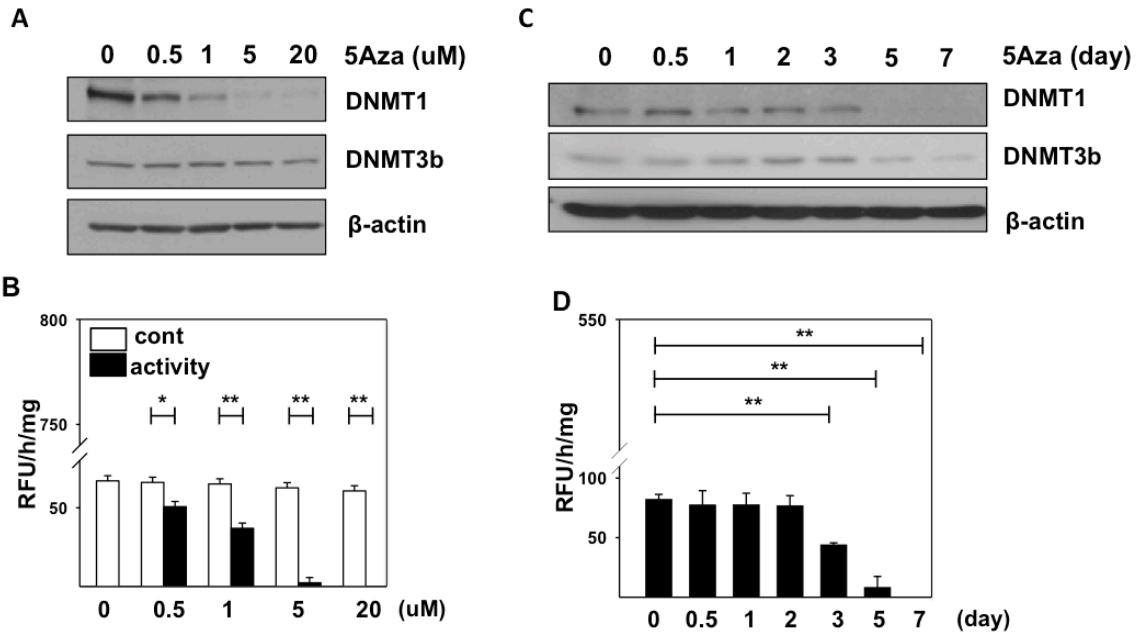

Figure 3.5: 5-Aza-2'-deoxycytidine decreased DNMT1 protein expression, activity, and global DNA methylation in HUVECs a dose- and time-dependent manner. (A) Western blot of DNMT1 protein expression in static HUVEC cells treated with 0, 0.5, 1, 5, and 20 µM 5Aza for 5 days (right) or with 5 µM 5Aza for a duration of 0, 0.5, 1, 2, 3, 5, or 7 days (left). (B) DNMT enzymatic activity in HUVEC cells treated with 0, 0.5, 1, 5, and 20 µM 5Aza for 5 days (right) or with 5 µM 5Aza for a duration of 0, 0.5, 1, 2, 3, 5, or 7 days (left). (C and D) DNMT enzymatic activity increases in HUVECs in OS conditions. This increase is blunted in a dose- and time-dependent manner by treatment with 5Aza.

SiRNA was transfected using oligofectamine (Invitrogen 12252-011) with 100nM final concentration of siDNMT1 (Dharmacon RNAi ON-TARGET plus SMART pool) or 100nM stealth RNAi negative control (medium GC content, Invitrogen 12935-112) in OptiMEM (Invitrogen 31985-088) for 6 hours followed by normal HUVEC media replacement. After 48 hours, shear stress (either LS or OS) was applied for an additional 24 hours. SiRNA dose optimization was done in static HUVECs in doses of 25, 50, 75, 100, 400nM of siRNA in a total volume of 0.5ml. After 6 hours of incubation with siRNA, media was replaced with standard HUVEC media, and RNA and protein were collected after 48 hours.

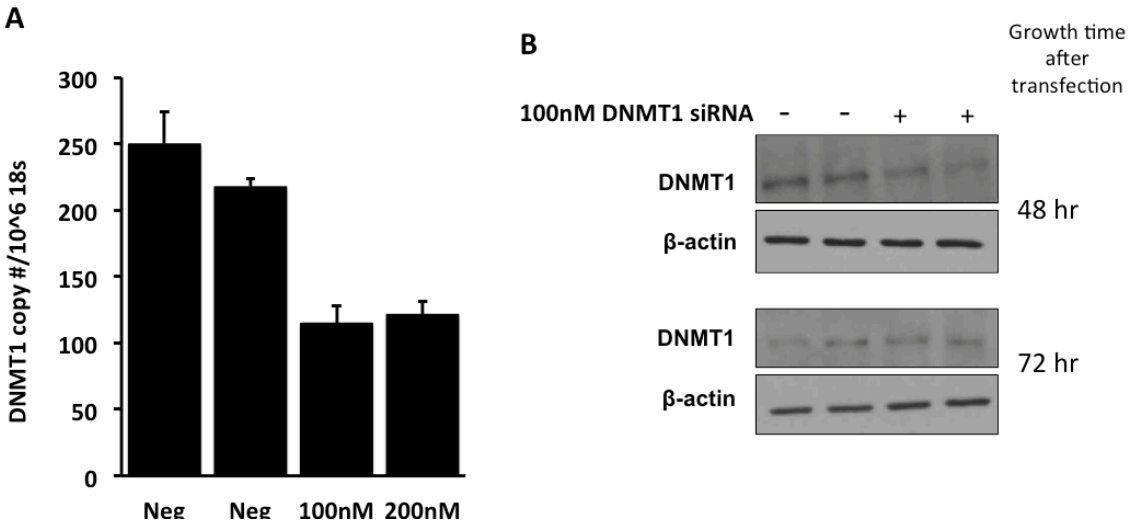

Figure 3.6: Dose (mRNA level) and time (protein level) curve optimization of DNMT1 siRNA. (A) DNMT1 mRNA expression was measured by qPCR in static HUVEC cells treated with either 100nM or 200nM of either negative control siRNA or siRNA targeting DNMT1 for 48 hours. (B) Western blot of DNMT1 protein expression in static HUVEC cells treated with 100nM of either negative control siRNA or siRNA targeting DNMT1 for either 48 or 72 hours.

Western Blot on Protein Extracts from HUVECs

Western Blotting was performed by the standard method using antibodies for the following: DNMT1 (Santa Cruz sc-20701), DNMT3a (Abcam ab23565), DNMT3b (Abcam ab2851), and β-actin (Sigma A5316), and HoxA5 (Abcam ab82645).

MspI/HpaII Restriction Enzyme Assay to Determine Global DNA Methylation Status *In Vitro*

Genomic DNA was collected and purified by the DNeasy Blood and Tissue kit (Qiagen) from HUVECs treated with either 5μM 5Aza or vehicle control for 5 days. Either MspI or HpaII (ThermoSci ER0541) were reacted with the genomic DNA according to the recommended protocol for the restriction enzymes. The reaction

products were run on a 2.5% agarose gel stained with ethidium bromide alongside a 100 bp ladder (NEB N3231L) and imaged under UV light. MspI and HpaII cut at the C/CGG recognition site. MspI cleaves regardless of the internal cytosine methylation status, while HpaII is blocked from cleavage by internal cytosine methylation.

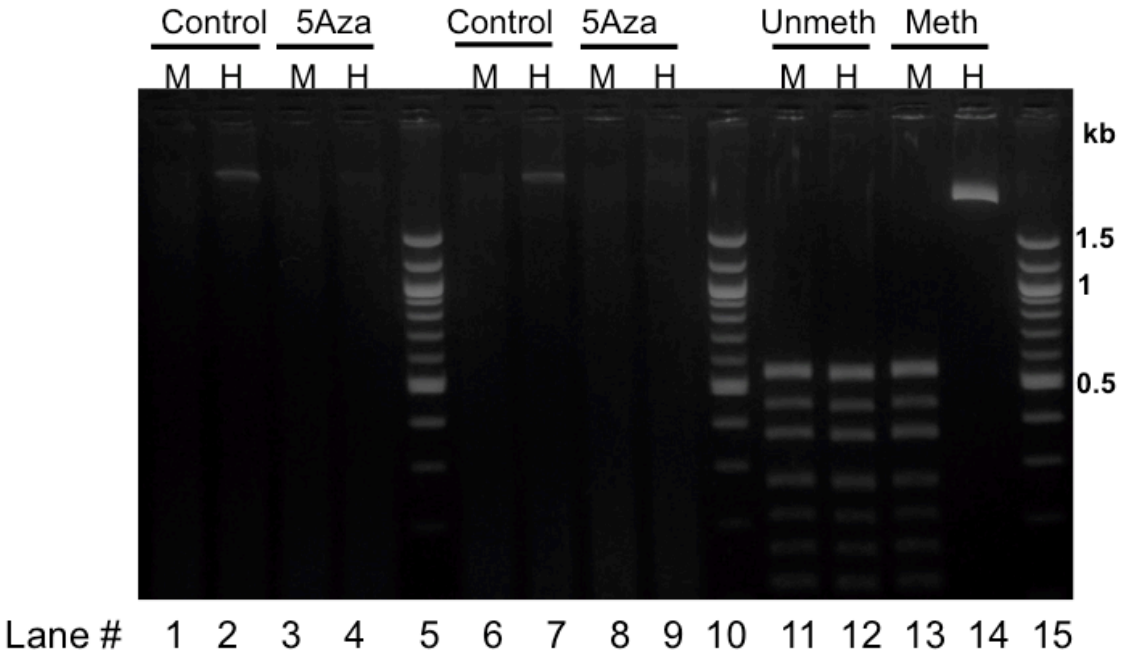

Figure 3.7: Results of the MspI/HpaII methylation restriction enzyme assay show that global methylation decreases in static HUVECs treated with 5uM 5Aza for 5 days. Lanes 5, 10, and 15 contain the molecular weight ladder (marked on the right of the figure). Lanes 1-4 and 6-9 are duplicates and lanes 11-14 are using either fully unmethylated or fully methylated DNA to show the effect of methylation on the restriction digest for the two enzymes. Lanes 2 and 6 contain genomic DNA from untreated HUVECs, and HpaII cleavage was blocked due to methylated cytosine. The band disappears in lane 4 and 9, when HpaII can cut the hypomethylated DNA from 5Aza-treated HUVECs.

DNMT Activity Assay

The DNMT enzymatic activity assay was performed according to the manufacturer's protocol (Epigentek, P-3010). Briefly, nuclear extracts from HUVEC that underwent either LS or OS for 24 hours, with or without 5Aza pre-treatment (5uM for 5

days before shear), were incubated with the DNMT substrate (unmethylated cytosine) and an antibody binding and fluorometric assay was used to measure the ratio of methylated to unmethylated cytosine to determine overall DNMT enzymatic activity.

Monocyte adhesion assay

HUVECs were pre-treated with either 5Aza or siRNA and were subjected to either LS or OS for 24 hours. Separately, human peripheral blood mononuclear leukocytes (THP-1 cells) were cultured in serum-containing RPMI medium (Fisher MT10040CM) and were labeled in serum-free RPMI with 5µl/ml 2'7'-bis-(2-carboxyethyl)-5-(and-6)-carboxyfluorescein (BCECF-AM; Molecular Probes B-1170) at 37°C for 30 minutes. As a positive control, HUVECs were activated by 1 ng/ml TNFα in serum-free RPMI for 3 hours to induce monocyte adhesion. After shear, each 10cm plate of HUVECs was exposed to the labeled THP-1 cells at a concentration of 5 x 10^5 THP-1 cells/ml (in a total of 6ml) for 30 minutes at 37°C. Non-adherent monocytes were washed away with HBSS (Fisher MT21023CV) and the bound monocytes were fixed with 4% paraformaldehyde for 5 minutes. Bound monocytes were imaged in 8 fields/plate via fluorescent and bright field microscopy and quantification was done using ImageJ.

In vivo 5Aza Treatment Scheme

Mice were treated by intraperitoneal injection at doses of 0.1, 0.2, or 0.4 mg/kg/day of 5-Aza-2'-Deoxycytidine (5Aza; Sigma) daily for four weeks (the acute d-flow-induced atherosclerosis model), or at 0.2 mg/kg/day for three months (the chronic diet-induced atherosclerosis model). Mouse weight was monitored weekly, and food and water intake and feces were monitored daily.

High Resolution Melting Curve Analysis to Quantify Global DNA Methylation *In Vivo*

Global genomic DNA methylation as represented by genomic repeat element methylation was quantified by LINE1 and B1 high resolution melting curve assays (HRM) for each mouse in the RRBS and array studies to determine the effect of 5Aza treatment. HRM was done according to the protocol set by Newman et al. [116]. Whole blood was collected by the submandibular technique one week after the start of 5Aza treatment. Genomic DNA was extracted from blood using the DNeasy Blood and Tissue kit (Qiagen) and genomic DNA was bisulfite converted using the Epitect Bisulfite Conversion kit (Qiagen). Bisulfite-converted genomic DNA was subjected to HRM using the F_unmeth_mLINE1 and R_unmeth_mLINE1, and the F_mod_unbiased_B1_Mm and R_mod_unbiased_B1_Mm primers from Newman et al. and normal qPCR methods as described above[116].

Statistical Analyses

Statistical analyses were performed using Graph-Pad Prism 5 (GraphPad Software). Error bars are reported as the standard error of the mean. Pairwise comparisons were done using two-tailed Student's t-tests. Multiple comparisons of means were performed using one-way analysis of variance followed by Tukey's multiple comparison tests. Differences between groups were considered significant at P-values below 0.05 (*) and the P-values are denoted separately for values below 0.01 (**).

Results

To identify flow-sensitive genes in arterial endothelium in vivo, endothelial-enriched RNA was obtained directly from mouse carotid arteries at various timepoints

post-partial carotid ligation surgery in C57BL/6 mice (Figure 3.3A) and applied to a microarray. Using this method, our lab previously identified ~600 "mechanosensitive" genes whose expression changes in ECs exposed to disturbed flow in the left carotid artery (LCA) as compared to unidirectional flow in the right carotid artery (RCA) for 12 and 48 hours.

Discovery of D-flow-induced DNMT1 Overexpression Using Microarray

DNMT1 was initially identified as a potential mechanosensitive gene in endothelial cells from these previous in vivo mRNA array studies described in detail in the methods section[17]. The mRNA array showed that *DNMT1* expression was ~2.4-fold higher in the left carotid artery (LCA, which was partially ligated and exposed to d-flow for 48h) than in the contralateral right carotid artery (RCA, exposed to s-flow)[17].

DNMT1 is Upregulated at the mRNA and Protein Level by D-flow Exposure to the Mouse Endothelium In Vivo

We validated this endothelial microarray data by qPCR, immunostaining, and western blot both in vivo and in vitro. *DNMT1* mRNA expression showed a significant increase by more than 2-fold in the LCA endothelium as compared to that of the RCA at 48 hours post-partial carotid ligation (Figure 3.8B). Similarly, robust DNMT1 protein expression was observed in the flow-disturbed LCA (48 hours post-ligation) compared to the contralateral RCA and sham-controlled LCA and RCA (Figure 3.8C). Importantly, a robust DNMT1 protein expression was also observed in endothelial cells in the lesser curvature (LC) of the aortic arch, which is naturally and chronically exposed to d-flow without the ligation surgery, but not in the greater curvature (GC, an atherosclerosis-resistant region, which is naturally exposed to s-flow) (Figure 3.8D and E). Interestingly,

DNMT1 expression was increased in the intimal and medial layers of the LCA (Figure 3.8C), suggesting that d-flow affected the protein expression in both endothelial and smooth muscle cells. Of the catalytically actives, DNA methyltransferase DNMT1 is the only one with increased expression by D-flow in vivo (Figure 3.9).

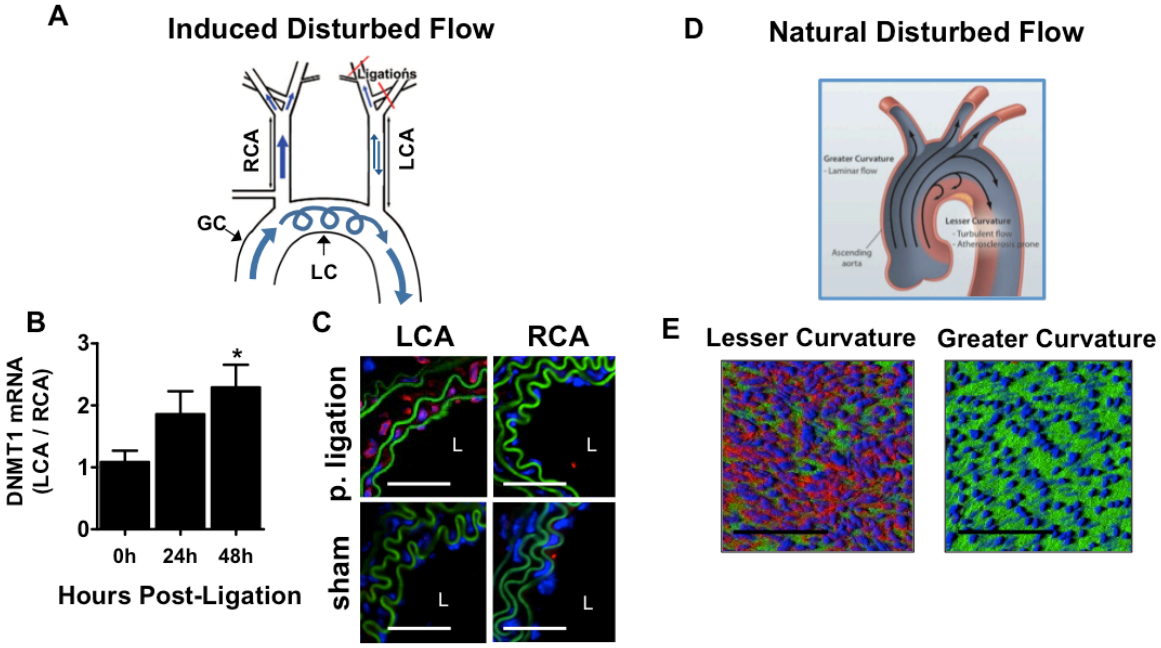

Figure 3.8: DNMT1 expression is induced by d-flow in endothelial cells in vivo and in vitro. Schematic diagram of the partial carotid ligation model, in which 3 of the 4 caudal branches of the left common carotid artery (LCA) are ligated, while the contralateral right common carotid artery (RCA) remains untouched as an internal control. Also depicted are the naturally, chronically flow-disturbed lesser curvature (LC) and the unidirectional- flow greater curvature (GC). (B) Validation of microarray results by qPCR was performed with endothelial-enriched total RNA obtained from the LCA and RCA at 0, 24, and 48 hours after ligation in C57BL/6 mice. *DNMT1* mRNA levels were normalized to 18S. Data are shown as the mean ± SEM. *$P < 0.05$, $n = 8$ (0 hours), $n = 9$ (24 hours), $n = 12$ (48 hours)[16]. (C) LCA and RCA frozen sections 48 hours after ligation (scale bars: 50 µm) and (E) the LC and GC (en face preparation; scale bars: 100 µm) from C57BL/6 mice without ligation surgery were stained with DNMT1 antibody (red)[16]. Nuclei are stained with DAPI (blue), and elastic laminae autofluoresce green. The lumen (L) is indicated. (D) Diagram of the endogenously s-flow (greater curvature) and d-flow(lesser curvature) regions of the aortic arch. Figure of arch adapted from http://ars.els-cdn.com/content/image/1-s2.0-S0270929512000447-gr1.jpg.

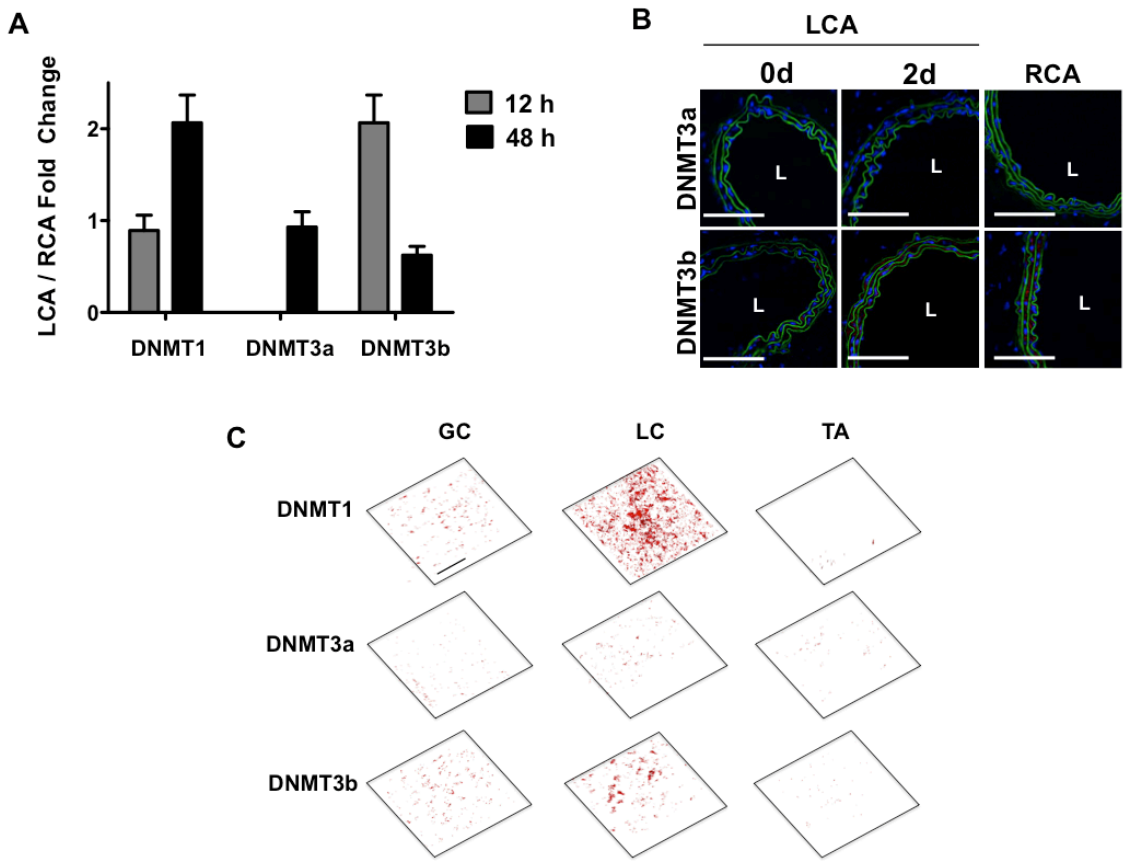

Figure 3.9: (A) q-PCR validation of microarray results demonstrating a time-course study of the fold-change in DNMT1, DNMT3a, and DNMT3b expression at 12 and 48 hours post-ligation in C57/BL6 mice. DNMT3a levels were undetectable by qPCR at 12 hours post-ligation. (B) Representative immunohistochemical staining of DNMT3a and DNMT3b protein (red) in carotid artery sections at 48 hours post-ligation in C57/BL6 mice. Nuclei are stained with DAPI in blue and the elastin laminae autofluoresce green. L indicates the lumen of the blood vessel. (C) Representative immunohistochemical staining of DNMT1, DNMT3a, and DNMT3b protein (red) in the naturally flow-disturbed lesser curvature (LC) and unidirectional flow greater curvature (GC) and thoracic aorta (TA) in C57/BL6 mice. Nuclei are stained with DAPI in blue and the elastin laminae autofluoresce green. [16]

DNMT1 is Overexpressed at mRNA and Protein Level in Cultured Endothelial Cells Exposed to D-Flow Using the Cone and Plate Viscometer

These in vivo data were further confirmed in cultured human endothelial cells (HUVECs) exposed to oscillatory shear stress (OS, mimicking d-flow in vitro) compared to unidirectional laminar shear stress (LS, mimicking s-flow in vitro) for 24 hours.

DNMT1 mRNA and protein expression were significantly higher in HUVECs exposed to OS as compared with LS (Figure 3.10A and B), which directly demonstrates that DNMT1 expression is regulated by OS in endothelial cells. DNMT3b was also upregulated at the mRNA and protein levels by d-flow, but to a much lesser extent. In contrast, expression of DNMT3a was barely detectable and did not show significant changes in protein level (Figure 3.10). These results indicate that the expression of DNMT1 is strongly regulated in a flow-dependent manner in endothelial cells in vivo and in vitro, and that the other catalytically active DNMTs (DNMT3a or DNMT3b) do not have a dramatic effect. Therefore, subsequent studies focused on the role of DNMT1.

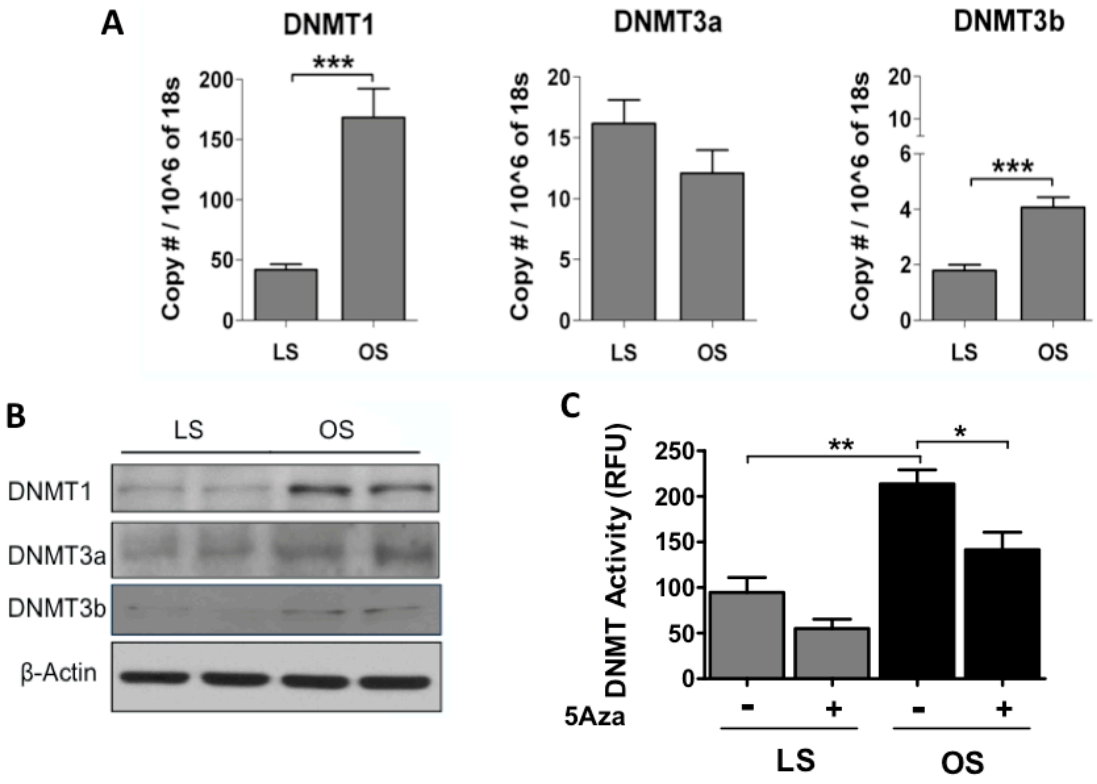

Figure 3.10: DNMT1, DNMT3a, and DNMT3b mRNA expression in HUVECs exposed to either LS or OS for 24h measured by qPCR (A) and protein expression measured by Western Blot (B). ***p<0.001. HUVECs exposed to LS (15 dyn/cm^2) or OS (±5 dyn/cm^2, at 1 Hz) for 24 hours were used for qPCR and Western blot

analyses for DNMT1 using 18S and β-actin as respective internal controls. (C) DNMT enzymatic activity increases in HUVECs in OS conditions. This increase is blunted by a 5-day 5μM treatment of 5Aza. [16]

DNMT1 Inhibition in Endothelial Cells by 5-Aza-2'deoxycytidine (5Aza) or siRNA Inhibits D-flow-induced Inflammation *In Vitro*

To determine the functional importance of DNMT1 in endothelial cells, human umbilical vein endothelial cells (HUVECs) were treated with either the DNMT inhibitor 5Aza or DNMT1 siRNA (siDNMT1). Optimization studies showed that 5Aza treatment in HUVECs decreased DNMT1 in a dose and time dependent manner (Figure 3.5). It was determined that a five day treatment of 5uM resulted in significant DNMT1 knockdown and a concomitant decreased DNMT activity with minimal cell death (Figure 3.5, Figure 3.10C, and Figure 3.11).[117] 5Aza has preferential targeting of DNMT1 in ECs as is reported in other cell types, and it was found that 5Aza could prevent OS-induced DNMT1 overexpression and hyperactivity (Figure 3.10C), and decrease global methylation (Figure 3.7). Dose and time optimization studies for DNMT1 siRNA determined that a 48h treatment with 100nM siRNA led to sufficient knockdown of DNMT1 protein expression under both laminar and oscillatory shear conditions (Figure 3.6 and Figure 3.12).

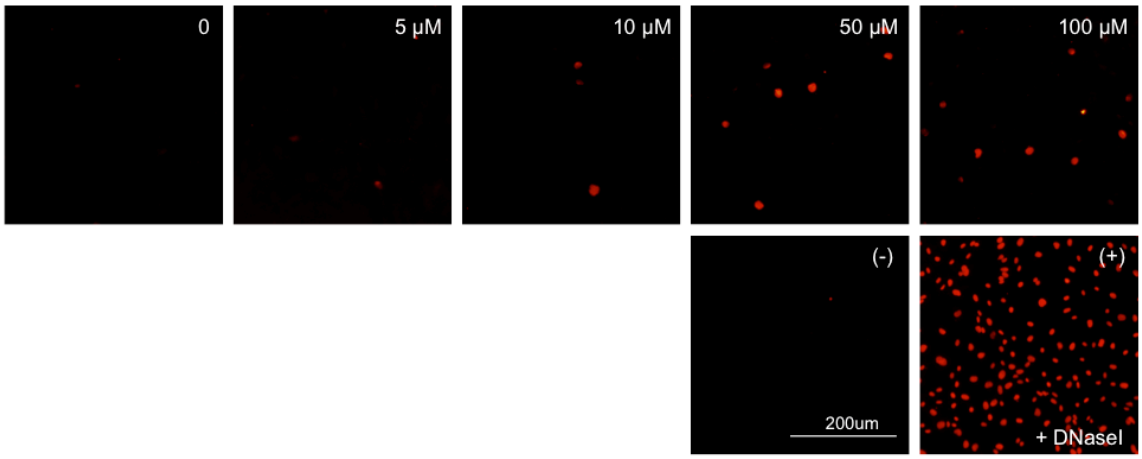

Figure 3.11: HUVEC TUNEL staining on a dose-curve treatment for 5 days of 5Aza showing endothelial apoptosis (red), using DNaseI treatment as a positive control for cell death.

Exposure to OS increased DNMT1 expression and DNMT activity compared to LS and 5Aza inhibited this increase (Figure 3.12A). Treatment with 5Aza significantly prevented OS-induced monocyte adhesion to HUVECs (Figure 3.12C). Moreover, siDNMT1 also decreased OS-induced DNMT1 expression as well as monocyte adhesion to HUVECs (Figure 3.12B and D). Together, these results suggest that DNMT1 plays a major role in OS-induced endothelial inflammation.

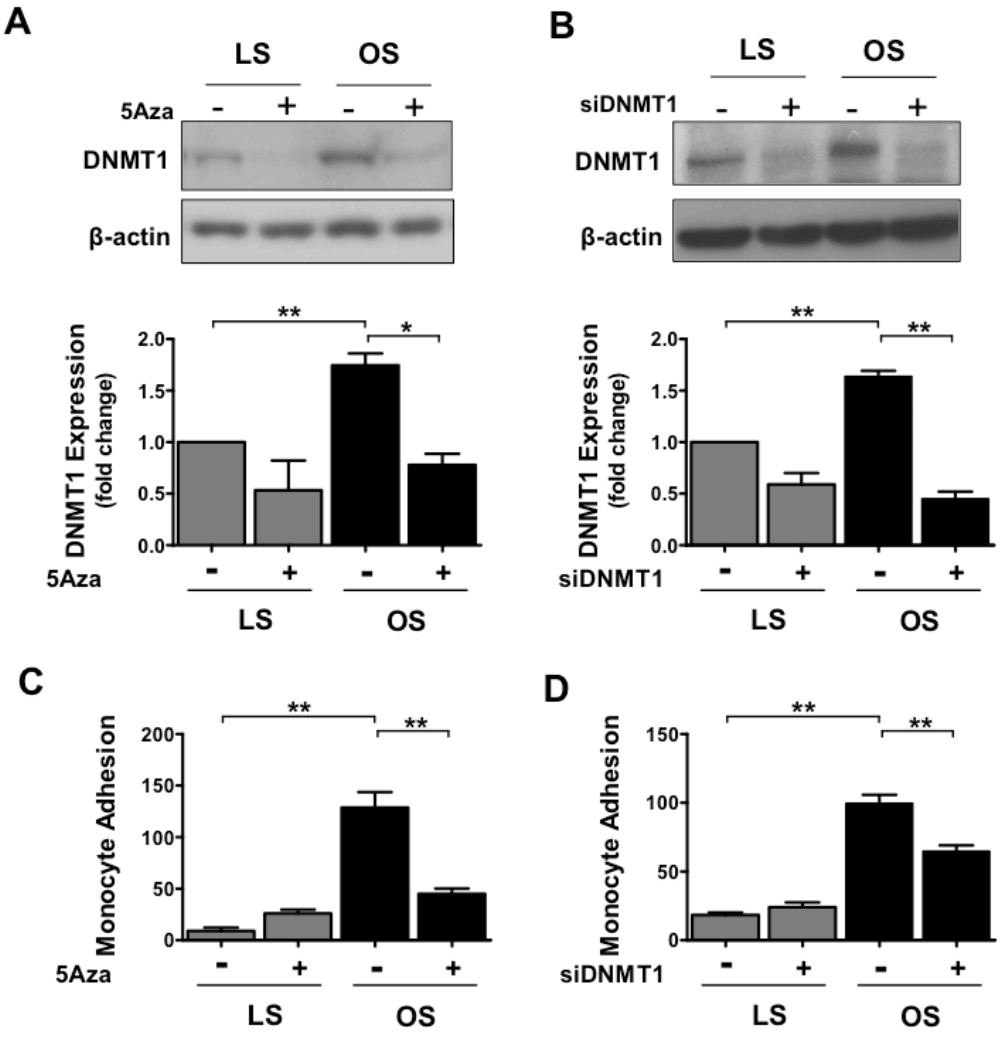

Figure 3.12: DNMT inhibition blocks OS-induced endothelial inflammation. HUVECs were pre- treated with either 5-aza-2′-deoxycytidine (5Aza) at 5 μM for 5 days or DNMT1 siRNA (siDNMT1) at 100 nM for 48 hours, and subsequently exposed to OS or LS for an additional 24 hours. (A and B) Cell lysates were then analyzed by Western blotting with the DNMT1 antibody and quantified by ImageJ analysis using β-actin as an internal control (n = 4 each, data are shown as the mean ± SEM. *$P < 0.05$; **$P < 0.01$). (C and D) Under the same conditions and following shear, endothelial inflammation was determined by quantification of the number of THP-1 monocytes adhered to sheared endothelial cells (n = 4 each, data are shown as the mean SEM. **$P < 0.01$). [16]

DNMT Inhibition by 5-Aza-2'deoxycytidine Blocks Atherosclerosis Development in Chronic and Acute Models of Atherosclerosis in Mice

We used two different ApoE$^{-/-}$ mouse models to study the role of DNMT in atherosclerosis: the acute partial carotid ligation model with western diet which rapidly develops atherosclerosis within 3 weeks [113], and the conventional western diet-fed model that chronically develops atherosclerosis in 3 months [101,118]. In the carotid ligation model, the LCA rapidly developed atherosclerosis within 3 weeks (Figure 3.13A), and this was inhibited by 5Aza treatment in a dose-dependent manner with 0.2 mg/kg/day being the lowest effective dose (Figure 3.13A and B). Immunostaining for the leukocyte marker CD45 showed a remarkable inhibitory effect of 5Aza on inflammatory cell infiltration at the 0.2 mg/kg/day dose (Figure 3.15A), which was consistent with the atherosclerosis data. In the conventional western diet model, 5Aza treatment (0.2 mg/kg/day) also significantly inhibited atherosclerosis development in the aortic arch and brachiocephalic arterial branch (Figure 3.13C and D). In both models, 5Aza treatment did not show a significant effect on the serum lipid profile (Figure 3.16A and C) and apparent health, but induced a smaller body weight gain than the control groups (acute study: 25 grams in control vs. 23 grams in 5Aza mice at 3 weeks; Chronic study: 34 grams in control vs. 31 grams in 5Aza group at 3 month) (Figure 3.16B and D). As an additional control, we examined the effect of d-flow, atherosclerosis, and 5Aza treatment on 5-methylcytosine (5mC) content by immunostaining. The dramatically induced 5mC level in the partially ligated LCA at the 3-week time-point was significantly reduced by 5Aza treatment in a dose-dependent manner (Figure 3.15B). Taken together, these results provide strong

support that 5Aza treatment prevented atherosclerosis by reducing DNMT expression and activity in the arterial wall.

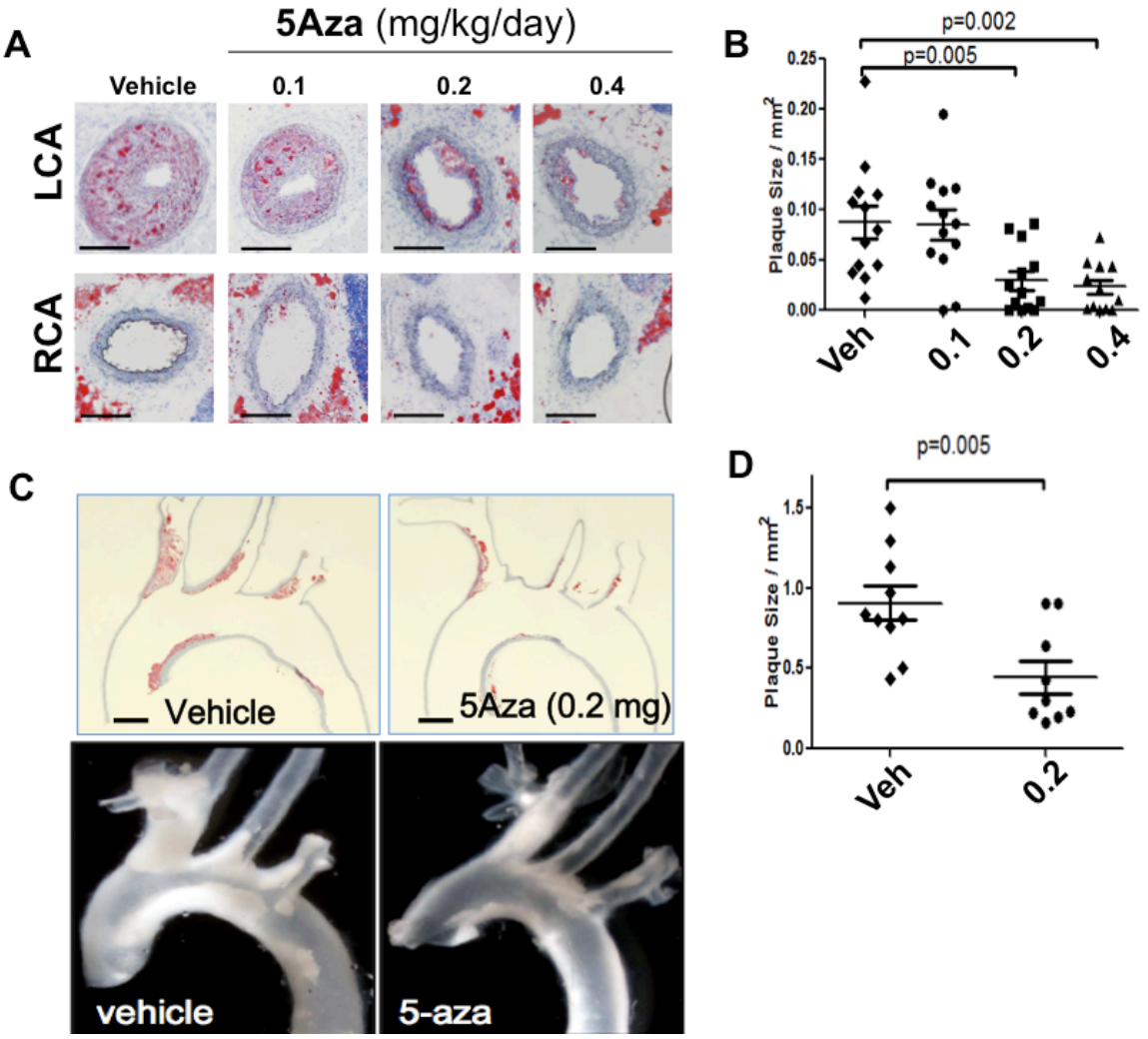

Figure 3.13: Treatment with the DNMT inhibitor 5Aza inhibits atherosclerosis. (A and B) Acute, partial carotid ligation model of atherosclerosis: *ApoE*$^{-/-}$ mice were given daily i.p. injections of 5Aza for 1 week at 0.1, 0.2, or 0.4 mg/kg/d, or saline as a vehicle control. Then, partial carotid ligation was done, and mice were fed a Western diet while continuing the same 5Aza treatment for 3 more weeks. Frozen sections of the carotid arteries were examined by oil red O staining (scale bars: 200 μm) (A), and plaque area quantification (mm^2) was done using ImageJ (B) (*n* = 13 each, data are shown as the mean ± SEM. ***P* < 0.005). (C and D) Chronic, diet-induced atherosclerosis model: *ApoE*$^{-/-}$ mice were fed a Western diet (without partial ligation surgery) and treated with 5Aza (vehicle or 0.2 mg/kg/d, daily i.p.

injections) for 3 months. Aortic arches were longitudinally sectioned and stained with oil red O (scale bars: 1 mm) (C), and plaque area (mm^2) was quantified (D) (*n* = 10 for vehicle, *n* = 9 for 5Aza, mean ± SEM. ***P* < 0.005). [16]

Global methylation is reduced by 5Aza treatment in the acute D-flow and chronic diet-induced models of atherosclerosis. The decreased melting temperature of bisulfite-converted repetitive DNA elements indicates a decrease in global DNA methylation, demonstrating the efficacy of 5Aza treatment (Figure 3.14).

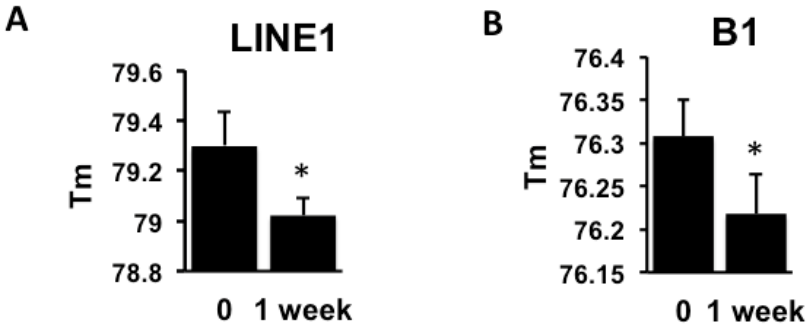

Figure 3.14: 5Aza treatment reduces global methylation in mouse blood cells. (A,B) High resolution melting curve analysis shows decreased methylation in the normally highly methylated LINE1 long interspersed (A) and B1 short interspersed (B) repeat elements of the genome. The analysis was done on blood genomic DNA collected by submandibular bleed just before beginning the 5Aza treatment and one week after the start of the daily 0.2 mg/kg/day 5Aza injections. (n=20; mean ± s.e.m; * p<0.05)[16]

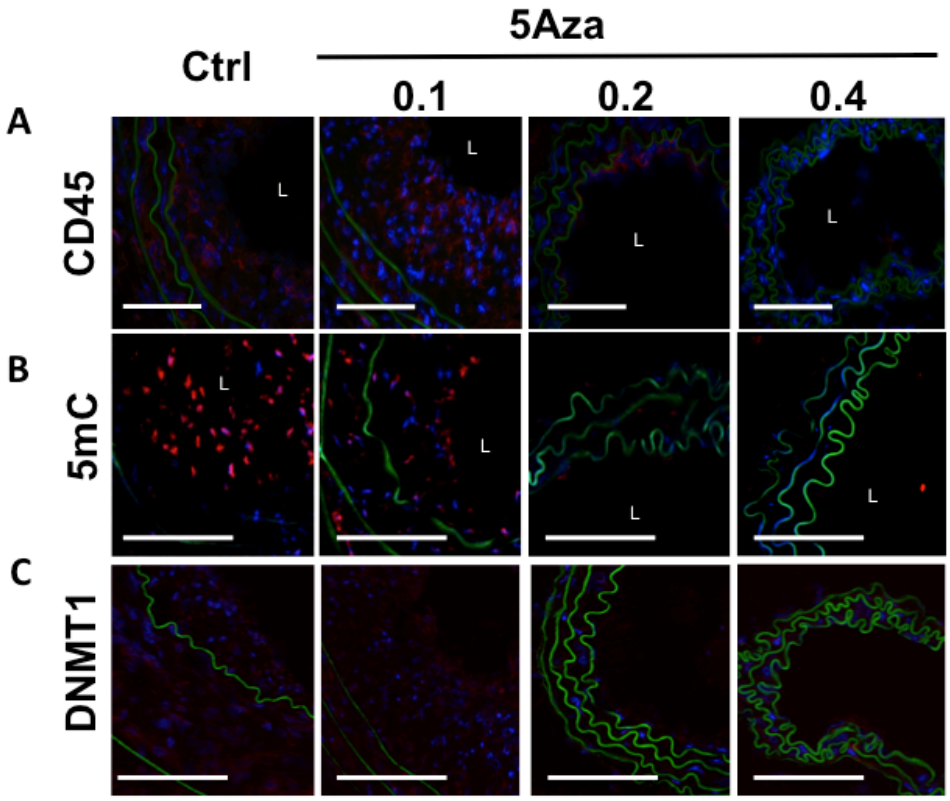

Figure 3.15: 5Aza treatment inhibits immune cell infiltration and DNA methylation in mice. (A) Representative immunohistochemical staining of CD45 (red) in the LCA of the acute, d-flow induced atherosclerosis model, demonstrating a dose-dependent decrease in immune cell infiltration after 4 weeks of 5Aza treatment from 0.1-0.4 mg/kg/day doses compared to the vehicle control (scale bar = 100 µm). (B-C) Representative images show immunostaining of 5-methylcytosine (B) and DNMT1 (C) in red in LCA frozen sections from the partially-ligated ApoE$^{-/-}$ mice as described in Figure 3, demonstrating a dose-dependent decrease in global DNA methylation and DNMT1 expression by 5Aza treatment (scale bars = 50 µm). Nuclei are stained with DAPI in blue and the elastin laminae autofluoresce green.

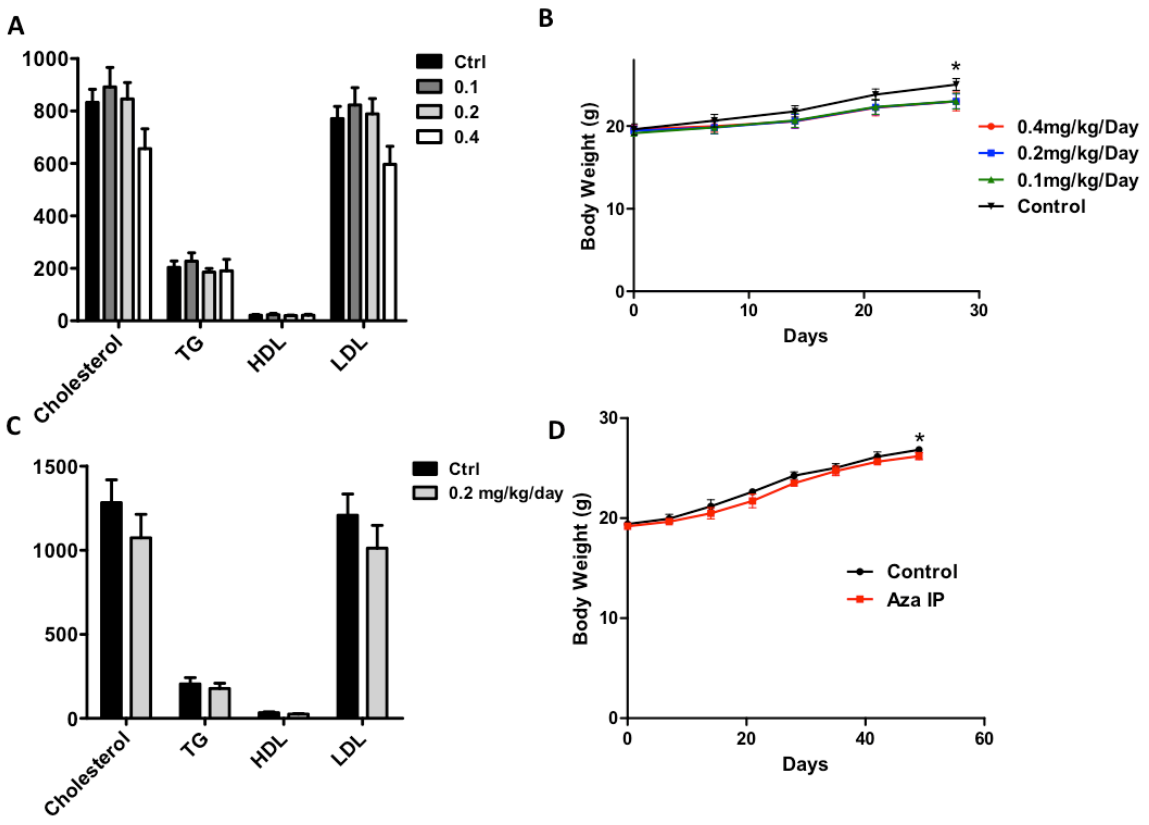

Figure 3.16: 5Aza has no major effects on serum lipid profiles and body weight. (A,C) Total blood serum cholesterol, triglycerides (TG), high density lipoprotein (HDL), and low density lipoprotein (LDL) in the acute, d-flow induced atherosclerosis model (A) and the chronic, diet-induced atherosclerosis model. Blood was collected from mice immediately before sacrifice. (B,D) Mouse body weights were measured weekly over the course of the 5Aza treatment in the acute, d-flow induced atherosclerosis model and in the chronic, diet-induced atherosclerosis model.[16]

Mechanoreceptors and MicroRNAs are Potential Upstream Regulators of the DNMT1 Shear Response

The miR29 family are Flow-Sensitive MicroRNAs that are validated to target DNMTs

These studies provide novel insight into the mechanism by which flow regulates gene expression in a DNMT1-dependent manner and uncovers novel genes involved in the endothelial flow response. However, much remains to be understood about the mechanism by which flow controls DNMT1. Our preliminary microarray data shows that

the miRNA29 family (mir29a, b, and c) is suppressed by d-flow and *in silico* analysis suggests that they may regulate DNMT1 directly. Using MirWalk, we performed a gene-microRNA interaction search and discovered 50 miRs that have been experimentally validated to target DNMT1. We compared this list of DNMT1-targeting miRs to our microarray dataset of global miR expression at 48 hours post-ligation, and we discovered that 18 miRs that can regulate DNMT1 are downregulated significantly (by more than 33%) by d-flow (Table 3.2). Future studies will be focused on the microRNA29 family (mir29a, b, and c) because they are known to regulate key biological functions, including epigenetics, cell cycle, and matrix remodeling, but miR29s have not been previously described in the context of endothelial biology.

Table 3.2: Validated microRNAs that target DNMT1 and suppressed in the d-flow LCA.

MicroRNA	Fold Change (LCA/RCA)
mmu-let-7a	0.04
mmu-let-7c	0.60
mmu-let-7d	0.50
mmu-let-7g	0.63
mmu-miR-1	0.03
mmu-miR-124	0.42
mmu-miR-126-5p	0.55
mmu-miR-146b*	0.67
mmu-miR-148b	0.12
mmu-miR-152	0.50
mmu-miR-155	0.13
mmu-miR-221	0.40
mmu-miR-29b	0.48
mmu-miR-29b*	0.14
mmu-miR-29c	0.35
mmu-miR-29c*	0.62
mmu-miR-302b	0.52
mmu-miR-302c*	0.53

Endothelial Cell Mechanoreceptors are Intermediate Players Between Flow Sensing and Overexpression of DNMT1

As an additional route of examining the potential upstream regulation of DNMT1, we developed a predictive model to understand how the activity of different endothelial cell mechanoreceptors affects the expression and activity of DNA Methyltransferase. Well-studied mechanosensors known to play a role in endothelial cell mechanotransduction (Appendix A Table A1) were subjected to systems biology analysis using Ingenuity Pathways Analysis to determine their potential network connectivity to DNMT1. No direct binding interactions were found to occur between mechanosensors and DNMT1. However, a highly interconnected protein interaction network emerged as a potential regulator of the DNMT1 shear response (Figure 3.17). This involved the primary mechanosensors Platelet/Endothelial Cell Adhesion Molecule 1 (PECAM1), caveolin 1 (CAV1), and Vascular Endothelial Growth Factor Receptor (VEGFR), and secondary signaling molecules cyclin D1 (CCND1), Protein Kinase B (PKB, or AKT), annexin A5 (ANXA5), and embryonic ectoderm development (EED). We developed a directional regulatory map and created a computational model of gene expression and protein activity in the system using Matlab (Appendix A, Figure 1 and Table 2). The model was further expanded to include the DNMT1 inhibitor 5-Aza-2'deoxycytidine to determine whether we could accurately predict behavior of the system upon perturbation of DNMT1 expression. 5Aza is also known to upregulate expression of the mechanoreceptor CAV1[119]. Several assumptions were used due to lack of literature available and to enable sufficiently simple model development for the scope of this

analysis (Appendix A) and it is emphasized that this model should not be interpreted as predictive of the actual system, but rather should be used as a basis to guide future experimental design to analyze the upstream regulation of DNMT1.

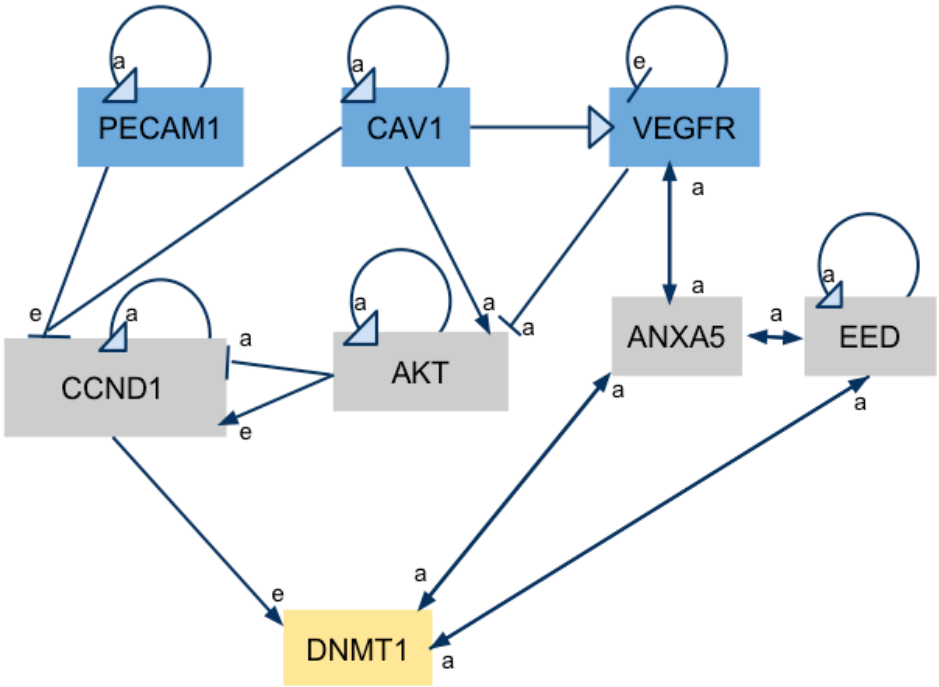

Figure 3.17: A Schematic Representation of the Endothelial Cell Mechanoreceptors and the Signal Transduction Pathway to DNMT1.

Using this model we tested all possible cases based on combinations of initial states (S) of the mechanosensors (simplified to either S=0: not expressed, inactive; S=1: expressed, inactive; and S=2: expressed, active). We found that a negative feedback mechanism turns off DNMT1 when *both* PECAM1 and CAV1 are expressed +/- active, and the state of VEGFR doesn't affect negative feedback (Appendix A, Figure 5). Additionally, when PECAM1 and CAV1 are not both expressed *together*, DNMT1 stays expressed and active indefinitely (Appendix A, Figure 6). Finally, the addition of 5Aza alters the dependence of negative autoregulation of DNMT1 on *both* PECAM1 and CAV1, so that *only* PECAM1 needs to be expressed to achieve negative autoregulation

(Appendix A, Figure A7 and A8).

Discussion

Prior to 2014, there had been no accounts of flow-regulated DNA methyltransferases (DNMTs) and their functional relevance to endothelial cell (EC) biology. 5-Aza-2'deoxycytdine (5Aza) and siRNA treatment allowed us to directly observe the functional consequence of DNMT1 inhibition on EC function. Results from *in vitro* studies predicated the question of a functional effect of DNMT1 inhibition on disease outcome. Our two *in vivo* models of acute d-flow-induced and chronic diet-induced atherosclerosis are robust and well-tested systems that we used to analyze DNMT inhibition effects. The question of whether DNMT1 inhibition affects EC inflammation *in vitro* and atherosclerotic plaque development *in vivo* had never been addressed before.

We showed that DNMT1 is a mechanosensitive gene upregulated by d-flow and that DNMT inhibition prevents d-flow-induced endothelial inflammation *in vitro* and atherosclerosis development *in vivo*. Given its dramatic flow-sensitivity, we expect that DNMT1 is the dominant DNMT involved in endothelial inflammation and atherosclerosis. However, it would also be interesting to examine the role of the other catalytically active DNMTs (DNMT3a and DNMT3b) in EC function, especially given our findings that DNMT3b is slightly upregulated by d-flow at the protein level (Figure 3.10) and that DNMT3a was found to be shear-responsive in ECs in other model systems[57,65]. In April 2014, Jiang et al. reported that DNMT3A is overexpressed by d-flow in human aortic endothelial cells (HAEC) and that this regulates Klf4 transcription.[65] Klf4, a key mediator of endothelial function, maintains an anti-

inflammatory, quiescent endothelial state in unidirectional flow conditions. The group showed that d-flow increases DNMT3A binding to the Klf4 promoter leading to DNA hypermethylation and blocking MEF2 (myocyte enhancer factor-2) binding. Using methods similar to ours, they showed that DNMT inhibition decreased Klf4 promoter methylation, increased its expression, and reversed the d-flow-induced dysregulation of downstream Klf4 targets eNOS, thrombomodulin (THBD), and monocyte chemoattractant protein-1 (MCP-1). This study demonstrates that in other experimental setups analyzing the shear effect on endothelium, other DNMTs also appear to be dysregulated. Additionally, DNA methylation via DNMTs plays a direct role in gene expression control. Before these studies, DNMTs in ECs had not been previously implicated as a mechanism for flow-mediated gene expression control.

In order to determine whether there is a further functional role for DNMT1 in atherosclerosis development, additional markers of EC dysfunction that increase in d-flow (including inflammation, apoptosis, proliferation, thrombosis and cell migration) could be examined in future studies. Additionally, the *in vivo* effect of EC-specific DNMT1 knockdown on plaque development can be tested. Due to the potential off-target and non-tissue-specific effects of 5Aza, the acute and chronic *in vivo* mouse atherosclerosis experiments done here can be repeated endothelial cell specific DNMT1 knockout mice as described in the Future Directions section of Chapter 6.

While we established that DNMT1 is upregulated in d-flow and plays a key role in atherosclerosis development, the mechanism of DNMT1 upregulation is unknown. The goal of the initial microRNA and mechanosensor computational analyses described here were to aid in the design of future experiments to analyze the upstream regulation of

DNMT1. We anticipate the usefulness of future studies to examine the effect of mir29, PECAM1, CAV1, or VEGFR silencing or overexpression on DNMT expression and activity, as well as EC biology and atherosclerosis development. Such potential studies are described in more detail in Chapter 6 Future Directions.

Overall, in Chapter 3 we found that DNMT1 is a functionally important mechanosensitive gene that plays a key role in endothelial cell (EC) inflammation *in vitro* and plaque development *in vivo*. D-flow-induced DNMT1 upregulation was verified at the transcript and protein level *in vitro* and in *vivo*. The role of DNMT1 in atherosclerosis development *in vivo* was tested using the DNMT1-specific inhibitor 5Aza on chronic and acute atherosclerosis models to determine the functional outcome of blocking DNMT1 overexpression in d-flow. Results show that DNMT1 inhibition by 5Aza blocks endothelial inflammation *in* vitro and atherosclerosis progression *in vivo,* implicating DNMT1 to have a key functional role in d-flow-induced EC dysfunction and atherosclerosis.

CHAPTER 4 DNA METHYLATION-DEPENDENT ENDOTHELIAL GENE EXPRESSION RESPONSE TO FLOW

Summary

In this study, we sought to determine the mechanism of action of DNMT1 overexpression and conversely inhibition by 5Aza in disturbed-flow-exposed endothelium. Since DNMT1 is known to methylation genomic DNA, and DNA methylation may control gene expression, we designed two parallel "omics" studies to examine the effects of both disturbed flow and DNMT inhibition on the endothelial cell DNA methylome and transcriptome *in vivo*. We carried out the reduced representation bisulfite sequencing (RRBS) study using endothelial-enriched genomic DNA (gDNA) obtained from the RCA and LCA of partially ligated mice at two different time points of two days and one week post-ligation. To further determine whether the flow-dependent DNA methylation changes were regulated in a DNMT-dependent manner, mice treated with 5Aza were compared to a saline vehicle control. Moreover, to determine which mechanosensitive genes has transcriptional dysregulation, potentially by DNA hypermethylation, we carried out a concomitant gene transcript microarray study using endothelial-enriched RNA obtained from the LCA and RCA of partially-ligated mice treated with either saline (RCA vs. LCA) or 5Aza (Aza-RCA vs. Aza-LCA). From these studies we found that DNMT inhibition by 5Aza rescues global gene expression in LCA to healthy state. While genome-wide and functional genomic elements did not have dramatic methylation changes under these conditions, we followed a specific hypothesis and found a subset of genes that had d-flow-induced promoter hypermethylation correlating with gene suppression, both were 5Aza-reversible. Based on a systems

biology and further bioinformatics analysis, we found that gene promoters containing cyclic AMP Response Elements (CRE) are preferentially methylated by d-flow in a 5Aza-dependent manner. We further discovered that, on the genome scale, CRE hypermethylation corresponds to decreased gene expression. These studies used "omics" datasets to uncover a key regulatory network regulated by DNA methylation that may provide a basis for novel therapeutic approaches for atherosclerosis. A substantial portion of Chapter 4 was published as follows: Dunn, J., Qiu, H., Kim, S., Jjingo, D., Hoffman, R., Kim, C. W., Jang, I., Son, D. J., Kim, D., Pan, C., Fan, Y., Jordan, I. K. Jo, H. Flow-dependent epigenetic DNA methylation regulates endothelial gene expression and atherosclerosis. *J Clin Invest* 124, 3187-3199[16].

Introduction

The Relationship Between DNA Methylation and Gene Expression

CG methylation in the promoter region of a gene, close to the transcription start site, is associated with repression of gene expression. Although debated, promoter methylation is thought to affect the transcription of genes in two ways.[120-122] First, methylation of DNA physically impedes the binding of transcriptional proteins to the gene. Second, methylated DNA is bound by methyl-CpG-binding domain proteins (MBDs). MBDs then recruit additional repressive proteins to the locus, such as histone and chromatin modifiers, and this complex causes chromatin compaction. The exact mechanism of crosstalk between DNA methylation and histone modifications remains a topic of extensive research.[123,124]

CG methylation in the gene body is less straightforward[125-127]. Initial studies on intragenic methylation indicated that gene body hypermethylation is correlated with

increased gene expression [128]. On the contrary, it has been argued that intragenic methylation causes chromatin compaction and blocks RNA Polymerase II binding, which prevents transcript elongation [129]. Gene body methylation may activate or repress genes depending on the location (exon/intron/alternative promoter), density (CpG Island), and extent of methylation [130]. For example, expressed genes may be associated with methylated gene bodies, and unmethylated intragenic CpG island EP300-bound enhancers, and vice-versa for silenced genes [127].

Methods to Analyze DNA methylation

MspI/HpaII

To examine the overall level of methylation at the genome level, a restriction enzyme digest can be done using MspI and HpaII (methylation insensitive and sensitive, respectively; both recognize the 5'-CCGG-3' restriction site). When DNA is hypermethylated globally, HpaII is blocked from cutting, but when DNA is hypomethylated, HpaII is able to cut.

Bisulfite Conversion and BS-Seq

Additional methylation assays rely on bisulfite technology, the gold standard in DNA methylation analysis [131]. Bisulfite salt deaminates unmethylated cytosines in genomic DNA, which converts them to uracil. However, methylated cytosines are protected from this chemical conversion and remain cytosine after bisulfite conversion. In this way, the only cytosines that remain in the genomic DNA are those that were originally methylated. After PCR amplification, the unmethylated cytosines become thymine, while methylated cytosines are still cytosine (Figure 4.1).

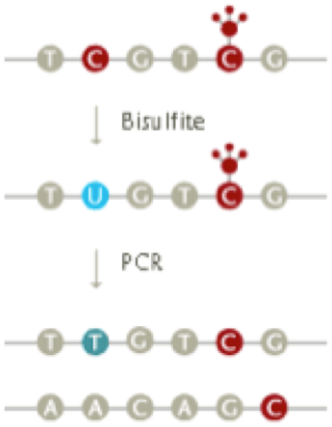

Figure 4.1: Scheme for Bisulfite Conversion. Adapted from http://www.epigenomics.com/en/science-and-technologies/bisulfite-technology/

There are several possible subsequent steps one can take with the bisulfite converted DNA. Bisulfite sequencing, for example, involves PCR amplification of the bisulfite-converted genomic DNA with specially designed PCR primers. Bisulfite sequencing primers are limited to regions that have no CG sites (any cytosine in the primer design region will always be converted to a U and will be represented as a T in primer design) but must encompass several CG sites in the amplified region in order to be a useful probe. Amplicon size is generally limited to 500bp or less due to genomic DNA fragmentation (to ~3kb fragments) during bisulfite conversion and due to the difficulty of specific primer design. Because bisulfite conversion alters the DNA sequence, comparison of the sequencing product to the reference sequence for that locus reveals cytosines that were methylated and unmethylated in given conditions. Bisulfite converted genomic DNA can also be subjected to high resolution melting curve analysis to determine the number of C's vs. T's in a specific region amplified by qPCR [132]. More methylated DNA will have more C's after bisulfite conversion, and will thus have a

higher melting temperature due to more hydrogen bonding between C-G bonds as compared with A-T bonds [116,133].

RRBS

Reduced Representation Bisulfite Sequencing (RRBS) enables researchers to determine genome-scale methylation patterns at the nucleotide resolution. [134-136] Genomic DNA is cut with the methylation-insensitive restriction enzyme MspI to enrich for sequences containing many CG sites, and fragments are then size-selected and cloned into a library for sequencing. RRBS enables researchers to probe relevant, CG-rich portions of the genome, eliminating the need for full genome sequencing. Conveniently, Meissner et al. further modified the RRBS technique to allow for as low as 30ng of input DNA, which makes it compatible for application with our *in vivo* mouse carotid artery ligation model [137]. RRBS is a cost-effective technique to scan the genome for interesting loci based on methylation changes [138].

OMICS approaches to DNA methylation and gene expression studies

Genome-Wide Analysis

With the advent of high throughput genome-wide analysis technology such as the microarray it became possible to study the expression of thousands of genes throughout the genome simultaneously [139]. This greatly impacted the field of vascular mechanobiology by enabling researchers to track a large host of genes in a controlled, well-defined environment. The resulting studies displayed clear evidence of the endothelial cells' keen ability to sense and convert mechanical stimuli into biochemical signaling responses. Microarray studies illuminated numerous key regulatory pathways

and their dynamics while also supporting the discovery of novel mechanosensitive genes and functional gene clusters. These datasets continue to support the working hypothesis that laminar, unidirectional flow upregulates "atheroprotective" genes and downregulates "atheropathogenic" genes while disturbed, reversing, or stagnant flows result in the opposite phenomenon of enhancing atheropathogenic genes and suppressing atheroprotective genes.

In 2001, the complementary DNA (cDNA) microarray was first utilized *in vitro* to study the effect of shear stress on gene expression profiles of cultured endothelial cells. Gimbrone et al. used the cDNA array to define gene expression profiles of 11,397 genes in cultured human umbilical vein endothelial cells (HUVEC) exposed to steady laminar flow, turbulent flow, or static flow over 24 hours. Functional tests determined that several "mechanosensitive" genes activated under laminar flow were, in fact, atheroprotective, and that the reciprocal was true regarding atheropathogenic genes.[6,20] Chien et al. discovered 125 differentially regulated mechanosensitive genes in human aortic endothelial cells (HAEC) exposed to laminar flow versus static conditions by a less comprehensive cDNA microarray but under more rigorous statistical testing as compared to Gimbrone.[26] Both groups used RT-PCR validation and array analyses described later in further detail. Broadly, it was found that gene expression profiles in endothelial cells exposed to laminar, unidirectional flow are distinctly different from those under disturbed flow, while static flow profiles have a strong resemblance to turbulent shear expression profiles. More specifically, laminar shear stress causes suppression of genes associated with inflammatory responses, matrix remodeling, and cell proliferation, and activates genes involved in signal transduction, cytoskeletal remodeling, and angiogenesis.

There are various approaches to microarray data analysis. Raw data can be analyzed in the most straightforward manner by comparison of the relative intensities of probe hybridization, expressed as a fold change, which represent the levels of differential transcript expression. Rigorous statistical analysis and filtering is necessary to lend significance to fold change values. Large datasets can be parsed by hierarchical clustering based on various criteria such as gene ontology, location in the genome, or expression patterns alluding to co-regulation. However, this method may disregard underlying trends and often cannot tease out complex biological interactions formed by specialized gene circuitry. The Gimbrone group created the analytical software Argus, which allows the integration of multiple experimental conditions to help account for this difficulty. Both open source and proprietary systems biological tools like Ingenuity Pathways Analysis have become available. In addition to systems-wide analyses, computational tools at the gene-specific level such as DAVID, amiGO, NCBI UniGene, and the UCSC Genome Browser, make gene ontology and functional studies quite feasible.

Integrative approaches to analyzing DNA methylation and gene expression datasets from high-throughput approaches such as microarray and next generation sequencing-based assays are highly useful to determine the interplay between these two "omics" datasets.

Cyclic AMP Response Elements and the Cyclic AMP Response Element Binding Protein CREB

Cyclic AMP response elements (CRE) were discovered in 1986 by separate analyses that converged on the importance of a sequence motif existing in the promoters of several cAMP-responsive genes, including somatostatin, proenkephalin, and

phosphoenolpyruvate carboxykinase (PEPCK) [140-142]. The finding that the 8 bp palindrome sequence 5'-TGACGTCA-3' conferred gene expression responsiveness in the presence of cAMP was later found to also exist in many other genes. [143] In fact, many cell cycle genes such as cyclins A and D1 contain CREs, as do an abundance of metabolic genes [143-146]. In additional to the full CRE (fCRE) motif TGACGTCA, CREs also exist in half-sites (hCRE) as CGTCA or TGACG [147,148]. As of the year 2001, there were 105 identified genes containing functional CREs (~50% containing the fCRE and the other 50% containing a hCRE) and the majority were found between -50 to -150bp upstream of the transcription start site [143]. Gene ontology analysis of CRE-containing genes revealed that 38% of all CRE-containing genes are transcription factors [149].

The cAMP response element binding protein (CREB) is a transcription factor that binds to cAMP response elements (CRE) of genes and regulates transcription. In this manner, CREB controls global gene expression and its dysregulation is linked to many developmental pathways and diseases. CREB can selectively distinguish its binding motif from that of AP1 (which is TGACTCA), and it is thought that two key lysines (304 and 305) are key for CREB recognition of the CRE site. Interestingly, lys304 mutation interrupts CREB binding to fCRE, but not to the hCRE [150]. Additionally, while fCRE has a higher overall binding affinity for CREB as compared to hCRE, the affinity of hCRE increases much more dramatically than that of fCRE upon CREB phosphorylation, and this has been implicated as a mechanism of fine-tuning gene expression of hCRE-containing genes [151,152]. Additional bZIP transcription factors, including C/EBPα, also bind to CRE [153].

It is known that methylation of the cytosine in CpG dinucleotide of both hCRE and fCRE blocks CREB binding, but can actually increase C/EBPα binding to hCRE [149,153,154]. Methylation-dependent CREB binding is a key mechanism in Wp gene silencing on the Epstein-Barr virus during viral-induced B cell to lymphoblastoid transformation, and also in hCRE control of the testis-specific expression/somatic cell silencing of Pdha2 [155-157]. CREB binding affinity may also relate to sequence motifs surrounding the CRE, for example Tax-responsive elements (TREs) contain the CGTCA motif but are surrounded by highly CG-rich flanking regions and TREs demonstrate a significantly lower binding affinity for CREB[158,159].

CREB was one of the first transcription factors found to have activity regulated by phosphorylation. It has been shown that protein kinase A (PKA) downregulation in ECs ecxposed to d-flow leads to decreased CREB phosphorylation and decreased CREB binding to CRE elements [160]. Interestingly, while cilostazol, a phosphodiesterase III inhibitor that increases cAMP and activates CREB, is used clinically to treat patients with PAD, its mechanism is still unclear, and it is contraindicated for heart failure patients.

Methods

Partial Carotid Ligation Surgery and 5Aza-2'deoxycytidine Treatment Schemes

To decrease complications arising from the hypercholesterolemic conditions in ApoE$^{-/-}$ mice, C57BL/6 mice were used for these studies. At the earlier timepoint, C57BL6 mice were partially ligated by Chanwoo Kim (see methods in Chapter 3 for detailed explanation) without any other treatment and gDNA was collected by Jessilyn Dunn and Soyeon Kim from the carotid arteries two days later to determine the effect of flow alone on DNA methylation. At the later timepoint, mice were pre-treated with saline

or 5Aza (0.2 mg/kg/day) for two weeks by intraperitoneal injection, then were partially ligated by Chanwoo Kim and the 5Aza treatment was continued for one week after. ligation.

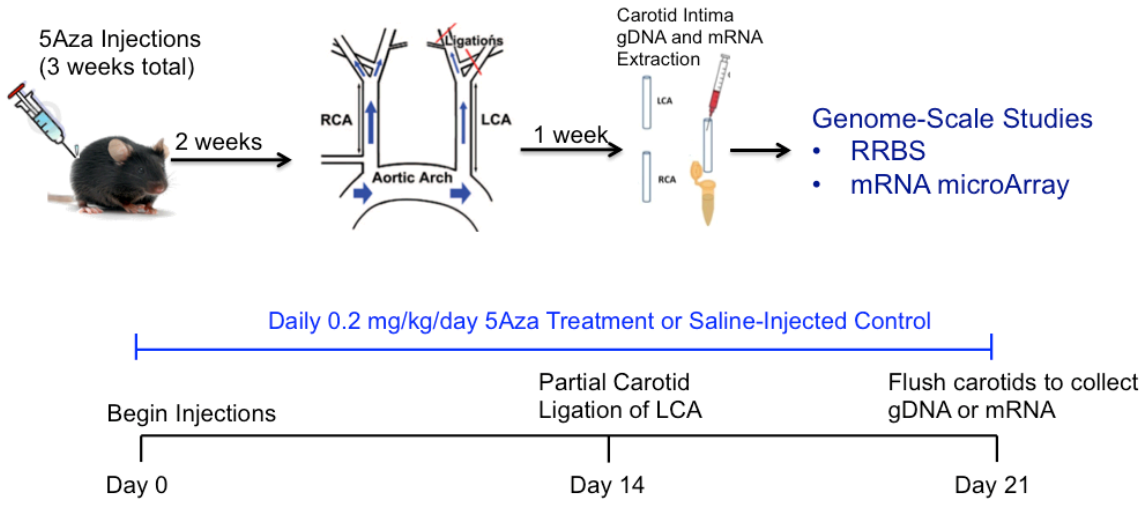

Figure 4.2: 5Aza treatment scheme to study the effect of Flow on Genome-Wide DNA Methylation (by reduced representation bisulfite sequencing, or RRBS) and Gene Expression (by microarray) Patterns in the Endothelium in vivo. C57BL/6 mice were treated with 5Aza or saline for 2 weeks at 0.2 mg/kg/day via *i.p.* injections. Then, partial carotid ligation was done and mice continued to receive the same 5Aza or saline treatment for 1 more week. Following sacrifice, endothelial-enriched genomic DNA (gDNA) was collected from the LCA and RCA.

Endothelial Cell Genomic DNA and RNA Preparation Quality Control

To measure the purity of endothelial cells in our gDNA and RNA preparations from flushing the carotid arteries, we performed a number of control experiments on C57Bl6 mice at 7 days post-ligation. The goal of these experiments was to determine the cell populations existing in our samples as a ratio of ECs to SMCs and immune cells. These control experiments included qPCR on eNOS, aSMA, and CD11B, single-gene bisulfite sequencing of eNOS, and immunohistochemistry and cell counting of ECs, SMCs, and immune cells using cell profiler (see Appendix B for details and results).

Genomic DNA and RNA Extraction from Mouse Carotid Arteries for Transcriptome and Methylome Studies

Microarray

Total intimal RNA was collected by flushing the RCA, LCA, Aza-RCA, and Aza-LCA with 150 µl of Qiazol and was purified using the miRNeasy Mini Kit (Qiagen). Three carotid RNA samples were pooled and the combined sample was amplified and reverse transcribed, and the cDNA was applied to Illumina Mouse WG6 microarray chips. The microarray detected 45,281 probes corresponding to 30,854 genes.

The two repeated timepoints in our lab's previous microarray studies using the Illumina and Affymetrix microarrays make it possible to verify the first microarray results. Previously published shear-sensitive genes were found to have similar expression patterns in our arrays, and numerous novel mechanosensitive genes were also discovered through this *in vivo* microarray study

RRBS

Genomic DNA was collected from mouse carotid arteries (as described previously) by flushing with 200 ul of a 1:1 solution of Buffer AL and nuclease-free water. Genomic DNA was purified using the DNeasy Blood and Tissue Kit (Qiagen) and 20 genomic DNA samples were pooled per RRBS sample. gDNA for the RCA, LCA, Aza-RCA, and Aza-LCA was examined for quantity and quality using the Nanodrop (Table 4.1) and samples were sent to Zymo Research Corp. where RRBS was carried out by bisulfite conversion, genome reduction by restriction enzyme digest and size selection, library preparation, and next generation sequencing.

Table 4.1: Quantity and quality of gDNA at 7 days (with or without 5Aza treatment) or 2 days post-ligation as measured by Nanodrop. The gDNA was submitted to Zymo Research for bisulfite conversion, RRBS library prep, sequencing, and alignment.

	Amount of gDNA (ng)	260/280 ratio
7 d Ctrl LCA	650.7	1.65
7 d Ctrl RCA	477.0	1.49
7 d Aza LCA	414.0	1.49
7 d Aza RCA	255.6	1.66
2 d LCA	1,550	1.64
2 d RCA	1,450	1.79

Computational Analysis of Genome-wide Methylome (Reduced Representation Bisulfite Sequencing) and Transcriptome (Microarray) Datasets

Next generation sequencing reads from the RRBS study were mapped to the Mm9 genome assembly by Zymo Research Corp. The resulting mapped files were analyzed by our lab. Methylome coverage was determined by dividing the number of unique CG sites covered by each individual RRBS dataset by the number of total CG sites in the Mm9 genome assembly (21,342,492 CG sites in chromosomes 1-19, X, and Y). Promoter coverage was determined by confining the RRBS and Mm9 assemblies to gene transcription start sites (TSS, as defined by the NCBI reference sequences database) ± 1kb (there are 2,130,470 CG sites in these Mm9 Assembly promoters), and then again

calculating coverage in these confined regions. The methylation ratio at each CG site was calculated by the number of methylated reads divided by the total number of reads at that site, and the percent methylation at each site is the methylation ratio multiplied by 100.

Heatmap correlation scatterplots were generated using the smoothScatter function in R. The log of the methylation ratios of only those unique CG sites covered by all four datasets were plotted and the R^2 values were determined by fitting linear models with the R lm function [10,161,162].

Analysis of the DNA methylation Levels Around the Transcription Start Site, Gene Body, and Transcription Termination Site and its Relationship to Gene Expression Levels

The average percentage (± standard error) methylation levels was calculated using 100bp windows spanning the transcription start site (TSS), gene-body, and transcription termination site (TTS), using the regions 3kb and 5kb upstream and downstream of the TSS respectively and 5kb and 3kb upstream and downstream of TTS, respectively, across five gene expression level bins. This analysis was done by Dr. Daudi Jjingo in collaboration with Dr. I. King Jordan [126].

Emergent Methylation Patterns

For the *a priori* emergent methylation pattern analysis to rank the average methylation ratio of each gene promoter from the four experimental groups at 7 days post-ligation, was done using only those CG sites confined to promoter regions (TSS ± 1kb). We calculated the promoter methylation ratio by the total number of methylated reads divided by the total number of all reads in the region, normalized to the number of CG sites in that region. This was done for each RRBS dataset, and then the methylation ratio for each gene promoter was compared between datasets and ranked from highest to

lowest methylation ratio. There are 24 possible combinatorial patterns that can result from this ranking analysis by ordering the 4 samples from highest to lowest, and we counted the number of genes that fell into each of the 24 possible pattern categories. This analysis was done in collaboration with Dr. Daudi Jjingo and Dr. I. King Jordan.

Promoter Cyclic Amp Response Element CpG Methylation

After discovering CREB as a common network regulator of the 11 gene subset discovered in Chapter 5, the RRBS datasets were subsequently mined to determine the methylation ratio for each sample (RCA, LCA, Aza-RCA, and Aza-LCA) specifically at the CpG dinucleotide within CRE sequences, and then again but for those CRE sequences specifically confined to gene promoter regions (TSS ± 1kb).

The RRBS datasets were analyzed for genomic and promoter (transcription start site ± 1kb) CG content and methylation status, as well as CRE element methylation status using the R Bioconductor packages BSGenome (specifically, the Mm9 Genome Assembly apprehended from the UCSC database), GenomicRanges, Genomic Features, and Biostrings.

The Relationship Between Promoter Cyclic Amp Response Element CpG Methylation and Gene Expression

First, the sequence of the promoters (+/- 1 kb from the transcription start site, or TSS) of all genes (34,000) in the Mm9 genome were downloaded from the UCSC Genome Browser. Those genes on the hap, un, and rand chromosome maps were removed from the set because they come from either alternate assemblies or unmapped contigs (hap: different haplotypes/alternative alleles that may cause duplicated sequences in the reference; un: unmapped regions; rand: random contigs whose exact location on the

chromosome is uncertain). This resulted in 33,826 promoter sequences included in the downstream analysis. We performed a string search for the three CRE motifs on this set of promoter sequences, and found that there were 9,556 genes containing CGTCA in their promoter, 9,536 containing TGACG, and 863 containing TGACGTCA. The genomic ranges of these gene promoter sequences were then mapped back to our RRBS CpG methylation data using only those sites covered by all RRBS datasets (3,232,969 CG sites) at a minimum of 10 reads per CG site. We were then able to map the promoter CRE CG methylation status of a gene to its expression using our microarray data to determine the relationship, which resulted in 4,286 genes containing CGTCA in their promoter, 3,326 containing TGACG, and 503 containing TGACGTCA (Figure 4.9).

Subsequently we filtered out those genes with the most dramatically changed promoter CRE CG site corresponding to the most dramatic gene expression changes by thresholding so that only those genes that followed our expected trends (hypermethylation and lower probe intensity in the LCA vs. RCA) were kept. For the thresholding values, we parameterized the data to account for both the CRE CG methylation change as well as the probe intensity change. Using this parameter (arbitrary units), the data was thresholded so that the difference between the flow-altered samples (measured by the length the line between the LCA and RCA datapoints for each gene, which is also the magnitude of the parameter change) in Figure 4.10 was greater than 100 and the slope of that line (the rate of change of the parameter) was less than -50.

CpG Methylation Analysis in Functional Genomic Regions

Global percent methylation for each of the RRBS datasets was determined using only those CG sites covered by all datasets (the intersection of the RRBS datasets:

3,232,969 CG sites). The values were calculated by averaging the methylation ratios across every CG site in the genome or only within specific regions, including enhancers (experimentally validated by the VISTA enhancer browser), promoters (+/- 1 kb from the transcription start site, or TSS), gene body (the region between the TSS and TTS), and transcription termination site (TTS; defined as within ± 1kb of a gene TTS).

The VISTA enhancer browser is a resource containing experimentally validated human and mouse noncoding fragments with gene enhancer activity. Putative enhancers are selected by the VISTA group based on their conservation across vertebrates and/or positive ChIP-Seq data of enhancer marks. A subsequent *in vivo* enhancer screen is done using enhancer/LacZ reporter transgenic mice to assess spatial expression during embryonic development, which enables identification of distant-acting transcriptional enhancers. "Positive" enhancers are defined as those experimentally validated by demonstrating reproducible expression in the same structure in at least three independent transgenic embryos. We used the genomic ranges for only positive mouse enhancer regions defined by VISTA (244 regions) to measure global enhancer methylation in our RRBS data (Figure 4.7).

Results

Quantification of Relative Cell Types for Endothelial Cell Genomic DNA and RNA Quality Control

One major complication of DNA methylation studies on samples taken directly from in vivo is the possibility for the inclusion of multiple cell types. To ensure that changes seen in our DNA methylation and gene expression data could be attributed to the endothelial response to experimental conditions rather than differential DNA methylation

or gene expression occurring across different cell types, we performed a brief study (Appendix B) to measure the number of contaminating cell types we could expect in our endothelial cell genomic DNA and RNA preparations. Detailed analysis of the results from these experiments indicate that we have minimal contamination from SMCs and immune cells in our endothelial preparations, and underscore the validity of our experimental and analytical methods for the following experiments.

Validation of 5-Aza-2'deoxycytidine Efficacy by High Resolution Melting Curve Analysis

As a control for 5Aza treatment, blood was collected one week after the start of the treatment and global DNA methylation was measured by high resolution melting curve analysis (HRM). This showed that global methylation decreased as early as one week after 5Aza treatment, demonstrating the efficacy of this treatment strategy (Chapter 3 Figure 15).

Reduced Representation Bisulfite Sequencing Data Analysis

The two RRBS datasets for the LCA and RCA at the early timepoint of two days post-ligation did not show a significant difference in methylation. Further analysis was performed using only the four RRBS datasets collected at the later timepoint of 1 week post-ligation, for which we also collected a concomitant transcriptome dataset for comparison and analysis.

The four RRBS datasets (RCA, LCA, Aza-RCA, and Aza-LCA) were mapped to the Mm9 (July 2007/NCBI37) mouse genome assembly, which contains a total of 21,342,492 CG sites. Our four RRBS datasets showed a methylome coverage of ~23% (4,967,716 unique CG sites on average) of all CG sites in the mouse genome, including

promoters, gene bodies, and intergenic regions (Table 4.2). Interestingly, ~53% (1,125,997 CG sites on average) of all CG sites in the promoter regions (defined as transcription start site ± 1kb) were covered by our RRBS datasets (Table 4.2), which shows a higher coverage in the promoter regions as compared to the other genomic sites.

Table 4.2: The number of CG sites in the Mm9 Genome Assembly and in each RRBS dataset, and the number of CG sites specifically in gene promoter regions (transcription start site ± 1kb) in each.

	Dataset	Total CGs	CGs in Promoters
	Mm9 Genome Assembly	21,342,492	2,130,470
RRBS Datasets	LCA	4,923,836	1,124,726
	RCA	4,584,088	1,068,670
	Aza-LCA	5,308,692	1,156,804
	Aza-RCA	5,054,246	1,153,786
	Average	4,967,716	1,125,997

To measure the DNA methylation changes at each CG site in the RRBS datasets, only those covered in all four datasets (RCA, LCA, Aza-RCA, and Aza-LCA) were selected for further analysis (3,232,969 unique CG sites). The methylation ratio at each CG site was compared between the RCA and LCA as well as the Aza-RCA and Aza-LCA using heatmap correlation scatterplots (Figure 4.3A and B). Of the 3.2 million CG sites examined, 4.1% (131,176 CG sites) showed hypermethylation by more than 40% in the LCA as compared to the RCA, whereas 93% showed no significant difference in methylation, defined as less than a 40% difference between the RCA and LCA (Figure 4.3A). 5Aza treatment reduced the number of hypermethylated CG sites in the LCA by more than 50% as compared to the saline group (from 131,176 to 55,224 CG sites), while

97% of the CG sites showed no significant difference between the Aza-RCA and Aza-LCA (Figure 4.3B). This result showed that the small number (4.1%) of CG sites that were hypermethylated in the LCA by d-flow was substantially reduced by the 5Aza treatment (to 1.7%), suggesting that d-flow regulates genome-wide DNA methylation patterns in a DNMT-dependent manner.

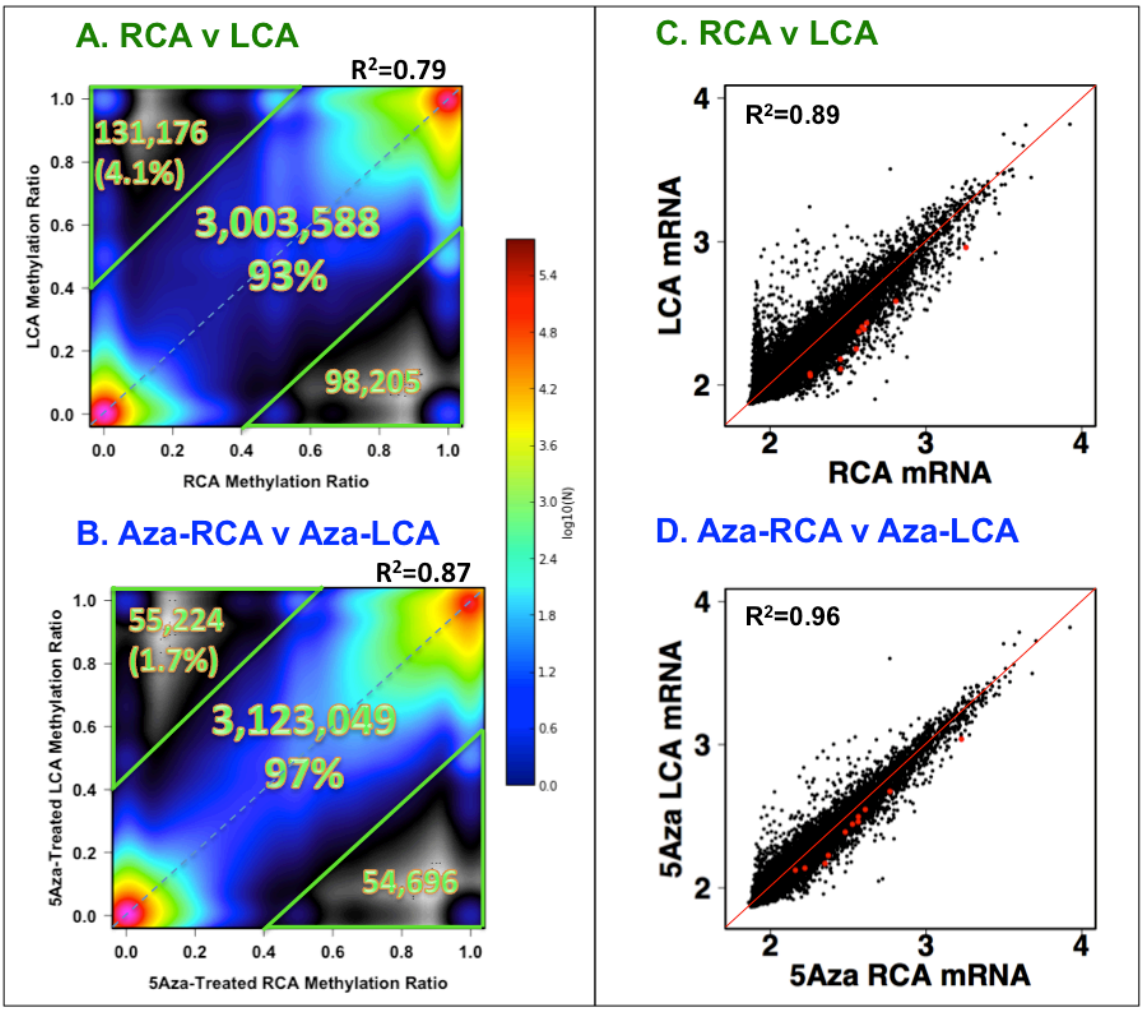

Figure 4.3: D-flow alters genome-wide DNA methylation patterns and gene expression in a 5Aza-dependent manner. (A and B) gDNA from 20 LCAs and RCAs each were pooled and the genome-level methylation was analyzed by RRBS (reduced representation bisulfite sequencing). Shown are density heat map correlation plots portraying the methylation status at each of 3,232,969 CG sites covered by the RRBS analyses. The numbers indicated in the upper (131,176), middle (3,003,588) and lower triangles (98,205) in (A) indicate hypermethylated, not

altered significantly and hypomethylated CG sites, respectively, in the partially ligated LCA compared to the RCA in saline-treated mice. Likewise, the numbers shown in (B) indicate the same as in (A), but in the LCA and RCA obtained from mice treated with 5Aza. (C and D) Following sacrifice, endothelial-enriched RNA obtained from 3 LCAs and RCAs were pooled as one sample, and 3 samples per condition (LCA and RCA from saline vs. 5Aza treated groups) were analyzed by the Illumina Mouse WG6 microarray. Shown are correlation scatterplots of gene expression values on the log scale. The 11 genes identified in Chapter 5 Figure 1 are represented as red dots in each plot.

Relationship Between Global CpG Methylation and Gene Expression

To determine how many of these mechanosensitive DNA methylation patterns at the promoters correlate to gene expression patterns, we compared the promoter DNA methylation data to the gene transcript array data. First, the gene array data analysis showed that expression of 1,319 genes (569 down- and 750 upregulated) changed by more than 33% in the LCA compared to the RCA (Figure 4.3B and D). Treatment with 5Aza decreased the number of differentially expressed genes to 385 (152 down- and 233 upregulated in the LCA) between the Aza-RCA and Aza-LCA (Figure 4.3C). Importantly, 5Aza treatment rescued the downregulation of 540 out of the 569 mechanosensitive genes in the LCA (Figure 4.3C and D), demonstrating the dominant effect of 5Aza treatment on mechanosensitive gene expression, either directly or indirectly (Figure 4.3B-D, Figure 4.4C and D).

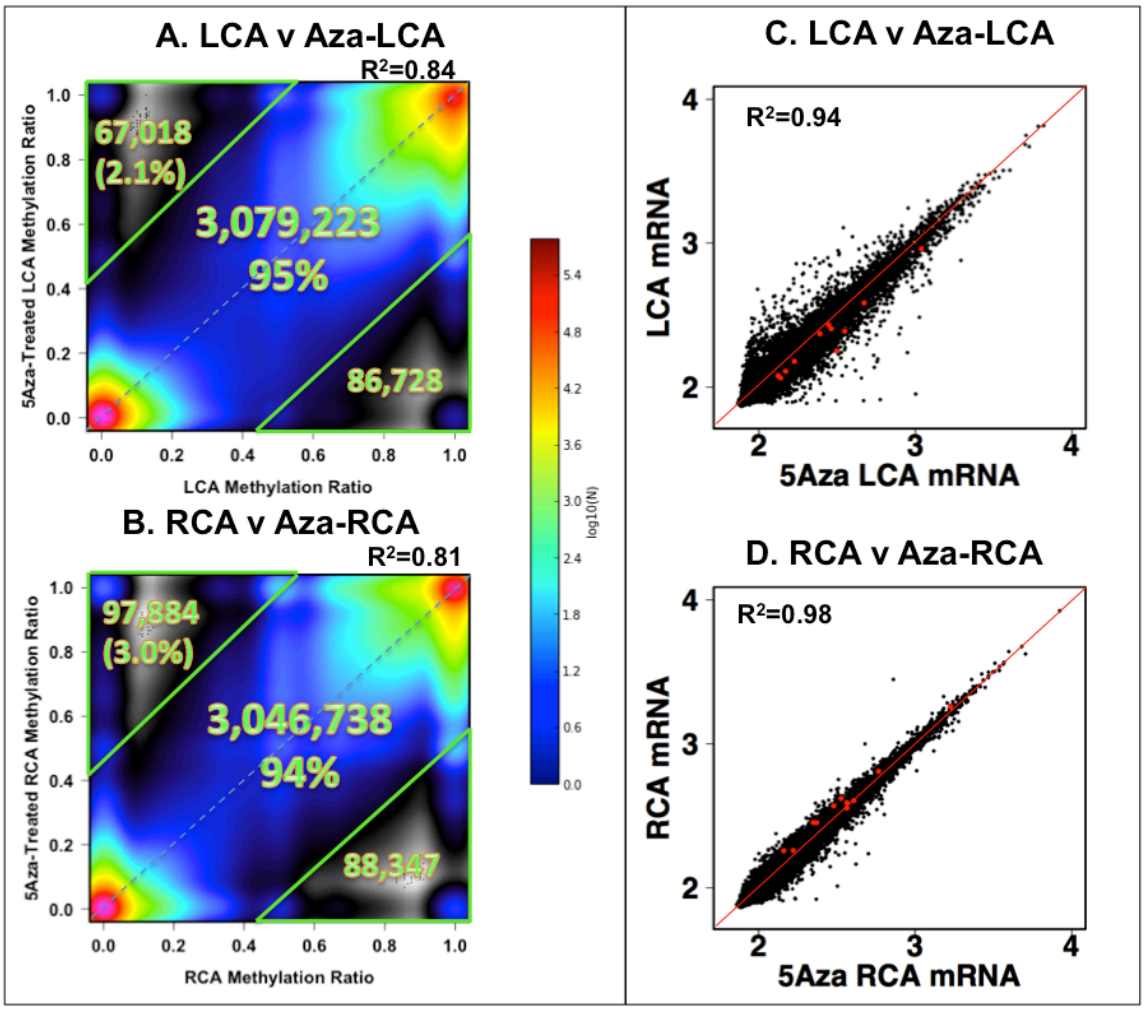

Figure 4.4: Genome-wide methylation and gene expression patterns in partially-ligated mouse carotids. (A,B) Heatmap correlation scatterplots of the methylomes of the LCA compared to the Aza-LCA and the RCA compared to the Aza-RCA. (C,D) Gene expression was compared between the LCA vs. Aza-LCA and RCA vs. Aza-RCA obtained from endothelial RNA as described in Figure 4.3.

Analysis of the DNA methylation levels around the transcription start site, gene body, and transcription termination site and its relationship to gene expression levels further analysis revealed that our RRBS and gene array datasets showed the expected pattern, wherein percent promoter methylation inversely correlated with gene expression levels on a global scale (Figure 4.5), whereas the same trends were not observed for the gene body (GB) and 3' gene regions surrounding the transcription termination sites

(TTS). This finding is consistent with previous reports showing a close correlation between promoter hypermethylation and gene silencing [126], validating that our RRBS and transcriptome data sets behave in an expected and reliable manner.

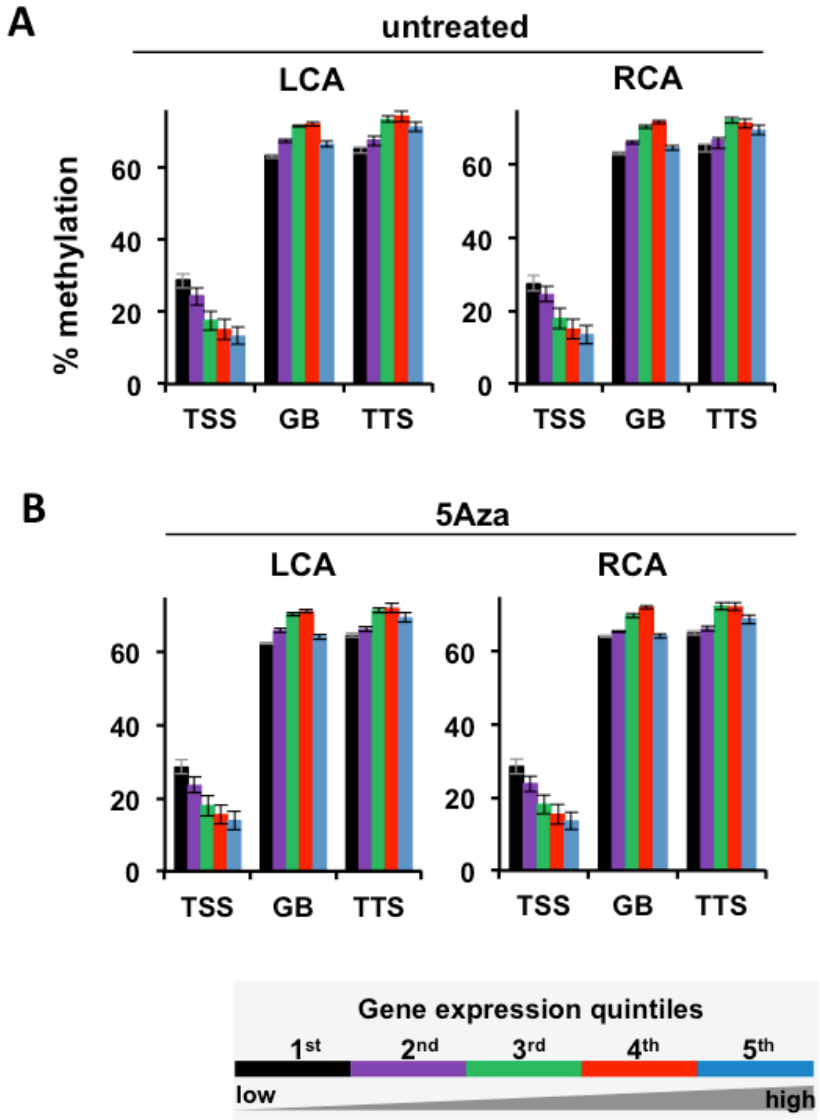

Figure 4.5: Global comparison of the RRBS data and the transcriptome data demonstrates that our datasets follow expected trends. Comparison of DNA methylation to gene expression for the LCA and RCA of (A) untreated and (B) 5Aza-treated mice for different regions of the genome: the transcription start site (TSS; the promoter is defined as within ± 1kb of a gene TSS), gene body (GB), and transcription termination site (TTS; defined as within ± 1kb of a gene TTS). The data for TSS shows the expected inverse correlation between promoter methylation and gene expression.

Emergent Methylation Patterns

An *a priori* methylation pattern analysis was performed to determine the global behavior of methylation changes across the samples at each CG site by ranking the methylation ratio of each gene promoter among the 4 groups. This revealed a pronounced emergent methylation pattern, wherein gene promoters in the LCA (2,086 out of 16,493 genes) were hypermethylated as compared to the RCA, Aza-LCA, and Aza-RCA (listed in decreasing order of methylation ratios, L>R>aL>aR; Figure 4.6). This supports our hypothesis that d-flow induces promoter hypermethylation in a subset of genes in the LCA in a DNMT-dependent manner.

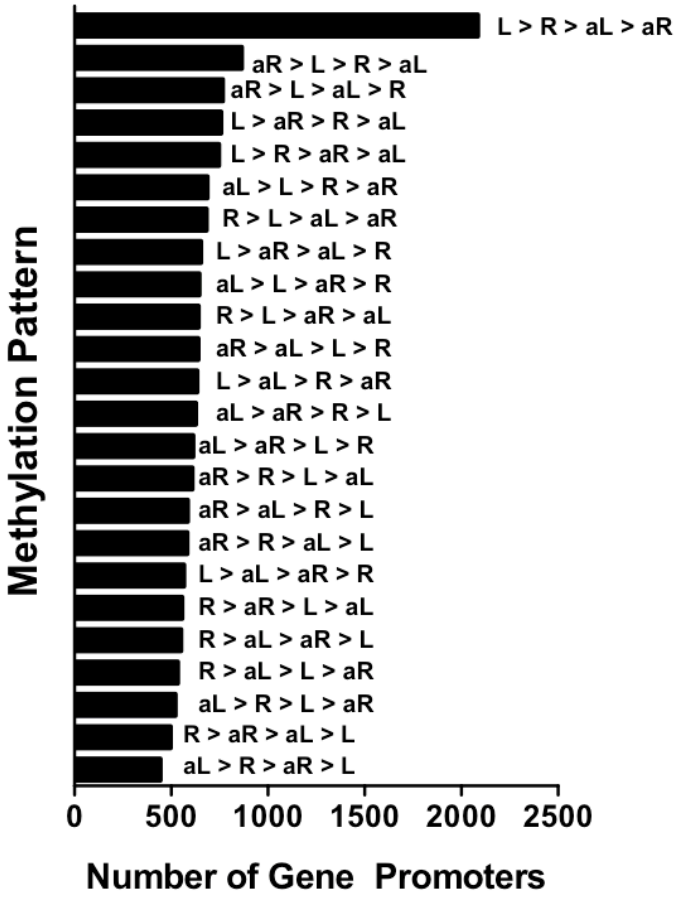

Figure 4.6: Emergent methylation pattern analysis. Analysis of gDNA methylation patterns existing in the RRBS datasets by ranking promoter methylation per gene for each RRBS sample (LCA=L, RCA=R, Aza-LCA=aL, and Aza-RCA=aR) revealed a pronounced emergent methylation pattern wherein gene promoters in the LCA are most methylated as compared to the RCA, Aza-LCA, and Aza RCA (in decreasing order).

Functional Genomic Region Methylation Analysis

In addition, and as expected based on literature reports, we found that overall promoter CGs were far less methylated (~29%) in comparison to genome-wide CGs (~78%) (Figure 4.7) [126]. These results were expected because it is well-established that promoter CGs are in general demethylated as compared to their genome-localized counterparts [163]. Enhancers had intermediate methylation levels (~43%) with slightly higher variability between the methylation levels of each enhancer due to the lower number of experimentally validated mouse enhancers (244) as compared to genes (~34,000) that existed in the VISTA enhancer database (Figure 4.7). Gene body methylation was slightly lower than genome-wide levels (~73%) and methylation near the 3'UTR in the transcription termination site (TTS) region was the most variable across RRBS samples, showing the strongest flow-dependent change at 2 days post-ligation (from 88% methylated in the RCA to 100% methylated in the LCA) (Figure 4.7).

Contrary to our hypothesis, however, the CG methylation status of each type of functional genomic region we analyzed was similar regardless of flow conditions and 5Aza treatment in the RCA, LCA, Aza-RCA and Aza-LCA (Figure 4.7), although this result is consistent with the small difference in the number of hypermethylated CG sites on the genome-wide level in LCA and Aza-LCA groups shown in Figure 4.3A and B. These results suggest a possibility that the 5Aza effect may be specific and limited to a relatively small number of genes.

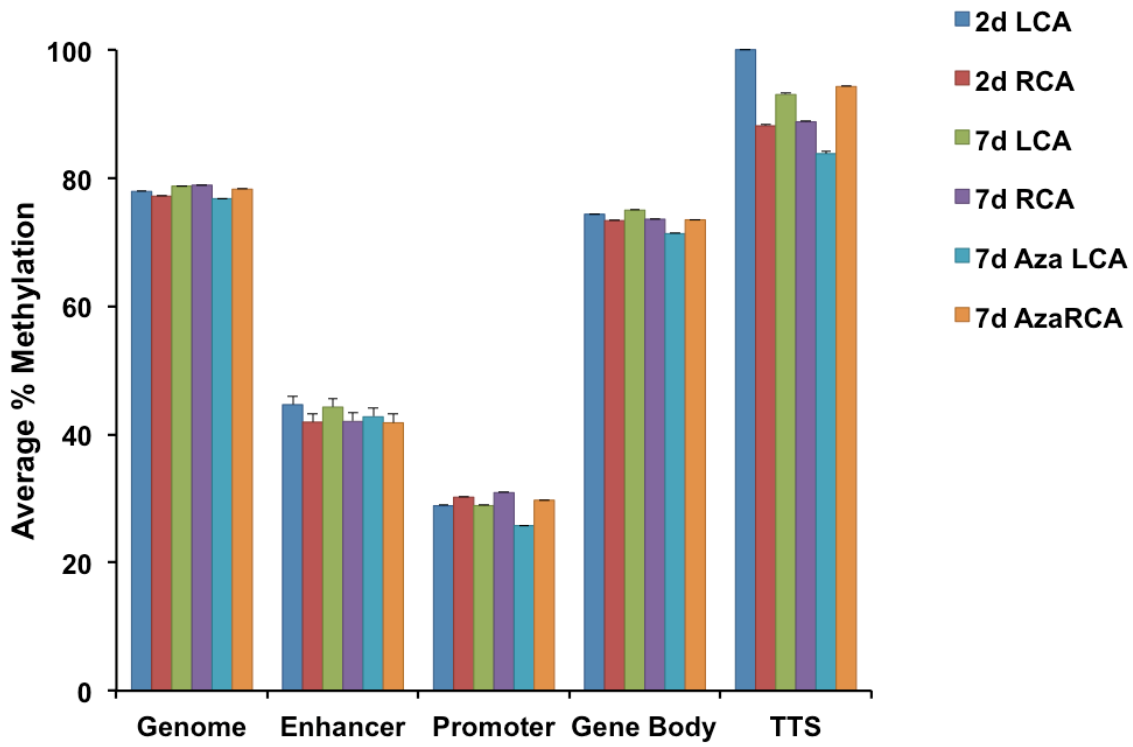

Figure 4.7: Global percent methylation for each of the RRBS datasets was determined using only those sites covered by all datasets (the intersection of the RRBS datasets). The values were calculated by averaging the methylation ratios across every CG site in the genome or only within specific regions, including enhancers (experimentally validated by the VISTA enhancer browser), promoters (+/- 1 kb from the transcription start site, or TSS), gene body (the region between the TSS and TTS), and transcription termination site (TTS; defined as within ± 1kb of a gene TTS).

Global and Promoter-specific Cyclic AMP Response Element CpG Methylation

We next examined whether the CRE elements across the genome display this property of d-flow-induced hypermethylation that can be prevented by 5Aza. We found that CRE sequences across the genome were nearly fully methylated (95-100%) in all four groups (Figure 4.8A). However, CRE elements within just the promoter regions showed significantly less methylation compared to that of genome-wide CREs (Figure 4.8B). In the LCA, the average percent methylation of promoter CREs was 8.7%, which

was decreased by ~2% in the Aza-LCA (Figure 4.8B). In both untreated and 5Aza-treated RCA, promoter CRE methylation was nearly zero, indicating the dramatic effect of s-flow in preventing methylation of promoter CRE elements in the RCA (Figure 4.8B). It is interesting to note that 5Aza treatment showed only a small reduction in average promoter CG site methylation while it dramatically decreased CG methylation at specific gene promoters such as *HoxA5, Klf3, Cmklr1,* and *Acvrl1*, indicating a targeted effect of 5Aza toward some gene promoters containing CREs.

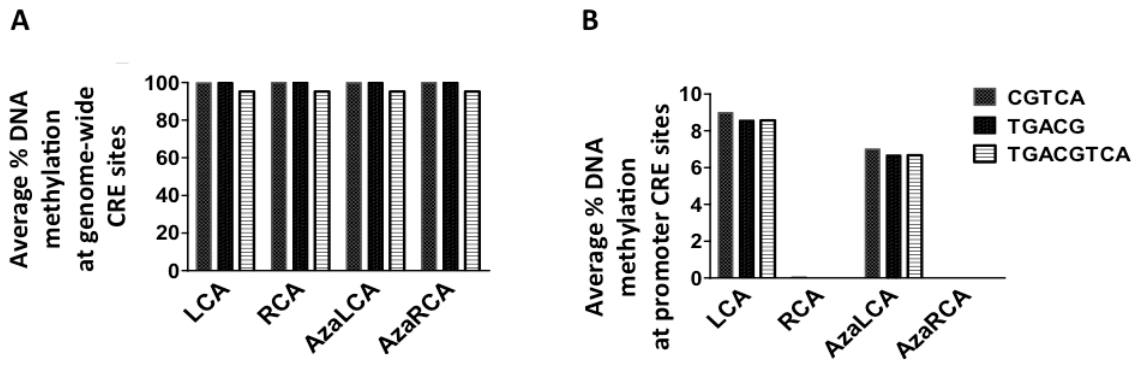

Figure 4.8: Global percent methylation for each of the RRBS datasets was calculated by averaging the methylation ratios across each CG site localized to CRE motifs in the genome (A) or only within promoter regions (B).

In Figure 4.8 we determined that on average, promoter CRE CG sites have ~10% increase in methylation in the LCA, and we next sought to determine whether there exists a subset of genes with a more dramatic change.

The Relationship Between Promoter CRE CpG Methylation and Gene Expression

Using the 33,826 promoter sequences obtained from the Mm9 Genome Assembly using the UCSC Genome Browser, our string search for the three CRE motifs resulted in 9,556 genes containing CGTCA in their promoter, 9,536 containing TGACG, and 863 containing TGACGTCA which could be mapped to CG sites covered by our RRBS

datasets for 4,286 (CGTCA), 3,326 (TGACG), and 503 (TGACGTCA) genes. A preliminary analysis plotting the gene expression (probe intensity as a surrogate marker) vs CRE CG methylation ratio showed that there was a strong correlation between the promoter CRE methylation status and gene probe intensity measured by the microarray study (Figure 4.9).

Based on these findings, we sought to discover whether flow affected a subset of these genes. We filtered the set of genes containing promoter CREs to determine whether there was a subset that had dramatic changes in promoter CRE methylation in d-flow conditions that could be linked with gene expression changes, and discovered a subset of genes for each CRE (Figure 4.10). Subsequently we focused the analysis to those genes with the most dramatically changed promoter CRE CG site corresponding to the most dramatic gene expression changes by thresholding so that only those genes that followed our expected trends (hypermethylation and lower probe intensity in the LCA vs. RCA) were kept (Figure 4.10). In this category, we observed that the most flow sensitive genes, occurring in the lower right hand quadrant of Figure 4.10D, contained a subset of genes we previously discovered by our initial filtering analysis, including HoxA5, Klf3, and Cmklr1 (Figure 5.4). We also discovered several novel flow sensitive genes, including Stim2, Lima1, Npr2, Slc29a1, and Pcdhga12 (Figure 4.10D). These genes display different sensitivities to 5Aza. For example, While Pcdhga12 and Lima1 expression increase due to 5Aza treatment, it does not appear to be due to a change in their CRE CG methylation status. This indicates that there may be an upstream signaling event that is affected by 5Aza and controls their downstream gene expression by a mechanism other than CRE CG methylation.

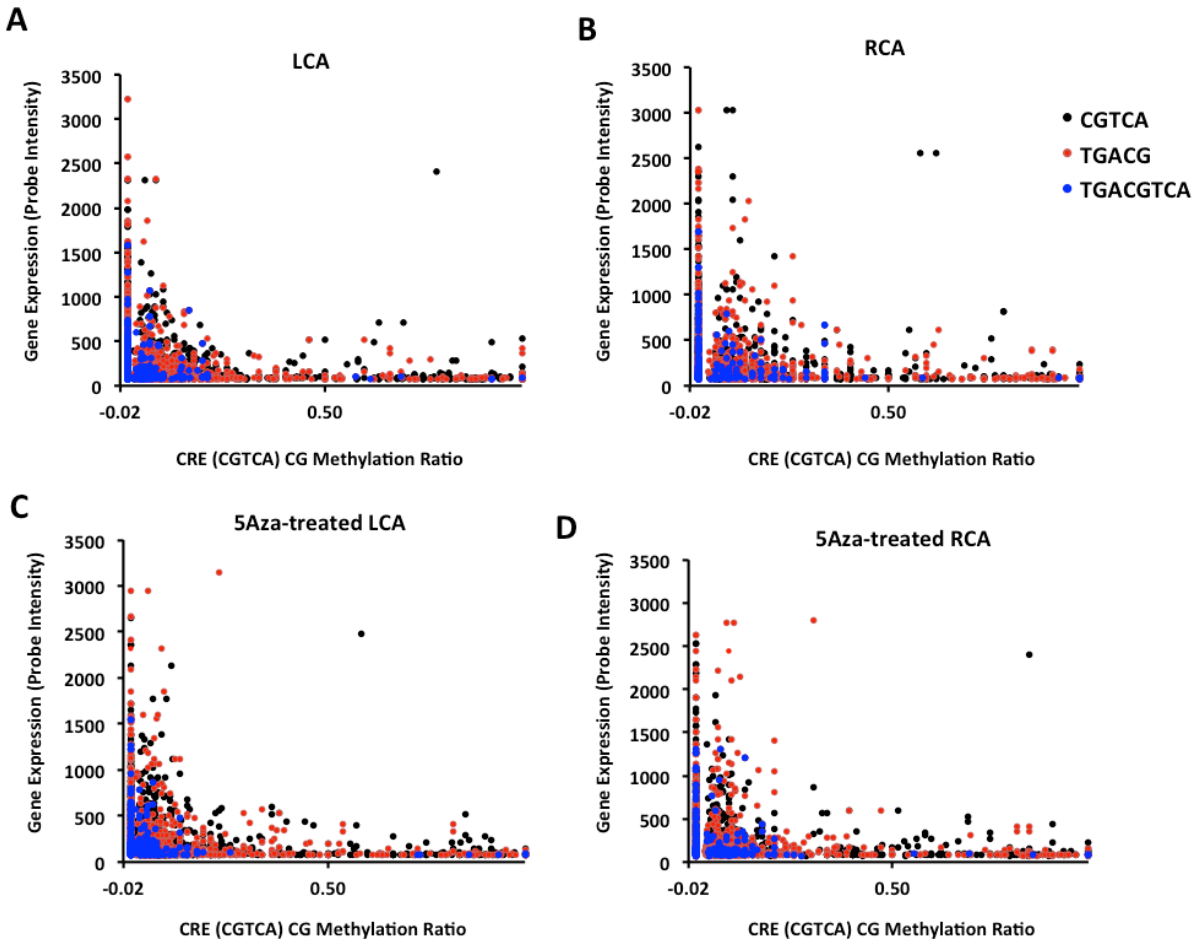

Figure 4.9: Global correlation between the methylation ratio of the promoter CRE and the corresponding gene's expression for each (A) the LCA, (B) RCA, (C) AzaLCA, and (D) AzaRCA, and for each CRE motif (CGTCA, TGACG, and TGACGTCA).

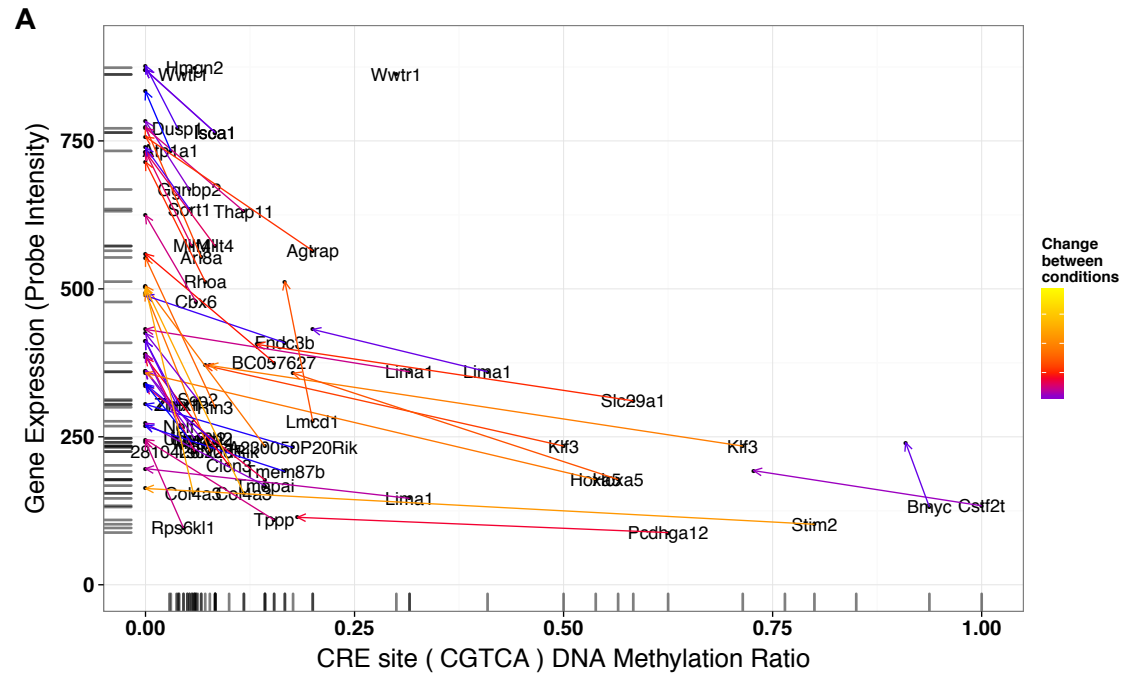

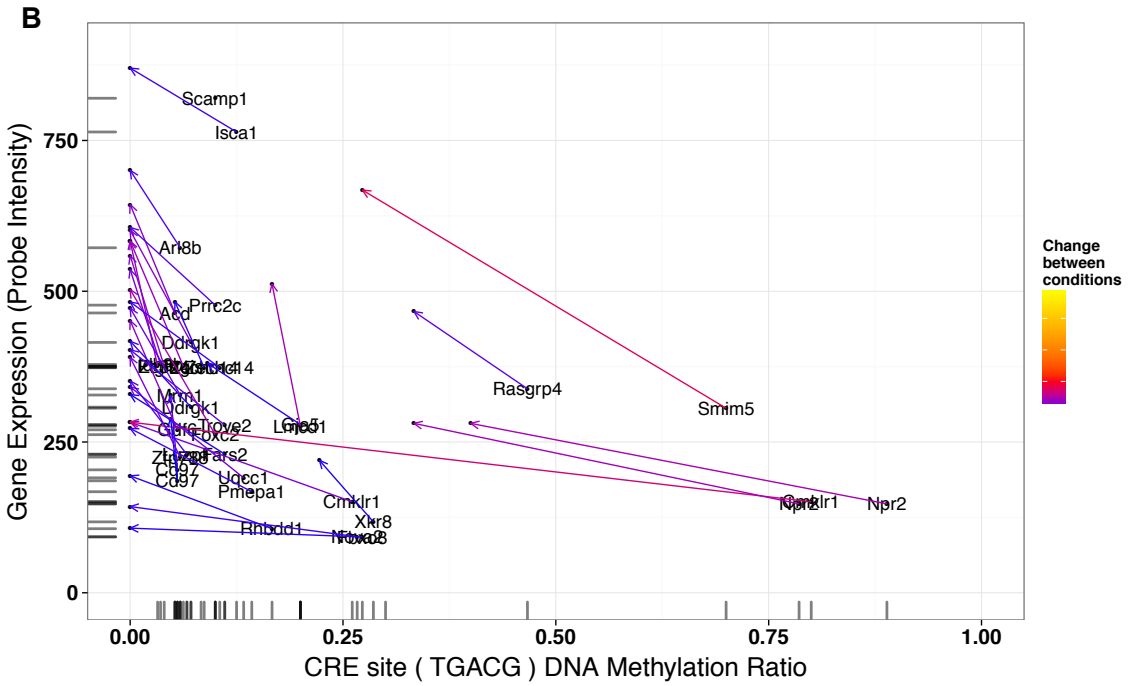

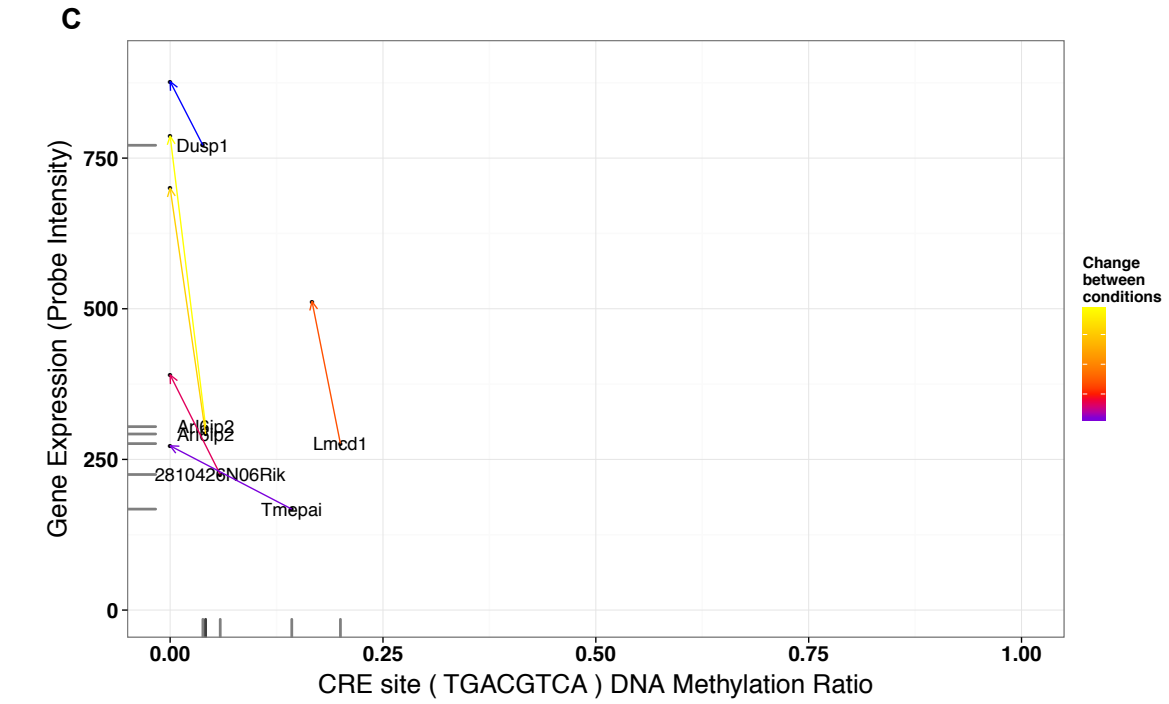

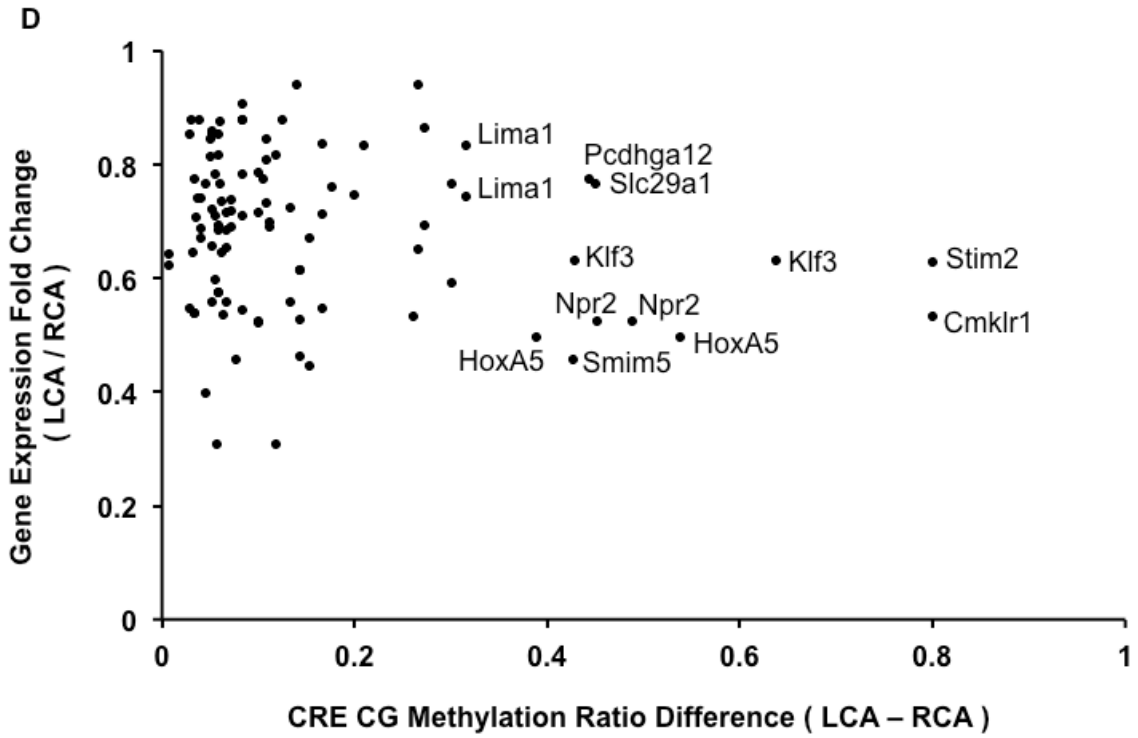

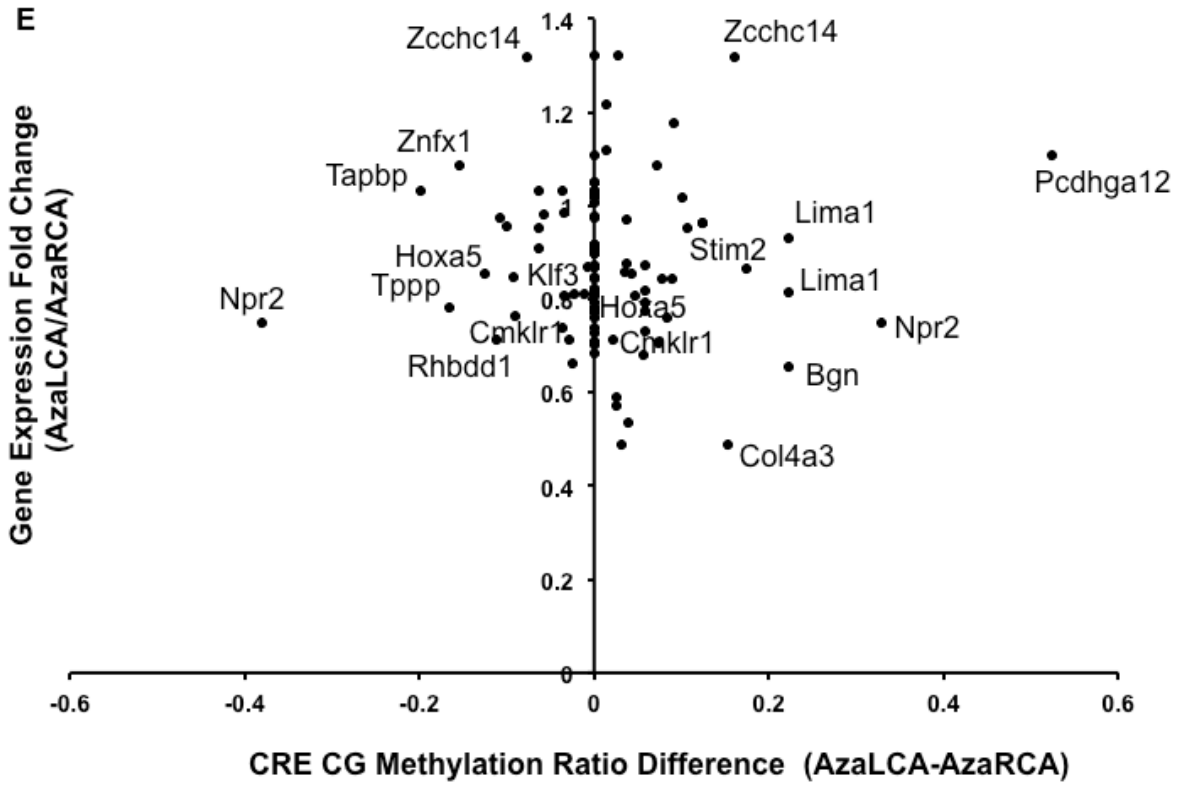

Figure 4.10: Trajectory and differentials plots showing the change between LCA and RCA for each CRE motif (CGTCA (A), TGACG (B), and TGACGTCA(C); (A-C) arrows point from LCA values for CRE methylation and gene expression to RCA values for the same). The differences between gene expression and methylation for all d-flow-hypermethylated CRE CG sites are plotted for the LCA v RCA (D) and the AzaLCA v AzaRCA (E).

Discussion

The studies described in Chapter 4 analyzing the concomitant endothelial methylome and transcriptome enabled us to examine the effects of shear stress and the role of DNMT1 in global EC DNA methylation and gene expression. We addressed the difficulty of tackling the widely unknown disease mechanism of atherosclerosis by limiting the scope of our project to a specific *a priori* hypothesis based on well-studied epigenetic mechanisms, and we recognize the limitations of such directed studies. We

used the knowledge that promoter CpG methylation causes gene supression to guide our studies and increase the likelihood of rapid, therapeutically actionable discoveries. The huge benefit of the data collected with our dual "omics" approach its availability and abundant potential for future analyses as new epigenetic mechanisms such as non-CpG methylation and functional genomic region methylation changes become clearer.

5Aza treatment showed a dramatic effect in rescuing the mechanosensitive gene expression patterns, recovering nearly 540 genes out of 569 genes that were suppressed by d-flow in the LCA (Chapter 5 Figure 1) while having minimal effect on the RCA gene expression (Figure 4.4D). The lack of any significant effect of 5Aza on the RCA gene expression was surprising, but it may indicate that the 5Aza effect is limited only to the d-flow-sensitive genes in the LCA. This may be due to the hyperproliferative nature of d-flow-exposed endothelial cells in the LCA while the RCA endothelial cells remain quiescent. This is consistent with the known effect of 5Aza, which functions in dividing cells such as those in leukemia and in the LCA endothelium. This notion is further corroborated by the lack of a widespread effect of 5Aza on the genome-wide DNA methylation patterns, although 5Aza did reduce the number of hypermethylated CG sites significantly for a limited subset of the methylome (from ~130,000 to ~55,000 sites in the LCA) and those CG sites may have a functional importance on gene expression (Figure 4.3A and B).

Given the known specificity of 5Aza action on highly proliferative myeloid cells as opposed to populations with a lower turnover rate, we were interested in exploring further whether the targeted effect of 5Aza in the LCA could be a result of altered rates on endothelial cell proliferation in altered shear stress conditions. It has been

demonstrated that overall rates of endothelial cell (EC) turnover in the artery are very low.[164] More specifically, ECs in atherosclerosis-resistant regions of the artery have an approximate life span of 12 months.[165] However, as demonstrated by multiple independent groups, when ECs are exposed to disturbed flow the turnover rate increases dramatically; ECs at these lesion-prone sites live for weeks and even shorter when animals age[165,166].

One of the most striking findings from our RRBS data was that CRE-localized promoter CG sites were not methylated at all (~0%) in the s-flow RCA, whereas CG sites across all regions of the promoter were ~30% methylated (Figure 4.7 and Figure 4.8). This suggests that there is an active hypomethylation mechanism that prevents these promoter CRE CG sites from being methylated.

Our computational analyses in Chapter 4 overlaying the concomitant endothelial methylome and transcriptome datasets that we collected were designed to ask very specific questions regarding the importance of DNA methylation in atherosclerosis development. We also performed *a posteriori* analyses to allow the data itself to dictate the direction of our further analyses. We found that DNMT inhibition by 5Aza rescues global gene expression in the LCA towards the s-flow state. While our first pass analysis did not demonstrate dramatic genome-wide or functional genomic element methylation changes under these conditions, we followed a specific hypothesis and found a subset of genes that had d-flow-induced promoter hypermethylation correlating with gene suppression in which both were 5Aza-reversible. Using systems biology to direct our second pass genome-scale bioinformatics analysis, we discovered that gene promoters containing cyclic AMP Response Elements (CRE) are preferentially methylated by d-

flow in a 5Aza-dependent manner. We further discovered that, on the genome scale, CRE hypermethylation corresponds to decreased gene expression. The studies presented in Chapter 4 used an "omics" approach to uncover a key gene regulatory network controlled by DNA methylation that plays an important role in the endothelial cell flow response.

CHAPTER 5 MASTER REGULATORS OF ENDOTHELIAL FUNCTION THAT ARE CONTROLLED BY DNA METHYLATION

Summary

To determine the mechanisms by which 5Aza inhibited atherosclerosis in vivo and endothelial cell inflammation in vitro, we tested the hypothesis that d-flow induces hypermethylation of anti-atherogenic endothelial cell genes at the promoter regions thereby silencing their expression, and that 5Aza treatment prevents this hypermethylation, leading to prevention of atherosclerosis.

The aim of Chapter 5 was to discover genes that are important in endothelial biology and regulated by DNA methylation. Detailed examination of the RRBS and microarray led to 11 genes that were hypermethylated and had suppressed expression in d-flow, and these were reversed by treatment with 5Aza. These included *HoxA5, Tmem184b, Adamtsl5, Klf3, Cmkrl1, Pkp4, Acvrl1, Dok4, Spry2, Zfp46,* and *F2rl1*. We also found that genes containing promoter cyclic AMP response elements (CRE) are enriched in these hypermethylated, d-flow suppressed genes.

Of note, *HoxA5* showed the most robust flow-dependent changes in promoter methylation and gene silencing that was significantly reversed by 5Aza treatment, indicating the potential importance of DNMT-dependent mechanosensitive gene regulation by promoter methylation. In addition to HoxA5, we found that the entire family of Hox genes, including the co-localized mir10 family, had strong flow-dependent methylation changes in the same manner as described for the 11 genes. A portion of Chapter 4 was published as follows: Dunn, J., Qiu, H., Kim, S., Jjingo, D., Hoffman, R., Kim, C. W., Jang, I., Son, D. J., Kim, D., Pan, C., Fan, Y., Jordan, I. K. Jo, H. Flow-

dependent epigenetic DNA methylation regulates endothelial gene expression and atherosclerosis. *J Clin Invest* 124, 3187-3199[16].

Introduction

Shear-Responsive Epigenetics

Histone Modifications and Chromatin Remodeling

Shear stress has been found to mediate chromatin remodeling and histone modifications and this is thought to play a role in shear-induced gene expression changes [33,34]. Early reports of shear-responsive epigenetics described novel pathways by which laminar shear mediates chromatin remodeling in cultured endothelial cells via histone H3/H4 acetylation and H3 phosphorylation [63,64].In ECs, LS activates genes with intrinsic histone acetyltransferase (HAT) activity, such as RSK-2 (ribosomal S6 kinase-2), MSK-1 (mitogen- and stress-activated kinase-1), and CREB/CBP (cAMP-responsive element–binding protein/CREB-binding protein) complexes. LS also deactivates histone deacetylases (HDACs), and induces histone H3/H4 acetylation and H3 phosphorylation in cultured ECs, and this regulates the key EC transcription factors Kruppel-like Factors 2 and 4 (Klf2, Klf4), and the EC-specific gene endothelial nitric oxide synthase (eNOS), via myocyte enhancer factor-2 (MEF2)[63,64,167]. Conversely, OS causes HDAC overexpression, and HDAC inhibition prevents OS-induced EC proliferation and EC inflammation in vivo and in vitro [168-170].

LS blocks HDACs from deacetylating the promoter of myocyte enhancer factor-2 (MEF2), and this enables MEF2 to be active and mediate KLF2 and eNOS expression in LS[167]. OS induces HDAC overexpression and accumulation in the nucleus via phosphatidylinositol 3-kinase (PI3K)/Akt signaling, which blocks the expression of anti-

inflammatory transcription factors Nrf2 (NF-E2-related factor 2, by HDAC2/3/5) and Mef2 (by HDAC1/2/3). It was further found that HDAC1/2/3 inhibition by siRNA or the class I-specific (HDAC1/2/3) inhibitor valproic acid prevented OS-induced EC proliferation in vivo and in vitro[168].

Endothelial-specific Gene Expression Mediated by Epigenetics

Early single gene epigenetic studies were mainly focused on defining markers of cellular differentiation down the endothelial lineage. Understanding the function and regulation of genes that have EC-specific expression is of keen interest to researchers because the loss of normally constitutively active EC genes is a hallmark of EC dysfunction.

Histone acetylation is important for both LS-induced and endothelial-specific expression of eNOS. HDAC inhibitor-induced increases in eNOS expression were linked to decreased DNA methylation of the eNOS promoter, and a trichostatin A (TSA) and 5Aza combination treatment synergistically increased eNOS expression in non-ECs [171]. This demonstrates the complementary interactions of histone modifications and DNA methylation. It was later found that the eNOS promoter is heavily methylated in non-ECs but demethylated in ECs, and that 5Aza treatment can induce eNOS expression in non-ECs that normally do not express eNOS [172]. This demonstrates that basal eNOS expression is regulated by DNA methylation. Methylation of the eNOS promoter blocks binding of Sp1, Sp3, and Ets1, and thus eNOS transcription [172].

In addition to eNOS, Roundabout 4 (Robo4) is an EC-specific gene whose expression is controlled by promoter DNA methylation in non-ECs which prevents binding of essential transcription factor SP1. Both the methylation and gene expression

status of Robo4 in non-ECs can be reversed by treatment with 5Aza. Interestingly, while Robo4 is suppressed by LS and eNOS is suppressed by OS, neither Robo4 nor eNOS has shear-responsive promoter DNA methylation changes [65,173-175]. Both eNOS and Robo4 lineage-specific epigenetic changes have been carefully dissected to show that Robo4-specific methylation patterns are established during the transition from ES to Flk-1+ mesodermal cells, while EC-specific eNOS DNA methylation and concomitant histone modifications appear in early proangiogenic cells [173,176].

Studies of epigenetically-moderated EC-specific gene expression were expanded to a repertoire of EC-specific genes, and highly important EC genes PECAM1 (CD31), von Willebrand factor (vWF), VE-cadherin, and intercellular adhesion molecule-2 have EC-specific promoter demethylation. As with other genes, 5Aza induced their expression in non-ECs and TSA had a synergistic effect [177]. These studies, taken together, demonstrate that DNA methylation is a key mechanism for EC-specific gene expression.

DNA Methylation is a Novel Epigenetic Mechanism that Regulates Endothelial Cell Responses to Shear Stress

Until recently, there had been little exploration on the potential for endothelial cell epigenetic responses to shear stress. In the spring of 2014, several research groups in vascular mechanobiology independently converged on the seminal finding that DNA methyltransferases are shear responsive proteins that regulate flow-mediated endothelial gene expression programs.

Klf4 is a key mediator of endothelial function and has been well documented to maintain an anti-inflammatory, quiescent endothelial state in unidirectional flow conditions[178-181]. Very recently, DNA methylation was discovered as a novel, flow-

mediated mechanism of endothelial Klf4 transcriptional regulation both in vitro and in vivo[65]. In this study, both DNMT3A expression and DNMT3A binding to the Klf4 promoter were found to increase due to d-flow. This led to DNA hypermethylation and decreased MEF2 binding. MEF2 is a key transcription factor that controls Klf4 upregulation in response to resveratrol in ECs[182]. DNMT inhibition by 5Aza or RG108 rescued Klf4 expression and reversed the DF-induced loss of downstream Klf4 targets eNOS and thrombomodulin (THBD), and the DF-induced overexpression of the proinflammatory monocyte chemoattractant protein-1 (MCP-1).

Shortly following these studies, Zhou et al. also reported that d-flow causes DNMT1 overexpression [66]. Comparing OS to pulsatile, unidirectional shear in HUVECs, they found that OS increases DNMT1 mRNA and protein levels, DNMT1 nuclear translocation, and 5-methyl-cytosine (5mC) content. 5Aza treatment inhibited the OS-induced DNMT1 expression and prevented increases in 5mC. Using a rat partial carotid ligation model, they demonstrated that d-flow also induced DNMT1 protein expression and increased 5mC content.

The genome-wide studies of DNA methylation and gene expression we recently completed provide a much broader view of flow-mediated global DNA methylation changes that regulate networks of genes and have a functional effect on atherosclerosis development in vivo.

The Homeobox and MicroRNA10 Gene Families

Hox genes are homeobox transcription factors whose homeodomains recognize and bind to specific DNA sequences, enabling the coordinate regulation of sets of genes. Hox

genes are highly conserved, known to be dysregulated in cancer, and are controlled in part by DNA methylation[183-188].

The four Hox gene clusters are well known to play key roles in developmental patterning of the anteroposterior axis of bilaterian animals. The Hox families exhibit a high level of self-interaction, forming 3-dimensional chromatin conformations known as a topological domains [189]. This global method of establishing a higher order genomic structure that also occurs specifically within Hox domains underscores the key importance of DNA domain interaction regulation by epigenetic mechanisms. Hox family members have been implicated in vascular remodeling, angiogenesis, and disease by orchestrating changes in gene expression, extracellular matrix, and integrins [190].

HoxA5 is known to regulate various vascular functions such as migration, angiogenesis, and inflammation by controlling specific endothelial genes [191-195]. HoxD3 and HoxB3 are pro-invasive, angiogenic genes that upregulate β3 and α5 integrins and Efna1 in ECs, respectively [196-199]. HoxA3 induces EC migration by upregulating metalloproteinase-14 (MMP14) and plasminogen activator urokinase receptor (uPAR) [200]. Conversely, HoxD10 and HoxA5 have the opposite effect of suppressing EC migration and angiogenesis, and stabilizing adherens junctions by upregulating TIMP1, downregulating uPAR and MMP14, and by upregulating Tsp2 and downregulating VEGFR2, Efna1, Hif1α and COX-2, respectively [192,193]. HoxA5 also upregulates the tumor suppressor p53 and Akt1 by downregulation of PTEN [194]. Suppression of HoxA5 has been shown to attenuate hemangioma growth [195]. HoxA5 has far-reaching effects on gene expression, causing ~300 genes to become upregulated upon its induction in breast cancer cell lines [201]. HoxA5 protein transduction domain overexpression prevents

inflammation shown by inhibition of TNFα-inducible monocyte binding to HUVECs [191,202]. Our study shows, for the first time, that HoxA5 is downregulated by d-flow in a DNA methylation-dependent manner and that HoxA5 suppresses endothelial inflammation.

Mir10a and Mir10b are located within the HoxB and HoxD clusters, respectively. Both the Hox and Mir10 families are highly evolutionarily conserved, known to be dysregulated in several cancers, and are controlled, at least in part, by DNA methylation.[183-188] Interestingly, Mir10a and Mir10b were both found to be suppressed, and HoxA1 overexpressed, in endothelial cells in pro-inflammatory, athero-susceptible disturbed flow regions both *in vitro* and *in vivo*.[79] Mir10a is a regulator of ~1,100 genes and was shown to directly target the inflammatory NFKB signaling network in endothelial cells.[79,203] The known shear-sensitive, anti-atherogenic, tumor suppressor gene Klf4 is experimentally validated as a direct target of Mir10b.[204] Mir10a and Mir10b differ by only one nucleotide and are experimentally validated to target a host of Hox genes. HoxA1, HoxA3, HoxD4, and HoxD10, are all targets of Mir10a, and Mir10b is thought to regulate HoxB4.[186,205,206] *De novo* methylation at the HoxD4 promoter has been observed as a result of Mir10a targeting.[206] While DNA methylation is known to be an important regulator of these genes under certain developmental and disease conditions, whether epigenetic DNA methylation in flow-exposed ECs is an important regulatory mechanism of atherosclerosis had not been previously explored. Additionally, Hox was not known to be a mechanosensitive gene family until now. The Hox/Mir10 clusters merit further study to understand their importance in EC biology and atherosclerosis.

Klf3

Klf3 is a transcription factor, but unlike Klf2 and Klf4, which are well-known mechanosensitive transcriptional activators, Klf3 is known to repress transcription[207-209]. Interestingly, both HoxA5 and Klf3 are suppressed in acute myeloid leukemia (AML), and the DNMT inhibitor 5Aza is used to treat this disease. While HoxA5 is known to be hypermethylated in AML, it has not yet been shown whether 5Aza directly targets these genes for demethylation [210,211]. AML is also treated with all-trans retinoic acid, a drug known to influence DNA methylation of a small number of specific genes and, also interestingly, this drug was shown to rescue Klf3 expression by an unknown mechanism [99,212]. It would be interesting to determine whether the therapeutic effects of 5Aza and all-trans retinoic acid on AML are mediated, at least in part, by rescuing Klf3 promoter hypermethylation.

Mechanosensitive MicroRNAs

Multiple reports in recent years have indicated the crucial role that miRNAs play in the endothelial response to shear stress, as the levels of these miRNAs are directly altered in response to shear stress. These miRNAs are known as mechanomiRs and many have now been directly implicated in the pathogenesis of atherosclerosis. While some miRNAs become upregulated in LS conditions, and thus would be considered atheroprotective, many become upregulated in OS conditions, and thus are thought to be atherogenic. Some atheroprotective miRNAs that have been discovered in vitro are miR-10a, miR-19a, miR-21, miR-23b, miR-101, and miR-143/145 [79,93,213-216].

Conversely, miR-21, miR-92a, and miR-663 are mechanosensitive atheromiRs that become highly expressed in OS conditions [217-219]. Also, miR-155 is a mechanosensitive

miRNA, but its role in atherosclerosis is unclear [220]. Given the fact that miRNAs have hundreds of gene targets, unsurprisingly, many miRNAs (such as miR-21, 181, and 155) have played both anti-atherogenic and pro-atherogenic roles depending on cell type and stimulus [221].

Although many miRNAs have been studied under in vitro conditions of shear stress, some miRNAs have directly been studied in mouse models of atherosclerosis. In 2013, our group discovered that a miR-712 becomes highly upregulated in endothelial regions exposed to d-flow in our murine model of disturbed flow-induced atherosclerosis. Furthermore, repression of miR-712 binding (by locked nucleic acid anti-miRNA) to its main target, tissue inhibitor of metalloproteinases (TIMP3), drastically inhibited endothelial dysfunction and atherosclerosis [222]. Additionally, we found that the human ortholog of miR-712, miR-205, is also mechanosensitive and mediates the same effects both in atherosclerosis and in abdominal aortic aneurysm [223]. Other miRNAs that have been demonstrated to directly play a role in atherosclerosis are miR-92a and miR-181b. Loyer and colleagues demonstrated that miR-92a inhibition by antagomiR treatment inhibited endothelial dysfunction and subsequent atherosclerosis in high-fat diet-fed LDL receptor$^{-/-}$ mice, whereas Sun et al. demonstrated that systemic injection of miR-181b in ApoE$^{-/-}$ mice led to its overexpression in endothelial cells and peripheral blood mononuclear cells (PBMCs) and subsequently inhibited NFκB activation and atherosclerosis development [224,225].

Methods

A Priori Filtering to Discover Mechanosensitive Genes Regulated by DNA Methylation Through DNA Methyltransferase

The differentially methylated and differentially expressed genes were parsed according to our hypothesis that d-flow–induced hypermethylation at the promoter suppresses gene expression, and that this could be reversed by 5Aza. We performed thresholding to filter out genes that are hypermethylated in the promoter and suppressed by d-flow in a 5Aza-preventable manner. Specifically, we looked for differentially methylated regions (DMRs) in gene promoters, defined by TSS ± 1 kb containing a minimum of 10 CG sites with a minimum difference in percent methylation (Δ % methylation = % methylation in the LCA – % methylation in the RCA) of 10. There were 421 such genes. We further parsed this list to genes whose promoter hypermethylation in LCA was prevented by 5Aza (Δ% methylation = % methylation in the Aza-LCA – % methylation in the Aza-RCA < 5), and this resulted in 335 genes. For the mRNA expression criteria, we looked for genes downregulated in LCA versus RCA (LCA/RCA < 0.67), which resulted in 569 genes, and then we further looked for genes whose expression in LCA was rescued by 5Aza (resulting in 540 genes). By combining these methylation and gene expression criteria, we extracted 11 genes that have d-flow–inducible hypermethylation and gene suppression that can be prevented by 5Aza. Of the resulting 11 genes, systems biology analysis via MetaCore revealed common regulation by the CREB transcription factor in 5 of the 11 genes (only 4 of which had RRBS coverage specifically at the CRE sequence).

Systems Biology Analysis Led to CREB as a Key Network Regulator

The GeneGO MetaCore program by Thomson Reuters is a data mining and pathways analysis tool that enables systems biology analysis of mammalian cells incorporating data from ligand-receptor binding interactions, cell signaling and regulation pathways, and metabolic pathways. We used this tool as recommended by the company to examine whether there were any common network regulators in our parsed gene set.

The discovery of a common transcription factor as a central node in the systems biology analysis of the gene set led to a JASPAR analysis to determine the consensus binding motif, and the specificity of binding, for CREB1.

The promoter sequences of the 11 genes (+/-1kb from the TSS) were obtained from the UCSC Genome Browser using the NCBI37/mm9 genome assembly. A string search was done for the consensus CREB binding motifs (TGACGTCA, TGACG, and CGTCA) on the positive strand of the promoter sequence, although strand configuration is unimportant due to the palindromic nature of the CRE sequence.

QPCR and Single Locus Bisulfite Sequencing

qPCR was done as described in Chapter 3 methods, and qPCR primers are listed in Bisulfite sequencing primers for HoxA5 (Chapter 3 Table 1) were designed using the MethPrimer program [226]. Genomic DNA collected from 4 mouse carotid arteries as described previously was pooled, purified using the DNeasy Blood and Tissue Kit (Qiagen) and was bisulfite converted using the Epitect bisulfite conversion kit (Qiagen). 10ng of bisulfite-converted DNA was subjected to PCR amplification using custom-design BS-PCR primers (Chapter 3 Table 1) at a Tm of 59.5°C.

siRNA and monocyte adhesion

siRNA and monocyte adhesion studies were performed as described in the methods section of Chapter 3. Dharmacon SmartPool siRNAs for HoxA5 and Klf3 were used.

Results

A Priori Filtering to Discover Mechanosensitive Genes Regulated by DNA Methylation Through DNA Methyltransferase

In order to determine the most robustly flow-sensitive genes that are controlled by DNA methylation, we compared the list of mechanosensitive genes that were hypermethylated at their promoter and downregulated in the LCA in a 5Aza-dependent manner to determine the genes that exhibit the expected correlation between methylation and gene expression. This comparative analysis revealed 11 flow-sensitive genes that were hypermethylated at their promoter and silenced by d-flow that could be rescued by 5Aza (Figure 5.1). These included *HoxA5, Tmem184b, Adamtsl5, Klf3, Cmkrl1, Pkp4, Acvrl1, Dok4, Spry2, Zfp46,* and *F2rl1*. Of note, *HoxA5* showed the most robust flow-dependent changes in promoter methylation and gene silencing that was significantly reversed by 5Aza treatment, indicating the potential importance of DNMT-dependent mechanosensitive gene regulation by promoter methylation.

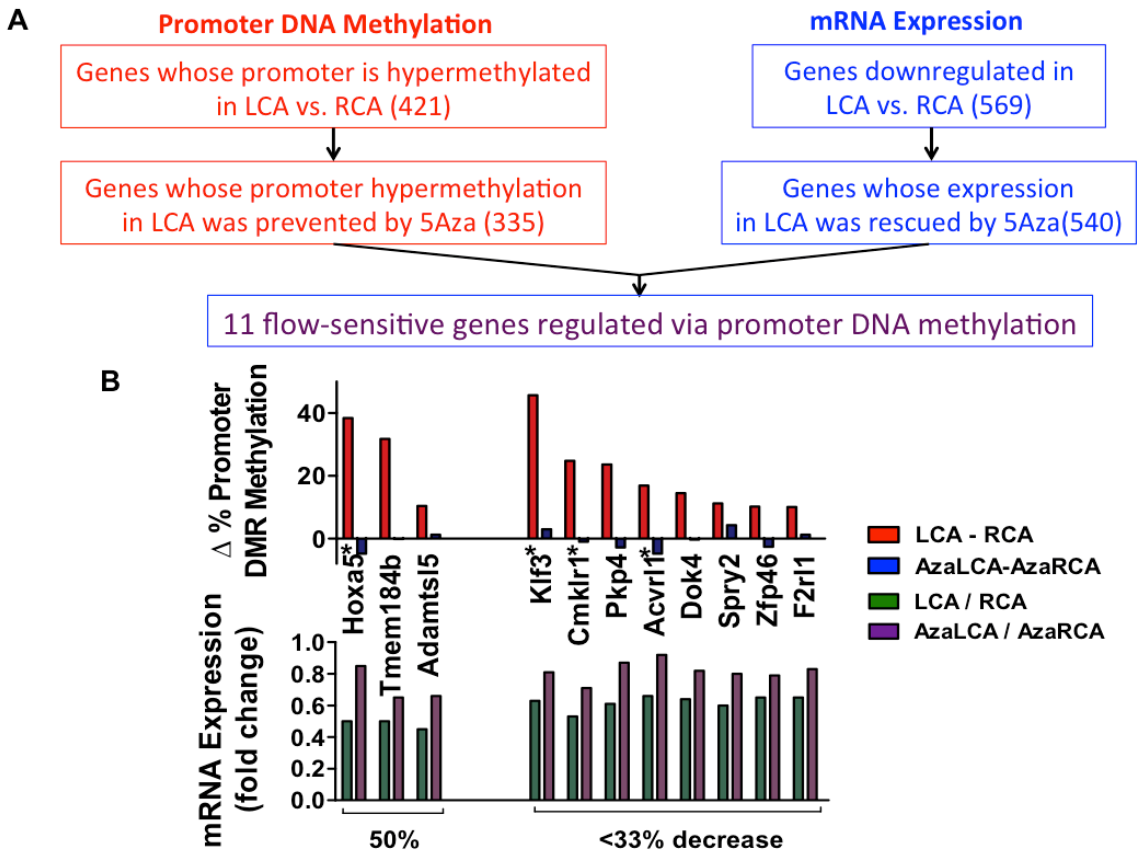

Figure 5.1: D-flow induces promoter hypermethylation corresponding to suppressed expression in a subset of flow-sensitive genes. (A and B) To identify mechanosensitive genes that are hypermethylated in their promoter and their gene expression downregulated in a 5Aza-dependent manner, the genes with hypermethylated promoters in the LCA that were rescued by 5Aza treatment were selected. Using the microarray data, the mechanosensitive genes that were downregulated by more than 33% in the LCA and rescued by 5Aza treatment were selected. These 2 selected gene lists were compared with each other, result- ing in 11 genes that were hyper- methylated in the promoters and downregulated in a 5Aza-dependent manner (data are shown as the mean ± SEM. *$P < 0.05$; **$P < 0.05$). Gene names containing hypermethylated promoter CRE sites in B are indicated with a single asterisk (*).

Systems Biology Analysis Uncovered Cyclic-AMP Response Element Binding Protein (CREB) as a Common Network Regulator

To explore whether there are any functional regulatory elements that are common within the promoter regions among the 11 genes, we first searched for common regulatory mechanisms of these genes. The systems biological analysis using GeneGo

MetaCore (Thomson Reuters) with these 11 genes as the input predicted CREB1 (CRE binding protein) as the transcription factor with the highest potential connectivity. Using JASPAR, we determined the CREB1 binding motif to be TGACGTCA (Figure 5.3). A thorough literature review revealed that CREB binds to both the full palindromic and also half sequence motifs (TGACGTCA, TGACG, and CGTCA).

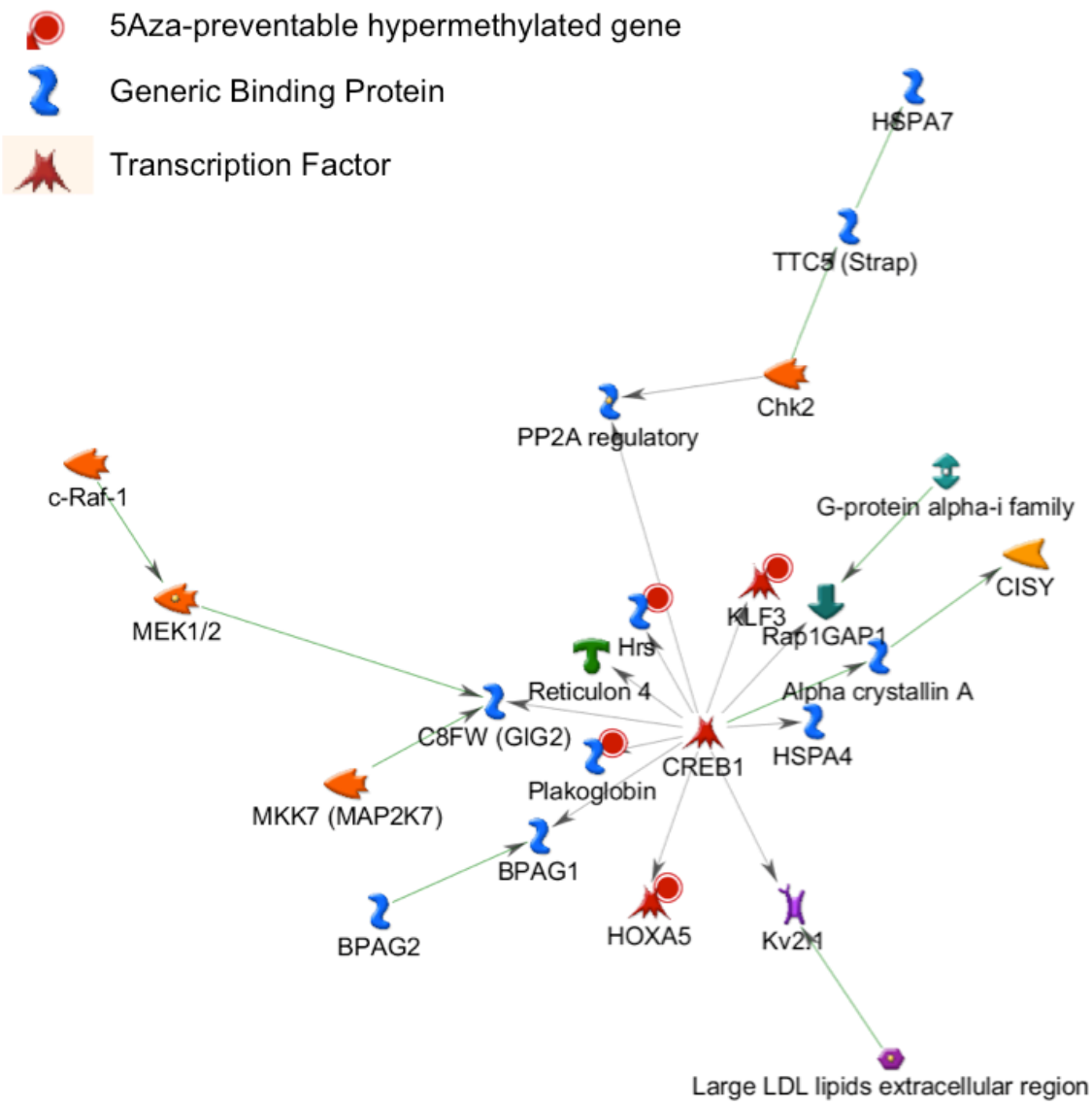

Figure 5.2: Systems biology analysis using MetaCore GeneGO shows CREB as a common network regulator in the parsed gene list. This zoomed in view of the

interaction network shows those 5Aza-rescuable, hypermethylated genes (HoxA5 and Klf3) predicted by MetaCore to have a direct binding interaction with CREB. Further sequence analysis revealed that 5 out of the 11 genes contain CREB binding sites (Figure 5.4).

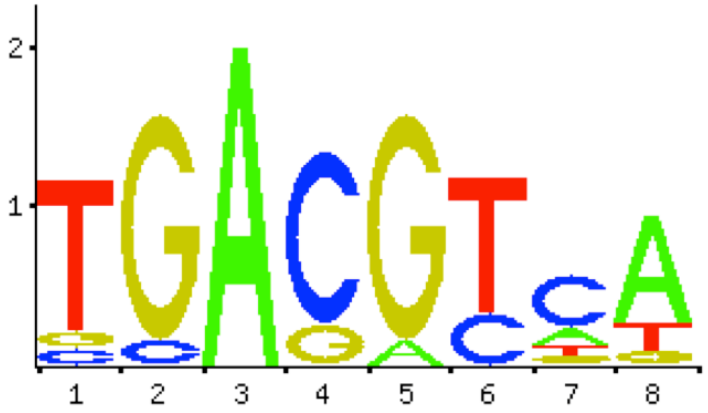

Figure 5.3: JASPAR TFBS search revealed the consensus CREB binding motif sequence of TGACGTCA. The size of the nucleotide corresponds to its importance in the binding interaction, with the third A being key to the interaction, and the other nucleotides having allowable variability of different levels and with different possible substitutions.

The Subset of D-Flow Hypermethylated and Suppressed Genes That Are 5Aza-Rescuable Are Enriched For Genes with CRE Motifs in Their Promoter

This led us to a computational sequence analysis designed to look for the full palindromic or half CRE sequences (TGACGTCA, TGACG, and CGTCA) within the differentially methylated regions (DMR) of the 11 gene promoters (+/- 1kb from the transcription start site). This search revealed that 5 of the 11 gene promoter DMRs

contained CRE sites, including *HoxA5, Klf3, Cmklr1, Acvrl1 and Spry2*. We then examined the DNA methylation status of these gene promoter DMRs at the specifically the CRE CG site and found that *HoxA5, Klf3, Cmklr1,* and *Acvrl1* indeed showed significant hypermethylation at this CG in the LCA, which was prevented by 5Aza treatment (Figure 5.4A-D). For example, percent methylation of the *HoxA5* promoter CRE CG site was dramatically higher in the LCA (55.6%) as compared to the RCA (11.5%), the Aza-LCA (17.2%), and the Aza-RCA (20.0%). The promoter CRE CG site in *Spry2*, however, was not fully covered by our RRBS data; therefore we could not determine its flow- and 5Aza-dependency.

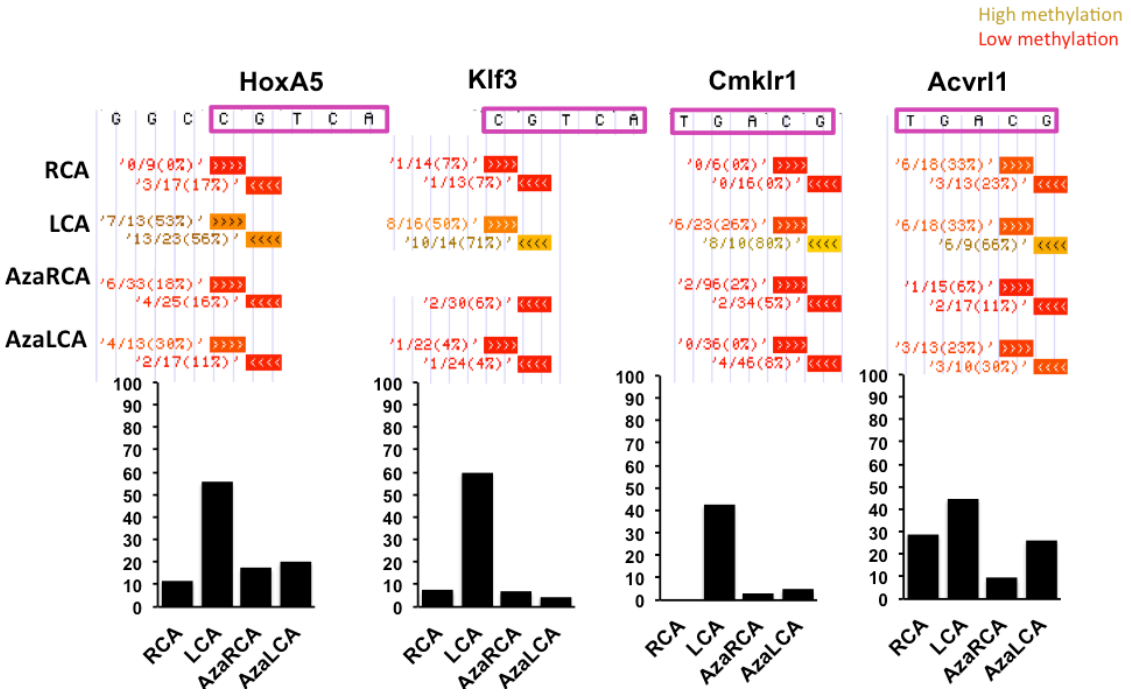

Figure 5.4: Gene promoters containing CRE are preferentially methylated by d-flow in a 5Aza-dependent manner. Of the 11 genes in Figure 5.1, *HoxA5*, *Klf3*, *Cmklr1*, and *Acvrl1* contain CREs in their promoter differentially methylated regions (DMRs). The methylation ratios (the number of methylated sequencing reads divided by the total number of sequencing reads) for the CG site within the CRE are displayed for each genomic DNA strand for the RCA, LCA, Aza-RCA, and Aza-LCA, and average values are shown below in bar graphs.

Detailed analysis of the RRBS DNA methylation data in the *HoxA* gene cluster is shown in Figure 5.5 using a UCSC genome browser track to display our RRBS data at the nucleotide resolution. The *HoxA5* promoter region was clearly hypermethylated in the d-flow LCA as compared to the s-flow RCA, the Aza-LCA, and the Aza-RCA (Figure 5.5A). This RRBS result was further confirmed by manual bisulfite sequencing of additional endothelial gDNA obtained from the RCA, LCA, Aza-RCA, and Aza-LCA, validating the RRBS data (Figure 5.5A). Further, we validated the *HoxA5* expression data obtained from the microarray study (Figure 5.5B) by qPCR (Figure 5.15C). The qPCR result showed that *HoxA5* expression was downregulated in the LCA by more than 50% compared to the RCA and was reversed by the 5Aza treatment, validating the microarray result.

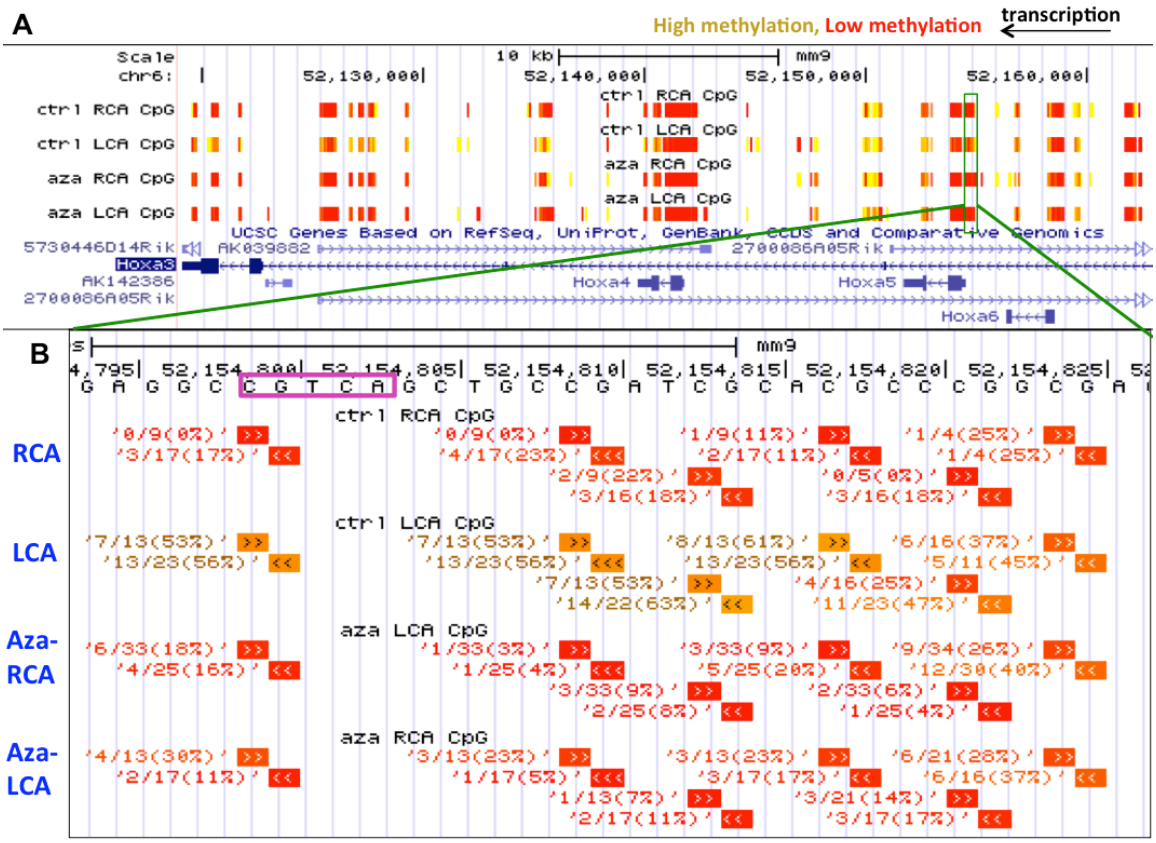

Figure 5.5: RRBS analysis reveals d-flow–induced *HoxA5* promoter hypermethylation. (A) DNA methylation data obtained from the RRBS study are shown using a University of California, Santa Cruz, browser track that displays our RRBS data sets. High methylation is denoted in yellow and low meth- ylation in red. (B) A zoomed-in view of the *HoxA5* methylation patterns displaying ratios with the number of methylated sequencing reads divided by the total number of sequencing reads at each individual CG site.

HoxA5 and Klf3 are Flow-sensitive Genes With Previously Unstudied Roles in Endothelial Biology

Given the potential role of the transcription factors HoxA5 and Klf3 as master regulators of gene expression networks, we further examined their relevance to the endothelial flow response. We found that HoxA5 is strongly suppressed in response to disturbed flow (DF) in vivo by microarray and qPCR (Figure 5.5C and D, respectively), and oscillatory shear (OS) in HUVECs in vitro at both the mRNA and protein level

(Figure 5.6A and B). We found that the CRE in the promoter of HoxA5 is homologous between mouse and human, further implicating its potential importance in human pathology, as well as enabling further study of HoxA5 in cultured human ECs (Figure 5.7).

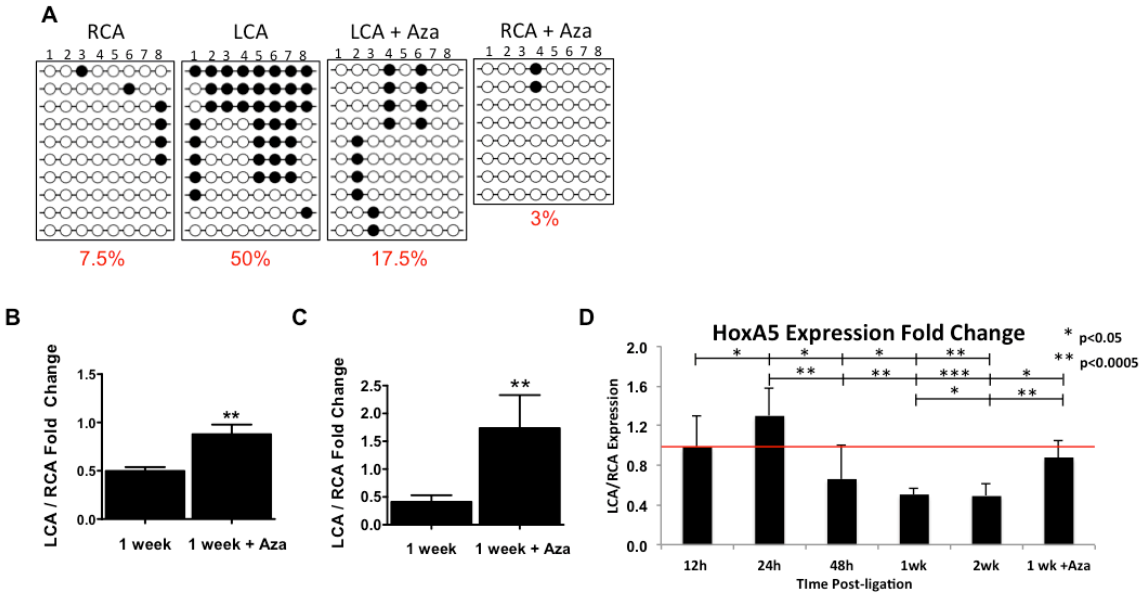

Figure 5.6: D-flow induces DNA hypermethylation of the *HoxA5* gene promoter and downregulates its expression in a 5Aza-dependent manner. (A) DNA methylation at the *HoxA5* promoter region in endothelial-enriched genomic DNA from the LCA and RCA at 1 week after partial ligation from mice treated with saline or 5Aza was fur- ther examined in independent samples by bisulfite sequencing. Black and white circles represent methylated and unmethylated cytosines, respectively. Eight CG sites (denoted by the columns) were probed in this assay, and 8 to 10 colonies (denoted by the rows) were chosen for analysis. Percentages below the figures denote the aver- age percent methylation for this region of the *HoxA5* promoter. (B and C) *HoxA5* gene expression was examined in endothelial-enriched RNA from the LCA and RCA obtained at 1 week after partial ligation from saline- or 5Aza-treated mice by microarray analysis. Data for B are shown as the mean ± SEM. **$P < 0.01$, $n = 3$ each and were validated by qPCR. Data for C are shown. (D) *HoxA5* gene expression was examined in endothelial-enriched RNA from the LCA and RCA obtained over a timecourse using microarray analysis.

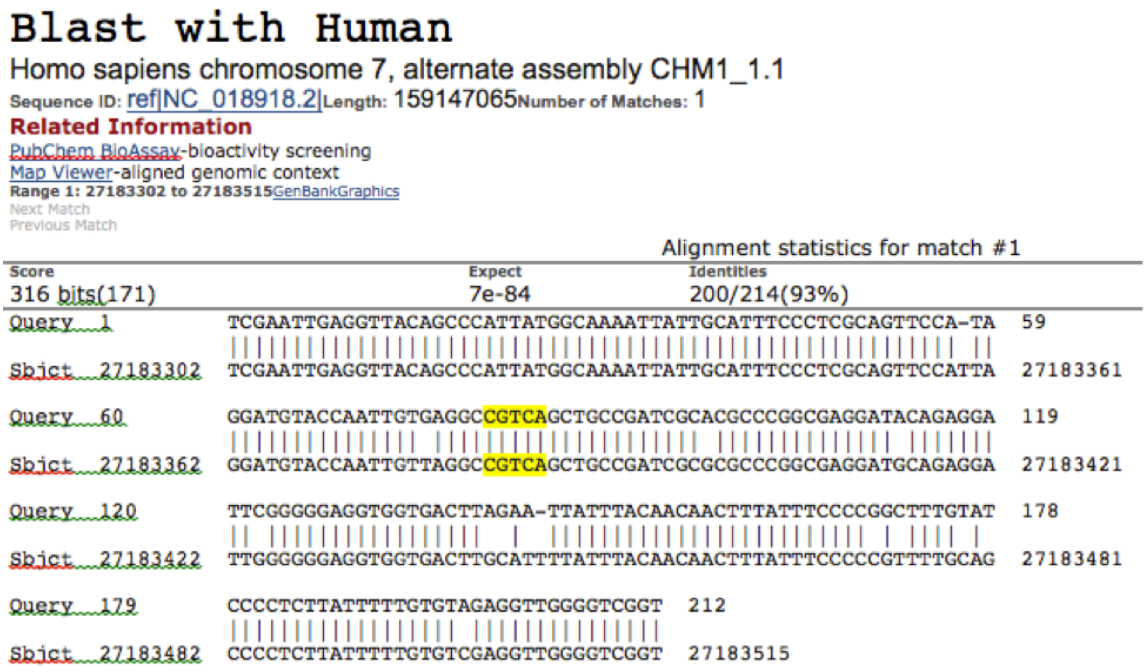

Figure 5.7: The sequence of the promoter CRE and surrounding region in HoxA5 is homologous in mouse (Sbjct) and human (Query).

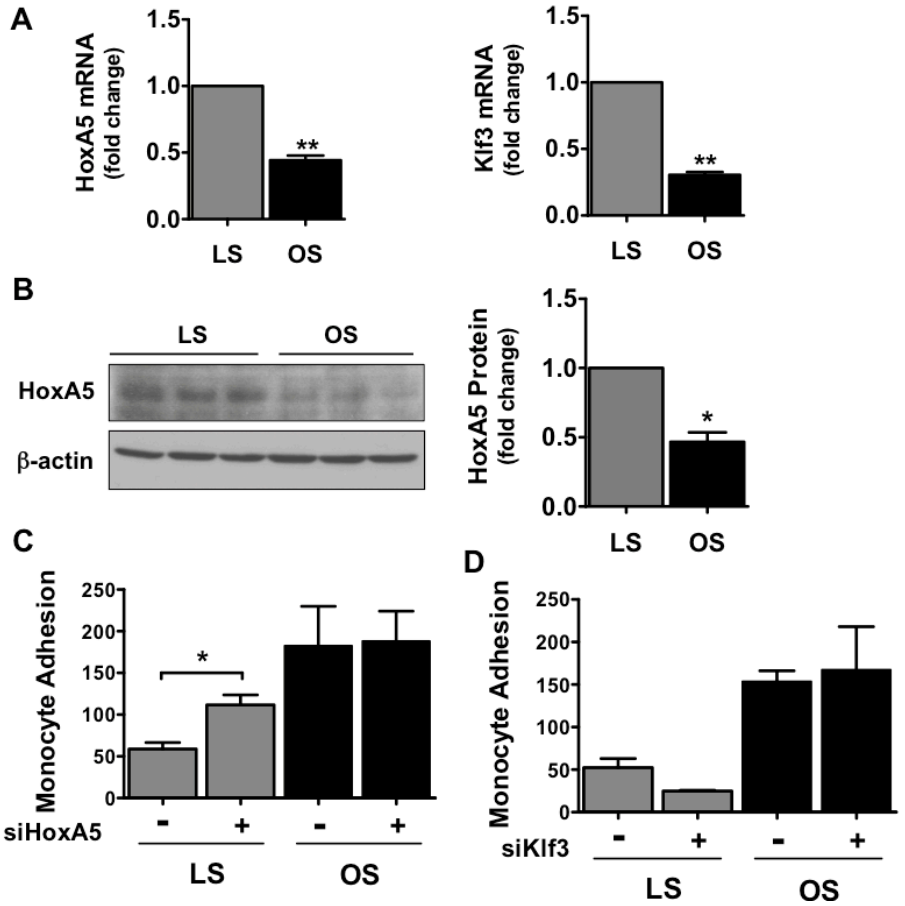

Figure 5.8: HoxA5 and Klf3 are suppressed by OS in vitro, and HoxA5 increases LS-suppressed endothelial inflammation. (A) *HoxA5* expression and *Klf3* expression are suppressed by OS compared with LS.HUVECs exposed to LS (15 dyn/cm2) or OS (±5 dyn/cm2, at 1 Hz) for 24 hours were used for qPCR using 18S as an internal control (*n* = 6 each, data are shown as the mean ± SEM. ***P* < 0.01). (B) Western blot analysis for HoxA5 was performed on the same samples from A using β-actin as the loading control. The bar graph shows the ImageJ Western blot quantification normalized to β-actin (*n* = 3 each, data are shown as the mean ± SEM; **P* < 0.05). (C and D) HUVECs were pre- treated with siRNA to *HoxA5* or *Klf3* (100 nM for 24 hours), and subsequently exposed to OS or LS for an additional 24 hours. Following shear, endothelial inflammation was determined by quantification of the number of THP-1 monocytes adhered to sheared endothelial cells (*n* = 3 each, data are shown as the mean SEM. **P* < 0.05)

Similarly, Klf3 mRNA expression is suppressed by d-flow both in vivo (Figure 5.1) and in vitro (Figure 5.6A). We were not able to determine Klf3 protein due to a lack of adequate antibody for western blot. To analyze the role of these transcription factors in endothelial inflammation, we performed monocyte adhesion assays using siRNAs to each HoxA5 and Klf3 in HUVECs under shear. We found that in the LS condition,

knockdown of HoxA5 significantly increased monocyte adhesion to HUVECs, simulating the OS condition of increased inflammation (Figure 5.6C). However, knockdown of Klf3 did not have a significant effect on endothelial inflammation, suggesting its potential importance in other flow-responsive pathways (Figure 5.6D).

We attempted to recapitulate the methylation changes seen in the HoxA5 promoter in vivo using cultured ECs but these changes do not appear to occur in cultured cells. We believe this can be attributed to the methylation changes that occur as a result of culturing cells under static, no flow conditions which has been well documented [227,228].

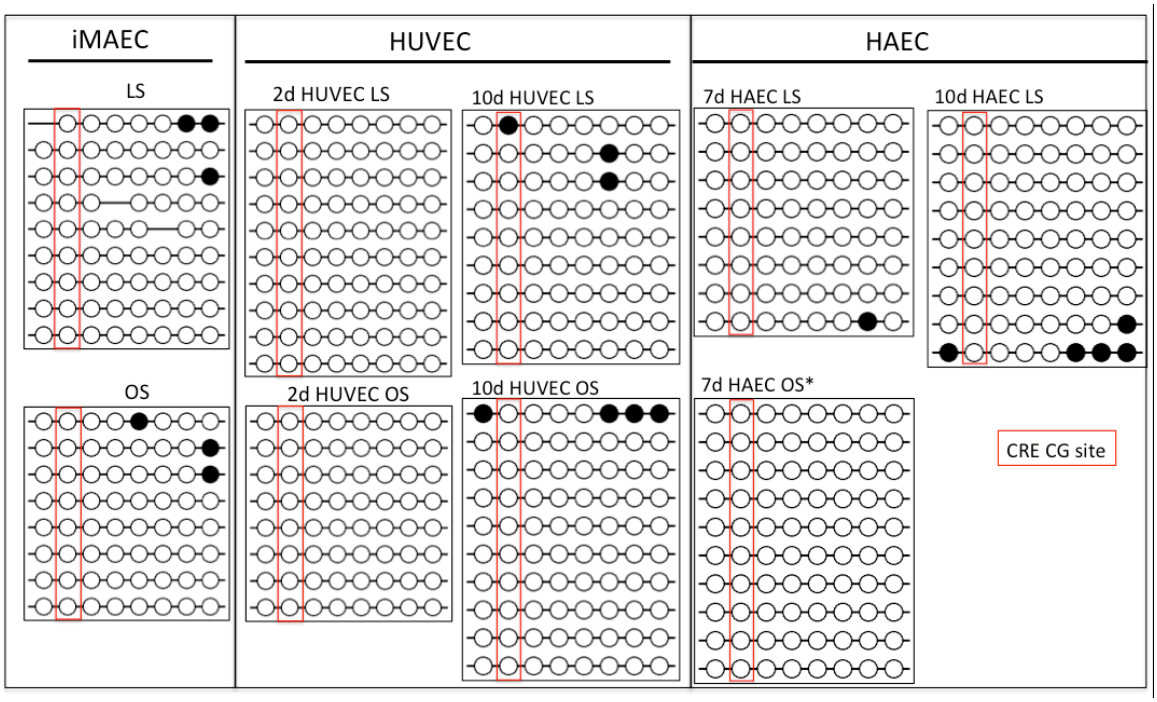

Figure 5.9: *In vitro* HoxA5 bisulfite sequencing using various endothelial cell types at multiple shear timepoints (immortalized mouse aortic endothelial cells (iMAEC) for 24 hour shear using the cone and plate system, human umbilical vein endothelial cells (HUVEC) and human aortic endothelial cells (HUVEC) both using the Ibidi system for long-term shear) in vitro shows that HoxA5 is essentially demethylated in all cases of cultured ECs regardless of flow conditions. The equivalent and homologous CRE CG site to our RRBS data is boxed in red.

We examined the expression of the 5 potentially CREB-regulated genes in vitro to determine whether their flow- and 5Aza-sensitivity demonstrated in vivo could be recapitulated in vitro. After 5 days of 5Aza treatment, HUVECs were subjected to 24h of shear and qPCR was done to determine gene expression levels. We found that OS downregulates expression of HoxA5, Klf3, and Cmklr1 (Figure 5.10). Additionally, 5Aza rescues expression of Klf3, Cmklr1, and Spry2 in LS, and also slightly rescues their expression in OS (Figure 5.10). These results also demonstrate the limitations of in vitro studies using cultured ECs, which often do not recapitulate biological events that occur in vivo.

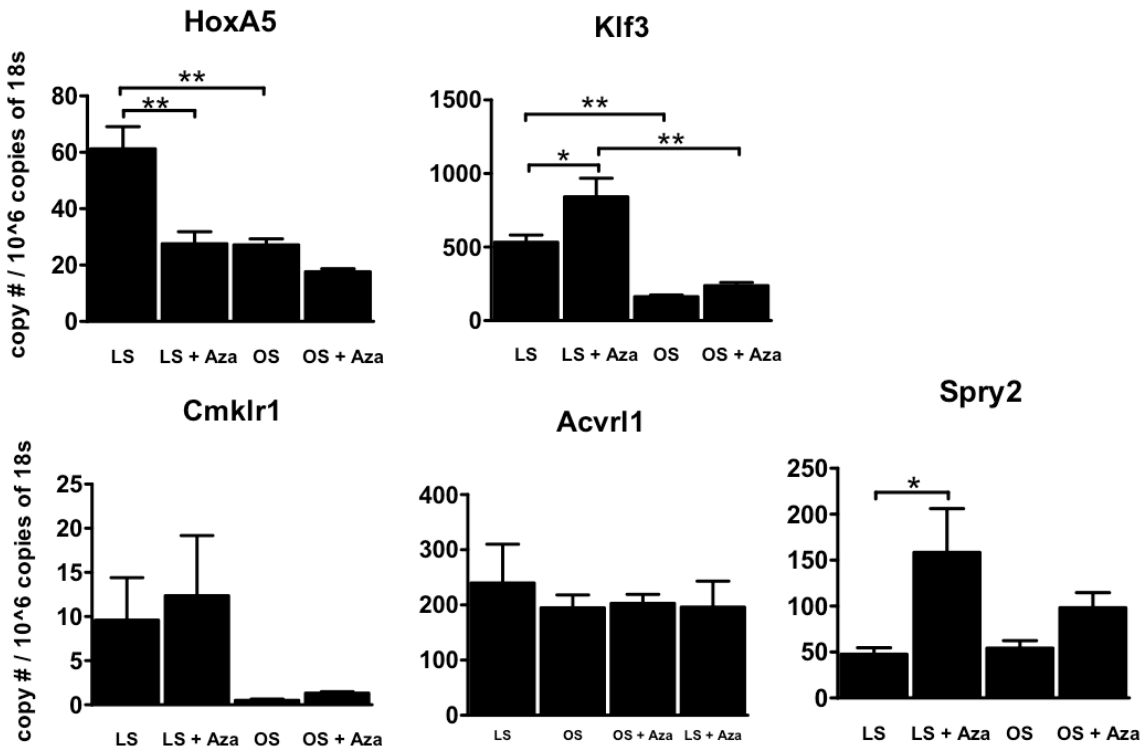

Figure 5.10: Shear- and 5Aza-sensitivity of the potential CREB-regulated genes in vitro (LS, AzaLS, AzaOS N=6; OS N=7)

Hox is a novel mechanosensitive gene family regulated by DNA methylation

The most prominent changes in DNA methylation in our RRBS dataset occur in the Hox gene family. Overall, there was very high coverage of CG sites localized to the Hox family gene clusters by our RRBS assay, and these sites exhibit the strongest and more densely packed changes in methylation in the d-flow LCA as compared to the non-d-flow RCA. These methylation changes occur mainly at key functional regions, including promoters where methylation is associated with gene suppression, intron/exon boundaries where methylation may be associated with alternative transcript expression, and surrounding microRNAs (Figure 5.11A and B). Many of these changes are also 5Aza-reversible (Figure 5.11A).

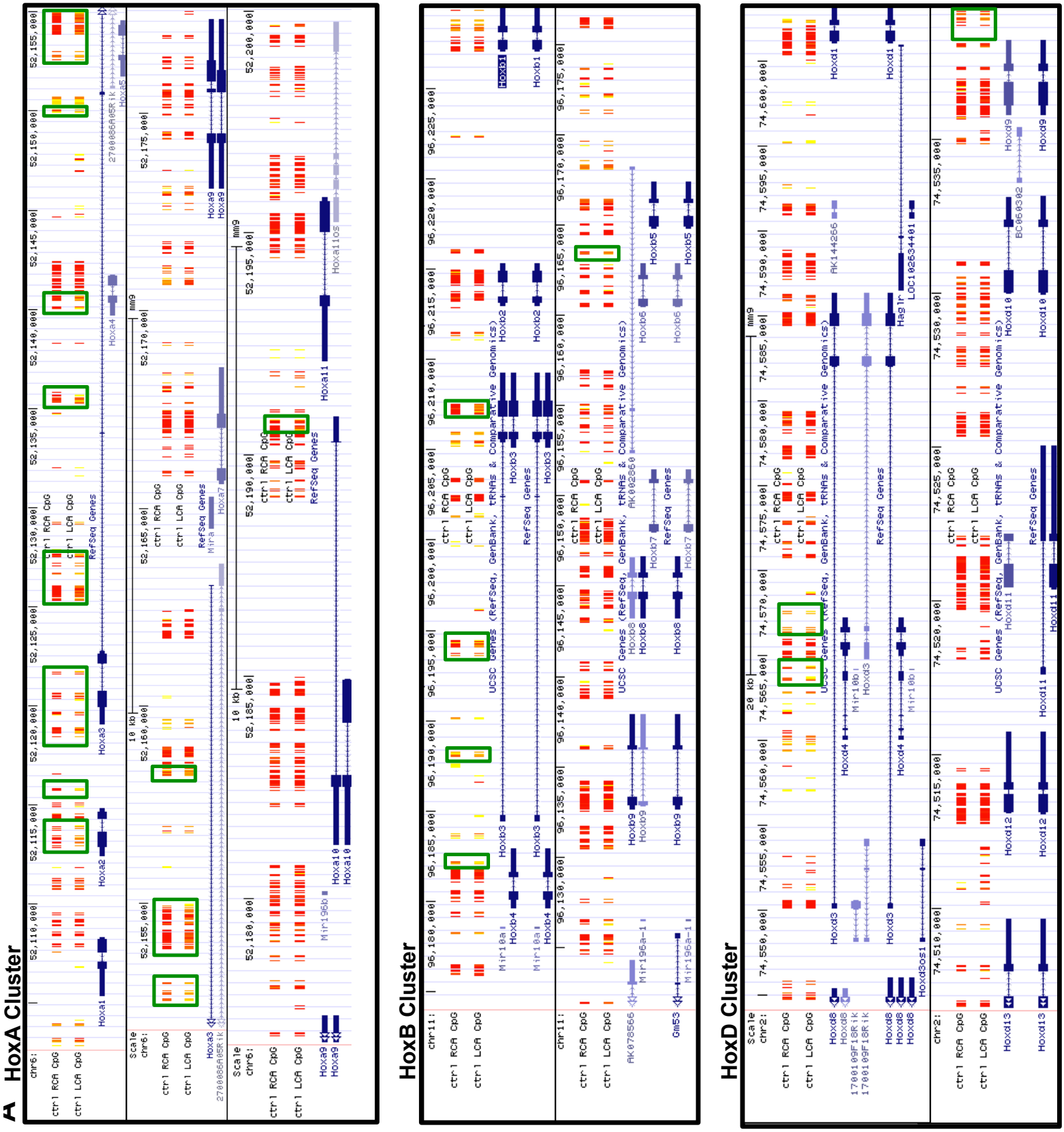

B

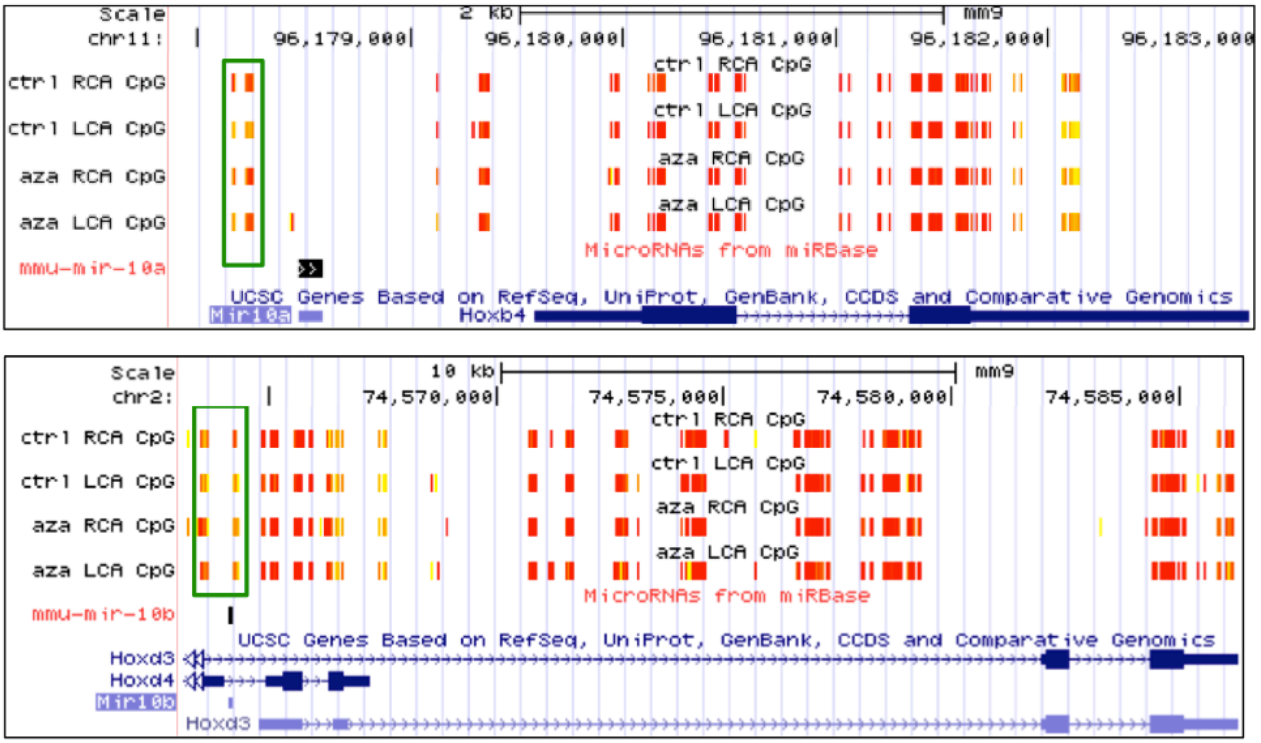

Figure 5.11: Flow regulates DNA methylation of the Hox family. (A) HoxA, HoxB, and HoxD gene family DNA methylation changes in endothelial cells due to disturbed flow are seen by reduced representation bisulfite sequencing (RRBS) using the mouse partial carotid ligation model. (B) RRBS data in UCSC Genome Browser showing 5Aza-reversible, d-flow-induced Hox promoter hypermethylation regions that also correspond to microRNAs: the Mir10a/HoxB4 shared promoter (upper panel) and the Mir10b/HoxD3 shared promoter (lower panel) are boxed in green. High methylation (yellow) and low methylation (red).

The Hox families exhibit a high level of self-interaction, forming 3-dimensional chromatin conformations known as a topological domains [189]. This global method of establishing a higher order genomic structure that also occurs specifically within Hox domains underscores the key importance of DNA domain interaction regulation by epigenetic mechanisms. Although the different Hox family subsets are located across different chromosomes, they appear to be co-regulated by methylation. In mouse, the HoxA, B, and D families are located on chromosomes 6, 11, and 2, respectively.

DNA methylation of Hox genes is a very well studied mechanism of their regulation in both development and cancer [229-231]. While it is known that Hox genes' DNA methylation status is a useful marker to distinguish between cell types for differentiation, we demonstrate below in Figure 5.12 that this is explicitly the case in the transition of cell type-specific differentiation. Comparison of the HoxA5 promoter methylation profile across cell types from the least differentiated (human embryonic stem cells) to the most endothelial-like (human umbilical vein endothelial cells, or HUVECs) using ENCODE datasets, as demonstrated by Shirodkar et al. for eNOS and VE-Cadherin, shows that the HoxA5 promoter is normally heavily methylated in non-differentiated cells and becomes demethylated as cells differentiate down the endothelial lineage (Figure 5.12B) [177,232]. We had difficulty recapitulating the in vivo HoxA5 shear responsive methylation changes using two different in vitro bioreactor systems to induce shear stress over cultured endothelial cells (Figure 5.9A). We determined that this was not due to experimental artifact caused by the bisulfite sequencing conditions (Figure 5.9B). This may be due to significant epigenetic changes occurring during EC culture under static conditions and raises an important consideration for the limitations of in vitro studies.

Further, the functional importance of the HoxA5 promoter region in transcriptional regulation is demonstrated in Figure 5.12A. Using Encyclopedia of DNA Elements (ENCODE) project data to determine locations of transcription factor/complex binding to DNA, we discovered enriched Pol2 and CTCF binding at the CpG-dense HoxA5 promoter in HUVECs, demonstrating transcriptional activity (Figure 5.12A). The HoxA locus is known to contain an insulator characterized by several CTCF binding sites

that separate the co-regulation of expression of HoxA1-7 and HoxA9-13 [233]. CTCF is a DNA insulator binding protein that marks the transition from tightly packed heterochromatin to relaxed euchromatin. Pol2 contains the active subunit for synthesizing RNA from the DNA template, and in combination with other RNA polymerase subunits, forms the DNA groove binding domain.

Our RRBS data indicates the key importance of genome-wide CREB binding sites (CRE) as a potential global regulator of gene expression. We expect that the HoxA5 promoter CRE methylation status regulates CREB binding and downstream expression of HoxA5, but unfortunately neither CREB nor its binding partners p300/CBP were covered by the ENCODE consortium endothelial Chromatin-IP datasets. However, our lab is actively exploring this hypothesis using alternative methods.

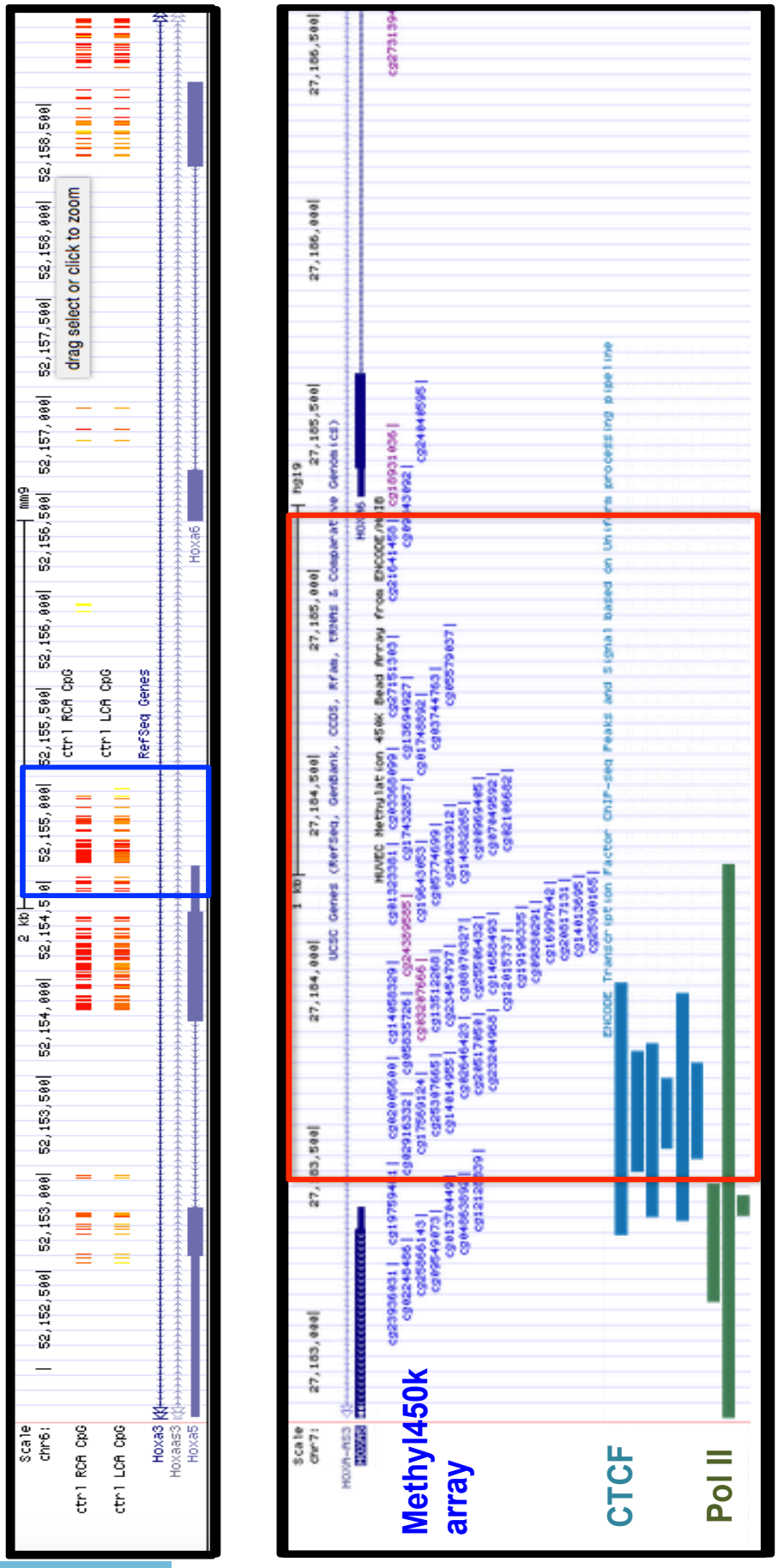

C

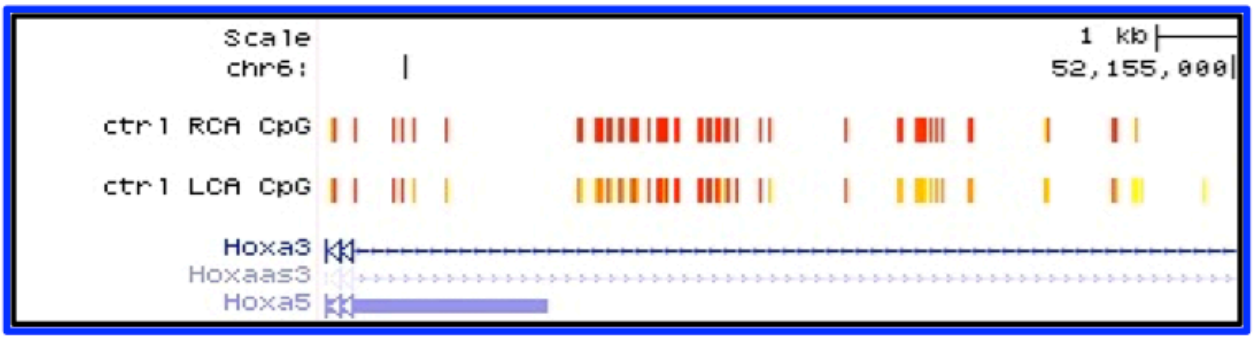

D

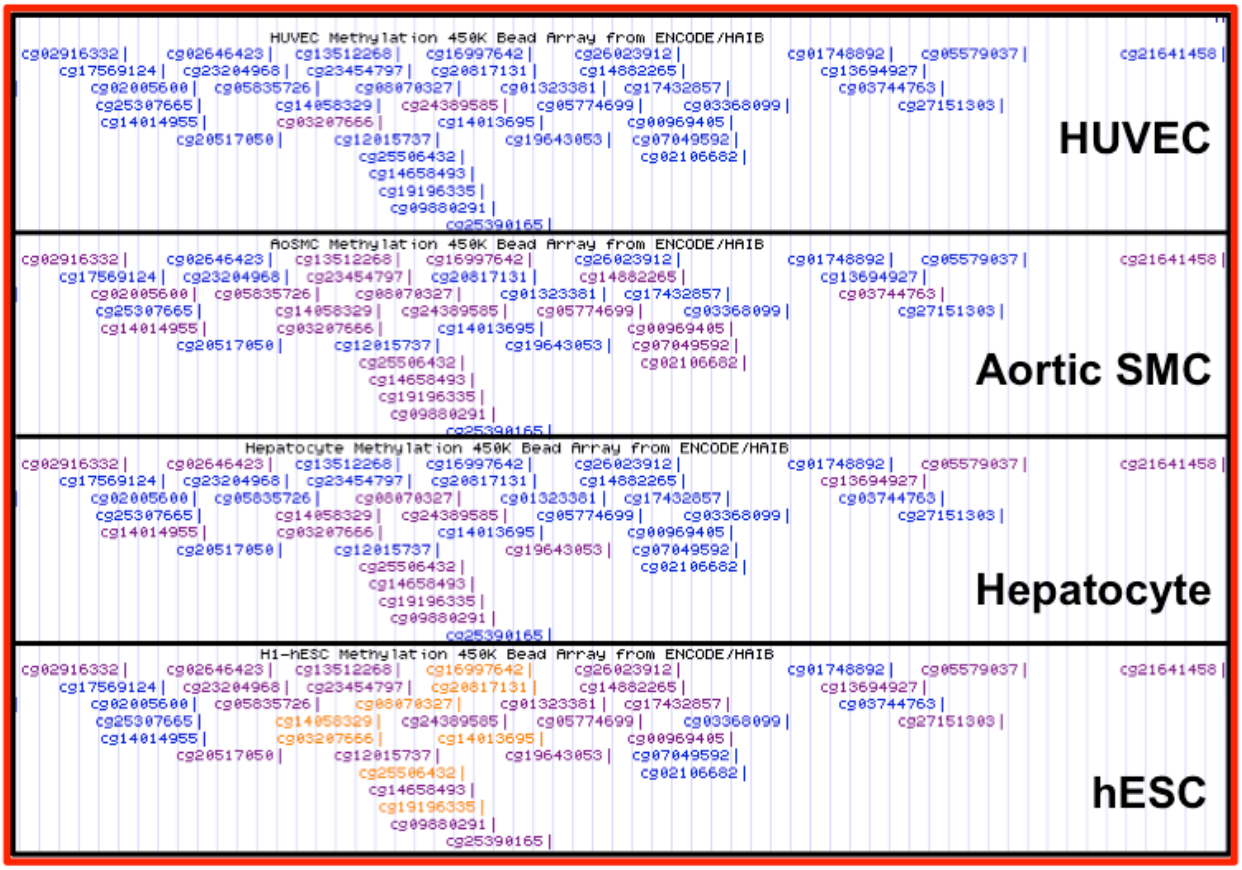

E

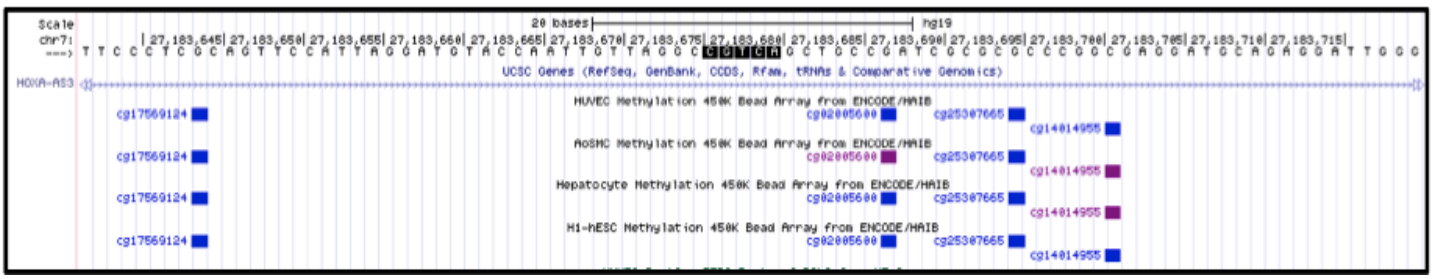

F

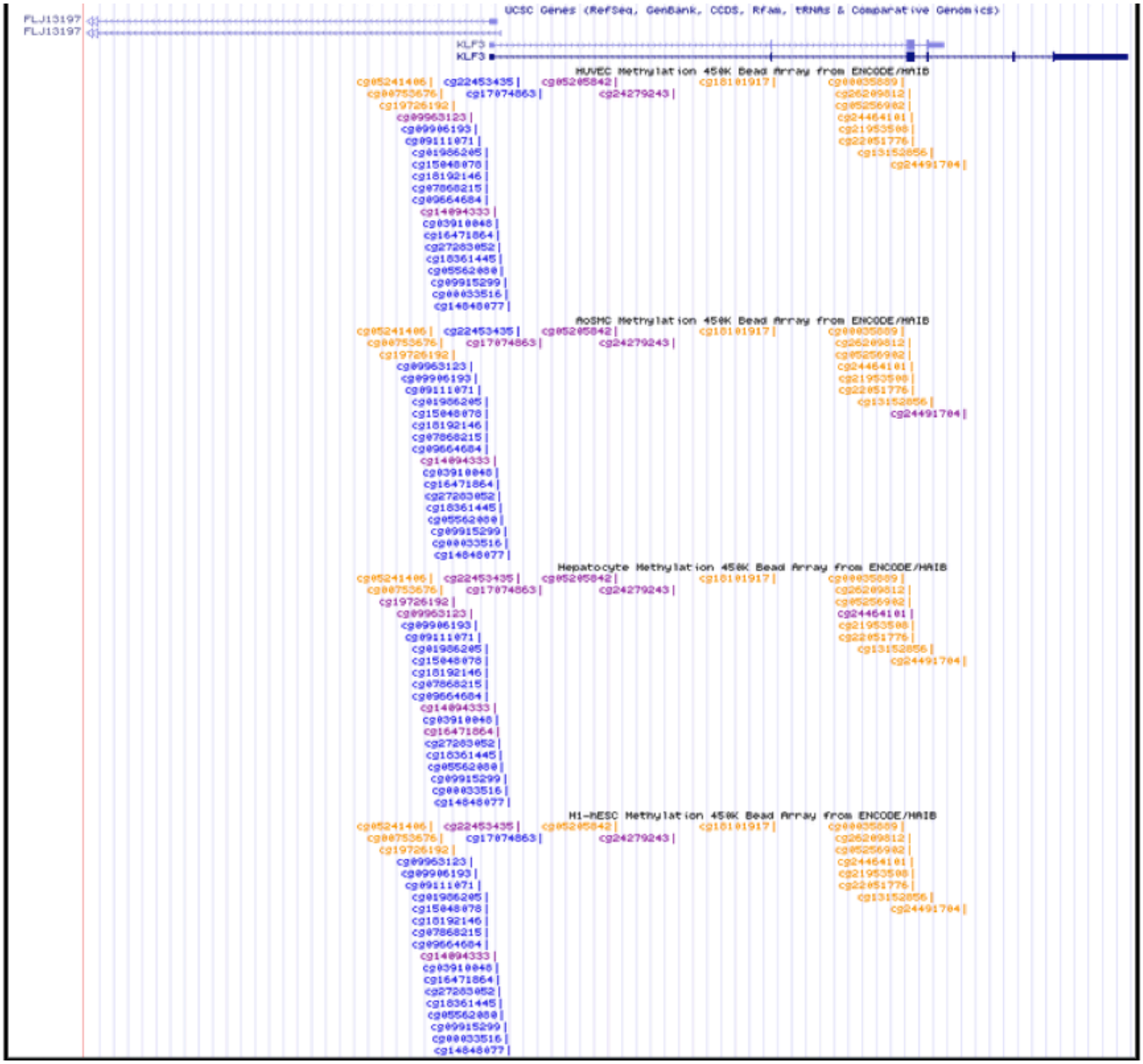

Figure 5.12: Flow- and differentiation-dependent methylation changes in the HoxA5 promoter. (A) UCSC Genome Browser view of the RRBS data showing flow-dependent methylation changes in the HoxA5 promoter. (B) The ENCODE consortium ChIP-Seq datasets for HUVEC show that the transcription factor CTCF and RNA Polymerase II are enriched at the HoxA5 promoter. (C) Zoomed-in view of the blue boxed area from panel A. UCSC Genome Browser screenshot of the ENCODE Methyl450k array datasets, in the region boxed in red in (B), shows a comparison of the HoxA5 promoter methylation profile across cell types from the least differentiated (human embryonic stem cells) to the most endothelial-like (human umbilical vein endothelial cells, or HUVECs). (D) Highly methylated regions are shown in orange, partially methylated regions in purple, and unmethylated regions in blue. (E) The HoxA5 promoter CRE is not covered by the ENCODE dataset. (F) ENCODE Methyl450k array data shows that, as opposed to

the case for HoxA5, Klf3 does not demonstrate significant change in its promoter methylation status across differentiated and non-differentiated cells.

The Mir10 family (Mir10a and Mir10b) lies within the Hox clusters and follows the criteria for 1) DF-induced suppression; 2) DF-induced promoter hypermethylation; and 3) 5Aza Inhibition of DF-induced promoter methylation. MiR10a and HoxB4 share a promoter and our RRBS data shows a differentially methylated region (DMR) following the proposed silencing pattern in this shared promoter. Additionally, MiR10b and HoxD3 share a promoter that also contains a DMR following the proposed silencing pattern (Figure 5.13). Other Hox genes also repeatedly demonstrate this pattern (Figure 5.11).

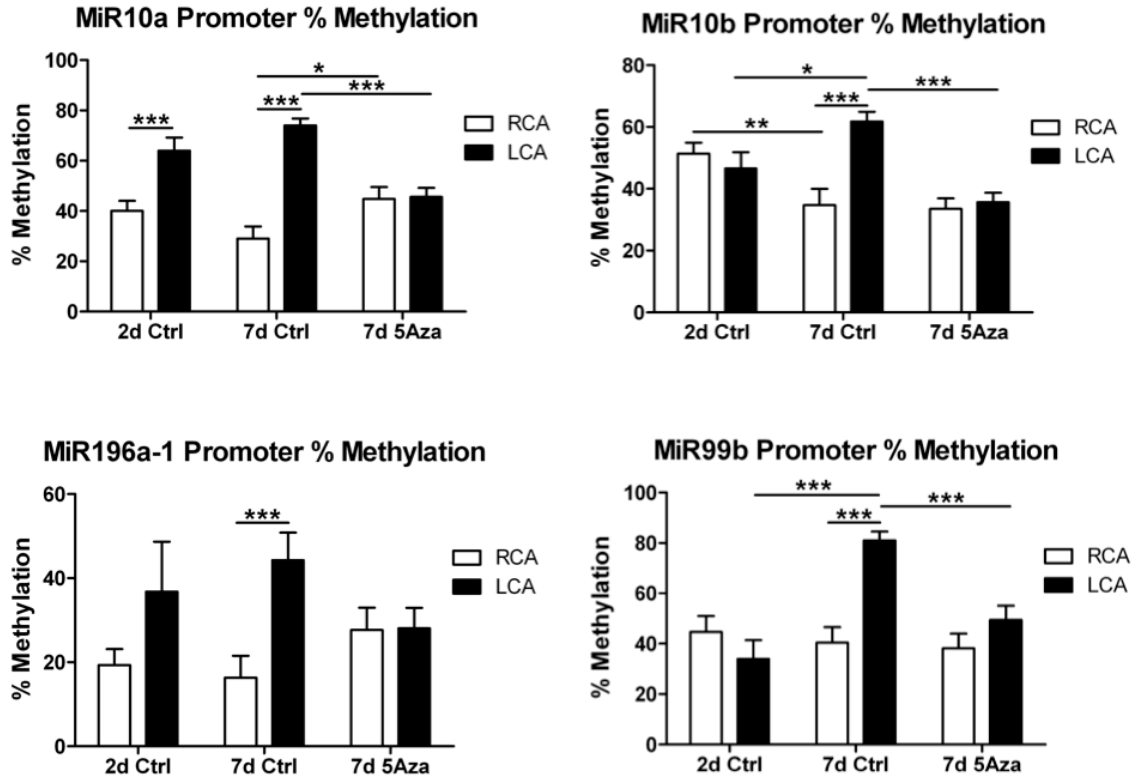

Figure 5.13: DNA methylation status of the MiR10a/HoxB4 and the MiR10b/HoxD3 shared promoters which each contain 16 CG and 23 CG sites, respectively (corresponding to the area boxed in green in Figure 5.11B).

The Hox genes with strong promoter differential methylation (RRBS) that are suppressed in d-flow (microarray) include A1, A2, A3, A4, A5, A9, B4, D3, D4 (Figure 5.11 and Figure 5.14). In vitro, HoxA1, A4, B4, D3, and D4 had trends toward downregulation by OS, but did not achieve statistical significance (Figure 5.15).

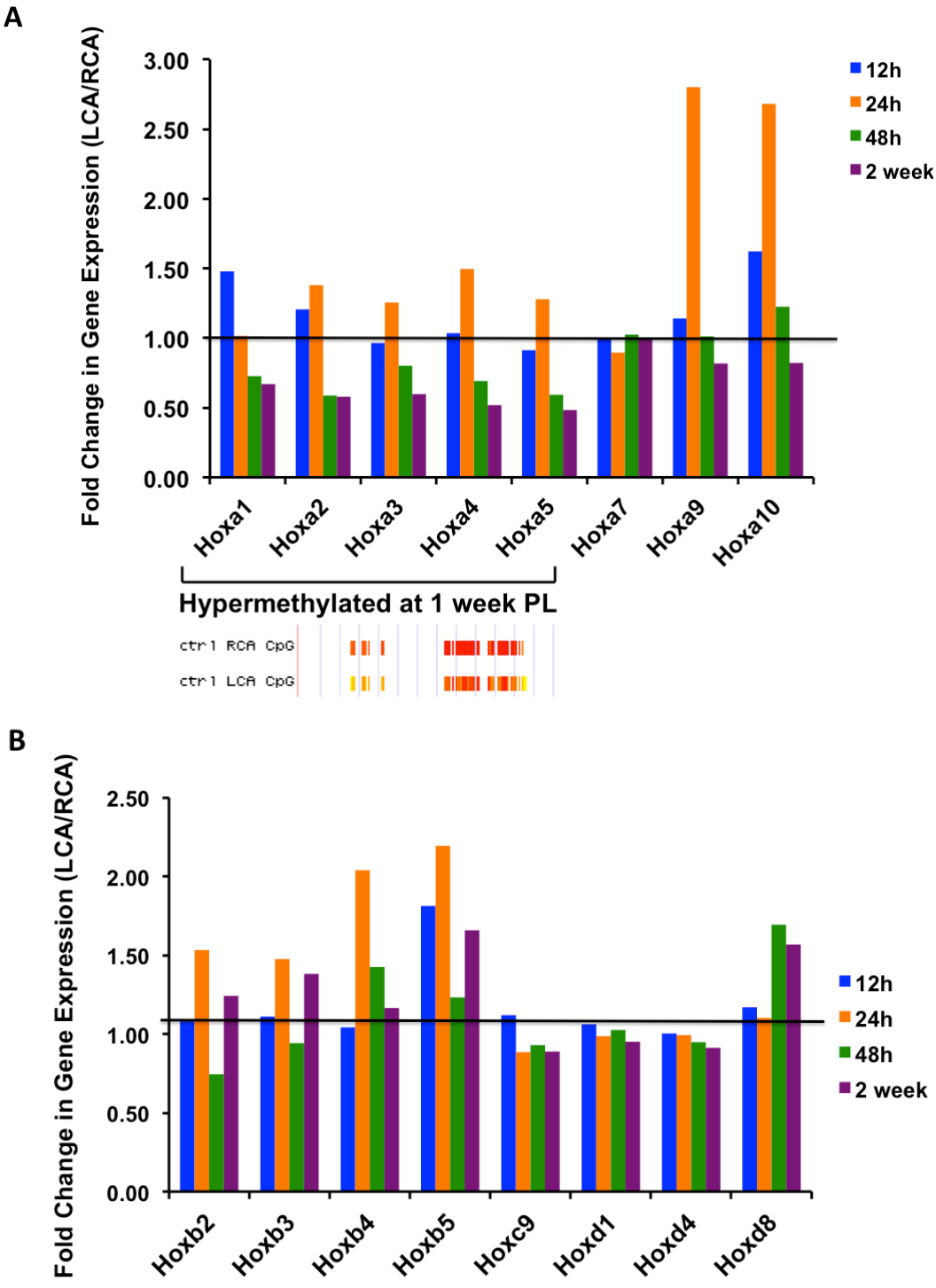

Figure 5.14: Gene array data for Hox Family Gene expression showing differentially expressed genes from (A) the HoxA cluster and (B) the other Hox genes.

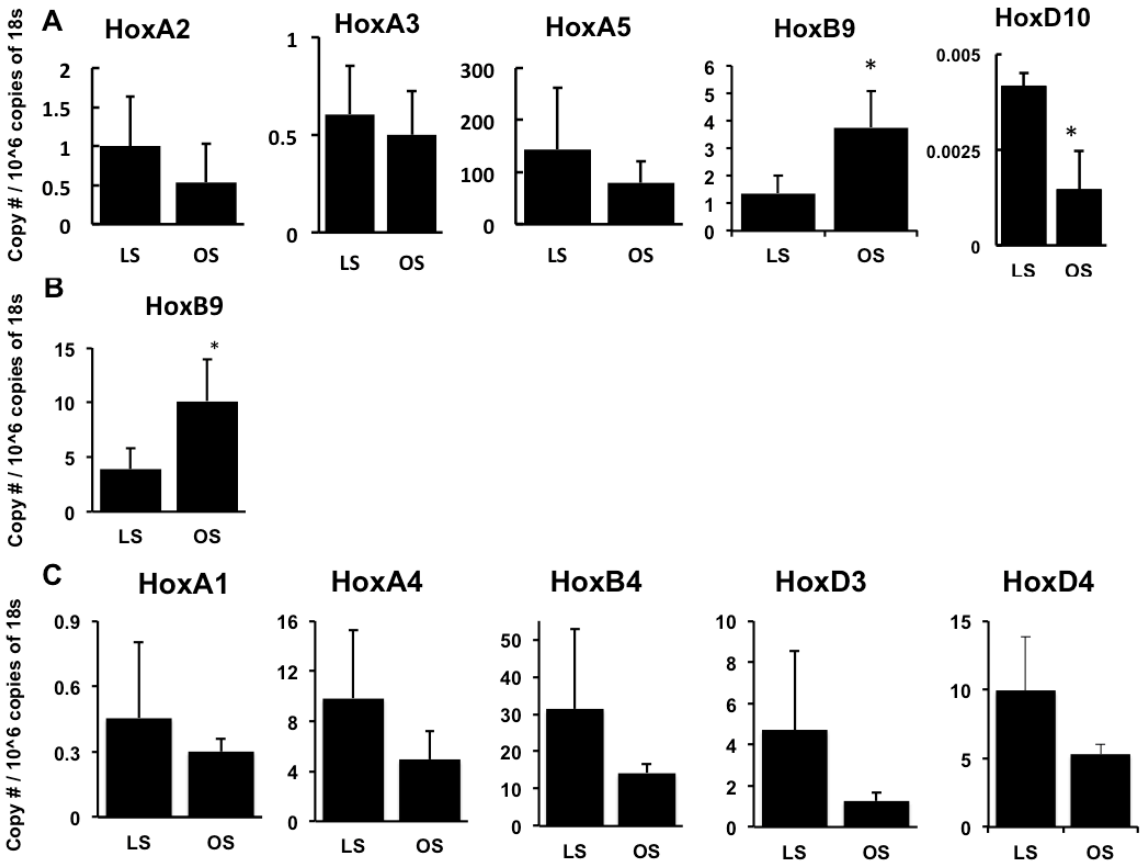

Figure 5.15: Shear-sensitivity of select Hox genes in vitro. HUVEC were subject to either LS or OS for 7 days using the Ibidi shear system (n=4 each).

Discussion

Using the DNA methylome and transcriptome datasets, our goal was to identify those genes that are hypermethylated in the promoter regions and silenced by d-flow, but that could be rescued by 5Aza treatment. Functional studies of DNA methylation patterns are complicated by the various, and often conflicting, reports of the role of specific methylation changes in gene expression control. The described study considered the functional consequences of specific methylation patterns by comparing the complementary transcriptome, and by performing rigorous single gene studies both *in vitro* and *in vivo* by a variety of methods including qPCR and bisulfite sequencing to

draw a definitive link between specific methylation patterns and the functional outcome of gene expression control. Ultimately these in vitro studies will be translated to disease development or prevention studies in vivo.

We would like to emphasize the importance of the user-defined threshold values in our method of gene discovery that, by using more strict criteria, enabled us to filter out a manageable number of genes for further study. This unbiased genome-wide comparative analysis revealed 11 genes that fit these criteria. This result was surprising at first, since most of the downregulated genes by d-flow in the LCA were rescued by 5Aza treatment (540 out of 569 genes), and because the promoter DNA methylation patterns were rescued by 5Aza in the majority of genes (335 out of 421 genes) (Figure 5.1). This discrepancy between the 5Aza effect on gene expression and methylation and the number of genes that fit our hypothesis could be due to the following possibilities that: 1) 5Aza may target a few master regulators such as transcription factors that could in turn regulate the rest of the mechanosensitive genes; 2) there are only a few key CG sites on promoters that could determine the binding of master transcription factors, which determines the expression of most of the mechanosensitive genes; and 3) the majority of other CG sites in the promoters do not necessarily lead to functional consequences. To test these possibilities, we first searched for potential master transcription factors that could regulate the 11 mechanosensitive and 5Aza-sensitive genes using the MetaCore analysis. This suggested CREB as a potential master transcription factor that could bind to 5 out of the 11 genes. The subsequent computational sequence-based analysis showed that 4 of these genes (*HoxA5*, *Klf3*, *Cmklr1*, and *Acvrl1*) contained a CG site in the promoter CRE that was hypermethylated by d-flow in a 5Aza-dependent manner (Figure 5.4). Our

results also suggest that d-flow induces hypermethylation in these promoter CRE CG sites by a DNMT-dependent mechanism (Figure 5.4 and Figure 5.5), which in turn has a major impact on gene expression.

We chose to study HoxA5 and Klf3 since they are transcriptional activators and repressors, respectively, potentially serving as a mechanosensitive master switch.[201,207] Our study implicates HoxA5 and Klf3 as novel mechanosensitive transcription factors regulated by DNA methylation that may serve as master regulators of global gene expression in response to flow. Interestingly, Klf3 is suppressed in acute myeloid leukemia (AML) and 5Aza is used to treat this disease, although it has not yet been shown whether 5Aza directly targets Klf3. AML is also treated with all-trans retinoic acid and, also interestingly, this drug was shown to rescue Klf3 expression by an unknown mechanism [99] Since all-trans retinoic acid is known to influence DNA methylation of a small number of specific genes [212], it would be interesting to test whether Klf3 is regulated by this mechanism in AML. Although our current study focused on examining the role of DNA methylation in vascular biology and disease, these results indicate that our work could have far-reaching implications across multiple diseases.

Our *in silico* analysis suggests CREB as another key transcription factor whose DNA binding is known to be regulated by methylation of the CRE sites of its target genes, such as HoxA5 and Klf3[149,154]. It was shown previously that protein kinase A (PKA) downregulation in d-flow leads to decreased CREB phosphorylation and decreased CREB binding to CRE elements [160]. Here, we identified a novel mechanism by which CREB binding to its gene targets may be decreased by d-flow via DNA methylation at their promoter CREs. We have been actively working to dissect the

detailed mechanism by which CREB may bind to the HoxA5 and Klf3 promoter CREs using chromatin immunoprecipitation assays combined with qPCR directed for the CRE. The results of this experiment combined with promoter CRE site-specific mutation or in vitro methylation of the CRE CG using luciferase assays with the Klf3 or HoxA5 promoters will enable us to better understand the mechanism by which the expression of these master transcription factors is controlled.

Functional studies of DNA methylation patterns are complicated by the various, and often conflicting, reports of the role of specific methylation changes in gene expression control. Here, we considered the functional consequences of specific methylation patterns by comparing the complementary transcriptome, and by performing single gene studies *in vitro* using qPCR, bisulfite sequencing, and EC inflammation assays. Follow-up studies initiated recently by new members in our lab will provide more in-depth analysis of a number of EC gene candidates that were illuminated by this study. This additional future work will help draw new definitive links between specific methylation patterns and the functional outcome of gene expression control and ultimately disease development or prevention. The results of this work compounded with future studies will continue to elucidate the epigenetic regulation of well known genes involved in atherogenesis and will also uncover novel shear sensitive genes and regulatory pathways that have yet to be discovered.

CHAPTER 6 DISCUSSION

Here, we demonstrate for the first time, to our knowledge, that blood flow epigenetically controls endothelial gene expression by regulating genome-wide DNA methylation patterns in a DNMT-dependent manner. Our novel findings have broad implications for understanding the biochemical mechanisms of atherogenesis and provide a basis for identifying potential therapeutic targets for atherosclerosis.

We found that d-flow induced expression of DNMT1 in mouse arterial endothelium in vivo and in cultured endothelial cells by oscillatory shear (OS) in vitro. The DNMT inhibitor 5-Aza-2'deoxycytidine (5Aza) or DNMT1 siRNA significantly reduced OS-induced endothelial inflammation. Moreover, 5Aza reduced lesion formation in two $ApoE^{-/-}$ mouse atherosclerosis models.

We applied a dual "omics" approach by overlaying concomitant endothelial methylome and transcriptome datasets to determine the mechanism by which 5Aza inhibited atherosclerosis in our murine models. We performed reduced representation bisulfite sequencing (RRBS) and microarray using endothelial-enriched gDNA and RNA, respectively, from the partially-ligated left carotid artery (LCA exposed to d-flow) and the right contralateral control (RCA) of mice treated with 5Aza or vehicle. Systems biological analyses using RRBS and transcriptome data revealed 11 mechanosensitive genes whose promoters were hypermethylated by d-flow, but rescued by 5Aza treatment. Of those, the two transcription factors *HoxA5* and *Klf3* contain cAMP-response-elements, and their methylation status could serve as a mechanosensitive master switch in gene expression. The results of our combined genome-wide studies demonstrate that d-flow controls epigenomic DNA methylation patterns in a DNMT-dependent manner, which in turn alters endothelial gene expression and induces atherosclerosis.

These robust experimental strategies involved various models of shear stress using different endothelial cell types, both in vivo and in vitro. The recurrent findings by our group and also by others reveal that epigenetic mechanisms, and particularly DNA methylation, are key in regulating vascular biology, endothelial gene expression, and the pathophysiology associated with atherosclerosis.

This project was the first of its kind to combine biomedical engineering approaches to understand the effect of mechanical forces on endothelial cell biology and cardiovascular disease development. We addressed the difficulty of tackling this widely unknown disease mechanism by limiting the scope of our project to a specific *a priori* hypothesis based on well-studied epigenetic mechanisms. However, our dual "omics" approach also allowed us to perform *a posteriori* analyses that enabled the discovery of previously unpredictable biological phenomena.

The genome-wide approaches used here to resolve the endothelial DNA methylome and transcriptome were confined by the available and practical technologies existing at the time of this study. The transcriptome was determined using Illumina Mouse WG6 microarray chips, which limited the breadth of the gene expression study to the set of probes covered by the array. This precluded the ability to detect most alternative transcripts and noncoding RNAs, which recent evidence suggests may be important consequences of differential methylation at alternative intragenic promoters and in functional genomic regions that are as of yet undefined. Additionally, variability can exist due to differences in the arrays themselves, the dye labeling, efficiency in RNA amplification and reverse transcription, and hybridization [234]. To address this to the best of our ability, we used biological replicates (n=3) consisting of pooled samples (3 carotid

arteries in each sample), and performed stringent quality control steps before and after the microarray process, including using the Bioanalyzer to analyze our purified RNA samples and qPCR validation of a subset of differentially expressed genes as determined by the microarray.

Reduced representation bisulfite sequencing (RRBS) is widely accepted for genome-scale methylation studies at the nucleotide resolution, although incomplete CG coverage is an inherent limitation of RRBS due to the MspI restriction enzyme digest, PCR, and sequencing steps [235]. These limitations produce partial genomic coverage, as evidenced by the 23% genomic and 53% promoter coverage of our RRBS assays. Additionally, we were only able to draw conclusions about differentially methylated regions with a functional effect on transcription by limiting our analysis to CG sites that were covered in all samples by *both* the microarray and RRBS. Therefore, genomic regions with partial coverage between samples or assays were not considered in this particular study, which could have resulted in overlooking potentially important methylation sites.

We would also like to emphasize the importance of the user-defined threshold values in our method of gene discovery using both the methylome and transcriptome datasets. Using very strict criteria enabled us to filter out a manageable number of genes for further study in the scope of this project; however, releasing the threshold stringencies would result in more target genes for additional studies.

Preexisting knowledge at the inception of this study surrounding DNA methylation, with a functional relevance to gene expression and disease, was mainly focused on CpG methylation in the promoter region of genes, especially in dense CpG-

rich regions known as CpG islands. We used this knowledge base to guide our studies and increase the likelihood of rapid discovery. However, we are aware that DNA methylation in other locales, including coding or noncoding gene regulatory regions, and at other motifs such as CpH (where H is A/T/C), are known to be important for controlling gene expression, alternative transcripts, chromatin conformation and genome stabilization [125,126,129,236]. While outside the scope of the current study, it would be quite interesting to examine whether there is d-flow-induced differential DNA methylation of non-CpG cytosines in endothelial cells, and whether any changes are localized to potentially functional genomic regions such as enhancers, promoters, intron/exon boundaries, transposable elements, 3'UTRs, transcription factor binding sites, and across the genome either sporadically or in the context of specific sequence motifs.

While DNA methylation at the 5' carbon of a cytosine base pair is the most well studied epigenetic covalent DNA modification, several others are known to exist and were recently implicated to be important in gene expression regulation, although their mechanisms are very unclear. These modifications include 5-hydroxymethylcytosine (5hC), 5-formylcytosine (5fC) and 5-carboxycytosine (5cC). Emerging methods of detection open up the possibility for future study of these cytosine modifications in endothelial biology and pathogenesis [237].

5-Aza-2'-deoxycytidine (5Aza, also known as Decitabine) is a nucleoside analog that traps DNMT1 in a covalent complex with DNA, and also preferentially targets DNMT1 via ubiquitin-dependent proteasomal degradation, resulting in DNMT1 inhibition [57]. 5Aza is an FDA approved drug and is currently used to treat myelodysplastic syndromes including leukemia [57-62], but its specific mechanism of action

and gene targets need to be further determined [58]. It should be noted that the dosing schedule for 5Aza affects treatment results depending on the dose, method of administration, and target tissue, especially due to its short half-life [62]. In this study, a high frequency, low-dosing strategy was applied to target the endothelium, maintain efficacy over time, and reduce toxicity. To address the potential off-target effects of 5Aza, we also used DNMT1 siRNA in our in vitro studies. However, the practical challenges associated with in vivo treatments using siRNAs precluded us from performing a DNMT1-specific inhibition study in vivo. During this project we began the development of endothelial-targeted DNMT1 knockout mice and in vitro characterization of novel DNMT1 chemical inhibitors described in Chapter 3. Both strategies can be exploited in future, more targeted in vivo studies of DNMT1.

We also recognize the potentially important effect of 5Aza treatment in cell types other than endothelial cells that are involved in atherogenesis, including smooth muscle cells and immune cells. While the aim of our study was to determine whether there is a novel epigenetic mechanism of flow-regulated endothelial gene expression and whether it plays a vital role in atherosclerosis development, it was recently shown by Cao et al. that the anti-atherosclerotic effect of 5Aza also has a mechanistic basis in the immune milieu [238]. Because atherosclerosis is a systemic disease caused by multi-cell type dysfunctions, a systems wide approach will be necessary to understand the role of global methylation changes and crosstalk between cell types in order to fully realize the therapeutic potential of epigenetic interventions.

Conclusions

The study presented here is the first to demonstrate that d-flow-induced global gene expression changes in endothelial cells are regulated at the genome level in a DNMT-and DNA methylation-dependent manner. We propose that d-flow induces DNMT1 expression in endothelial cells, which in turn stimulates DNA methylation in specific promoter CRE sites of mechanosensitive, master transcription factors including *HoxA5* and *Klf3*. These master genes may then regulate expression of the majority of other mechanosensitive genes, resulting in endothelial dysfunction and atherosclerosis. We further propose that the DNMT inhibitor 5Aza targets these mechanosensitive master regulators to restore anti-atherogenic gene expression profiles. In conclusion, our study provides a novel insight into the mechanism by which flow regulates gene expression in a DNMT-dependent manner and uncovers novel genes involved in the endothelial cell flow response.

Future Directions

The goal of this project was to determine how the endothelial DNA methylome changes in response to flow, and how this in turn alters gene expression and regulates atherosclerosis development. We show that blood flow epigenetically controls endothelial gene expression by regulating genome-wide DNA methylation in CRE sequence motifs and at specific gene promoters in a DNMT-dependent manner. Several genes were identified that merit further study as potential therapeutic and diagnostic candidates, and lab members who recently joined our team are actively initiating these detailed studies.

In Chapter 3 we establish that DNMT1 is upregulated in d-flow and that it plays a key role in atherosclerosis development. However, the upstream mechanism controlling

DNMT1 overexpression in this system is largely unknown. To address this, we performed preliminary studies on the mir29 family and we also developed a computational model of known mechanosensors that may control DNMT1 through biochemical signaling pathways. These preliminary studies will aid in future experimental design and validation of upstream regulators of DNMT1. Future studies involving pharmacological inhibitors and anti-miRs can be tested *in vitro* and *in vivo* to uncover the role of Mir29 in the flow regulation of DNMT1. In addition to the Mir29 family, we may explore additional d-flow-suppressed miRs that are validated to target DNMT1, including the Let-7 family, as well as the other miRs listed in Chapter 3 Table 2. PECAM1, CAV1, and VEGFR are three of the most important mechanosensors involved in atherosclerosis development, but conflicting findings on their expression and activity in disturbed flow and atherosclerosis have been reported.[239,240] Our model predicts that a loss of PECAM1 and CAV1 leads to increased DNMT1 expression and future experiments using knockdown or overexpression of each of these mechanoreceptors individually will enable elucidation of the mechanism of the regulation of the DNMT1 shear response.

While DNMT1 is the most dramatically altered DNMT at both the mRNA and protein level by d-flow in vitro, given our findings that DNMT3b is slightly upregulated by d-flow at the protein level (Chapter 3 Figure 11) and that DNMT3a has been found to be shear-responsive in ECs in other model systems [57,65], we believe that the DNMT family as a whole warrants further investigation. We foresee the benefit of future studies to analyze the role of the other catalytically active DNMTs (DNMT3a and DNMT3b) in EC functions. Additionally, these studies leave room for further analysis of the role of

DNMT1 in other EC biological functions in addition to inflammation. In Chapter 3 we show that DNMT1 inhibition reduces inflammation in ECs *in vitro* and plaque development *in vivo*. In order to determine whether there is a further functional role for DNMT1 in atherosclerosis development, additional markers of EC dysfunction that increase in d-flow (including inflammation, apoptosis, proliferation, thrombosis and cell migration) could be examined using either knockdown or overexpression of DNMT1 in future studies. We expect that certain specific markers will be more strongly affected by DNMT1 knockdown, which will implicate key gene regulatory pathways that can be examined further by systems biology and gene ontology studies.

Drawing upon epigenetics-based cancer diagnostics currently in use, it is foreseeable that epigenetic targets such as DNMTs, specific gene promoter DNA methylation, histone modifications, and miRNAs could serve as biomarkers for cardiovascular disease diagnosis as well as targets for therapeutic intervention. In Chapter 3 we show that DNMT1 inhibition by 5Aza blocks d-flow-induced atherosclerosis development *in vivo* in ApoE$^{-/-}$ mice. To address potential off-target effects and non-tissue-specific effects of 5Aza, we began developing endothelial-targeted DNMT1 knockout mice to test EC-specific DNMT1 knockdown on plaque development *in vivo* using the acute and chronic mouse atherosclerosis models. Full-body DNMT1 knockout is embryonic lethal[90]. Fortunately, floxed DNMT1 mice are commercially available (UC Davis- DNMT1$^{tm2Jae\ fl/fl}$ mice) and we have begun cross breeding these mice with endothelial-targeted Cre mice on an ApoE$^{-/-}$ background (VE-Cadherin-Cre$^{+/-}$/ApoE$^{-/-}$ mice) that we already have in our lab. This will likely enable us to generate endothelial-

specific DNMT1 knockout mice (DNMT1$^{tm2Jae\ fl/fl}$/VE-Cadherin-Cre$^{+/-}$/ApoE$^{-/-}$) for subsequent chronic and acute atherosclerosis studies.

We also began in vitro characterization of novel DNMT1 chemical inhibitors such as SGI-1027. SGI-1027 is a novel DNMT inhibitor that may become used routinely in place of 5Aza due to the cytotoxic effects of 5Aza treatment (both Decitabine and Vidaza) caused by their incorporation into DNA. SGI-1027 is a cell-permeable quinoline-based non-nucleoside compound that inhibits DNMT1, DNMT3a, and DNMT3b and results in selective degradation of DNMT1. The mode of action of DNMT inhibition is thought to be by competing with AdoMet (S-adenosyl-L-methionine, SAM) for the enzyme's cofactor binding site. SGI-1027 has been shown to be more effective than Decitabine in reactivating methylation-silenced tumor suppressor genes without inducing genome-wide hypomethylation or caspase-3 activation. We performed dose optimization studies for novel DNMT1 chemical inhibitors that may be useful in future studies to increase specificity of DNMT1 inhibition and reduce potential off-target effects (Figure 6.1)[241].

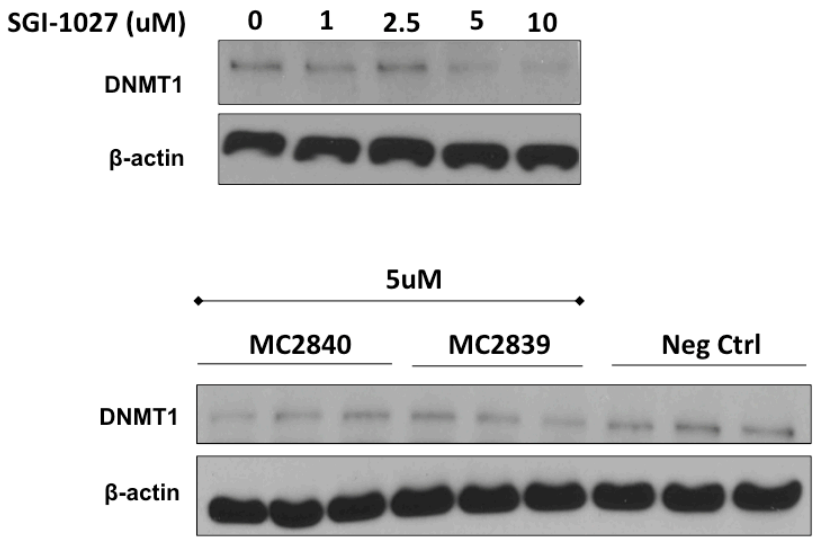

Figure 6.1: Novel chemical inhibitors specific to DNMT1. Dose curve for SGI-1027 (top) and single dose at 5uM of inhibitors MC2839 and MC2840 (bottom). Inhibitors were generously provided by Dr. Xiaodong Cheng.

The fact that ten-eleven-translocation (TET) enzymes convert 5mC into 5hmC, which acts as an intermediate step to demethylated cytosine, introduces the important concept of site-specific DNA demethylation, which could play an important role in both regulating DNA methylation patterns as well as in establishing aberrant demethylation in disease[242]. Directing DNMT or TET to specific DNA sequences could one day be used as epigenetic editing techniques[243,244].

Our computational analyses in Chapter 4 overlaying the concomitant endothelial methylome and transcriptome datasets that we collected were designed to ask very specific questions regarding the importance of DNA methylation in atherosclerosis development. We addressed the difficulty of tackling the widely unknown disease mechanism of atherosclerosis by limiting the scope of our project to a specific *a priori* hypothesis based on well-studied epigenetic mechanisms, and we recognize the limitations of such directed studies. The huge benefit of the data collected with our dual

"omics" approach is the abundant potential for future analyses. For example, these RRBS datasets could be the subject of computational analyses to examine changes in non-CpG cytosine methylation, as well as CpG methylation changes in other functional regions such as introns, exons, intron/exon boundaries, transposable elements, and additional transcription factor binding sites or sequence motifs, among others. As a specific example, it would be interesting to examine whether other known transcription factor binding sites that have binding motifs very similar to the CRE sequence also have differential methylation for particular genes or on the genome scale. For example, JunD, CST6, and TGA1 all have similar sequence motifs to the CREB binding motif (Figure 6.2).

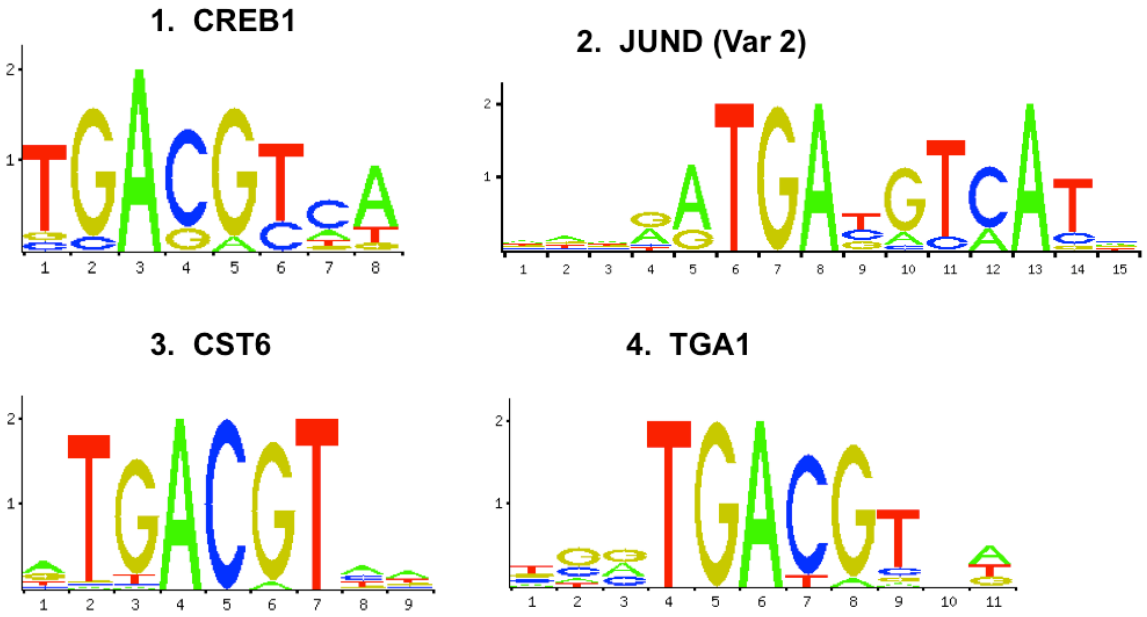

Figure 6.2: JASPAR TFBS search shows other transcription factors that bind to a similar sequence to CRE.The size of the nucleotide corresponds to its importance in the binding interaction, and stacked nucleotides at a single position have potential substitutions that affect the TF binding by different levels (corresponding to the height of the letter).

Very recent major technological developments in next generation sequencing now make it possible to repeat our transcriptome study using RNA sequencing to avoid sources of error due to microarray experimental setups. This would enable the discovery of flow-regulated differential expression of alternative transcripts and noncoding RNAs, as well as novel transcribed regions of the genome.

Functional studies of DNA methylation patterns are complicated by the various, and often conflicting, reports of the role of specific methylation changes in gene expression control. In Chapter 5, we considered the functional consequences of specific promoter CpG methylation patterns by comparing the complementary methylome and transcriptome, and by performing single gene studies *in vitro* using qPCR, bisulfite sequencing, and EC inflammation assays. Follow-up studies initiated recently by new members in our lab will provide more in-depth analysis of a number of EC gene candidates that were illuminated by this study, including *Tmem184b, Adamtsl5, Cmkrl1, Pkp4, Acvrl1, Dok4, Spry2, Zfp46,* and *F2rl1,* as well as additional functional studies on *HoxA5* and *Klf3*. This future work will help draw more definitive links between specific methylation patterns and the functional outcome of gene expression control and ultimately disease development or prevention.

Although our current study focused on examining the role of DNA methylation in vascular biology and disease, the results in Chapter 5 indicate that our work could have far-reaching implications across multiple diseases. While 5Aza is currently used in the clinic to treat acute myeloid leukemia (AML), this drug has many potential side effects, limiting its therapeutic utility not only for atherosclerosis, but also for AML. Therefore, it is crucial to develop more targeted, clinically relevant therapeutic approaches for

cardiovascular disease by understanding the mechanism of key epigenetically-controlled genes. Defining the mechanisms by which HoxA5 and Klf3 are regulated and control cell function in endothelial cells may also help shed light on other disease mechanisms such as AML.

With the understanding that global inhibition of the DNA methylation machinery would be an unwise therapeutic strategy given the key role that DNA methylation plays in both the global gene expression program as well as in genome stability, we foresee the major impact of this study as the identification of specific target genes that directly play a role in EC biological functions that regulate atherosclerosis. The results of this body of work compounded with future findings will continue to elucidate the epigenetic regulation of well known genes involved in atherogenesis and will also uncover novel shear sensitive genes and regulatory pathways that have yet to be discovered.

Appendix A

Modeling Endothelial Cell Mechanoreceptors as Regulators of DNA Methyltransferase

Methods

In order to create a manageable model with the most relevant and accurate datasets available, a literature search was done to include the most prominent and well-studied mechanoreceptors that play a role in endothelial cell mechanotransduction (Table A1).

Table A1: Mechanoreceptors Involved in Endothelial Cell Mechanotransduction of Flow Environment[1]

Ion Channels	Cell- Cell and Cell-Matrix Junctions
• TRP (transient Receptor Potential) Channels a. TRPP1/TRPP2 (PC1/2 encoded by PKD1/2) b. TRPV4 c. TRPC3 d. TRPM7 • P2RX4 purinoreceptors • Inward Rectifying K+ Channels • Outward Rectifying Cl- Channels	• Integrins • PECAM1 • Adherens Junctions a. VE Cadherin • Tyrosine Kinase Receptors • Caveolae • GPCRs/G-proteins • Glycocalyx • Cytoskeleton

This list was reduced using the Ingenuity Pathways Analysis (IPA) toolkit, a proprietary algorithm that performs a systematic literature search on molecules of interest. IPA outputs the molecules' connectivity based on publications detailing the mode of interaction of two or more species. This toolkit can also perform predictive analyses based on gene or protein sequence similarity; however, this function was not applied for the prescribed project. Only published data describing molecular interactions was used to create the model in order to maintain the highest level of accuracy possible.

To produce the initial model, mechanoreceptors in Table A1 were used alongside DNMT1 as inputs into IPA and the 'build-connect' function was used to uncover true connections reported in the literature. No interactions existed directly between DNMT1 and a mechanoreceptor. This falls in line with literature reports that DNMT1 in general terminates

signaling cascades to directly transduce the biochemical signal into transcriptional changes. Due to lack of primary connectivity between species in the model, the 'build-grow' function was used to expand the network to putative secondary and tertiary interactions and the 'build-connect' function was iterated, restricting the resulting map to 100 molecules.

This map was overly expansive given the desired scope of this particular model and thus the map was trimmed. We isolated only secondary and tertiary interactions in which intermediate signaling molecules had either a direct connection to a mechanoreceptor and also to DNMT1, or had just one intermediate signaling molecule. A highly interconnected map emerged from this analysis involving three mechanoreceptors, Platelet/Endothelial Cell Adhesion Molecule 1 (PECAM1), caveolin 1 (CAV1), and Vascular Endothelial Growth Factor Receptor (VEGFR), and four intermediate signaling molecules, cyclin D1 (CCND1), Protein Kinase B (PKB, or AKT), annexin A5 (ANXA5), and embryonic ectoderm development (EED) (Figure A1).

The nature and directionality of each connection in this conceptual model was expanded upon using literature reports. The findings could be summarized into a basic description of how the upstream molecule regulated either the expression or activity of the downstream molecule in the connection. Table A2 was created using this information.

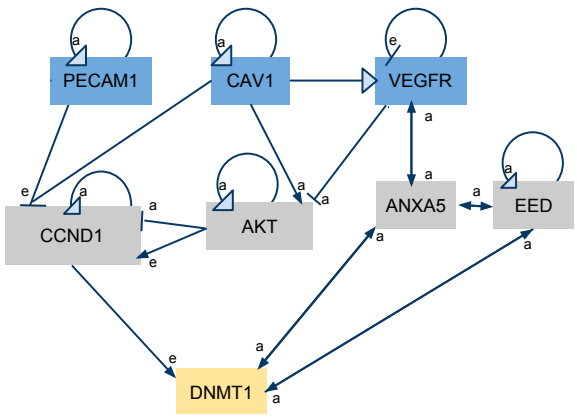

Figure A1: A Schematic Representation of the Endothelial Cell Mechanoreceptors and the Signal Transduction Pathway to DNMT1 ('a' denotes activity and 'e' denotes expression).

Table A2: Interactions between molecules. P- signifies that a molecule is phosphorylated.

Regulated → Regulators ↓	PECAM1	CAV1	VEGFR	CCND1	Akt	Anxa5	EED	DNMT1
PECAM1	Homdimerizes with PECAM1 on other cell surfaces	X	X	↓ expression	X	X	X	X
CAV1	X	•Homodimerizes & complexes with multiple proteins •P-Cav1 translocates from cytoplasm to plasma membrane	↑ P-VEGFR	↓ expression	↑Akt activation, ↑P-Akt	X	X	X
VEGFR	X	X	Neg autoreg	X	unbound VEGFR ↓ Akt activation	Binding	X	X
CCND1	X	X	X	Homodimerizes & complexes with Cdk4	X	X	X	↑ expression
Akt	X	X	X	↑ expression, ↓P-CCND1	•Translocates: cytoplasm to nucleus •Homodimerizes	X	X	X
Anxa5	X	X	Binding	X	X	X	Binding	Binding
EED	X	X	X	X	X	Binding	homodimerizes	Binding
DNMT1	X	X	X	X	X	Binding	Binding	X

In order to convert this information into a computational model, it was necessary to first define two crucial states for each molecule, expression (E), and activity (A). When E=0, the molecule is not expressed (this ignores the basal expression level, which is very low and negligible, and is assumed to be present even when E=0), and when E=1, the molecule is maximally expressed. When A=0, the molecule is inactive, and when A=1, the molecule is maximally active. A third state called (S) takes both the expression and activity into consideration, and three new states can be defined: S=0: not expressed, inactive; S=1: expressed, inactive; S=2: expressed, active. Assumptions were justified by literature evidence as detailed below:

Assumptions and Logic Rules

1. Activity and expression of the upstream "regulator" molecule are the two dominant factors affecting its downstream activity. This assumption should not affect the integrity of the model.

2. The effect of the upstream regulator on the expression or activity of the regulated molecule can be estimated by "Tri Boolean" logic[†]:
   a. If the regulator (r) decreases expression of the downstream molecule (d)[†]

	$E_{d(t+1)}$	$A_{d(t+1)}$
$S_{r(t)}$=0 or 1	No change	No change
$S_{r(t)}$=2	0	No change

   b. If the regulator (r) increases expression of the downstream molecule (d)

	$E_{d(t+1)}$	$A_{d(t+1)}$
$S_{r(t)}$=0 or 1	No change	No change
$S_{r(t)}$=2	1	No change

   c. If the regulator (r) decreases activity of the downstream molecule (d)

	$E_{d(t+1)}$	$A_{d(t+1)}$
$S_{r(t)}$=0 or 1 (non binding)	No change	No change
$S_{r(t)}$=1 (binding)	No change	1
$S_{r(t)}$=2 (binding or non)	No change	1

   d. If the regulator (r) increases activity of the downstream molecule (d)

	$E_{d(t+1)}$	$A_{d(t+1)}$
$S_{r(t)}$=0 or 1 (non binding)	No change	No change
$S_{r(t)}$=1 (binding)	No change	0
$S_{r(t)}$=2 (binding or non)	No change	0

[†]Assumes that the regulator must be both expressed and active (S=2) to alter the activity or expression of the downstream molecule, except in the case of a binding interaction, in which the regulator only needs to be expressed, but not necessarily active, to cause its downstream effect.

3. If both binding partners are expressed (E_r=1 and E_d=1) then they will bind and perform their function. Binding is dominated by chemical interactions and isn't a function that requires activity, so only presence of the molecule is necessary.
4. Homodimerization and heterodimerization interactions increase the activity of the proteins involved, and binding of two proteins does not affect the expression of either constituent.

This assumption is justified for this model in particular because as activation by complexing is a hallmark of the constituents in this system. This would not necessarily hold true in other molecular networks.

5. If two interactions of equal an opposite affect are combined, then there is no resulting change. Thus, molecules are not weighted based on their ability to affect a downstream molecule (all affects are assumed to be equal).

To test the model's ability to recapitulate experimental findings, we perturbed system with the inclusion of 5' Azacytidine, a DNMT1 inhibitor that has been used to treat various cancers because it blocks the methylation of anti-tumorigenic genes. Preliminary data from our lab shows that 5' Azacytidine also inhibits the formation of atherogenic plaques, however, the mechanism behind this remains unclear. 5' Azacytidine was shown to have an effect on both DNMT1 and the mechanoreceptor CAV1.

A sensitivity analysis was done to discover whether there is correlation between the initial conditions of the mechanoreceptors and the time for the system to reach steady state. For this model, steady state was defined by the time (t) when the state S of each molecule in the system was equivalent to the state S at the next time step (t+1). In this event, the system cannot be perturbed out of steady state because no conditions in the current state may change (this model excludes noise and random perturbations that would truly exist in a stochastic system).

Results

In the first trial run, all possible initial states of the mechanoreceptors were used to find trends in the system. For all trials, the intermediate molecules (IM) were assumed to be expressed, because when IM are not expressed, DNMT1 will never become activated (Figure A3). The cases are divided by sets of initial conditions that conferred the same or similar results.

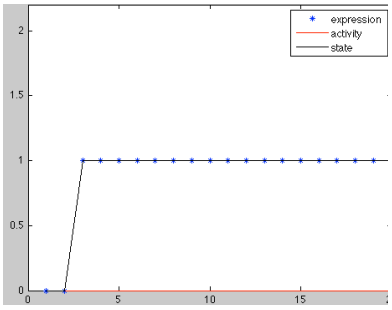

Figure A2: The case where S=0 for all IM. DNMT1 never becomes active. This state is ignored for trials varying mechanoreceptor states.

Case 1. All 3 mechanoreceptors are expressed +/- active, or both M1 and M2 are expressed +/- active (but not necessarily M3)

Table A3: Initial Conditions for Case 1

M1	M2	M3
1 or 2	1 or 2	0, 1, or 2

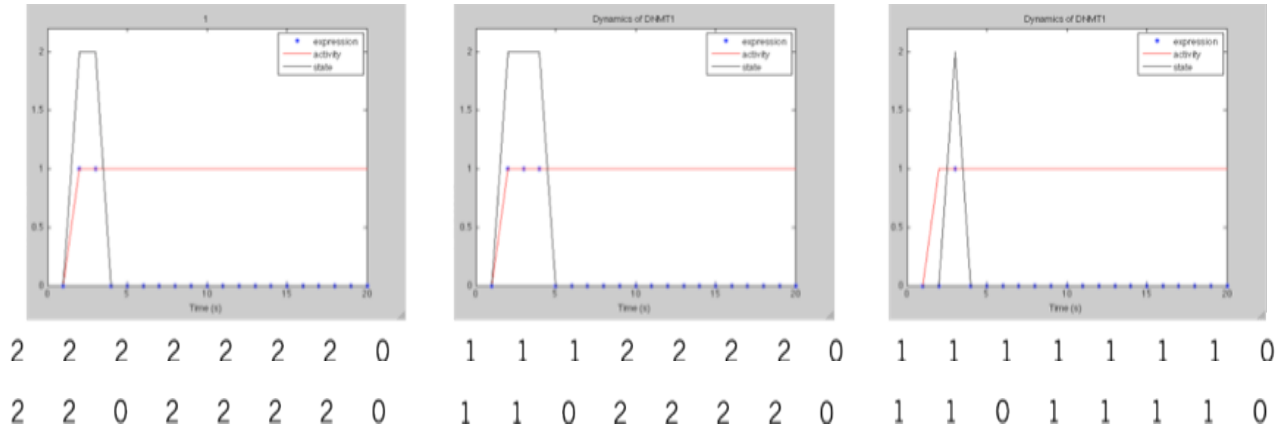

Figure A3: The Dynamics of DNMT1 activity given different initial conditions. The numbers underneath the plots represent the state S of each molecule in the system for the above plot (the first 3 values are for M1, M2, and M3, the next four values are the intermediate molecules of the signaling pathway, and the last value is DNMT1). In the third graph, activity precedes expression due to the initial state setup, as described in the discussion section.

The conclusion based on the above results is that negative feedback turns off DNMT1 when ***both*** M1 and M2 are expressed +/- active, and that the state of M3 doesn't affect Negative feedback.

Case 2. M1 or M2 or M3; M1&M3; M2&M3; No receptors expressed/active

Table A4: Initial Conditions for Case 2

M1	M2	M3
1 or 2	0	0
1 or 2	0	1 or 2
0	1 or 2	1 or 2
0	1 or 2	0

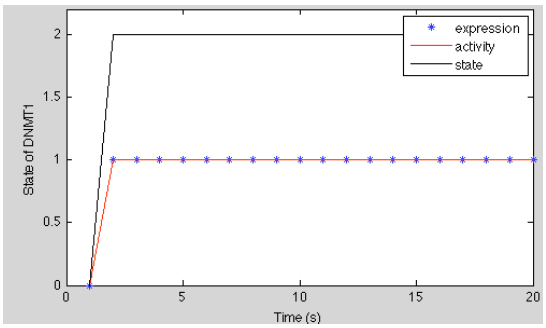

Figure A4: The Dynamics of DNMT1 activity given the different initial conditions in Table A4.

The conclusion based on the above results is that when M1 and M2 are not both expressed together, DNMT1 stays expressed and active indefinitely

Case 3. The addition of the DNMT1 inhibitor 5' Azacytidine under the previous initial conditions

Case 1 Initial Conditions

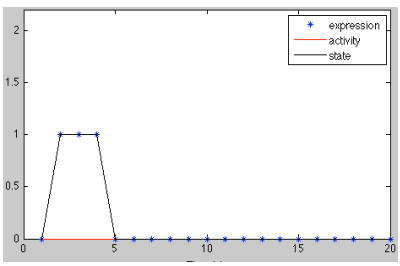

Case 2 Initial Conditions

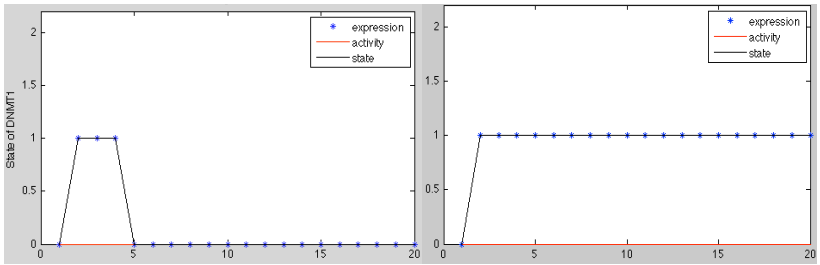

Figure A4: The Dynamics of DNMT1 expression and activity under administration of 5' Azacytidine (a DNMT1 inhibitor). (Right) M1 & M2, M1 & M3, M1 only (Left) None, M2 & M3, M2 only, M3 only

The addition of 5' Azacytidine causes the joint dependence of negative autoregulation on both M1 and M2 to be lost. Here, only M1 needs to be expressed to achieve negative autoregulation. The effects of expressed, or both expressed and active (denoted expressed +/- active) IM were also tested and the results are shown below in Figure A4.

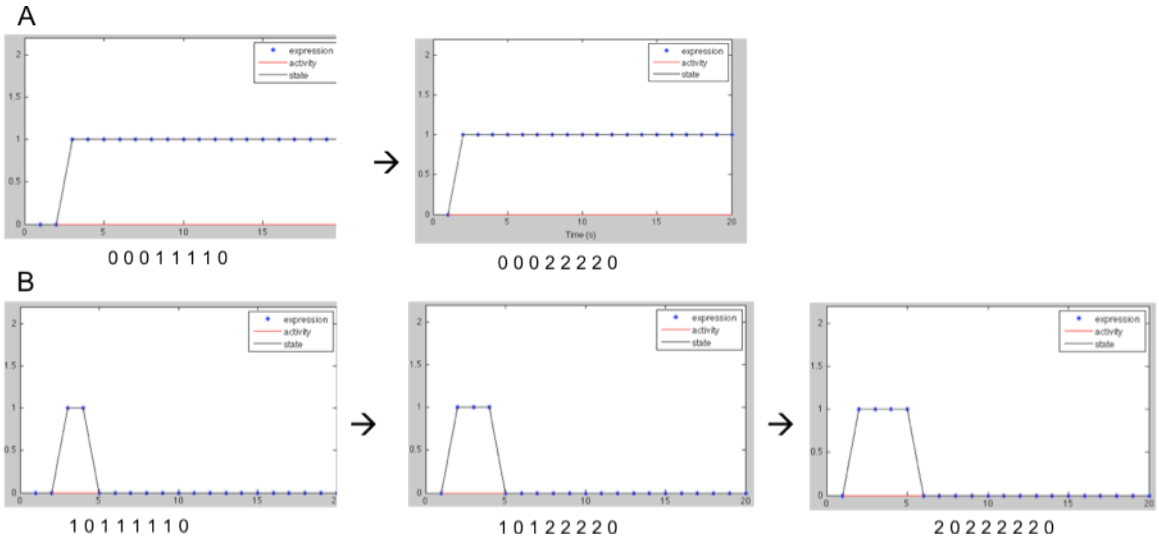

Figure A5: The effects of varying the initial states of IM from S=1 to S=2 for Case 3 (DNMT1 inhibitor) so the effects on expression can be viewed in solation. (A) Delay in expression of DNMT1when IM are expressed but not active. (B) Delay, so shorter length of time of expression of DNMT1 when IM are expressed but not active. When M are expressed but inactive, shorter length of expression than when M are both expressed and active.

Sensitivity Analysis

The sensitivity analysis was done to test how the various initial conditions affect the time for the system to reach steady state. In this case, all possible initial states were tested (combinations of each molecule, where S=0, 1, or 2). Steady state is defined as the time when the state of each molecule does not deviate at the next timepoint. It was found that under certain

conditions, shown below in Tables A5 and A6, the system reached steady state, however under the conditions in Table A7, the system never reached steady state.

Table A5: Initial Conditions where steady state is reached at timestep 3 (top) or timestep 4 (bottom).

M1	M2	M3	IM
0	0	1 or 2	2

M1	M2	M3	IM
0	0	1	1
0	0	0	0

Table A6: Initial Conditions where steady state is never reached.

M1	M2	M3	IM
1	1	1	1 or 2
1	0	0 or 1	1 or 2
0	1	0 or 1	1 or 2
1	1	0	1 or 2

It was found that under the conditions where steady state is not reached, one or more of the following 3 conditions are found to oscillate: M1 and/or M2 oscillate between active and inactive (S=1 or S=2) and IM4 between expressed and not expressed (S=0 or S-1).

Discussion

Table A7: S Matrix

E	A	S
0	0	0
0	1	0
1	0	1
1	1	2

It would have been possible to set the initial conditions with an S matrix for all possible initial states of each molecule (Tab. 8). The current model, however, initiates separate E and A matrices to allow a state where E=0 and A=1 that accounts for basal expression at E=0. The S matrix would equate the state where E, A=0 to E=0, A=1, but this neglects the activation of the basally expressed molecules. The current model maintained this state because it wasn't clear if this detail would be important. However, this complicated matters because the initial states expanded from 6,561 possibilities (3^8) to 65,536 (2^8*2^8) possibilities. The method of programming also had redundancy in combining the E and A matrices. In the future expanded model this redundancy must be corrected or the method stated above for the S matrix will be implemented (and the basally expressed molecules will not be able to be activated in the model).

In the first trial, to make the number of plots manageable, the initial conditions were only changed for the mechanoreceptor molecules since these molecules are a major control element of

the system. Then, the values of the intermediate molecules were varied synchronously. Graphs for each set of initial conditions were only plotted in the case where the dynamics of DNMT1 changed from the previous initial conditions. In the future model, a more systematic approach to plotting only the relevant graphs with important dynamical changes will be necessary to avoid a large number of redundant plots.

The model proved useful for depicting the overall dynamics of DNMT1 expression and activity for different initial conditions. It was found that this model predicts a negative feedback mechanism for DNMT1 expression under certain initial conditions. Two mechanoreceptors (M1/PECAM1 and M2/ CAV1) are implicated to be vital to the negative feedback system, while the third mechanoreceptor (M3, or VEGFR) is not found to be involved in this negative feedback. When VEGFR is expressed +/- active in the absence of PECAM1 and CAV1 expression, DNMT1 remains expressed indefinitely.

In disturbed flow conditions, three major mechanoreceptors, PECAM1, CAV1, and VEGFR, are involved in the development of atherosclerotic lesions, and DNMT1 expression is upregulated by an unknown mechanism. It has been shown that PECAM1-/- mice have reduced atherosclerotic lesions size,[15] and that CAV1 expression is upregulated in atherosclerosis (but CAV1 is deactivated under disturbed flow)[16]. This model predicts that a loss of PECAM1 and CAV1 leads to increased DNMT1 expression, but the literature supports the idea that decreased expression of these mechanoreceptors leads to slowed atherosclerosis progression (which would imply lower DNMT1 levels). These conflicting results are not clear because there remain gaps in the literature, and also several assumptions were made for this working model, so the results may not be predictive of actual system. A brief discussion of the validity of important model assumptions follows.

1. The assumption that the effect of the upstream regulator on the expression or activity of the regulated molecule can be estimated by "Tri Boolean" logic leads to inaccuracy in the model and should be modified with data that quantitatively describes the extent to which the upstream regulator affects the expression or activity of the regulated molecule (e.g. downstream protein expression for regulator knockdown or overexpression by Western Blot can be semi-quantified by ImageJ).

2. The assumption that the effects of a molecule are not weighted by the specific molecule in question adds some uncertainty to the model, and the combinatorial effects of molecules will have to be determined by further mining of the literature to find available data.

3. The assumption that if both binding partners are expressed then they will bind and perform their function should be modified in future studies. The rate of binding isn't "all or nothing," but rather depends on the relative amount of each molecule as well as their affinity to bind. The goal of this model was to support the educated design process of future experiments to study the role of mechanoreceptors in the expression of DNMT1 during the progression of atherosclerosis. It is likely that future experiments will involve knocking down or upregulating expression or activity of each of these mechanoreceptors individually and testing the changes in the state of DNMT1 to further clarify the mechanisms.

References

1 Ngai et al. Vascular Responses to Shear Stress: The Involvement of Mechanosensors in Endothelial Cells. The Open Circulation and Vascular Journal, (2010) Vol 3, 85-94.

2 Mamdouh et al. Targeted recycling of PECAM from endothelial surface-connected compartments during diapedesis. Nature, (2003) Vol 421, 748-52.

3 Lupu et al. Caveolin-1 enhances tissue factor pathway inhibitor exposure and function on the cell surface. The Journal of Biological Chemistry, (2005). Vol 280, (23): 22308-17.

4 Hulit et al. The cyclin D1 gene is transcriptionally repressed by caveolin-1. The Journal of Biological Chemistry, (2000) Vol 275, (28):21203-9.

5 Wen et al. Lipocortin V May Function as a Signaling Protein for VEGFR-2/Flk-1. Biochemical and Biophysical Research Communications, (1999) Vol 258, 713-721.

6 Shihab et al. Angiotensin II regulation of vascular endothelial growth factor and receptors Flt-1 and KDR (VEGFR2) / Flk-1 in cyclosporine nephrotoxicity. Kidney International, (2002) Vol 62, 422-433.

7 Sunet al. Identification of a novel domain at the N terminus of Cav-1 that controls rear polarization of the protein and caveolae formation. Journal of Biological Chemistry, (2007). Vol 282, (10):7232-41.

8 Jung et al.: Expression of DNA Methyltransferase 1 Is Activated by Hepatitis B Virus X Protein via a Regulatory Circuit Involving the p16 INK4a -Cyclin D1-CDK4/6-pRb-E2F1 Pathway. Cell, (2007).

9 Ohsawa et al. Molecular cloning and characterization of annexin V-binding proteins with

highly hydrophilic peptide structure. Journal of Neurochemistry, (1996) Vol 67, 89-97.
10 Datta et al. AH/PH domain-mediated interaction between Akt molecules and its potential role in Akt regulation. Molecular and cellular biology. (1995). Vol 15, (4):2304-10.
11 Tsujita et al. (2006). Nuclear targeting of Akt antagonizes aspects of cardiomyocyte hypertrophy. PNAS, Vol 103, (32):11946-51.
12 Salinas et al. Inhibition of PKB/Akt1 by C2-ceramide involves activation of ceramide-activated protein phosphatase in PC12 cells. Molecular and cellular neurosciences, (2000) Vol 15, (2):156-69.
13 Sewalt et al. Characterization of interactions between the mammalian polycomb-group proteins Enx1/EZH2 and EED suggests the existence of different mammalian polycomb-group protein complexes. Molecular and cellular biology, (1998) Vol 18, (6):3586-95.
14 Lohuizen et al.: Interaction of mouse polycomb-group (Pc-G) proteins Enx1 and Enx2 with Eed: indication for separate Pc-G complexes. Molecular and cellular biology, (1998) Vol 18, (6):3572-9.
15 Harry et al. Endothelial Cell PECAM-1 Promotes Atherosclerotic Lesions in Areas of Disturbed Flow in ApoE-Deficient Mice. Arteriosclerosis, Thrombosis, and Vascular Biology, (2008) Vol 28, 2003.
16 Frank et al. Caveolin-1 and caveolae in atherosclerosis: differential roles in fatty streak formation and neointimal hyperplasia. Curr Opin Lipidol, (2004) Vol 15, (5):523-9.
17 Ilan et al. Platelet-Endothelial Cell Adhesion Molecule-1 (CD31), a Scaffolding Molecule for Selected Catenin Family Members Whose Binding Is Mediated by Different Tyrosine and Serine / Threonine Phosphorylation. Biochemistry, (2000) Vol 275, (28):21435-21443.

Appendix B

Quantification of Endothelial Purity in genomic DNA and RNA preparations from mouse carotid arteries

Our lab recently showed that partial ligation of the mouse carotid artery induces disturbed flow with characteristic low and oscillatory wall shear stress, which in turn rapidly induces atherosclerosis, directly demonstrating the causal relationship between disturbed flow and atherosclerosis.[1] The goal of the studies detailed in Appendix B were to non-EC infiltration in our mouse partial carotid ligation model of atherosclerosis, which we have used to capture gene expression and epigenetic changes in endothelial cells caused by disturbed blood flow (d-flow).

One major complication of DNA methylation studies on samples taken directly from in vivo is the possibility for the inclusion of multiple cell types. To ensure that changes seen in our DNA methylation and gene expression data could be attributed to the endothelial response to experimental conditions rather than differential DNA methylation or gene expression occurring across different cell types, we performed a brief study to measure the number of contaminating cell types we could expect in our endothelial cell genomic DNA and RNA preparations.

Given our methods involving flushing of the complete vasculature, including the carotids, with saline prior to flushing with cell lysis buffer, we do not expect to see contamination of blood or other circulating cells. However, it is well established that immune cells invade the vessel wall to sites of injury. Because our disturbed flow conditions increase inflammatory signaling in the surrounding region, we expect that there should be some level of immune cell infiltration into the vessel wall, however, whether these cells would lie directly on the endothelial surface, causing them to be lysed along with our endothelial cells, was unknown.

It is well established that ligation increases the number of monocytes in the media and developing intima in mouse partial-ligation models.[2] Previously, our lab determined there are almost no monocyte, macrophage, or NK cell infiltrates (CD11B+ cells) in the intima.[1] However, we did not characterize the total number of white blood cells present on the intima of the LCA or RCA. Here, we performed CD45+ cell staining and FACs to examine all leukocyte cell infiltrates, including T-cells and B-cells.

I. Methods

1) qPCR

To assess EC purity for our mRNA preparations, we examined gene expression for the EC-specific platelet endothelial cell adhesion molecule 1 (PECAM1), smooth muscle cell-specific alpha smooth muscle actin (αSMA), and immune-specific cluster of differentiation molecule 11B (CD11B) markers. C57Bl6 mice were partially ligated and carotid arteries were flushed with Qiazol lysis buffer at 7 days post-ligation. RNA was collected and purified as described in the methods section of Chapter 4.

2) eNOS Bisulfite Sequencing

Endothelial Nitric Oxide Synthase (eNOS) is a well-known EC-specific gene that is demethylated only in ECs, enabling its cell-specific expression[3]. We performed bisulfite sequencing on eNOS in our LCA/RCA model because others have shown that eNOS DNA methylation increases in endothelial cells exposed to d-flow. gDNA was collected from the carotid arteries using the same scheme as for qPCR, but flushing with Buffer and gDNA isolation as described in the Chapter 4 methods. Additionally, the leftover carotid tissue after flushing was saved and digested with Buffer AL, and genomic DNA was extracted by the same method. Bisulfite sequencing was done according to the protocol by Chan et al., using their primers listed in Table B1 and qPCR cycling methods detailed in their publication[3].

Table B1: Bisulfite sequencing primers to analyze DNA methylation in the mouse eNOS promoter[3]

m_eNOS_Mu-409S	AGATAGGAGAGGAGTAAGGGTGAATTT
m_eNOS_Mu+73AS	CCCTAAACCACAAAATAACCCAAACTC
m_eNOS_Mu-230S	GGTTTTTATTTATTAGTTTTAGTTTTT
m_eNOS_Mu+57AS	AACCCAAACTCCTAACCCACACTCTTC

3) Immunohistochemistry and cell counting algorithm

C57Bl6 mice were partially ligated and *en face* staining was done on the carotids either before or after flushing with Buffer AL at 7 days post-ligation. Frozen blocks containing the heart, aortic arch, and carotid arteries were prepared in TissueTek and stored at –80°C.

Immunohistochemistry was performed on sections from the frozen blocks using the following antibodies at a 1:50 dilution: VE-Cadherin (sc-6458; Santa Cruz Biotechnology), CD45 (13-0454; eBioscience), and DAPI (1:10,000).

The stained carotids were imaged using confocal microscopy. The field of view of each image was 0.25 mm^2. The total number of cells present in the region was quantified using DAPI nuclear stain, the number of endothelial cells was quantified by the number of cells staining positive for VE-Cadherin, and the number of immune Cells was quantified by the number of cells staining positive for CD45. The CD45+ stain includes all leukocyte groups: Granulocytes, Monocytes, T lymphocytes, T helper cells, Cytotoxic T cells, B lymphocytes, Thrombocytes, Dendritic cells.

To determine the ratio of endothelial and immune cells in the carotid intima, we developed and validated an automated method to count total cells, endothelial cells only, and CD45+ cells only using CellProfiler. The steps in our CellProfiler macro included first separating the confocal image by color filters into an RGB image.

We then used the Blue image (DAPI-only) to define and remove SMCs from the total cell count. SMCs are easily identified according to their nuclear shape (Figure B1). We used eccentricity of the nucleus (blue stained area) as a measure of elongation to separate between ECs and non-ECs because EC's are known to align with flow. We used published images by Ferrara et al. to define the nuclear eccentricity for a non-SMC as < 0.88, and for a SMC as > 0.88.[4] For reference, the eccentricity of a perfectly straight line is 1, and the eccentricity of a perfect circle is 0. We next counted the number of non-SMC nuclei (nucleus eccentricity < 0.88) and used this as the total cell count (ECs + intimal cell infiltrates). Automated cell counts for ECs, SMCs, and immune cells using Cell Profiler were validated by undergraduate researcher Daniel Kim for 50 images.

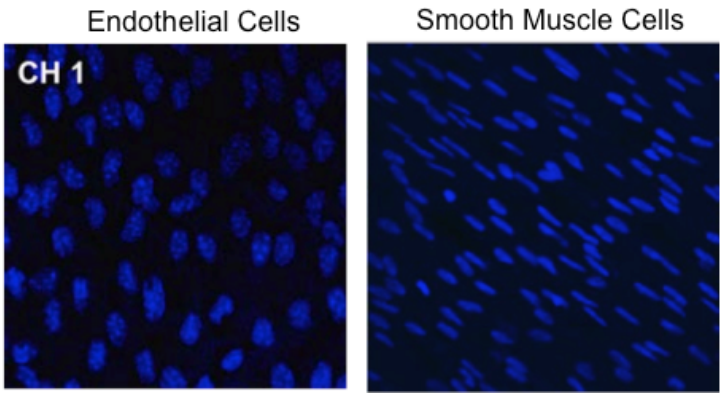

Figure B1: Differences in nuclear morphology found by Ferrara et al. are evident by nuclear staining of ECs and SMCs.[4]

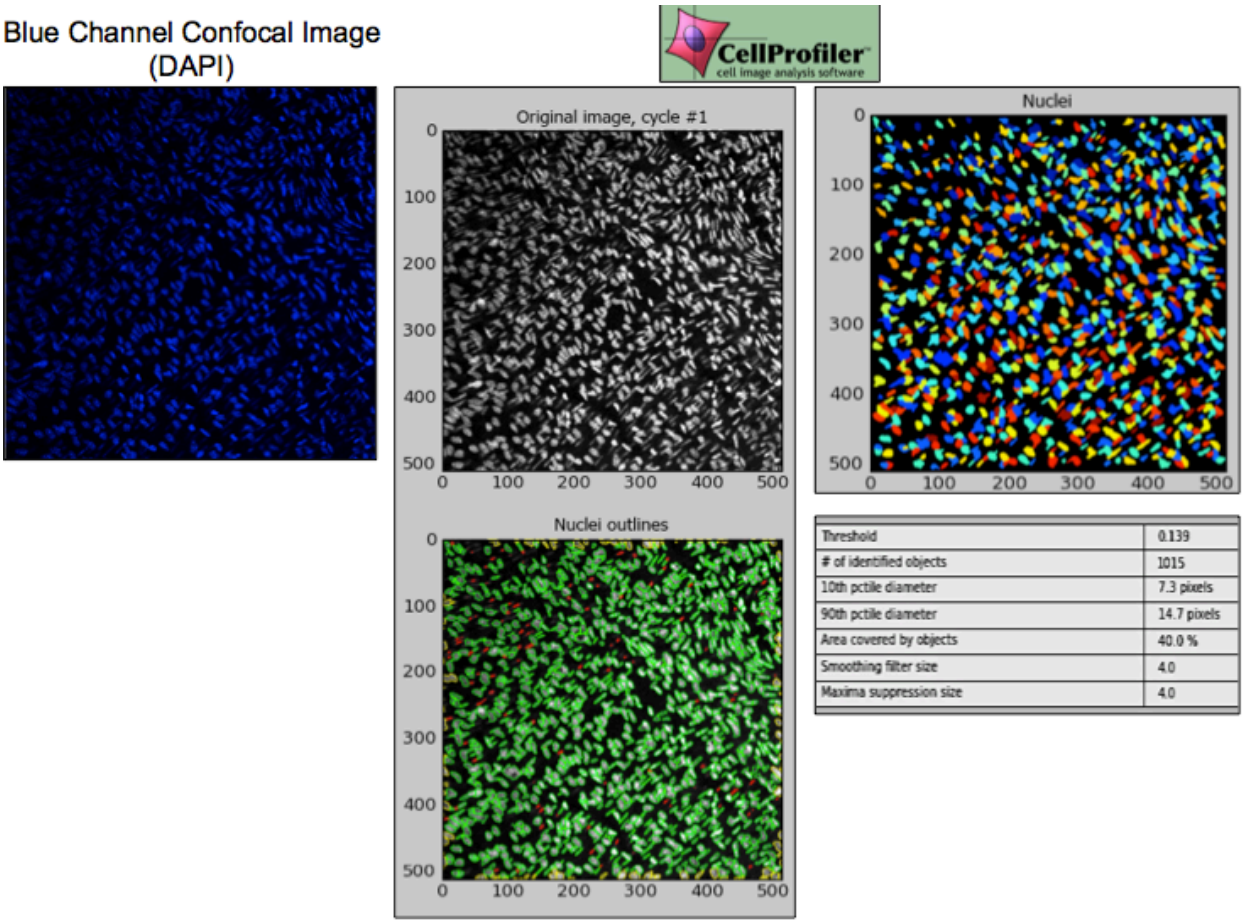

Figure B2: Cell Profiler macro was developed to count the number of endothelial cells based on their nuclear morphology. The ellipticity of objects identified by DAPI stain (nuceli; Blue channel image to left) was used as a threshold to distinguish between ECs and SMCs

To further determine the breakdown of ECs vs immune cells, we used the red image to count the number of CD45+ stained cells. We then determined the number of ECs by subtracting the number of CD45+ cells from the number of non-SMC cells. We validated this approach for determining the number of ECs using VE-Cadherin staining for ECs on separate samples.

A workflow for the Cell Profiler macro is as follows:

1. Separate the image into the Red, Green, and Blue (RGB) components
2. Using the blue image (the DAPI stain), separate by eccentricity
   - Define non-EC cell nucleus eccentricity <0.88
   - Count # EC nuclei
3. Using the CD45+ red image:
   - Count the number positive stained cells
   - Calculate the total # ECs = [nonSMC cells - CD45+ cells]
4. Validate the EC count using the VECadherin+ green image:
   - # ECs ≈ # VECadherin-positive cells

4) Fluorescence Activated Cell Sorting (FACs)

FACs studies were performed with the help of Noah Alberts-Grill and Amir Rezvan. Secondary staining of CD45-biotin was performed using streptavidin-conjugated Qdot 655. Immunofluorescence was detected using a LSR II flow cytometer, using AccuCount Ultra Rainbow Fluorescent Particles to determine absolute cell numbers. All flow analyses were performed using FlowJo analysis software (v5.0).

II. Results

1) qPCR

As expected, we found that a low level of smooth muscle cell (SMC) and immune cell marker gene expression in our preparations. The levels of aSMA were consistent among all preps and CD11B was increased only in the LCA, with a reduction in its expression upon 5Aza treatment. This indicated that gene expression changes we observe could potentially be due to contaminating cell types, particularly of the immune milieu.

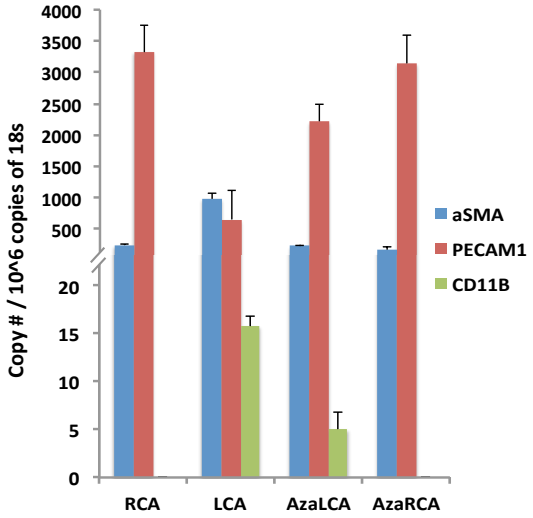

Figure B3: Endothelial, Smooth Muscle, and Immune cell marker expression in endothelial-enriched carotid artery RNA preparations

2) eNOS Bisulfite Sequencing

Bisulfite sequencing of the eNOS promoter of gDNA from both endothelial-enriched and leftover tissue samples demonstrate that in the RCA endothelial-enriched gDNA, eNOS is demethylated at the promoter. In the LCA, eNOS is hypermethylated (~50% of clones are fully methylated), but upon treatment with 5Aza this hypermethylation is diminished. In the leftover samples consisting mainly of smooth muscle cells and fibroblasts, the eNOS promoter is heavily methylated. This indicates the validity of our endothelial-enriched gDNA preparation methods

from the carotid arteries, and that the ratio of infiltrating cells to ECs is not sufficient to contribute to BS-Seq results significantly.

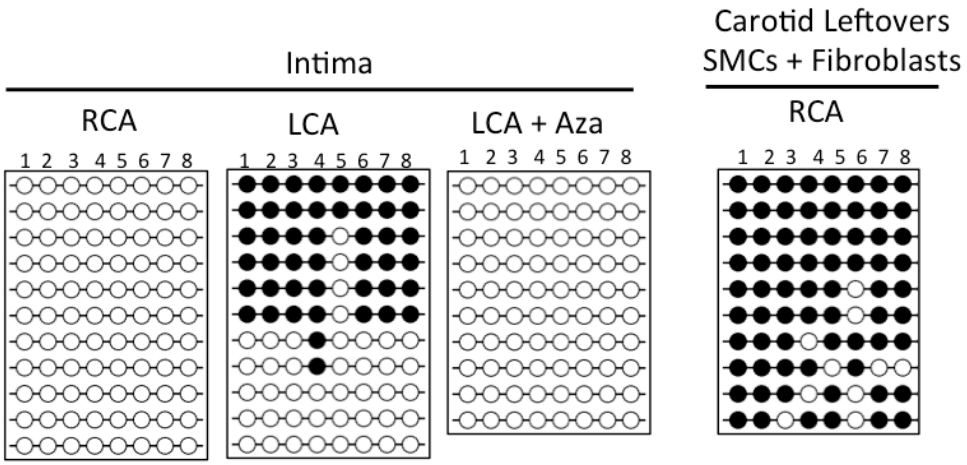

Figure B4: DNA methylation of EC and non-EC cells in the carotid arteries.

As a specific example of this analysis, CG site #4 in Figure B4 has a methylation ratio of 8/11 methylated CG sites, and so the eNOS promoter at site #4 in the LCA is ~73% methylated. If this result were due solely to infiltration of non-EC populations into our gDNA preparation, infiltrating cells would have to make up > 73% of the total cell population (8/11) in the LCA. This is because under normal circumstances endothelial cells are never methylated at this site (see site #4 of the RCA (Figure B4), and refer to Chan et al)[3], and thus any methylation present would either have to come from infiltrating cells or increased methylation in ECs. Further results from cell counting below indicate that infiltrating cell types comprise a minimal subset of the the gDNA preparation, and thus we can attribute these methylation changes to endothelial cell DNA methylation changes rather than an increase in the number of non-ECs in the gDNA preparation.

3) Immunohistochemistry and cell counting

The cell profiler algorithms were able to distinguish well between ECs, SMCs, and immune cells. As can be seen in Figure B5 (lower panel), the EC nuclei line up with VECad+ cells, whereas the SMC nuclei do not. As a validation of our methods, we found that the number of EC's we observed in the carotids and aortic arch were consistent with literature reports of EC densities in the LC, GC, and descending thoracic aorta (DT), where an EC density of ≈2500 ECs

per millimeter squared was reported in the murine aorta (Table B2).[5] Final calculations of EC numbers is listed in Table B3.

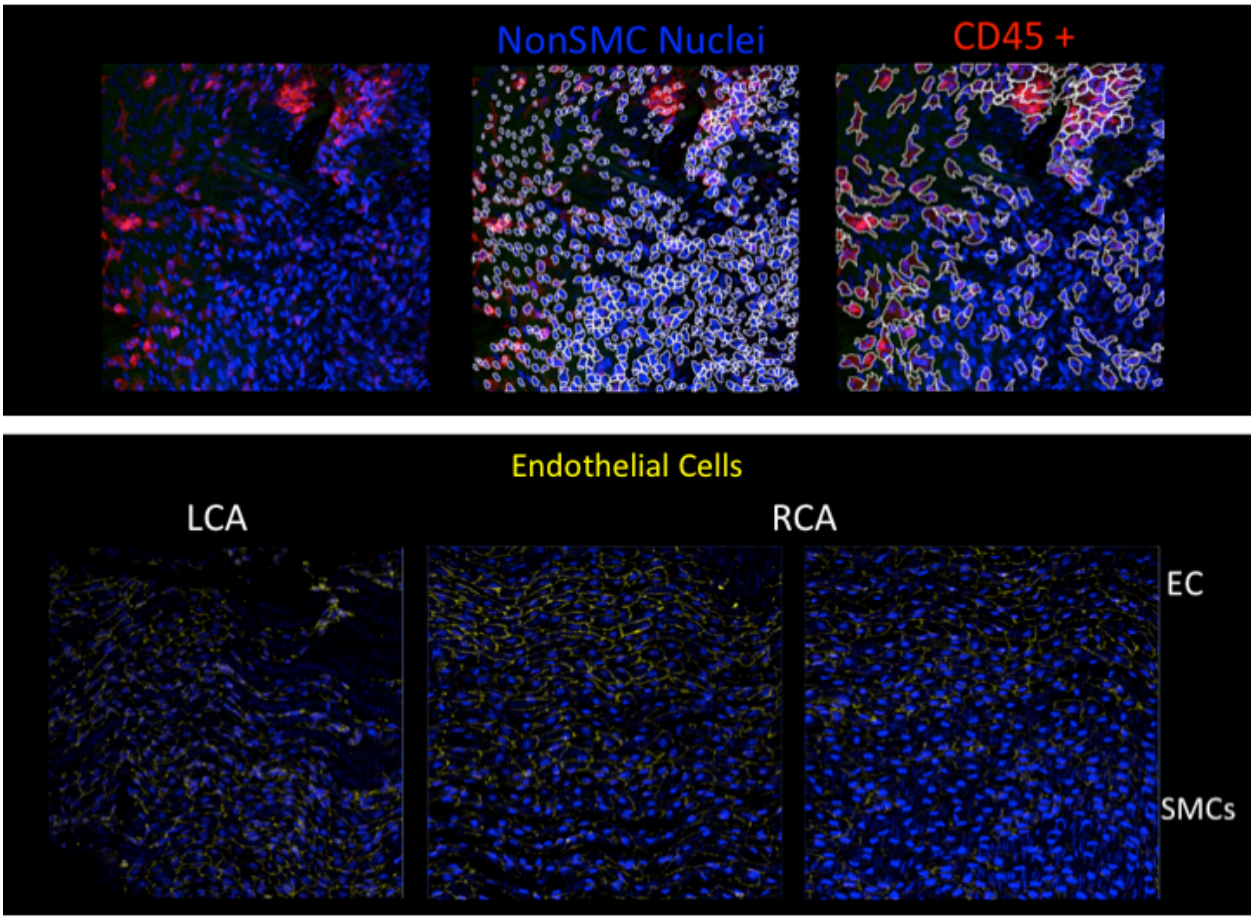

Figure B5: Representative images output from the Cell Profiler cell counting algorithm, showing processing steps from original RGB image (left) to capture of all non-SMC nuclei (center) to capture of CD45+ cells only (right). (upper) and VE-Cadherin/DAPI co-stain (lower) (20X magnification, 0.25 mm^2 field of view)

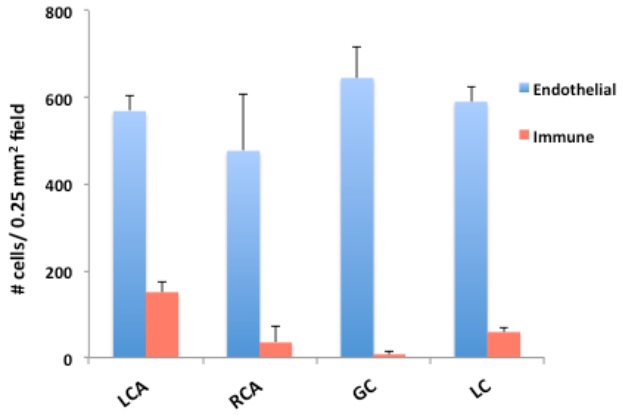

Figure B6: Number of EC's and Immune cells in either the vessel wall or the GC and LC per field view (n=3; each carotid imaged twice)

Table B2: Number of EC's observed in the carotids and aortic arch (left) are consistent with literature reports (right)[5]

	Nuclei/mm²	ECs/mm²	CD45+ cells/mm²
LCA	2875	2272	604
RCA	2050	1906	144
GC	2603	2577	26
LC	2596	2359	237

Table I. Number of nuclei or endothelial cells (EC) and nuclear density in different segments of mouse aorta

	Nuclei/mm²	EC/mm²	Density[a]
LC	3,415 ±74.4[b, c] *n*[d] = 6	2,431 ± 57.8 *n* = 12	1.40
GC	2,691 ± 88.91 *n* = 3	2,685 ± 93.25 *n* = 10	1.00
DT	2,657 ± 103.3 *n* = 3	2,549 ± 148.4 *n* = 4	1.04

[a]Nuclei/EC.
[b]Mean ± SE.
[c]P < 0.001 when compared with the EC number in LC.
[d]Total number of areas counted.

Although we have EC-enriched gDNA, there may be some heterogeneity due to contaminating cell types that have contributed their methylation signatures. We found our preparations to be at least 80% endothelial cells (Table B3).

Table B3: The percent of EC vs. Immune cell populations existing on the inner surface of the vessel wall as determined by IHC staining and cell counting using Cell Profiler.

	% ECs	% CD45+ cells
LCA	80.2	19.8
RCA	94.4	5.6
GC	98.7	1.3

LC	90.7	9.3

4) FACs validation of cell counts

Our FACs analysis demonstrated a higher immune cell infiltration into the vascular wall than shown by the previous studies. However, these experiments were done on the whole vessel wall rather than just the intima, and thus we expect that a major portion of these infiltrating leukocytes are coming from regions of the blood vessel wall other than the intimal layer. This is supported by our previous experiments examining just the intimal layer. Additionally, we only performed two replicates (n=2, each contains 5 mouse carotids pooled), and although each replicate shows significant immune cell infiltration into the LCA of C57Bl6 mice 7 days post-ligation, we cannot conclude whether these results are statistically significant from this data alone.

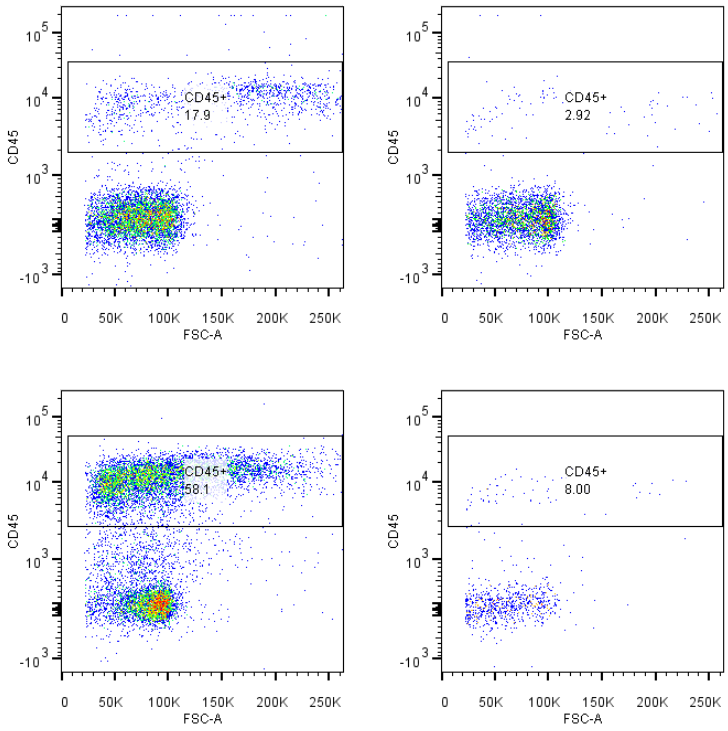

Figure B7: FACs data of leukocyte infiltration into the carotid artery wall using whole digested arteries.

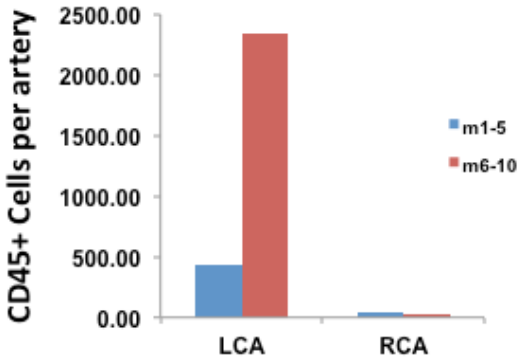

Figure B8: Number of CD45+ cells per artery. Each sample is 5 mouse carotid arteries pooled. Two samples are shown above.

Discussion

While our carotid intima DNA preparations using the flushing method are endothelial-enriched, they are not 100% endothelial pure. We do expect some contributions of genetic material from non-endothelial cells, particularly infiltrating leukocytes, that settle on the intima of the vascular walls. It is of vital importance to understand the level of endothelial cell purity of our genomic DNA or RNA preparations obtained by flushing the intimal layer of the carotid artery. We thus undertook this study to quantify the number of CD45+ cells (which includes all leukocyte groups: Granulocytes, Monocytes, T lymphocytes, T helper cells, Cytotoxic T cells, B lymphocytes, Thrombocytes, Dendritic cells- cite).

Detailed analysis of the results from these experiments indicate that we have minimal contamination from SMCs and immune cells in our endothelial preparations, and underscore the validity of our experimental and analytical methods for the following experiments.

1 Nam, D. *et al.* Partial carotid ligation is a model of acutely induced disturbed flow, leading to rapid endothelial dysfunction and atherosclerosis. *Am J Physiol Heart Circ Physiol* **297**, H1535-1543, doi:10.1152/ajpheart.00510.2009 (2009).

2 Korshunov, V. A. & Berk, B. C. Flow-induced vascular remodeling in the mouse: a model for carotid intima-media thickening. *Arterioscler Thromb Vasc Biol* **23**, 2185-2191, doi:10.1161/01.ATV.0000103120.06092.14 (2003).

3 Chan, Y. *et al.* The cell-specific expression of endothelial nitric-oxide synthase: a role for DNA methylation. *J Biol Chem* **279**, 35087-35100, doi:10.1074/jbc.M405063200 (2004).

4 Ferrara, D. E. *et al.* Quantitative 3D fluorescence technique for the analysis of en face preparations of arterial walls using quantum dot nanocrystals and two-photon excitation laser scanning microscopy. *American journal of physiology. Regulatory, integrative and comparative physiology* **290**, R114-123, doi:10.1152/ajpregu.00449.2005 (2006).

5 Jongstra-Bilen, J. *et al.* Low-grade chronic inflammation in regions of the normal mouse arterial intima predisposed to atherosclerosis. *The Journal of experimental medicine* **203**, 2073-2083, doi:10.1084/jem.20060245 (2006).

REFERENCES

1 Mozaffarian, D. *et al.* Executive summary: heart disease and stroke statistics-2015 update: a report from the american heart association. *Circulation* **131**, 434-441, doi:10.1161/CIR.0000000000000157 (2015).

2 Libby, P. & Theroux, P. Pathophysiology of coronary artery disease. *Circulation* **111**, 3481-3488, doi:10.1161/CIRCULATIONAHA.105.537878 (2005).

3 Corti, R., Hutter, R., Badimon, J. J. & Fuster, V. Evolving concepts in the triad of atherosclerosis, inflammation and thrombosis. *Journal of thrombosis and thrombolysis* **17**, 35-44, doi:10.1023/B:THRO.0000036027.39353.70 (2004).

4 Fruchart, J. C., Nierman, M. C., Stroes, E. S., Kastelein, J. J. & Duriez, P. New risk factors for atherosclerosis and patient risk assessment. *Circulation* **109**, III15-19, doi:10.1161/01.CIR.0000131513.33892.5b (2004).

5 Akimoto, S., Mitsumata, M., Sasaguri, T. & Yoshida, Y. Laminar shear stress inhibits vascular endothelial cell proliferation by inducing cyclin-dependent kinase inhibitor p21(Sdi1/Cip1/Waf1). *Circ Res* **86**, 185-190 (2000).

6 Garcia-Cardena, G., Comander, J. I., Blackman, B. R., Anderson, K. R. & Gimbrone, M. A. Mechanosensitive endothelial gene expression profiles: scripts for the role of hemodynamics in atherogenesis? *Ann N Y Acad Sci* **947**, 1-6 (2001).

7 Chatzizisis, Y. S. *et al.* Role of endothelial shear stress in the natural history of coronary atherosclerosis and vascular remodeling: molecular, cellular, and vascular behavior. *J Am Coll Cardiol* **49**, 2379-2393, doi:10.1016/j.jacc.2007.02.059 (2007).

8 Chien, S., Li, S. & Shyy, Y. J. Effects of mechanical forces on signal transduction and gene expression in endothelial cells. *Hypertension* **31**, 162-169 (1998).

9 He, X. H. *et al.* [Effect of chronic enhanced external counterpulastion on gene expression profiles of arterial endothelial cells of pigs fed with high-cholesterol diet]. *Nan fang yi ke da xue xue bao = Journal of Southern Medical University* **28**, 1195-1197 (2008).

10 White, S. J. *et al.* Characterization of the differential response of endothelial cells exposed to normal and elevated laminar shear stress. *J Cell Physiol* **226**, 2841-2848, doi:10.1002/jcp.22629 (2011).

11 Gimbrone, M. A., Jr., Topper, J. N., Nagel, T., Anderson, K. R. & Garcia-Cardena, G. Endothelial dysfunction, hemodynamic forces, and atherogenesis. *Annals of the New York Academy of Sciences* **902**, 230-239; discussion 239-240 (2000).

12 Chappell, D. C., Varner, S. E., Nerem, R. M., Medford, R. M. & Alexander, R. W. Oscillatory shear stress stimulates adhesion molecule expression in cultured human endothelium. *Circ Res* **82**, 532-539 (1998).

13 Dhawan, S. S. *et al.* Shear stress and plaque development. *Expert review of cardiovascular therapy* **8**, 545-556, doi:10.1586/erc.10.28 (2010).

14 Abumiya, T., Sasaguri, T., Taba, Y., Miwa, Y. & Miyagi, M. Shear stress induces expression of vascular endothelial growth factor receptor Flk-1/KDR through the CT-rich Sp1 binding site. *Arterioscler Thromb Vasc Biol* **22**, 907-913 (2002).

15 Topper, J. N., Cai, J., Falb, D. & Gimbrone, M. A., Jr. Identification of vascular endothelial genes differentially responsive to fluid mechanical stimuli: cyclooxygenase-2, manganese superoxide dismutase, and endothelial cell nitric oxide synthase are selectively up-regulated by steady laminar shear stress. *Proc Natl Acad Sci U S A* **93**, 10417-10422 (1996).

16 Dunn, J. *et al.* Flow-dependent epigenetic DNA methylation regulates endothelial gene expression and atherosclerosis. *J Clin Invest* **124**, 3187-3199, doi:10.1172/JCI74792 (2014).

17 Ni, C. W. *et al.* Discovery of novel mechanosensitive genes in vivo using mouse carotid artery endothelium exposed to disturbed flow. *Blood* **116**, e66-73, doi:10.1182/blood-2010-04-278192 (2010).
18 Libby, P. Inflammation in atherosclerosis. *Arterioscler Thromb Vasc Biol* **32**, 2045-2051, doi:10.1161/ATVBAHA.108.179705 (2012).
19 Libby, P., Ridker, P. M. & Hansson, G. K. Progress and challenges in translating the biology of atherosclerosis. *Nature* **473**, 317-325, doi:10.1038/nature10146 (2011).
20 Garcia-Cardena, G., Comander, J., Anderson, K. R., Blackman, B. R. & Gimbrone, M. A., Jr. Biomechanical activation of vascular endothelium as a determinant of its functional phenotype. *Proc Natl Acad Sci U S A* **98**, 4478-4485, doi:10.1073/pnas.071052598 (2001).
21 Chien, S. Mechanotransduction and endothelial cell homeostasis: the wisdom of the cell. *Am J Physiol Heart Circ Physiol* **292**, H1209-1224, doi:10.1152/ajpheart.01047.2006 (2007).
22 Davies, P. F. Flow-mediated endothelial mechanotransduction. *Physiol Rev* **75**, 519-560 (1995).
23 Nagel, T., Resnick, N., Atkinson, W. J., Dewey, C. F., Jr. & Gimbrone, M. A., Jr. Shear stress selectively upregulates intercellular adhesion molecule-1 expression in cultured human vascular endothelial cells. *J Clin Invest* **94**, 885-891, doi:10.1172/JCI117410 (1994).
24 Berliner, J. A. *et al.* Atherosclerosis: basic mechanisms. Oxidation, inflammation, and genetics. *Circulation* **91**, 2488-2496 (1995).
25 Skogsberg, J. *et al.* Transcriptional profiling uncovers a network of cholesterol-responsive atherosclerosis target genes. *PLoS Genet* **4**, e1000036, doi:10.1371/journal.pgen.1000036 (2008).
26 Chen, B. P. *et al.* DNA microarray analysis of gene expression in endothelial cells in response to 24-h shear stress. *Physiological genomics* **7**, 55-63 (2001).
27 Robertson, K. D. DNA methylation and chromatin - unraveling the tangled web. *Oncogene* **21**, 5361-5379, doi:10.1038/sj.onc.1205609 (2002).
28 Jaenisch, R. & Bird, A. Epigenetic regulation of gene expression: how the genome integrates intrinsic and environmental signals. *Nat Genet* **33 Suppl**, 245-254, doi:10.1038/ng1089 (2003).
29 Ansel, K. M., Lee, D. U. & Rao, A. An epigenetic view of helper T cell differentiation. *Nature immunology* **4**, 616-623, doi:10.1038/ni0703-616 (2003).
30 de Laat, W. & Grosveld, F. Spatial organization of gene expression: the active chromatin hub. *Chromosome research : an international journal on the molecular, supramolecular and evolutionary aspects of chromosome biology* **11**, 447-459 (2003).
31 Fahrner, J. A. & Baylin, S. B. Heterochromatin: stable and unstable invasions at home and abroad. *Genes & development* **17**, 1805-1812, doi:10.1101/gad.1123303 (2003).
32 Ragoczy, T., Telling, A., Sawado, T., Groudine, M. & Kosak, S. T. A genetic analysis of chromosome territory looping: diverse roles for distal regulatory elements. *Chromosome research : an international journal on the molecular, supramolecular and evolutionary aspects of chromosome biology* **11**, 513-525 (2003).
33 Illi, B. *et al.* Shear stress-mediated chromatin remodeling provides molecular basis for flow-dependent regulation of gene expression. *Circ Res* **93**, 155-161, doi:10.1161/01.RES.0000080933.82105.29 (2003).
34 Illi, B. *et al.* Epigenetic histone modification and cardiovascular lineage programming in mouse embryonic stem cells exposed to laminar shear stress. *Circ Res* **96**, 501-508, doi:10.1161/01.RES.0000159181.06379.63 (2005).
35 Jeltsch, A. Beyond Watson and Crick: DNA methylation and molecular enzymology of DNA methyltransferases. *Chembiochem* **3**, 274-293 (2002).

36 Eckhardt, F. *et al.* DNA methylation profiling of human chromosomes 6, 20 and 22. *Nat Genet* **38**, 1378-1385, doi:10.1038/ng1909 (2006).
37 Gardiner-Garden, M. & Frommer, M. CpG islands in vertebrate genomes. *Journal of molecular biology* **196**, 261-282 (1987).
38 Bestor, T. H., Gundersen, G., Kolsto, A. B. & Prydz, H. CpG islands in mammalian gene promoters are inherently resistant to de novo methylation. *Genetic analysis, techniques and applications* **9**, 48-53 (1992).
39 Takai, D. & Jones, P. A. Comprehensive analysis of CpG islands in human chromosomes 21 and 22. *Proc Natl Acad Sci U S A* **99**, 3740-3745, doi:10.1073/pnas.052410099 (2002).
40 Strichman-Almashanu, L. Z. *et al.* A genome-wide screen for normally methylated human CpG islands that can identify novel imprinted genes. *Genome Res* **12**, 543-554, doi:10.1101/gr.224102. Article published online before print in March 2002 (2002).
41 Rollins, R. A. *et al.* Large-scale structure of genomic methylation patterns. *Genome Res* **16**, 157-163, doi:10.1101/gr.4362006 (2006).
42 Li, M. & Chen, S. S. The tendency to recreate ancestral CG dinucleotides in the human genome. *BMC evolutionary biology* **11**, 3, doi:10.1186/1471-2148-11-3 (2011).
43 Duncan, B. K. & Miller, J. H. Mutagenic deamination of cytosine residues in DNA. *Nature* **287**, 560-561 (1980).
44 Jones, P. A. & Baylin, S. B. The fundamental role of epigenetic events in cancer. *Nat Rev Genet* **3**, 415-428, doi:10.1038/nrg816 (2002).
45 Rideout, W. M., 3rd, Coetzee, G. A., Olumi, A. F. & Jones, P. A. 5-Methylcytosine as an endogenous mutagen in the human LDL receptor and p53 genes. *Science* **249**, 1288-1290 (1990).
46 Turunen, M. P. & Yla-Herttuala, S. Epigenetic regulation of key vascular genes and growth factors. *Cardiovasc Res* **90**, 441-446, doi:10.1093/cvr/cvr109 (2011).
47 Nazarenko, M. S. *et al.* Methylation profiling of DNA in the area of atherosclerotic plaque in humans. *Molecular Biology* **45**, 561-566, doi:10.1134/s0026893311030125 (2011).
48 Wierda, R. J., Geutskens, S. B., Jukema, J. W., Quax, P. H. & van den Elsen, P. J. Epigenetics in atherosclerosis and inflammation. *J Cell Mol Med* **14**, 1225-1240, doi:10.1111/j.1582-4934.2010.01022.x (2010).
49 Hiltunen, M. O. & Yla-Herttuala, S. DNA methylation, smooth muscle cells, and atherogenesis. *Arterioscler Thromb Vasc Biol* **23**, 1750-1753, doi:10.1161/01.ATV.0000092871.30563.41 (2003).
50 Hiltunen, M. O. *et al.* DNA hypomethylation and methyltransferase expression in atherosclerotic lesions. *Vascular medicine* **7**, 5-11 (2002).
51 Huang, Y. S., Zhi, Y. F. & Wang, S. R. Hypermethylation of estrogen receptor-alpha gene in atheromatosis patients and its correlation with homocysteine. *Pathophysiology : the official journal of the International Society for Pathophysiology / ISP* **16**, 259-265, doi:10.1016/j.pathophys.2009.02.010 (2009).
52 Post, W. S. *et al.* Methylation of the estrogen receptor gene is associated with aging and atherosclerosis in the cardiovascular system. *Cardiovasc Res* **43**, 985-991 (1999).
53 Chang, P. Y. *et al.* Homocysteine inhibits arterial endothelial cell growth through transcriptional downregulation of fibroblast growth factor-2 involving G protein and DNA methylation. *Circ Res* **102**, 933-941, doi:10.1161/CIRCRESAHA.108.171082 (2008).
54 Jamaluddin, M. S., Yang, X. & Wang, H. Hyperhomocysteinemia, DNA methylation and vascular disease. *Clin Chem Lab Med* **45**, 1660-1666, doi:10.1515/CCLM.2007.350 (2007).

55 Issa, J. P. CpG-island methylation in aging and cancer. *Current topics in microbiology and immunology* **249**, 101-118 (2000).
56 Liu, C. *et al.* Transcriptional regulation of 15-lipoxygenase expression by promoter methylation. *Exp Cell Res* **297**, 61-67, doi:10.1016/j.yexcr.2004.02.014 (2004).
57 Ghoshal, K. *et al.* 5-Aza-deoxycytidine induces selective degradation of DNA methyltransferase 1 by a proteasomal pathway that requires the KEN box, bromo-adjacent homology domain, and nuclear localization signal. *Mol Cell Biol* **25**, 4727-4741, doi:10.1128/MCB.25.11.4727-4741.2005 (2005).
58 Mossman, D., Kim, K. T. & Scott, R. J. Demethylation by 5-aza-2'-deoxycytidine in colorectal cancer cells targets genomic DNA whilst promoter CpG island methylation persists. *BMC Cancer* **10**, 366, doi:10.1186/1471-2407-10-366 (2010).
59 Liu, Z. *et al.* 5-Aza-2'-deoxycytidine induces retinoic acid receptor-beta(2) demethylation and growth inhibition in esophageal squamous carcinoma cells. *Cancer Lett* **230**, 271-283, doi:10.1016/j.canlet.2005.01.012 (2005).
60 Christman, J. K. 5-Azacytidine and 5-aza-2'-deoxycytidine as inhibitors of DNA methylation: mechanistic studies and their implications for cancer therapy. *Oncogene* **21**, 5483-5495, doi:10.1038/sj.onc.1205699 (2002).
61 Issa, J. P. *et al.* Phase II study of low-dose decitabine in patients with chronic myelogenous leukemia resistant to imatinib mesylate. *J Clin Oncol* **23**, 3948-3956, doi:10.1200/JCO.2005.11.981 (2005).
62 Lemaire, M. *et al.* Importance of dose-schedule of 5-aza-2'-deoxycytidine for epigenetic therapy of cancer. *BMC Cancer* **8**, 128, doi:10.1186/1471-2407-8-128 (2008).
63 Chen, W., Bacanamwo, M. & Harrison, D. G. Activation of p300 histone acetyltransferase activity is an early endothelial response to laminar shear stress and is essential for stimulation of endothelial nitric-oxide synthase mRNA transcription. *J Biol Chem* **283**, 16293-16298, doi:10.1074/jbc.M801803200 (2008).
64 Illi, B. *et al.* Shear stress-mediated chromatin remodeling provides molecular basis for flow-dependent regulation of gene expression. *Circ Res* **93**, 155-161, doi:10.1161/01.RES.0000080933.82105.29 (2003).
65 Jiang, Y. Z. *et al.* Hemodynamic Disturbed Flow Induces Differential DNA Methylation of Endothelial Kruppel-Like Factor 4 (KLF4) Promoter In Vitro and In Vivo. *Circ Res*, doi:10.1161/CIRCRESAHA.115.303883 (2014).
66 Zhou, J., Li, Y. S., Wang, K. C. & Chien, S. Epigenetic Mechanism in Regulation of Endothelial Function by Disturbed Flow: Induction of DNA Hypermethylation by DNMT1. *Cell Mol Bioeng* **7**, 218-224, doi:10.1007/s12195-014-0325-z (2014).
67 Jones, P. A. & Martienssen, R. A blueprint for a Human Epigenome Project: the AACR Human Epigenome Workshop. *Cancer Res* **65**, 11241-11246, doi:10.1158/0008-5472.CAN-05-3865 (2005).
68 Anderson, K. P., Kern, C. B., Crable, S. C. & Lingrel, J. B. Isolation of a gene encoding a functional zinc finger protein homologous to erythroid Kruppel-like factor: identification of a new multigene family. *Mol Cell Biol* **15**, 5957-5965 (1995).
69 Topper, J. N. & Gimbrone, M. A., Jr. Blood flow and vascular gene expression: fluid shear stress as a modulator of endothelial phenotype. *Molecular medicine today* **5**, 40-46 (1999).
70 Bussolari, S. R., Dewey, C. F., Jr. & Gimbrone, M. A., Jr. Apparatus for subjecting living cells to fluid shear stress. *The Review of scientific instruments* **53**, 1851-1854 (1982).
71 Davies, P. F. & Tripathi, S. C. Mechanical stress mechanisms and the cell. An endothelial paradigm. *Circ Res* **72**, 239-245 (1993).
72 Resnick, N. *et al.* Platelet-derived growth factor B chain promoter contains a cis-acting fluid shear-stress-responsive element. *Proc Natl Acad Sci U S A* **90**, 7908 (1993).

73 Davis, M. E., Grumbach, I. M., Fukai, T., Cutchins, A. & Harrison, D. G. Shear stress regulates endothelial nitric-oxide synthase promoter activity through nuclear factor kappaB binding. *J Biol Chem* **279**, 163-168, doi:10.1074/jbc.M307528200 (2004).
74 Nam, D. *et al.* Partial carotid ligation is a model of acutely induced disturbed flow, leading to rapid endothelial dysfunction and atherosclerosis. *Am J Physiol Heart Circ Physiol* **297**, H1535-1543, doi:10.1152/ajpheart.00510.2009 (2009).
75 Hsiai, T. K. *et al.* Monocyte recruitment to endothelial cells in response to oscillatory shear stress. *Faseb J* **17**, 1648-1657, doi:10.1096/fj.02-1064com (2003).
76 Shyy, Y. J., Hsieh, H. J., Usami, S. & Chien, S. Fluid shear stress induces a biphasic response of human monocyte chemotactic protein 1 gene expression in vascular endothelium. *Proc Natl Acad Sci U S A* **91**, 4678-4682 (1994).
77 Hajra, L. *et al.* The NF-kappa B signal transduction pathway in aortic endothelial cells is primed for activation in regions predisposed to atherosclerotic lesion formation. *Proc Natl Acad Sci U S A* **97**, 9052-9057 (2000).
78 Lin, K. *et al.* Molecular mechanism of endothelial growth arrest by laminar shear stress. *Proc Natl Acad Sci U S A* **97**, 9385-9389, doi:10.1073/pnas.170282597 (2000).
79 Fang, Y., Shi, C., Manduchi, E., Civelek, M. & Davies, P. F. MicroRNA-10a regulation of proinflammatory phenotype in athero-susceptible endothelium in vivo and in vitro. *Proc Natl Acad Sci U S A* **107**, 13450-13455, doi:10.1073/pnas.1002120107 (2010).
80 Zaragoza, C., Marquez, S. & Saura, M. Endothelial mechanosensors of shear stress as regulators of atherogenesis. *Current opinion in lipidology* **23**, 446-452, doi:10.1097/MOL.0b013e328357e837 (2012).
81 Tzima, E. *et al.* A mechanosensory complex that mediates the endothelial cell response to fluid shear stress. *Nature* **437**, 426-431, doi:10.1038/nature03952 (2005).
82 White, G. E., Gimbrone, M. A., Jr. & Fujiwara, K. Factors influencing the expression of stress fibers in vascular endothelial cells in situ. *The Journal of cell biology* **97**, 416-424 (1983).
83 Davies, P. F. Hemodynamic shear stress and the endothelium in cardiovascular pathophysiology. *Nat Clin Pract Cardiovasc Med* **6**, 16-26, doi:10.1038/ncpcardio1397 (2009).
84 Tarbell, J. M., Shi, Z. D., Dunn, J. & Jo, H. Fluid Mechanics, Arterial Disease, and Gene Expression. *Annu Rev Fluid Mech* **46**, 591-614, doi:10.1146/annurev-fluid-010313-141309 (2014).
85 Noguchi, N. & Jo, H. Redox going with vascular shear stress. *Antioxid Redox Signal* **15**, 1367-1368, doi:10.1089/ars.2011.4011 (2011).
86 Bestor, T. H. The DNA methyltransferases of mammals. *Hum Mol Genet* **9**, 2395-2402 (2000).
87 Hsieh, C. L. The de novo methylation activity of Dnmt3a is distinctly different than that of Dnmt1. *BMC Biochem* **6**, 6, doi:10.1186/1471-2091-6-6 (2005).
88 Suzuki, M. RNA Interference-Mediated Knockdown of DNA Methyltransferase 1 Leads to Promoter Demethylation and Gene Re-Expression in Human Lung and Breast Cancer Cells. *Cancer Res* **64**, 3137-3143, doi:10.1158/0008-5472.can-03-3046 (2004).
89 Li, E., Beard, C. & Jaenisch, R. Role for DNA methylation in genomic imprinting. *Nature* **366**, 362-365, doi:10.1038/366362a0 (1993).
90 Li, E., Bestor, T. H. & Jaenisch, R. Targeted mutation of the DNA methyltransferase gene results in embryonic lethality. *Cell* **69**, 915-926 (1992).
91 Biniszkiewicz, D. *et al.* Dnmt1 overexpression causes genomic hypermethylation, loss of imprinting, and embryonic lethality. *Mol Cell Biol* **22**, 2124-2135 (2002).
92 Okano, M. & Li, E. Genetic analyses of DNA methyltransferase genes in mouse model system. *The Journal of nutrition* **132**, 2462S-2465S (2002).

93 Chen, K. *et al.* MicroRNA-101 mediates the suppressive effect of laminar shear stress on mTOR expression in vascular endothelial cells. *Biochem Biophys Res Commun* **427**, 138-142, doi:10.1016/j.bbrc.2012.09.026 (2012).

94 Qin, X. *et al.* MicroRNA-19a mediates the suppressive effect of laminar flow on cyclin D1 expression in human umbilical vein endothelial cells. *Proceedings of the National Academy of Sciences* **107**, 3240-3244, doi:10.1073/pnas.0914882107 (2010).

95 Weber, M., Baker, M. B., Moore, J. P. & Searles, C. D. MiR-21 is induced in endothelial cells by shear stress and modulates apoptosis and eNOS activity. *Biochemical and biophysical research communications* **393**, 643-648, doi:http://dx.doi.org/10.1016/j.bbrc.2010.02.045 (2010).

96 Fang, Y., Shi, C., Manduchi, E., Civelek, M. & Davies, P. F. MicroRNA-10a regulation of proinflammatory phenotype in athero-susceptible endothelium in vivo and in vitro. *Proceedings of the National Academy of Sciences* **107**, 13450-13455, doi:10.1073/pnas.1002120107 (2010).

97 Marin, T. *et al.* Mechanosensitive microRNAs-role in endothelial responses to shear stress and redox state. *Free radical biology & medicine* **64**, 61-68, doi:10.1016/j.freeradbiomed.2013.05.034 (2013).

98 Wu, W. *et al.* Flow-Dependent Regulation of Krüppel-Like Factor 2 Is Mediated by MicroRNA-92a. *Circulation* **124**, 633-641, doi:10.1161/circulationaha.110.005108 (2011).

99 Humbert, M. *et al.* Deregulated expression of Kruppel-like factors in acute myeloid leukemia. *Leukemia research* **35**, 909-913, doi:10.1016/j.leukres.2011.03.010 (2011).

100 Wei, Y., Nazari-Jahantigh, M., Neth, P., Weber, C. & Schober, A. MicroRNA-126, -145, and -155: a therapeutic triad in atherosclerosis? *Arteriosclerosis, thrombosis, and vascular biology* **33**, 449-454, doi:10.1161/ATVBAHA.112.300279 (2013).

101 D.J. Son, S. K., W. Takabe, C.W. Kim, C.W. Ni, N.A. Grill, I. Jang, S. Kim, W. Kim, S.W. Kim, A. Baker, J.W. S, K. Ferrara, H. Jo. The atypical mechanosensitive microRNA-712 derived from pre-ribosomal RNA induces endothelial inflammation and atherosclerosis. . *Nature Communications*, doi:10.1038/ncomms4000 (2013).

102 Fabbri, M. *et al.* MicroRNA-29 family reverts aberrant methylation in lung cancer by targeting DNA methyltransferases 3A and 3B. *Proc Natl Acad Sci U S A* **104**, 15805-15810, doi:10.1073/pnas.0707628104 (2007).

103 Takada, S., Berezikov, E., Choi, Y. L., Yamashita, Y. & Mano, H. Potential role of miR-29b in modulation of Dnmt3a and Dnmt3b expression in primordial germ cells of female mouse embryos. *Rna* **15**, 1507-1514, doi:10.1261/rna.1418309 (2009).

104 Braconi, C., Huang, N. & Patel, T. MicroRNA-dependent regulation of DNA methyltransferase-1 and tumor suppressor gene expression by interleukin-6 in human malignant cholangiocytes. *Hepatology* **51**, 881-890, doi:10.1002/hep.23381 (2010).

105 Braconi, C. *et al.* microRNA-29 can regulate expression of the long non-coding RNA gene MEG3 in hepatocellular cancer. *Oncogene* **30**, 4750-4756, doi:10.1038/onc.2011.193 (2011).

106 Ding, D. P. *et al.* miR-29c induces cell cycle arrest in esophageal squamous cell carcinoma by modulating cyclin E expression. *Carcinogenesis* **32**, 1025-1032, doi:10.1093/carcin/bgr078 (2011).

107 Chang, T. C. *et al.* Widespread microRNA repression by Myc contributes to tumorigenesis. *Nat Genet* **40**, 43-50, doi:10.1038/ng.2007.30 (2008).

108 Chen, K. C. *et al.* OxLDL up-regulates microRNA-29b, leading to epigenetic modifications of MMP-2/MMP-9 genes: a novel mechanism for cardiovascular diseases. *Faseb J* **25**, 1718-1728, doi:10.1096/fj.10-174904 (2011).

109 Sato, N., Maehara, N., Su, G. H. & Goggins, M. Effects of 5-aza-2'-deoxycytidine on matrix metalloproteinase expression and pancreatic cancer cell invasiveness. *Journal of the National Cancer Institute* **95**, 327-330 (2003).
110 Chernov, A. V., Sounni, N. E., Remacle, A. G. & Strongin, A. Y. Epigenetic control of the invasion-promoting MT1-MMP/MMP-2/TIMP-2 axis in cancer cells. *J Biol Chem* **284**, 12727-12734, doi:10.1074/jbc.M900273200 (2009).
111 Fang, J. *et al.* Epigenetic changes mediated by microRNA miR29 activate cyclooxygenase 2 and lambda-1 interferon production during viral infection. *Journal of virology* **86**, 1010-1020, doi:10.1128/JVI.06169-11 (2012).
112 Ogasawara, A. *et al.* Fluid shear stress-induced cyclooxygenase-2 expression is mediated by C/EBP beta, cAMP-response element-binding protein, and AP-1 in osteoblastic MC3T3-E1 cells. *J Biol Chem* **276**, 7048-7054, doi:10.1074/jbc.M008070200 (2001).
113 Nam, D. *et al.* Partial carotid ligation is a model of acutely induced disturbed flow, leading to rapid endothelial dysfunction and atherosclerosis. *American journal of physiology. Heart and circulatory physiology* **297**, H1535-1543, doi:10.1152/ajpheart.00510.2009 (2009).
114 Nam, D. *et al.* A model of disturbed flow-induced atherosclerosis in mouse carotid artery by partial ligation and a simple method of RNA isolation from carotid endothelium. *Journal of visualized experiments : JoVE*, doi:10.3791/1861 (2010).
115 Schmittgen, T. D. & Livak, K. J. Analyzing real-time PCR data by the comparative C(T) method. *Nat Protoc* **3**, 1101-1108 (2008).
116 Newman, M. *et al.* Sensitive quantitative analysis of murine LINE1 DNA methylation using high resolution melt analysis. *Epigenetics* **7**, 92-105, doi:10.4161/epi.7.1.18815 (2012).
117 Sampath, D., Rao, V. A. & Plunkett, W. Mechanisms of apoptosis induction by nucleoside analogs. *Oncogene* **22**, 9063-9074, doi:10.1038/sj.onc.1207229 (2003).
118 Park, J. G. *et al.* Peroxiredoxin 2 deficiency exacerbates atherosclerosis in apolipoprotein E-deficient mice. *Circ Res* **109**, 739-749, doi:10.1161/CIRCRESAHA.111.245530 (2011).
119 Jin, Z. *et al.* Temporal evolution in caveolin 1 methylation levels during human esophageal carcinogenesis. *BMC Cancer* **14**, 345, doi:10.1186/1471-2407-14-345 (2014).
120 Song, F. *et al.* Association of tissue-specific differentially methylated regions (TDMs) with differential gene expression. *Proc Natl Acad Sci U S A* **102**, 3336-3341, doi:10.1073/pnas.0408436102 (2005).
121 Grunau, C., Hindermann, W. & Rosenthal, A. Large-scale methylation analysis of human genomic DNA reveals tissue-specific differences between the methylation profiles of genes and pseudogenes. *Hum Mol Genet* **9**, 2651-2663 (2000).
122 Weber, M. *et al.* Chromosome-wide and promoter-specific analyses identify sites of differential DNA methylation in normal and transformed human cells. *Nat Genet* **37**, 853-862, doi:10.1038/ng1598 (2005).
123 Hashimoto, H., Vertino, P. M. & Cheng, X. Molecular coupling of DNA methylation and histone methylation. *Epigenomics* **2**, 657-669 (2010).
124 Schnekenburger, M., Talaska, G. & Puga, A. Chromium cross-links histone deacetylase 1-DNA methyltransferase 1 complexes to chromatin, inhibiting histone-remodeling marks critical for transcriptional activation. *Mol Cell Biol* **27**, 7089-7101, doi:10.1128/MCB.00838-07 (2007).
125 Maunakea, A. K. *et al.* Conserved role of intragenic DNA methylation in regulating alternative promoters. *Nature* **466**, 253-257, doi:10.1038/nature09165 (2010).
126 Jjingo, D., Conley, A. B., Yi, S. V., Lunyak, V. V. & Jordan, I. K. On the presence and role of human gene-body DNA methylation. *Oncotarget* **3**, 462-474 (2012).

127 Varley, K. E. *et al.* Dynamic DNA methylation across diverse human cell lines and tissues. *Genome Res* **23**, 555-567, doi:10.1101/gr.147942.112 (2013).
128 Jones, P. A. The DNA methylation paradox. *Trends in genetics : TIG* **15**, 34-37 (1999).
129 Lorincz, M. C., Dickerson, D. R., Schmitt, M. & Groudine, M. Intragenic DNA methylation alters chromatin structure and elongation efficiency in mammalian cells. *Nature structural & molecular biology* **11**, 1068-1075, doi:10.1038/nsmb840 (2004).
130 Ball, M. P. *et al.* Targeted and genome-scale strategies reveal gene-body methylation signatures in human cells. *Nat Biotechnol* **27**, 361-368, doi:10.1038/nbt.1533 (2009).
131 Frommer, M. *et al.* A genomic sequencing protocol that yields a positive display of 5-methylcytosine residues in individual DNA strands. *Proc Natl Acad Sci U S A* **89**, 1827-1831 (1992).
132 Stanzer, S. *et al.* Rapid and reliable detection of LINE-1 hypomethylation using high-resolution melting analysis. *Clin Biochem* **43**, 1443-1448, doi:10.1016/j.clinbiochem.2010.09.013 (2010).
133 Candiloro, I. L., Mikeska, T. & Dobrovic, A. Assessing combined methylation-sensitive high resolution melting and pyrosequencing for the analysis of heterogeneous DNA methylation. *Epigenetics* **6**, 500-507 (2011).
134 Meissner, A. *et al.* Reduced representation bisulfite sequencing for comparative high-resolution DNA methylation analysis. *Nucleic Acids Res* **33**, 5868-5877, doi:10.1093/nar/gki901 (2005).
135 Meissner, A. *et al.* Genome-scale DNA methylation maps of pluripotent and differentiated cells. *Nature* **454**, 766-770, doi:10.1038/nature07107 (2008).
136 Gu, H. *et al.* Preparation of reduced representation bisulfite sequencing libraries for genome-scale DNA methylation profiling. *Nat Protoc* **6**, 468-481, doi:10.1038/nprot.2010.190 (2011).
137 Gu, H. *et al.* Genome-scale DNA methylation mapping of clinical samples at single-nucleotide resolution. *Nat Methods* **7**, 133-136, doi:10.1038/nmeth.1414 (2010).
138 Rohde, C., Zhang, Y., Reinhardt, R. & Jeltsch, A. BISMA--fast and accurate bisulfite sequencing data analysis of individual clones from unique and repetitive sequences. *BMC bioinformatics* **11**, 230, doi:10.1186/1471-2105-11-230 (2010).
139 Schena, M., Shalon, D., Davis, R. W. & Brown, P. O. Quantitative monitoring of gene expression patterns with a complementary DNA microarray. *Science* **270**, 467-470 (1995).
140 Montminy, M. R., Sevarino, K. A., Wagner, J. A., Mandel, G. & Goodman, R. H. Identification of a cyclic-AMP-responsive element within the rat somatostatin gene. *Proc Natl Acad Sci U S A* **83**, 6682-6686 (1986).
141 Comb, M., Birnberg, N. C., Seasholtz, A., Herbert, E. & Goodman, H. M. A cyclic AMP- and phorbol ester-inducible DNA element. *Nature* **323**, 353-356, doi:10.1038/323353a0 (1986).
142 Short, J. M., Wynshaw-Boris, A., Short, H. P. & Hanson, R. W. Characterization of the phosphoenolpyruvate carboxykinase (GTP) promoter-regulatory region. II. Identification of cAMP and glucocorticoid regulatory domains. *J Biol Chem* **261**, 9721-9726 (1986).
143 Mayr, B. & Montminy, M. Transcriptional regulation by the phosphorylation-dependent factor CREB. *Nat Rev Mol Cell Biol* **2**, 599-609, doi:10.1038/35085068 (2001).
144 Desdouets, C. *et al.* Cell cycle regulation of cyclin A gene expression by the cyclic AMP-responsive transcription factors CREB and CREM. *Mol Cell Biol* **15**, 3301-3309 (1995).
145 Lee, R. J. *et al.* pp60(v-src) induction of cyclin D1 requires collaborative interactions between the extracellular signal-regulated kinase, p38, and Jun kinase pathways. A role for cAMP response element-binding protein and activating transcription factor-2 in pp60(v-src) signaling in breast cancer cells. *J Biol Chem* **274**, 7341-7350 (1999).

146 D'Amico, M. *et al.* The integrin-linked kinase regulates the cyclin D1 gene through glycogen synthase kinase 3beta and cAMP-responsive element-binding protein-dependent pathways. *J Biol Chem* **275**, 32649-32657, doi:10.1074/jbc.M000643200 (2000).
147 Fink, J. S. *et al.* The CGTCA sequence motif is essential for biological activity of the vasoactive intestinal peptide gene cAMP-regulated enhancer. *Proc Natl Acad Sci U S A* **85**, 6662-6666 (1988).
148 Yamamoto, K. K., Gonzalez, G. A., Biggs, W. H., 3rd & Montminy, M. R. Phosphorylation-induced binding and transcriptional efficacy of nuclear factor CREB. *Nature* **334**, 494-498, doi:10.1038/334494a0 (1988).
149 Zhang, X. *et al.* Genome-wide analysis of cAMP-response element binding protein occupancy, phosphorylation, and target gene activation in human tissues. *Proc Natl Acad Sci U S A* **102**, 4459-4464, doi:10.1073/pnas.0501076102 (2005).
150 Craig, J. C. *et al.* Consensus and variant cAMP-regulated enhancers have distinct CREB-binding properties. *J Biol Chem* **276**, 11719-11728, doi:10.1074/jbc.M010263200 (2001).
151 Nichols, M. *et al.* Phosphorylation of CREB affects its binding to high and low affinity sites: implications for cAMP induced gene transcription. *Embo J* **11**, 3337-3346 (1992).
152 Weih, F., Stewart, A. F., Boshart, M., Nitsch, D. & Schutz, G. In vivo monitoring of a cAMP-stimulated DNA-binding activity. *Genes & development* **4**, 1437-1449 (1990).
153 Rishi, V. *et al.* CpG methylation of half-CRE sequences creates C/EBPalpha binding sites that activate some tissue-specific genes. *Proc Natl Acad Sci U S A* **107**, 20311-20316, doi:10.1073/pnas.1008688107 (2010).
154 Iguchi-Ariga, S. M. & Schaffner, W. CpG methylation of the cAMP-responsive enhancer/promoter sequence TGACGTCA abolishes specific factor binding as well as transcriptional activation. *Genes & development* **3**, 612-619 (1989).
155 Tierney, R. J. *et al.* Methylation of transcription factor binding sites in the Epstein-Barr virus latent cycle promoter Wp coincides with promoter down-regulation during virus-induced B-cell transformation. *Journal of virology* **74**, 10468-10479 (2000).
156 Iannello, R. C. *et al.* Methylation-dependent silencing of the testis-specific Pdha-2 basal promoter occurs through selective targeting of an activating transcription factor/cAMP-responsive element-binding site. *J Biol Chem* **275**, 19603-19608, doi:10.1074/jbc.M001867200 (2000).
157 Iannello, R. C. *et al.* Regulation of Pdha-2 expression is mediated by proximal promoter sequences and CpG methylation. *Mol Cell Biol* **17**, 612-619 (1997).
158 Kwok, R. P. *et al.* Control of cAMP-regulated enhancers by the viral transactivator Tax through CREB and the co-activator CBP. *Nature* **380**, 642-646, doi:10.1038/380642a0 (1996).
159 Lundblad, J. R. *et al.* The human T-cell leukemia virus-1 transcriptional activator Tax enhances cAMP-responsive element-binding protein (CREB) binding activity through interactions with the DNA minor groove. *J Biol Chem* **273**, 19251-19259 (1998).
160 Boo, Y. C. Shear stress stimulates phosphorylation of protein kinase A substrate proteins including endothelial nitric oxide synthase in endothelial cells. *Experimental & molecular medicine* **38**, 63-71, doi:10.1038/emm.2006.8 (2006).
161 J. M. Chambers and T. J. Hastie, W. B. C., (1992).
162 Rogers, G. N. W. a. C. E. Symbolic descriptions of factorial models for analysis of variance. *Applied Statistics* **22**, 392-399 (1973).
163 Weber, M. *et al.* Distribution, silencing potential and evolutionary impact of promoter DNA methylation in the human genome. *Nat Genet* **39**, 457-466, doi:10.1038/ng1990 (2007).
164 Schwartz, S. M. & Benditt, E. P. Cell replication in the aortic endothelium: a new method for study of the problem. *Lab Invest* **28**, 699-707 (1973).

165 Schwartz, S. M. & Benditt, E. P. Aortic endothelial cell replication. I. Effects of age and hypertension in the rat. *Circ Res* **41**, 248-255 (1977).
166 Xu, Q. Disturbed flow-enhanced endothelial turnover in atherosclerosis. *Trends in cardiovascular medicine* **19**, 191-195, doi:10.1016/j.tcm.2009.12.002 (2009).
167 Wang, W. *et al.* Fluid shear stress stimulates phosphorylation-dependent nuclear export of HDAC5 and mediates expression of KLF2 and eNOS. *Blood* **115**, 2971-2979, doi:10.1182/blood-2009-05-224824 (2010).
168 Lee, D. Y. *et al.* Role of histone deacetylases in transcription factor regulation and cell cycle modulation in endothelial cells in response to disturbed flow. *Proc Natl Acad Sci U S A* **109**, 1967-1972, doi:10.1073/pnas.1121214109 (2012).
169 Inoue, K. *et al.* Histone deacetylase inhibitor reduces monocyte adhesion to endothelium through the suppression of vascular cell adhesion molecule-1 expression. *Arterioscler Thromb Vasc Biol* **26**, 2652-2659, doi:10.1161/01.ATV.0000247247.89787.e7 (2006).
170 Wang, J., Mahmud, S. A., Bitterman, P. B., Huo, Y. & Slungaard, A. Histone deacetylase inhibitors suppress TF-kappaB-dependent agonist-driven tissue factor expression in endothelial cells and monocytes. *J Biol Chem* **282**, 28408-28418, doi:10.1074/jbc.M703586200 (2007).
171 Gan, Y. *et al.* Role of histone deacetylation in cell-specific expression of endothelial nitric-oxide synthase. *J Biol Chem* **280**, 16467-16475, doi:10.1074/jbc.M412960200 (2005).
172 Chan, Y. *et al.* The cell-specific expression of endothelial nitric-oxide synthase: a role for DNA methylation. *J Biol Chem* **279**, 35087-35100, doi:10.1074/jbc.M405063200 (2004).
173 Okada, Y. *et al.* Endothelial cell-specific expression of roundabout 4 is regulated by differential DNA methylation of the proximal promoter. *Arterioscler Thromb Vasc Biol* **34**, 1531-1538, doi:10.1161/ATVBAHA.114.303818 (2014).
174 Park, K. W. *et al.* Robo4 is a vascular-specific receptor that inhibits endothelial migration. *Dev Biol* **261**, 251-267 (2003).
175 Suchting, S., Heal, P., Tahtis, K., Stewart, L. M. & Bicknell, R. Soluble Robo4 receptor inhibits in vivo angiogenesis and endothelial cell migration. *Faseb J* **19**, 121-123, doi:10.1096/fj.04-1991fje (2005).
176 Ohtani, K. *et al.* Epigenetic regulation of endothelial lineage committed genes in pro-angiogenic hematopoietic and endothelial progenitor cells. *Circ Res* **109**, 1219-1229, doi:10.1161/CIRCRESAHA.111.247304 (2011).
177 Shirodkar, A. V. *et al.* A mechanistic role for DNA methylation in endothelial cell (EC)-enriched gene expression: relationship with DNA replication timing. *Blood* **121**, 3531-3540, doi:10.1182/blood-2013-01-479170 (2013).
178 Hamik, A. *et al.* Kruppel-like factor 4 regulates endothelial inflammation. *J Biol Chem* **282**, 13769-13779, doi:10.1074/jbc.M700078200 (2007).
179 Wu, W. *et al.* Flow-Dependent Regulation of Kruppel-Like Factor 2 Is Mediated by MicroRNA-92a. *Circulation* **124**, 633-641, doi:10.1161/CIRCULATIONAHA.110.005108 (2011).
180 Hamik, A. & Jain, M. K. MiRrored regulation of KLF2 and KLF4. *Arterioscler Thromb Vasc Biol* **32**, 839-840, doi:10.1161/ATVBAHA.112.245563 (2012).
181 Huddleson, J. P., Ahmad, N., Srinivasan, S. & Lingrel, J. B. Induction of KLF2 by fluid shear stress requires a novel promoter element activated by a phosphatidylinositol 3-kinase-dependent chromatin-remodeling pathway. *J Biol Chem* **280**, 23371-23379, doi:10.1074/jbc.M413839200 (2005).
182 Villarreal, G., Jr. *et al.* Defining the regulation of KLF4 expression and its downstream transcriptional targets in vascular endothelial cells. *Biochem Biophys Res Commun* **391**, 984-989, doi:10.1016/j.bbrc.2009.12.002 (2010).

183 Tanzer, A., Amemiya, C. T., Kim, C. B. & Stadler, P. F. Evolution of microRNAs located within Hox gene clusters. *Journal of experimental zoology. Part B, Molecular and developmental evolution* **304**, 75-85, doi:10.1002/jez.b.21021 (2005).
184 Illingworth, R. *et al.* A novel CpG island set identifies tissue-specific methylation at developmental gene loci. *PLoS biology* **6**, e22, doi:10.1371/journal.pbio.0060022 (2008).
185 Rossig, L. *et al.* Histone deacetylase activity is essential for the expression of HoxA9 and for endothelial commitment of progenitor cells. *The Journal of experimental medicine* **201**, 1825-1835, doi:10.1084/jem.20042097 (2005).
186 Han, L., Witmer, P. D., Casey, E., Valle, D. & Sukumar, S. DNA methylation regulates MicroRNA expression. *Cancer biology & therapy* **6**, 1284-1288 (2007).
187 Pei, L. *et al.* Genome-wide DNA methylation analysis reveals novel epigenetic changes in chronic lymphocytic leukemia. *Epigenetics* **7**, 567-578, doi:10.4161/epi.20237 (2012).
188 Rauch, T. A., Wu, X., Zhong, X., Riggs, A. D. & Pfeifer, G. P. A human B cell methylome at 100-base pair resolution. *Proc Natl Acad Sci U S A* **106**, 671-678, doi:10.1073/pnas.0812399106 (2009).
189 Dixon, J. R. *et al.* Topological domains in mammalian genomes identified by analysis of chromatin interactions. *Nature* **485**, 376-380, doi:10.1038/nature11082 (2012).
190 Gorski, D. H. & Walsh, K. The role of homeobox genes in vascular remodeling and angiogenesis. *Circ Res* **87**, 865-872 (2000).
191 Lee, J. Y. *et al.* Human HOXA5 homeodomain enhances protein transduction and its application to vascular inflammation. *Biochem Biophys Res Commun* **410**, 312-316, doi:10.1016/j.bbrc.2011.05.139 (2011).
192 Myers, C., Charboneau, A., Cheung, I., Hanks, D. & Boudreau, N. Sustained expression of homeobox D10 inhibits angiogenesis. *Am J Pathol* **161**, 2099-2109, doi:10.1016/S0002-9440(10)64488-4 (2002).
193 Rhoads, K. *et al.* A role for Hox A5 in regulating angiogenesis and vascular patterning. *Lymphatic research and biology* **3**, 240-252, doi:10.1089/lrb.2005.3.240 (2005).
194 Arderiu, G. *et al.* HoxA5 stabilizes adherens junctions via increased Akt1. *Cell adhesion & migration* **1**, 185-195 (2007).
195 Zhu, Y. *et al.* Restoring transcription factor HoxA5 expression inhibits the growth of experimental hemangiomas in the brain. *Journal of neuropathology and experimental neurology* **68**, 626-632, doi:10.1097/NEN.0b013e3181a491ce (2009).
196 Boudreau, N., Andrews, C., Srebrow, A., Ravanpay, A. & Cheresh, D. A. Induction of the angiogenic phenotype by Hox D3. *The Journal of cell biology* **139**, 257-264 (1997).
197 Boudreau, N. J. & Varner, J. A. The homeobox transcription factor Hox D3 promotes integrin alpha5beta1 expression and function during angiogenesis. *J Biol Chem* **279**, 4862-4868, doi:10.1074/jbc.M305190200 (2004).
198 Myers, C., Charboneau, A. & Boudreau, N. Homeobox B3 promotes capillary morphogenesis and angiogenesis. *The Journal of cell biology* **148**, 343-351 (2000).
199 Chen, Y. *et al.* Retroviral delivery of homeobox D3 gene induces cerebral angiogenesis in mice. *Journal of cerebral blood flow and metabolism : official journal of the International Society of Cerebral Blood Flow and Metabolism* **24**, 1280-1287, doi:10.1097/01.WCB.0000141770.09022.AB (2004).
200 Mace, K. A., Hansen, S. L., Myers, C., Young, D. M. & Boudreau, N. HOXA3 induces cell migration in endothelial and epithelial cells promoting angiogenesis and wound repair. *J Cell Sci* **118**, 2567-2577, doi:10.1242/jcs.02399 (2005).
201 Chen, H. *et al.* Identification of transcriptional targets of HOXA5. *J Biol Chem* **280**, 19373-19380, doi:10.1074/jbc.M413528200 (2005).
202 Chen, Y. & Gorski, D. H. Regulation of angiogenesis through a microRNA (miR-130a) that down-regulates antiangiogenic homeobox genes GAX and HOXA5. *Blood* **111**, 1217-1226, doi:10.1182/blood-2007-07-104133 (2008).

203 Huang, H. *et al.* miR-10a contributes to retinoid acid-induced smooth muscle cell differentiation. *J Biol Chem* **285**, 9383-9389, doi:10.1074/jbc.M109.095612 (2010).
204 Tian, Y. *et al.* MicroRNA-10b promotes migration and invasion through KLF4 in human esophageal cancer cell lines. *J Biol Chem* **285**, 7986-7994, doi:10.1074/jbc.M109.062877 (2010).
205 Garzon, R. *et al.* MicroRNA fingerprints during human megakaryocytopoiesis. *Proc Natl Acad Sci U S A* **103**, 5078-5083, doi:10.1073/pnas.0600587103 (2006).
206 Tan, Y. *et al.* Transcriptional inhibiton of Hoxd4 expression by miRNA-10a in human breast cancer cells. *BMC molecular biology* **10**, 12, doi:10.1186/1471-2199-10-12 (2009).
207 Pearson, R. C., Funnell, A. P. & Crossley, M. The mammalian zinc finger transcription factor Kruppel-like factor 3 (KLF3/BKLF). *IUBMB life* **63**, 86-93, doi:10.1002/iub.422 (2011).
208 Villarreal, G., Jr. *et al.* Defining the regulation of KLF4 expression and its downstream transcriptional targets in vascular endothelial cells. *Biochem Biophys Res Commun* **391**, 984-989, doi:10.1016/j.bbrc.2009.12.002 (2010).
209 Lin, Z. *et al.* Kruppel-like factor 2 (KLF2) regulates endothelial thrombotic function. *Circ Res* **96**, e48-57, doi:10.1161/01.RES.0000159707.05637.a1 (2005).
210 Strathdee, G., Sim, A., Soutar, R., Holyoake, T. L. & Brown, R. HOXA5 is targeted by cell-type-specific CpG island methylation in normal cells and during the development of acute myeloid leukaemia. *Carcinogenesis* **28**, 299-309, doi:10.1093/carcin/bgl133 (2007).
211 Kim, S. Y. *et al.* Level of HOXA5 hypermethylation in acute myeloid leukemia is associated with short-term outcome. *The Korean journal of laboratory medicine* **30**, 469-473, doi:10.3343/kjlm.2010.30.5.469 (2010).
212 Miftakhova, R. *et al.* DNA methylation in ATRA-treated leukemia cell lines lacking a PML-RAR chromosome translocation. *Anticancer research* **32**, 4715-4722 (2012).
213 Qin, X. *et al.* MicroRNA-19a mediates the suppressive effect of laminar flow on cyclin D1 expression in human umbilical vein endothelial cells. *Proc Natl Acad Sci U S A* **107**, 3240-3244, doi:10.1073/pnas.0914882107 (2010).
214 Weber, M., Baker, M. B., Moore, J. P. & Searles, C. D. MiR-21 is induced in endothelial cells by shear stress and modulates apoptosis and eNOS activity. *Biochem Biophys Res Commun* **393**, 643-648, doi:10.1016/j.bbrc.2010.02.045 (2010).
215 Wang, K. C. *et al.* Role of microRNA-23b in flow-regulation of Rb phosphorylation and endothelial cell growth. *Proc Natl Acad Sci U S A* **107**, 3234-3239, doi:10.1073/pnas.0914825107 (2010).
216 Kohlstedt, K. *et al.* AMP-activated protein kinase regulates endothelial cell angiotensin-converting enzyme expression via p53 and the post-transcriptional regulation of microRNA-143/145. *Circ Res* **112**, 1150-1158, doi:10.1161/CIRCRESAHA.113.301282 (2013).
217 Zhou, J. *et al.* MicroRNA-21 targets peroxisome proliferators-activated receptor-alpha in an autoregulatory loop to modulate flow-induced endothelial inflammation. *Proc Natl Acad Sci U S A* **108**, 10355-10360, doi:10.1073/pnas.1107052108 (2011).
218 Fang, Y. & Davies, P. F. Site-specific microRNA-92a regulation of Kruppel-like factors 4 and 2 in atherosusceptible endothelium. *Arterioscler Thromb Vasc Biol* **32**, 979-987, doi:10.1161/ATVBAHA.111.244053 (2012).
219 Ni, C. W., Qiu, H. & Jo, H. MicroRNA-663 upregulated by oscillatory shear stress plays a role in inflammatory response of endothelial cells. *Am J Physiol Heart Circ Physiol* **300**, H1762-1769, doi:10.1152/ajpheart.00829.2010 (2011).
220 Weber, M., Kim, S., Patterson, N., Rooney, K. & Searles, C. D. MiRNA-155 targets myosin light chain kinase and modulates actin cytoskeleton organization in endothelial

cells. *Am J Physiol Heart Circ Physiol* **306**, H1192-1203, doi:10.1152/ajpheart.00521.2013 (2014).
221 Hergenreider, E. *et al.* Atheroprotective communication between endothelial cells and smooth muscle cells through miRNAs. *Nature cell biology* **14**, 249-256, doi:10.1038/ncb2441 (2012).
222 Son, D. J. *et al.* The atypical mechanosensitive microRNA-712 derived from pre-ribosomal RNA induces endothelial inflammation and atherosclerosis. *Nat Commun* **4**, 3000, doi:10.1038/ncomms4000 (2013).
223 Kim, C. W. *et al.* Prevention of abdominal aortic aneurysm by anti-microRNA-712 or anti-microRNA-205 in angiotensin II-infused mice. *Arterioscler Thromb Vasc Biol* **34**, 1412-1421, doi:10.1161/ATVBAHA.113.303134 (2014).
224 Loyer, X. *et al.* Inhibition of microRNA-92a prevents endothelial dysfunction and atherosclerosis in mice. *Circ Res* **114**, 434-443, doi:10.1161/CIRCRESAHA.114.302213 (2014).
225 Sun, X. *et al.* Systemic delivery of microRNA-181b inhibits nuclear factor-kappaB activation, vascular inflammation, and atherosclerosis in apolipoprotein E-deficient mice. *Circ Res* **114**, 32-40, doi:10.1161/CIRCRESAHA.113.302089 (2014).
226 Li, L. C. & Dahiya, R. MethPrimer: designing primers for methylation PCRs. *Bioinformatics* **18**, 1427-1431 (2002).
227 Tompkins, J. D. *et al.* Epigenetic stability, adaptability, and reversibility in human embryonic stem cells. *Proc Natl Acad Sci U S A* **109**, 12544-12549, doi:10.1073/pnas.1209620109 (2012).
228 Bentivegna, A. *et al.* DNA Methylation Changes during In Vitro Propagation of Human Mesenchymal Stem Cells: Implications for Their Genomic Stability? *Stem cells international* **2013**, 192425, doi:10.1155/2013/192425 (2013).
229 Torres-Martin, M. *et al.* Genome-wide methylation analysis in vestibular schwannomas shows putative mechanisms of gene expression modulation and global hypomethylation at the HOX gene cluster. *Genes Chromosomes Cancer*, doi:10.1002/gcc.22232 (2014).
230 Tsumagari, K. *et al.* DNA methylation and differentiation: HOX genes in muscle cells. *Epigenetics & chromatin* **6**, 25, doi:10.1186/1756-8935-6-25 (2013).
231 Laurent, L. *et al.* Dynamic changes in the human methylome during differentiation. *Genome Res* **20**, 320-331, doi:10.1101/gr.101907.109 (2010).
232 Raney, B. J. *et al.* ENCODE whole-genome data in the UCSC genome browser (2011 update). *Nucleic Acids Res* **39**, D871-875, doi:10.1093/nar/gkq1017 (2011).
233 Kim, Y. J., Cecchini, K. R. & Kim, T. H. Conserved, developmentally regulated mechanism couples chromosomal looping and heterochromatin barrier activity at the homeobox gene A locus. *Proc Natl Acad Sci U S A* **108**, 7391-7396, doi:10.1073/pnas.1018279108 (2011).
234 Jaluria, P., Konstantopoulos, K., Betenbaugh, M. & Shiloach, J. A perspective on microarrays: current applications, pitfalls, and potential uses. *Microbial cell factories* **6**, 4, doi:10.1186/1475-2859-6-4 (2007).
235 Hongcang Gu, C. B., Tarjei S Mikkelsen,, Natalie Jäger , Z. D. S., Eleni Tomazou Andreas Gnirke, Eric S Lander, & & Meissner, A. Genome-scale dna methylation mapping of clinical samples at single-nucleotide resolution. *Nat Methods* **7**, doi:10.1038/nmeth.1414
10.1038/NMETH.1414 (2010).
236 Guo, J. U. *et al.* Distribution, recognition and regulation of non-CpG methylation in the adult mammalian brain. *Nature neuroscience* **17**, 215-222, doi:10.1038/nn.3607 (2014).
237 Kriaucionis, S. & Tahiliani, M. Expanding the epigenetic landscape: novel modifications of cytosine in genomic DNA. *Cold Spring Harbor perspectives in biology* **6**, a018630, doi:10.1101/cshperspect.a018630 (2014).

238 Cao, Q. *et al.* Inhibiting DNA Methylation by 5-aza-2'-deoxycytidine Ameliorates Atherosclerosis Through Suppressing Macrophage Inflammation. *Endocrinology*, en20141595, doi:10.1210/en.2014-1595 (2014).
239 Harry, B. L. *et al.* Endothelial cell PECAM-1 promotes atherosclerotic lesions in areas of disturbed flow in ApoE-deficient mice. *Arterioscler Thromb Vasc Biol* **28**, 2003-2008, doi:10.1161/ATVBAHA.108.164707 (2008).
240 Frank, P. G. & Lisanti, M. P. Caveolin-1 and caveolae in atherosclerosis: differential roles in fatty streak formation and neointimal hyperplasia. *Current opinion in lipidology* **15**, 523-529 (2004).
241 Datta, J. *et al.* A new class of quinoline-based DNA hypomethylating agents reactivates tumor suppressor genes by blocking DNA methyltransferase 1 activity and inducing its degradation. *Cancer Res* **69**, 4277-4285, doi:10.1158/0008-5472.CAN-08-3669 (2009).
242 Wu, H. & Zhang, Y. Mechanisms and functions of Tet protein-mediated 5-methylcytosine oxidation. *Genes & development* **25**, 2436-2452, doi:10.1101/gad.179184.111 (2011).
243 Gregory, D. J., Mikhaylova, L. & Fedulov, A. V. Selective DNA demethylation by fusion of TDG with a sequence-specific DNA-binding domain. *Epigenetics* **7**, 344-349, doi:10.4161/epi.19509 (2012).
244 Jurkowska, R. Z. & Jeltsch, A. Silencing of gene expression by targeted DNA methylation: concepts and approaches. *Methods Mol Biol* **649**, 149-161, doi:10.1007/978-1-60761-753-2_9 (2010).

VITA

JESSILYN P. DUNN

DUNN was born in Hollywood, Florida. She attended Nova High School in Davie, Florida, and earned a B.S. in Biomedical Engineering from the Johns Hopkins University in Baltimore, Maryland in 2010 before joining the Georgia Institute of Technology and Emory University to pursue her doctorate in Biomedical Engineering. When she is not working on her research, Dunn enjoys spending time with her family and friends, dancing, running, and swimming, gardening, and painting.